Investigating the role of the SNARE protein, Tlg2, in *Leishmania mexicana*

Kirstin Anne Spence

Doctor of Philosophy

University of York

Biology

January 2022

Abstract

Soluble *N*-ethylmaleimide-sensitive factor adaptor proteins receptors (SNARE) proteins are essential components of intracellular membrane trafficking yet are critically understudied in trypanosomatid parasites. Although 27 SNARE-domain containing proteins have been identified in *Leishmania major*, no functional characterisation has yet been undertaken. In yeast, Tlg2 is a SNARE protein that forms part of the *trans*-Golgi network and mediates fusion events between endosomes and the late Golgi. It also plays a role in autophagy, although the mechanisms behind this are not fully understood. Bioinformatic analysis of the *Leishmania mexicana* genome revealed homologues of Tlg2, its SNARE complex partners and two Sec1/Munc18 (SM) Vps45 regulatory proteins. Overexpression of ectopic Tlg2 in *L. mexicana* promastigotes did not result in any observed phenotypes but demonstrated that the protein is exclusively expressed during logarithmic growth. In contrast, *tlg2* null mutants displayed growth and morphological phenotypes, as well as delayed expression of *SHERP* mRNA (a marker for metacyclogenesis). Addback of an ectopic wild-type Tlg2 ($Tlg2^{WT}$) rescued the null mutants. Addback of a F10A/L11A mutant ($Tlg2^{FL}$) that is predicted to disrupt a high-affinity pocket-mode of binding to Vps45, was unable to rescue the null mutant phenotypes, suggesting a role for the N-terminal motif in protein function. *L. mexicana tlg2*Δ displayed decreased virulence in macrophage infection assays and a change in Atg8 expression (an autophagy marker) at early promastigote lifecycle stages. Finally, use of immunoprecipitation assays revealed that $Tlg2^{WT}$ formed protein complexes with several Golgi and endosomal-associating proteins, whereas $Tlg2^{FL}$ associated more with proteins involved in translation, protein degradation and stress response. Taken together, this data demonstrates a role for Tlg2 in parasite growth and differentiation, with the N-terminal motif playing an important part in this SNARE protein's function.

Table of contents

List of tables

List of figures

List of appendices

Acknowledgements

Firstly, I would like to thank my supervisors, Pegine Walrad and Nia Bryant, for all their help, guidance and support throughout my PhD. It has been a great experience and I am thankful to have had the opportunity to be part of their labs. I am also grateful for the feedback and suggestions of my FRP/TAP members, Jeremy Mottram and Chris MacDonald. Additionally, I would like to thank the BBSRC and the University of York for providing me with the finances and facilities, respectively, to carry out my PhD.

Particular thanks go to members of the University of York Technology Facility. Graeme Park for his help with setting up and using the flow cytometry machines and also for all the fun chats we've had. Grant Calder for his help with the confocal microscopy. Sally James for helping me with the qPCR and answering my random queries. Chris Taylor and Adam Dowle for everything you did for prepping my IP mass spec samples and the subsequent analysis. I would also like to thank Cooper Grace for his NGS analysis and for helping me understand the data.

I could not have done this PhD without my fellow members of the Walrad lab. I am so grateful to Tiago Ferreira, who was such a massive help when I was first starting and who answered any of my queries with a never-ending supply of patience. I would also like to thank Natalia Teles for all her help with the macrophage infection assays, for all her great ideas and discussions and for just generally being an awesome person. I am incredibly grateful to Josh Bramley for all his help with getting those final few Western blots done, and for taking a weight off my shoulders at a stressful time. Last, but definitely not least, I would like to thank Ewan Parry for being the best fellow PhD friend I could ask for. For all our chats, for all the opportunities to bounce ideas off each other, for having a moan together and for frolicking in the snow. I am so happy we joined the Walrad lab at the same time!

Finally, I am very thankful to my friends and family for their emotional support. To my mum and dad for always being positive and inviting me round for homemade pizza nights. To Kris Paraschiv and Sonja Srdanović for being my cheerleaders, for the tea-chats and for all their empathy and support. Additional thanks to Sonja for putting me up in Iceland and allowing me to have a well-earned break. I would especially like to thank my partner, William Cheng, for being my rock, my logical half and for all the cups of tea and coffee that he brought me when I've been tied to my desk. I also cannot forget my cat, Cora, who has been my snuggle-buddy for all the many hours of writing.

Author's declaration

I declare that this thesis is a presentation of original work and I am the sole author, unless otherwise stated. The next generation sequencing analysis presented in chapter 3 was done in collaboration with Dr Cooper Grace, Jeffares lab, University of York. The macrophage infection assay presented in chapter 5 was done in collaboration with Dr Natalia Teles, Walrad lab, University of York. The immunoprecipitation work presented in chapter 5 was done in collaboration with Dr Adam Dowle, MAP lab, TF, University of York.

This work has not previously been presented for an award at this, or any other, University. All sources are acknowledged as References.

Chapter 1 – Introduction

The leishmaniases are considered a neglected tropical disease, yet are second only to malaria in terms of global parasite-related fatalities, with somewhere between 20,000 - 40,000 deaths reported annually (Alvar et al., 2012). *Leishmania* are single-celled obligate parasites that are transmitted to mammalian hosts through the bite of an infected sand fly. An important aspect of the *Leishmania* lifecycle is the parasite's transition to and from extracellular and intracellular forms, depending on whether it is residing in the sand fly or mammalian host respectively. Autophagy has previously been identified as playing a key role in the parasite's ability to differentiate between these forms (Besteiro et al., 2006; Giri & Shaha, 2019), yet the mechanisms behind this process are relatively understudied in this organism. Alongside the autophagy-related (Atg) proteins, which were first discovered in yeast (Tsukada & Ohsumi, 1993), additional proteins and complexes are known to be involved in autophagy, including the soluble N-ethylmaleimide-sensitive factor attachment protein receptor (SNARE) proteins (Nair et al., 2011). Bioinformatic analysis has confirmed the presence of SNAREs in *Leishmania* (Besteiro et al., 2006), yet little-to-no functional data has been published for these proteins to date. This study focuses on one such SNARE protein, Tlg2, which is involved in trafficking through the *trans*-Golgi network (TGN) (Abeliovich et al., 1998). In yeast, *Δtlg2* cells display a marked decrease in autophagy, as well as being more vulnerable to osmotic stress (Nair et al., 2011; Struthers et al., 2009). This chapter will discuss what is currently known about Tlg2 in eukaryotes and the potential implications for *Leishmania*, with a particular focus on parasite differentiation and the role that SNAREs play.

1.1 Leishmaniasis

1.1.1 Epidemiology of leishmaniasis

Leishmaniasis is the collective name for a range of diseases caused by ~20 species of parasites in the *Leishmania* genus. Close to 100 countries are endemic for leishmaniasis, with an estimated 700,000 - 1 million new cases reported annually (WHO, 2021; WHO, 2021). The three main forms of leishmaniasis are cutaneous, mucocutaneous and visceral, with the disease presentation dependent on the *Leishmania* species, as well as host factors, co-infections and the geographic location.

Cutaneous leishmaniasis (CL) is the most common form of the disease and is present across the Old World and the New World. In 2020, over 80% of new CL cases arose in Afghanistan, Algeria, Brazil, Colombia, Iraq, Pakistan and the Syrian Arab Republic (WHO, 2021). CL has several clinical manifestations but most commonly presents as singular, potentially ulcerating,

lesions that self-heal over several months or years. In the Old World, species such as *Leishmania (L.) major*, *L. tropica* and *L. aethiopica* are some of the causative agents of CL, whereas in the New World they are *L. mexicana*, *L. amazonensis*, *L. braziliensis* and *L. guyanensis* (de Vries et al., 2015). In rarer cases of infection with *L. aethiopica*, *L. mexicana* or *L. amazonensis* a poor host immune response can lead to diffuse CL (DCL), with spreading of non-ulcerative nodules/papules across the body. Although not usually life-threatening, CL can leave permanent and disfiguring scarring, which can lead to social ostracism and poor mental health (Yanik et al., 2004).

A more severe progression of CL (termed mucocutaneous (M) CL) is when lesions occur around the nasal-pharyngeal area, potentially resulting in the destruction of mucous membranes around the nose, mouth and throat. MCL is more common in the New World, with *L. braziliensis*, *L. amazonensis* and *L. guyanensis* as the leading causes, and may result in permanent facial disfigurement or even death through secondary infections (Burza et al., 2018).

Finally, visceral leishmaniasis (VL) is the systemic form of the disease, with approximately 50,000 - 90,000 new cases each year, and is responsible for almost all the deaths resulting from leishmaniasis. Ten countries account for 95% of new VL cases: India, Iraq, Nepal, China, Brazil, Ethiopia, Kenya, Somalia, Sudan and South Sudan (WHO, 2021). In VL, *Leishmania* parasites (either *L. donovani* or *L. infantum*) infect organs and tissues such as the liver, spleen, bone marrow or lymph nodes, leading to a wide range of symptoms. Most commonly, VL presents with fever, weight loss, anaemia and hepatosplenomegaly and is almost 100% fatal in those left untreated (Burza et al., 2018). Cases of VL-HIV co-infection are common and lead to more severe progression for both diseases, along with a higher likelihood of treatment failure and relapse (Lindoso et al., 2018).

Post-kala-azar dermal leishmaniasis (PKDL) is a late-stage complication of VL, derived from *L. donovani* infections, and typically occurs in patients who have been successfully treated for VL. PKDL is generally self-healing and is characterised by a hypopigmented macular or maculopapular/nodular rash that spreads across the face and body, with residual parasites residing in the skin (Zijlstra, 2016). Because of this, PKDL is considered to be an important reservoir for ongoing transmission of VL (le Rutte et al., 2019).

1.1.2 Leishmaniasis treatment and current challenges

Treatments for leishmaniasis are complicated and vary based on parasite species, clinical manifestations, geographical factors and co-infections. Traditionally, VL has been treated using pentavalent antimonial monotherapy, of which there are two formulations: sodium

stibogluconate (SSG) and meglumine antimoniate (MA). SSG is more commonly used than MA and across Africa and South America is considered the first-line treatment for VL caused by *L. donovani* (Burza et al., 2018). However, in the Indian subcontinent, the efficacy of pentavalent antimonials has been demonstrated to be decreasing since the late 1990s and is therefore no longer the recommended treatment (Das et al., 2005; Sundar et al., 2000). Further disadvantages of pentavalent antimonials are the long regimens (at least 20 - 28 days) of daily, painful, intramuscular injections or intravenous infusions, along with adverse side effects (nausea, vomiting, pancreatitis, cardio- and hepatotoxicity) (Moore & Lockwood, 2010).

More recent treatments, such as amphotericin B (AmB) and miltefosine (MF), were originally used as antifungal and anticancer drugs respectively, but were subsequently discovered to have leishmanicidal properties. When pentavalent antimonials began to lose efficacy in Indian states, AmB was used as an alternative first-line treatment, but this in turn presented issues of high cost and potentially life-threatening toxicities (Chappuis et al., 2007). A safer lipid formation, liposomal amphotericin B (LAmB), which can be administered intravenously as either a single high dose or at lower doses over 3 - 6 days, is now the recommended treatment for VL on the Indian subcontinent and for all *L. infantum* infections (Burza et al., 2018). However, the use of LAmB also presents issues of high cost and reliable storage, due to the requirement for an uninterrupted cold chain, which can be problematic in developing countries that lack the necessary infrastructure and resources (de Pina Carvalho et al., 2021; Maintz et al., 2014).

MF, currently the only orally administered anti-leishmaniasis drug, is commonly used in combination with LAmB, but is also available as a monotherapy for both VL and CL. MF is generally well tolerated but may result in relatively mild gastrointestinal issues. However, it is not recommended for women who are pregnant and should be used cautiously for women of child-bearing age due to its teratogenic and reproductive toxicities (Dorlo et al., 2012). Intramuscular injection of paromomycin (PM), a broad-spectrum antibiotic with leishmanicidal properties, can also be used to treat VL and has the advantages of being cost-effective and relatively safe (Sundar & Chakravarty, 2008; Wiwanitkit, 2012). To avoid parasites developing drug resistance, PM is typically administered in combination with either LAmB or MF in the Indian subcontinent or with pentavalent antimonials in East Africa (Burza et al., 2018). Topical ointment of PM with either methylbenzethonium chloride or gentamycin can also be used to treat Old World or New World CL respectively (D. H. Kim et al., 2009; Sosa et al., 2019). Additional CL therapies include thermotherapy (localised application of 50°C heat) and intralesional injections of antimonials, with or without liquid nitrogen-based cryotherapy (Burza et al., 2018).

With VL, HIV co-infection adds further complications due to issues of treatment failure and subsequent fatalities, greater susceptibility to drug toxicities and relapse. VL can also cause an increase in HIV viral-load, faster disease progression into AIDS and decreased response to antiretroviral therapy (Lindoso et al., 2018; Olivier et al., 2003).

1.1.3 Vectors of leishmaniasis and control strategies

The natural vectors of the *Leishmania* parasite are females of the small, winged insect commonly known as the sand fly. Of the subfamily *Phlebotominae*, there are approximately 1000 species of sand flies, but less than 10% of them are known vectors of *Leishmania*. Although there are six recognised genera of phlebotomine sand flies, only two are considered medically important: either the *Phlebotomus* in the Old World or *Lutzomyia* in the New World (Bates, 2008; Munstermann, 2019).

Due to their small size (~3mm) making them susceptible to dehydration, the majority of sand flies are active between dusk and dawn, when conditions are more favourable. They tend to rest during the day in comparatively cool and humid locations (e.g. caves, forests or dense vegetation, animal burrows, rock fissures, latrines and cellars) (Killick-Kendrick, 1999). Both male and female sand flies feed on sap and other natural sugar sources, but only the females require blood meals to provide the nutrients necessary for egg production (Ready, 2013). They feed on a variety of animals, including mammals, birds and reptiles. Some sand fly species only require one blood meal per gonotrophic cycle, whereas others require multiple blood meals, which increases the likelihood of ongoing *Leishmania* transmission (Killick-Kendrick, 1999; Ready, 2013).

Due to the difficulty of locating larval sites and the primarily outdoor biting (exophagic) and outdoor resting (exophilic) behaviour of female sand flies, control strategies can be difficult to implement. However, where sand flies venture into indoor environments (i.e. peridomestic species) residual spraying of insecticides and insecticide-treated nets have been demonstrated to reduce the prevalence of leishmaniasis (Balaska et al., 2021; Chowdhury et al., 2011; Joshi et al., 2009). For areas with predominantly exophilic species, ultra-low volume space spraying of insecticides in outdoor environments can help reduce the population of local sand fly vectors (Balaska et al., 2021; Britch et al., 2011). An additional control strategy that is often employed in areas where *L. infantum*, the causative species of human zoonotic VL, predominates (e.g. Latin America) is to target the natural canine hosts by using insecticide-impregnated collars. Evidence indicates that this approach can help reduce VL incidence in both domestic dogs and the local human population (Gálvez et al., 2018; Yimam & Mohebali, 2020).

1.2 *Leishmania* parasites

1.2.1 Biology and lifecycle of *Leishmania*

Leishmania undergo a digenetic lifecycle which utilises a sand fly vector and a mammalian host. *Leishmania* are broadly described as having two main cell types: the extracellular, flagellated promastigote that resides within the sand fly midgut and the intracellular, non-motile amastigote that is primarily found within mammalian macrophages. Within the promastigote cell type there are distinct developmental forms that are either proliferative or quiescent, depending on whether their role is to populate the midgut or prepare for transmission into the mammalian host. The general morphology of promastigotes is an elongated cell body and extended flagellum, with some variety in the size of the cell body and length of flagellum depending on the developmental form. In contrast, amastigotes have a smaller, more rounded body with a very short flagellum (Sunter & Gull, 2017). These changes in morphology reflect the differing environments in which the cell types are exposed to. The ovoid cell shape and long flagellum of the promastigotes are required for the parasites to traverse through and adhere to the sand fly midgut (Gluenz et al., 2015; Killick-Kendrick et al., 1974). In contrast, the small spherical shape of the amastigotes helps to protect them from the harsh intracellular conditions of the mammalian macrophages, with the short immobile flagellum possibly playing a sensory role (Gluenz et al., 2010; Sunter & Gull, 2017).

The *Leishmania* life cycle is initiated when a sand fly takes a bloodmeal from an infected mammalian host (Fig. 1). Amastigotes are ingested along with the blood meal, which is then encased in a peritrophic matrix (PM) as it enters the sand fly mid gut. The PM is an acellular semi-permeable membrane that is composed of chitin, proteins and glycoproteins and is designed to protect the midgut epithelium from pathogenic or mechanical damage (Lehane, 1997; Pruzinova et al., 2015). Initially, *Leishmania* amastigotes that reside within the PM differentiate into procyclic promastigotes, a weakly mobile but highly proliferative form. This differentiation is likely to be triggered by the drop in temperature and increase in pH experienced within the sand fly midgut, but additional, unknown, chemical triggers may also be required (Sunter & Gull, 2017). Approximately 2 – 3 days post-blood meal procyclic promastigotes differentiate into non-proliferative nectomonad promastigotes, which, with their higher mobility, are able to escape the PM and adhere to the midgut epithelial microvilli via their flagellum. This adherence is crucial in preventing the promastigotes from being expulsed when the sand fly defecates (Rogers et al., 2002; Sunter & Gull, 2017).

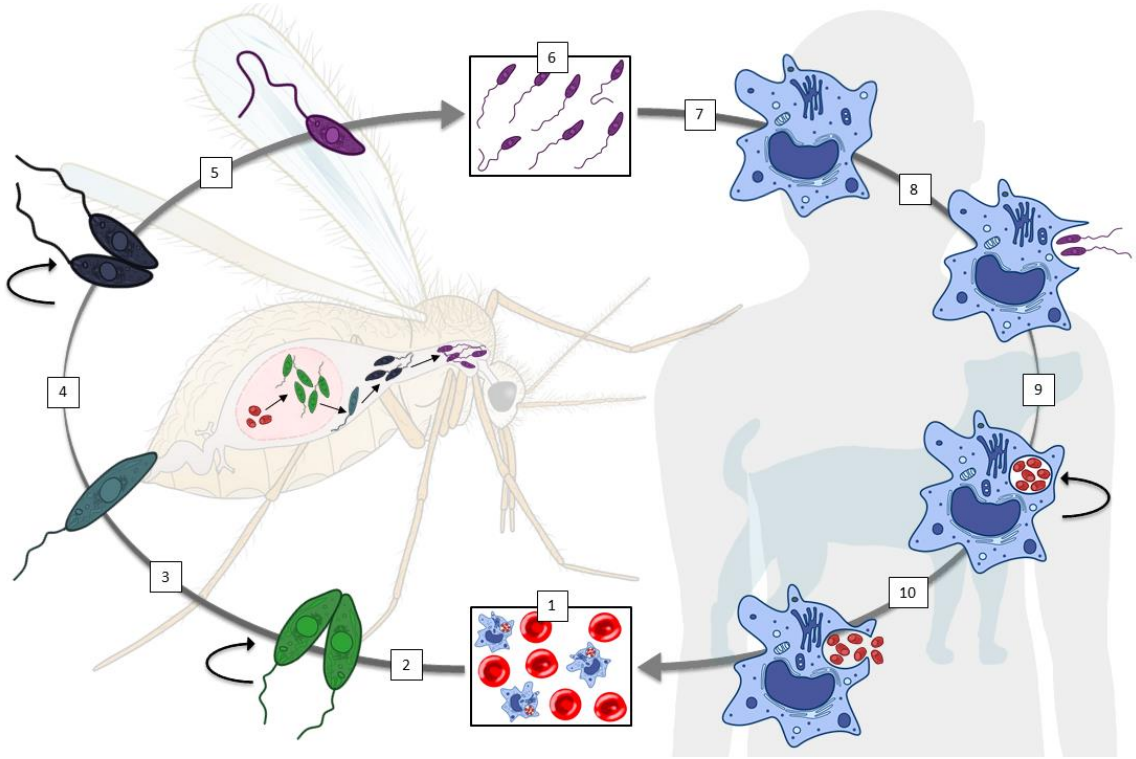

Figure 1. *Schematic depicting the lifecycle of* Leishmania. A sand fly takes a blood meal from an infected mammalian host and ingests amastigotes (1). The amastigotes differentiate into procyclic promastigotes within the sand fly midgut, which then undergo rapid proliferation (2). Procyclic promastigotes morph into nectomonad promastigotes that escape the peritrophic matrix and attach to the midgut microvilli to prevent being expelled when the sand fly defecates (3). Nectomonad promastigotes then migrate to the anterior midgut where they differentiate into the replicative leptomonad promastigote (4). Within the stomodeal valve of the sand fly the leptomonad form transitions into the infective metacyclic promastigote (5), which are then deposited into the skin of a mammalian host when the sand fly takes a blood meal (6). Macrophages are recruited to the site of the bite (7) and phagocytose the metacyclic promastigotes (8). Metacyclic promastigotes reside within a macrophage phagolysosome, where they differentiate into amastigotes, which then proliferate (9) before disseminating and infecting further macrophages (10).

After migration, nectomonad promastigotes undergo a further differentiation into leptomonad promastigotes, a second proliferative form that then populates the sand fly anterior midgut (Gossage et al., 2003). The final differentiation step within the sand fly involves the leptomonad promastigotes transforming into either the mammalian infective metacyclic promastigotes or into haptomonad promastigotes. The role of haptomonad promastigotes is somewhat ambiguous but involves adherence to the cuticle lining of the sand fly stomodeal valve via hemidesmosomal structures that reside on their short, bulbous flagellum. This adherence is thought to either prevent their transmission into a mammalian host, thus maintaining long-term infection in the sand fly, or inducing damage to the stomodeal valve by secreting chitinases,

which in turn causes reflux of the parasites into the bite site when the sand fly is taking a blood meal (Hendry & Vickerman, 1988; Kimblin et al., 2008; Sunter & Gull, 2017; Volf et al., 2004).

An interesting feature of *Leishmania* infections in the sand fly is the production of a proteophosphoglycan-rich promastigote secretory gel (PSG). This PSG is produced by leptomonad promastigotes in the lumen of the anterior midgut and is believed to be the primary site of metacyclogenesis for the parasites (the differentiation of leptomonads to the metacyclic promastigotes). Metacyclic promastigotes are highly motile and are characterised by their long flagellum (>2x the length of the cell body) and slender cell body, which adapts them to traversing and populating the PSG (Rogers, 2012). In turn, PSG distends the anterior midgut of infected sand flies and forces the stomodeal valve to remain open, which then affects sand fly feeding behaviour and promotes *Leishmania* transmission by the reflux of parasites (Rogers et al., 2002). Regurgitation of the PSG into the sand fly bite site is also thought to enhance the infectivity of the *Leishmania* promastigotes in the mammalian host (Rogers et al., 2004). An interesting phenomenon of the *Leishmania* promastigote life cycle is the conversion of metacyclic promastigotes back into leptomonad-like forms (termed retroleptomonad promastigotes) when sand flies take additional blood meals. This process has been demonstrated to amplify parasite numbers in the sand fly vector over 100-fold, due to the subsequent proliferation of the retroleptomonad promastigotes, and, consequently, enhance vector infectivity and ongoing transmission potential (Serafim et al., 2018).

Within the skin of the mammalian host there is an infiltration of neutrophils and macrophages that localise to the site of the sand fly bite. *Leishmania* metacyclic promastigotes are rapidly phagocytosed primarily by the neutrophils, but do not appear to establish long-term infections in this cell type (Beattie & Kaye, 2011; Laufs et al., 2002; Peters et al., 2008). Instead, macrophages appear to phagocytose the *Leishmania* metacyclic promastigotes after they have been released from infected neutrophils that are undergoing apoptosis (Peters et al., 2008; Ritter et al., 2009). This phagocytosis of promastigotes is a receptor-mediated process; with the interaction of *Leishmania* lipophosphoglycan (LPG) and GP63 glycoprotein with macrophage complement receptors (i.e. CR1, CR2 and CR3) implicated as the main cell entry pathway (Polando et al., 2013; Domínguez & Toraño, 1999; Russell, 1987; Liu & Uzonna, 2012). LPG is also believed to play an important role in the intracellular survival of *Leishmania*, by protecting these parasites from oxidants and lysis by complement (Späth et al., 2003). Once inside macrophages, metacyclic promastigotes are enclosed in a host cell-derived membrane termed the phagosome. Fusion of the phagosome with endosomes, and eventually the lysosome, result in the phagolysosome, which is where the metacyclic promastigotes differentiate into amastigotes (Beattie & Kaye, 2011). Triggers for this differentiation event (also termed

amastigogenesis) are likely to involve the increase in temperature and drop in pH of moving from the extracellular sand fly environment to the intracellular phagolysosome (Barak et al., 2005; Zilberstein & Shapira, 1994). *In vitro* studies have demonstrated that *Leishmania* typically undergo morphogenesis to amastigotes between 10 – 24 hours, with full maturation taking up to 120 hours (Barak et al., 2005; Tsigankov et al., 2014). Old World and New World *Leishmania* species differ in their lifestyles within macrophages, with Old World amastigotes, such as those from *L. major*, residing singly within small phagolysosomes. In contrast, New World species, such as *L. mexicana*, have multiple amastigotes within a larger phagolysosome (Castro et al., 2006). After amastigote maturation, the parasites undergo division and proliferation, to increase the likelihood of transmission back to the sand fly vector when they take a blood meal (Beattie & Kaye, 2011).

1.2.2 *Leishmania* cell structure

As mentioned in the previous section, *Leishmania* have two main morphological forms: the promastigote and the amastigote. A major feature of the promastigote is the flagellum, which is located at the anterior of the cell and has a 9+2 arrangement of the axoneme, which is indicative of its role in cellular motility. In contrast, the amastigote form of *Leishmania* have a very short, immotile flagellum with a 9+0 axoneme arrangement. This ultrastructure is more commonly found in eukaryotic cilia and is indicative of a sensory/signalling function (Wheeler et al., 2015). Another notable feature of *Leishmania* parasites is an invagination of the plasmid membrane located at the base of the flagellum, named the flagella pocket. Like in other trypanosomatids, the flagella pocket in *Leishmania* is an essential part of the endomembrane system and is the only site of endo- and exocytosis. Consequently, is crucial for cell viability (Field & Carrington, 2009; Halliday et al., 2021).

Leishmania cells contain many of the classic eukaryotic organelles, such as the nucleus, endoplasmic reticulum (ER), Golgi apparatus, lysosome and the mitochondria (Fig. 2). However, unlike what is seen in mammalian cells, *Leishmania* contain one large mitochondria, that can be up to 12% of the cell volume. A unique aspect of the mitochondria in *Leishmania*, and other kinetoplastids, is the presence of a kinetoplast; a disc-like shaped organelle located next to the flagella pocket that contains the mitochondrial DNA (kDNA). kDNA is composed of a mix of maxi- and minicircles that make up approximately 30% of the cell's total DNA (Fidalgo & Gille, 2011). Another unique feature of kinetoplastids are the glycosomes, membrane-bound peroxisome-like organelles that contain most of the parasite's glycolytic enzymes, with the consequent compartmentalisation of glycolysis to these organelles. Additionally, glycosomes contain enzymes for other processes, including the pentose-phosphate

pathway and β-oxidation of fatty acids. Glycosome are thought to contribute to the rapid metabolic adaptation required for *Leishmania* and other parasitic trypanosomes due to the changing environments of their life cycles (Hannaert et al., 2003; Michels et al., 2006).

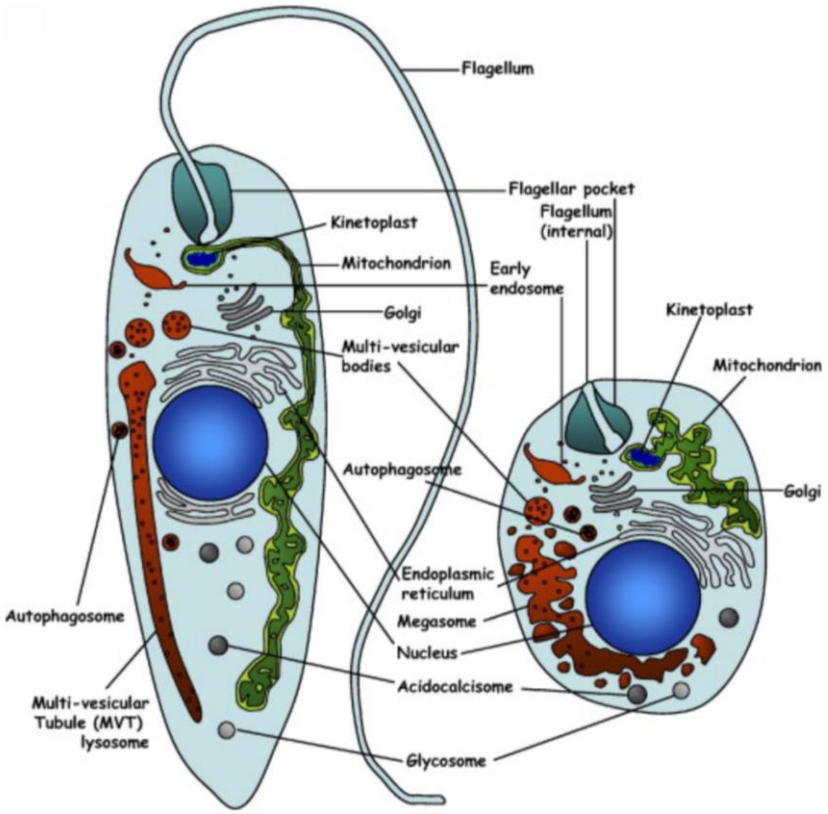

Figure 2. *Subcellular organisation of* Leishmania. Illustrative representation of the organelles found within *Leishmania* promastigotes (left) and amastigotes (right). Reproduced partial image from Besteiro et al. (2007).

1.2.3 *Leishmania* gene regulation

The mechanisms of gene regulation and expression is an unusual feature of kinetoplastids that differs from many eukaryotic cells. Unlike in other organisms, kinetoplastids have an almost complete absence of transcriptional control. Instead, nuclear protein-coding genes are transcribed by RNA polymerase II into multi-gene pre-mRNA arrays from polycistronic transcriptions units (PTUs) (Clayton, 2016; Johnson et al., 1987; Martínez-Calvillo et al., 2003). Transcription is usually bidirectional and is typically initiated in divergent strand-switch regions (where two PTUs are orientated 'head-to-head') enriched with specific histone variants and modifications. Termination of transcription usually occurs in regions where PTU's are 'tail-to-tail', known as convergent strand-switch regions, also characterised by histone variants and other epigenetic modifications (Anderson et al., 2013; Siegel et al., 2009). One such

modification is β-D-glucosyl-hydroxymethyluracil, also known as base J, which is predominantly located in telomeric repeats but is also found in RNA polymerase II termination sites. In *Leishmania*, base J is required for maintaining the appropriate termination of polycistronic transcription (van Luenen et al., 2012). Processing of the pre-mRNA arrays into mature mRNAs occurs co-transcriptionally and involves *trans* splicing of a 39 nt capped Spliced Leader sequence at the 5' end, along with cleavage and polyadenylation at the 3' end (Clayton, 2016; Parsons et al., 1984; LeBowitz et al., 1993). Because of these transcription mechanisms, gene regulation in kinetoplastids typically occurs at the post-transcriptional or post-translation level.

As differentiation of the parasites into their distinct developmental forms occurs, so too does differential expression of genes that are required for the various metabolic processes undertaken by the cells. For example, transcriptome analysis has revealed that proliferative forms such as the procyclic promastigotes and amastigotes have upregulation of genes related to DNA replication, glucose catabolism and cell-cycle regulation in comparison to the quiescent nectomonad and metacyclic promastigotes forms. In contrast, nectomonad and metacyclic promastigotes demonstrate transcriptome increases in genes involved in stress response, autophagy and cell-cycle arrest (Alcolea et al., 2019; Inbar et al., 2017). When comparing metacyclic against procyclic promastigotes there is an upregulation of genes related to fatty acid biosynthesis and ATP-coupled proton transport (Alcolea et al., 2019; Dillon et al., 2015). As promastigotes differentiate into amastigotes there is a concurrent down regulation of flagellar motility genes, whilst genes that are upregulated include cell surface proteins, peptidases and membrane transporters (such as *amastin*) (Fiebig et al., 2015; Ruy et al., 2019).

Differential expression can also be seen on the protein level, with a recent study showing almost 1200 proteins with stage-specific enrichment when analysing procyclic promastigotes, metacyclic promastigotes and macrophage-derived amastigotes. Interestingly, a significant proportion of these proteins were RNA-binding proteins, demonstrating the importance of stage-specific post-transcriptional regulation in these parasites (de Pablos et al., 2019). These differential expression profiles can also be taken advantage of in terms of utilising stage-specific upregulated genes/proteins as life cycle markers. For example, Sherp, a small membrane associated protein, is a commonly used marker for metacyclic promastigotes on both the mRNA and protein level, whilst amastins have been used as amastigote markers (de Pablos et al., 2019; Doehl et al., 2017; Giraud et al., 2019; Rafati et al., 2006).

1.3 Autophagy

1.3.1 The process of autophagy

Autophagy is a highly conserved cellular process that involves the degradation and recycling of cytoplasmic components, such as proteins and organelles, to provide the macromolecules and energy necessary for cell survival. Autophagy occurs at basal levels in all eukaryotic cells to maintain cellular homeostasis but is upregulated during times of stress. Three main types of autophagy have been described: macroautophagy, microautophagy and chaperone-mediated autophagy (CMA). Macroautophagy involves the sequestering of cytoplasmic components into a double-membraned vesicle, which eventually fuses with the cell vacuole/lysosome to deliver its cargo for degradation (Wen & Klionsky, 2016) (Fig. 3). In contrast, in microautophagy the cargo is directly captured by the vacuole/lysosome by protrusion or invagination of the organelle's membrane, forming intralysosomal vesicles, with eventual degradation (Mijaljica et al., 2011). Finally, CMA has only been described in mammalian cells and involves the recognition of individual proteins with specific KFERQ pentapeptide motif by chaperones to target them to the lysosome, where they are unfolded and then translocated across the lysosomal membrane (Arias & Cuervo, 2011). This section will detail the process and mechanisms of macroautophagy, which will hereafter be referred to autophagy.

In yeast, autophagy is initiated at a single site proximal to the vacuole, which is known as the phagophore assembly site (PAS). In mammalian cells, there are multiple initiation sites, with studies indicating that omegasomes (subdomains of the ER) may serve as these initiation sites (Hayashi-Nishino et al., 2009). At the PAS a transient double-membrane begins to form, known as the phagophore, with sequential expansion around the cargo bound for degradation. The origin of the phagophore membrane remains unclear, but various studies have suggested membrane donations from the ER, mitochondria, the Golgi apparatus and the plasma membrane (Hailey et al., 2010; Hayashi-Nishino et al., 2009; Ravikumar et al., 2010; Takahashi et al., 2011). This expanded phagophore eventually fully sequesters the cargo and fuses together to form a double-membraned autophagosome, which is turn fuses to the vacuole/lysosome, whereby a single membraned autophagic body is released into the lysosomal lumen. The autophagic body and its contents are then degraded by lipases and hydrolases, with the resultant macromolecules recycled back into the cell. (Parzych & Klionsky, 2014; Wen & Klionsky, 2016). An additional fusion step between the autophagosome and early or late endosomes results in a structure known as an amphisome, which can in turn fuse to vacuole/lysosome (Berg et al., 1998; Ganesan & Cai, 2021).

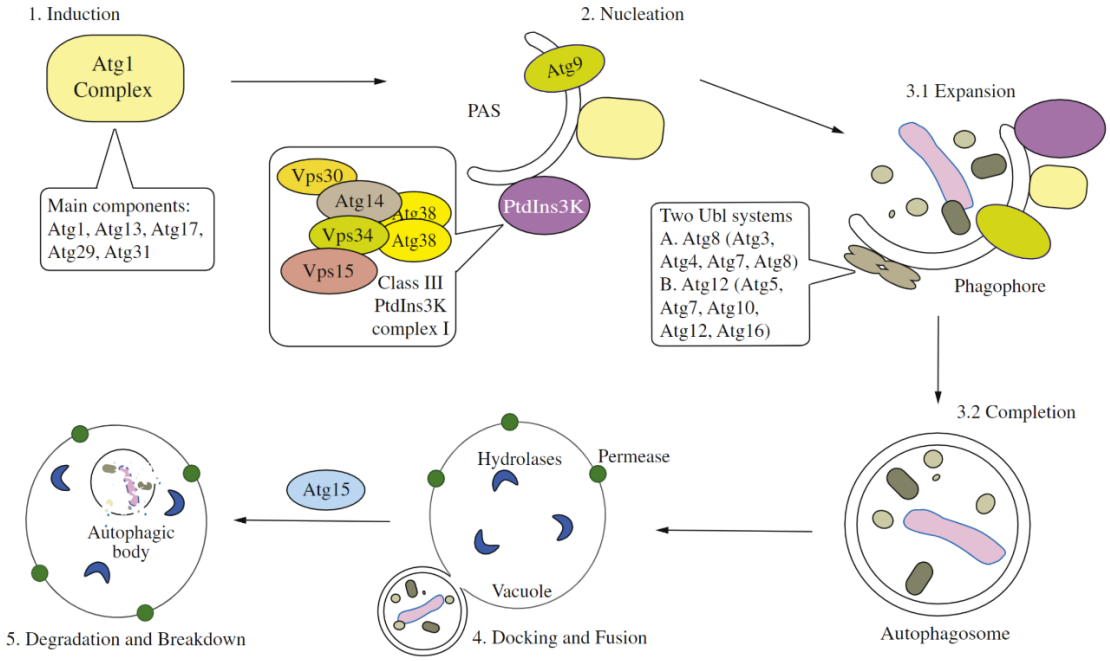

Figure 3. *An overview of macroautophagy*. Schematic demonstrating the different stages of macroautophagy, as characterised in yeast, and highlighting the key Atg proteins and complexes that are involved in each step. Reproduced from Wen & Klionsky, 2016.

1.3.2 The machinery of autophagy

The first autophagy-defective mutants were characterised in yeast. (Tsukada & Ohsumi, 1993). A proteinase-deficient yeast strain was mutagenized and, using light microscopy, those mutants that did not accumulate vacuolar autophagic bodies under nitrogen starvation were isolated. Genetic analysis of these mutants highlighted 15 genes that were involved in autophagy, which were designated as *APG* genes. Further discovery and development led to a unified nomenclature for the autophagy-related (*ATG*) genes, with at least 41 so far being characterised in yeast (Klionsky et al., 2003, 2016). The process of autophagy can be broken down into five stages, with a variety of proteins and complexes that are recruited (Fig. 3). Stage I (induction) is the initiation of the PAS and is regulated by the Atg1-Atg13 kinase complex, which comprises of at least Atg1, Atg13 and the Atg17-Atg31-Atg29 subcomplex. This complex is crucial in autophagy as it recruits further Atg proteins to the PAS and is involved in phosphorylation of downstream targets (Papinski et al., 2014; Suzuki et al., 2007; Yin et al., 2016).

Stage II (nucleation) recruits the class III phosphatidylinositol 3-kinase (PI(3)K) complex to the PAS, which comprises the lipid kinase Vps34, the regulatory kinase Vps15, Vps30/Atg6, Atg14 and Atg38. The PI(3)K complex is essential in the production of phosphatidylinositol-3-

phosphate (PI(3)P), which helps to correctly localise and recruit additional Atg proteins that are involved in autophagosome biogenesis (Burman & Ktistakis, 2010; Yin et al., 2016).

Expansion and completion of the phagophore (stage III) relies on two ubiquitin-like (Ubl) conjugation systems: the Atg12–Atg5-Atg16 complex and the Atg8 system. The Atg12–Atg5-Atg16 complex is formed by the covalent conjugation of Atg12 to Atg5 via the Atg7 E1-like enzyme. Noncovalent binding to Atg16 allows the formation of larger complexes. The Atg8 conjugation system culminates in Atg8 being conjugated to lipid phosphatidylethanolamine (PE). Precursors of Atg8 are cleaved upon synthesis by the cysteine protease Atg4, exposing a glycine residue at the Atg8 C-terminus. This is then activated by Atg7, which is consequently transferred to the E2-like enzyme Atg3 where the glycine is conjugated to PE. The Atg12–Atg5–Atg16 complex also functions as an E3-like enzyme for Atg8-PE conjugation (Shpilka et al., 2012; Yin et al., 2016). Atg8 is unique in that it is the only Atg protein that is known to associate with the completed autophagosome, with Atg8-PE found on the luminal and cytosolic aspects of the autophagosome membrane (Nair et al., 2012). An additional protein, Atg9, plays an important role in directing membranes to the expanding phagophore, and cycles between the PAS and peripheral structures in a Atg1 complex-dependant manner (Parzych & Klionsky, 2014; Reggiori et al., 2004). Atg9 also acts as a bridge between endocytosis and autophagy within the cell. Induction of autophagy via amino acid starvation or treatment with rapamycin has been demonstrated to induce a switch in the distribution and trafficking of Atg9 within the cell; from within the endocytic TGN to peripheral LC3 (mammalian homologue of Atg8) positive endosomes (Young et al., 2006). In neuronal cells, defects in endocytosis result in mis-localisation of Atg9 and disruption of autophagy in the pre-synapses (Yang et al., 2022).

Docking and fusion (Stage IV) of the autophagosome to the lysosome requires SNARE mediated membrane fusion. In mammals, the SNARE involved was identified as Syntaxin 17 (Stx17), which in turn is mediated by the homotypic fusion and protein sorting (HOPS)-tethering complex and the Rab 7 GTPase (Balderhaar & Ungermann, 2013; Jiang et al., 2014). The final stage of autophagy is degradation. Atg15 is a lipase that helps to breakdown the autophagic body within the lysosome, thus releasing the cargo for degradation by hydrolases (Epple et al., 2001; Wen & Klionsky, 2016).

1.3.3 Regulation of autophagy

Autophagy's critical role in maintaining cellular homeostasis means that any deviation in this process can result in cellular dysfunction and disease. As such, it is important that autophagy is properly regulated. One of the main negative regulators of autophagy is the mechanistic target

of rapamycin (mTOR), also known as TOR in yeast. mTOR is a serine/threonine protein kinase that is involved in the formation of two complexes: mTORC1 and mTORC2 (Dunlop & Tee, 2014). The core components of mTORC1 are mTOR, rapamycin-associated protein of TOR (Raptor) and GβL (Kim et al., 2003). mTOR is a key coordinator of cell growth; by sensing environmental cues (such as nutrient availability and changes to amino acids and nitrogen levels) it is able to regulate anabolic and catabolic cellular processes. mTORC1 has an anabolic role and is involved in cell growth and proliferation in nutrient-rich conditions, promoting ribosome biogenesis and the initiation of protein translation (Dunlop & Tee, 2014; Laplante & Sabatini, 2012; Proud, 2007). Consequently, in nutrient-rich conditions, autophagy is downregulated by the direct phosphorylation of Atg1, Atg13 and Atg14 by mTORC1, which prevents the formation and activation of the Atg1-Atg13 and PI(3)K complexes that are essential for autophagy induction and nucleation (Kamada et al., 2010; Yuan et al., 2013). In contrast, under nutrient starvation, mTORC1 dissociates from these complexes, allowing the dephosphorylation of the Atg proteins and subsequent activation of autophagy (Hosokawa et al., 2009).

Other regulators of autophagy are activated in response to cellular glucose levels. In a manner similar to mTORC1, when glucose levels are abundant, the cAMP-dependent protein kinase (PKA) pathway phosphorylates both Atg1 and Atg13 and prevents Atg13 from localising to the PAS (Stephan et al., 2009). Additionally, autophagy can be regulated by AMP-activated protein kinase (AMPK) in a glucose-dependant manner. When glucose levels are depleted, AMPK can initiate autophagy by inhibiting the activity of mTORC1 through phosphorylation of Raptor, or by activating the tuberous sclerosis complex 1/2 (TSC1/2), which in turn negatively regulates mTORC1 (Russell et al., 2014; Yin et al., 2016).

1.3.4 Autophagy and its role in differentiation in *Leishmania*

Due to the cellular remodelling of *Leishmania* parasites as they progress though their lifecycle, and the metabolic demands of adapting to the change in environments, autophagy plays a vital role in these organisms (Besteiro et al., 2006; Williams et al., 2013). Many of the Atg proteins and autophagy-related complexes that have been identified in yeast and other model organisms also appear to be present in *Leishmania* when conducting genome searches. However, autophagy is still a relatively understudied pathway in *Leishmania* and other trypanosomatids and there are several Atg proteins with no apparent homologues in these parasitic organisms (Brennand et al., 2012; Herman et al., 2006; Rigden et al., 2009). Additionally, of the proteins that have been identified, only a few have undergone functional analysis that has confirmed their role in autophagy. In *Leishmania*, these include Atg8, Atg4, Atg5, Atg10 and an Atg12

protein. In contrast to yeast, four Atg8 families, encompassing 25 genes, have been identified in *L. major* (Williams et al., 2009). This is also distinct from other trypanosomatids, such as *T. cruzi* and *T. brucei,* which have either two or three Atg8 genes, respectively (Brennand et al., 2012; Williams et al., 2009). Of the four Atg8 families in *Leishmania,* only two have an apparent role in autophagy. In another deviation from yeast, *Leishmania* have two copies of Atg4 (Atg4.1 and Atg4.2), as opposed to one.

Due to their low sequence homology, Atg5 and Atg12, and subsequently the Atg12–Atg5-Atg16 complex involved in autophagosome expansion, were initially believed to be absent in *Leishmania*. However, when the Atg8 proteins were characterised in *L. major*, an additional Atg8-like protein was demonstrated to be functionally homologous to yeast Atg12 in complementation assays, along with Atg5 and Atg10 proteins (Williams et al., 2009). Several *Leishmania atg* null mutants showed defects in autophagy. *atg5*Δ *L. major* promastigotes were deficient in the formation of autophagosomes and displayed a reduced ability to differentiate into metacyclic promastigotes and survive in macrophages (Williams et al., 2012). Similarly, both *atg4.1*Δ and *atg4.2*Δ had an effect on autophagy, although the *atg4.2*Δ phenotypes were more severe. Deletion of Atg4.2 resulted in an accumulation of autophagosomes that were unable to fuse with lysosomes and the promastigotes were defective in metacyclogenesis (Williams et al., 2013).

In addition to the Atg proteins, other proteins have been identified as being essential for autophagy and differentiation in *Leishmania*. One such protein is Vps4, which is an ATPase that plays a crucial role in endosomal sorting and the formation of multivesicular bodies (MVB), a type of multivesicular late endosome. Mutations of Vps4 in *Leishmania* promastigotes result in disruption of transport through the endocytic pathway to the lysosome, which leads to defects in autophagy. This in turn impacts the parasites' ability to withstand starvation and they are unable to differentiate into metacyclic promastigotes (Besteiro et al., 2006). Studies have also demonstrated that two cysteine peptidases (CPA and CPB) are responsible for proteolysis within the *Leishmania* vacuole. Promastigotes lacking both of these proteins display an excessive accumulation of non-degraded autophagosomes within the lysosome, which has deleterious effects on parasite survival in response to stress and in their ability to undergo differentiation (Williams et al., 2006).

1.4 SNARE proteins

1.4.1 The SNARE family of proteins

The soluble N-ethylmaleimide-sensitive-factor attachment protein receptors (SNAREs) are a highly conserved family of proteins that are essential components of intracellular membrane fusion. The formation of SNARE protein complexes brings two opposing membranes into close proximity to facilitate membrane fusion. SNARE proteins are characterised by the presence of a C-terminal 60 – 70aa region known as the SNARE motif. The SNARE motif is composed of a repeated pattern of heptad hydrophobic residues that promote the formation of an α-helical secondary structure, with the hydrophobic side chains all projecting from the same side of the helix. These secondary structures in turn form a parallel four-helical bundle when SNARE complexes form, with the side chains forming 16 stacked layers that provide stability within the core bundle (Antonin et al., 2002; Poirier et al., 1998; Ungar & Hughson, 2003). Often, the SNARE motif is located adjacent to a C-terminal transmembrane domain (TMD) that anchors the SNARE protein to its resident membrane. Certain SNARE proteins do not contain a TMD but instead bind to membranes through C-terminal lipid modifications such as farnesylation and palmitoylation (Fukasawa et al., 2004).

SNARE proteins can be categorised as either Q- or R-SNAREs. The α-helical SNARE domain contains a hydrophilic side chain that forms a part of the central ionic 'zero' layer in the otherwise hydrophobic SNARE complex core bundle. The hydrophilic residue that resides on this side chain is either a glutamine (Q) or an Arginine (R), the discovery of which gave rise to the classification of Q- or R-SNAREs (Fasshauer et al., 1998; Sutton et al., 1998). A proposed role for this ionic layer is to prevent misalignment of the four helices in the SNARE complex due to the hydrogen-bonded network of the hydrophilic residues. Alternatively, charge repulsion would prevent more than one R-SNARE from being present in the complex, thus promoting an asymmetrical complex composition of three Q-SNAREs and one R-SNARE (Ossig et al., 2000; Ungar & Hughson, 2003).

Q-SNAREs can be further divided into three main subfamilies, the Qa-, Qb- and Qc-SNAREs, that are characterised by their N-terminal domains and positions within the SNARE complex. Qa-SNAREs, otherwise known as syntaxins, contain an independently folded N-terminal extension that forms an antiparallel three-helix bundle, which is known as the Habc domain. This domain is present on all Qa-SNAREs, and is highly structurally conserved, but can also be found in some Qb- and Qc- SNAREs (Antonin et al., 2002; Dietrich et al., 2003; Fernandez et al., 1998; Misura et al., 2002). The Habc domain controls syntaxin entry into SNARE

complexes through adoption of either a ‘closed’ conformation, whereby the Habc domain interacts with the SNARE motif and prevents SNARE complex formation, or an ‘open’ conformation, in which the Habc domain disassociates from the SNARE motif and promotes syntaxin entry into SNARE complexes (Dietrich et al., 2003; Dulubova et al., 1999). Evidence of these two conformations were first discovered in Syntaxin 1a (Stx1a), a SNARE involved in synaptic membrane fusion, but were later demonstrated, through use of X-ray crystallography, to also occur in the yeast Sso1p Qa-SNARE, which mediates fusion of secretory vesicles at the plasma membrane (Hughson et al., 2000).

Other N-terminal domains of Q-SNAREs include a Px domain, which is found on the yeast Qc-SNARE Vam3 and is involved in vacuolar targeting and membrane binding through its interactions with PI(3)P (Lu et al., 2002). Another protein, SNAP-25, is unique amongst the SNARE family due to the presence of two SNARE motifs and is nominally designated as a ‘Qbc-SNARE’. Membrane binding of SNAP-25 is unusual in that it doesn’t occur at a C-terminal TMD, but instead occurs via palmitoylation of the linker region between the two SNARE motifs (Jahn & Scheller, 2006).

A subset of R-SNAREs, the Longins, are conserved across all eukaryotes and are characterised by their extended N-terminal longin domain, which is comprised of a five-stranded β-sheet that is flanked by an α-helix on one side and two α-helix on the opposite side. A later evolutionary subset of R-SNAREs, the Brevins, have a short and variable N-terminal domain and are not present in all eukaryotes, including *Leishmania* (Besteiro et al., 2006; Rossi et al., 2004). Similarly to the Habc domain, the longin domain has a regulatory role in SNARE complex entry and subsequent membrane fusion but it also appears to be important for regulating the localisation of Longins to their required membrane sites (Daste et al., 2015).

1.4.2 The regulation of SNAREs

As previously mentioned, SNAREs are an essential component of intracellular membrane fusion events. Evidence demonstrates that SNARE proteins are able to form SNARE complexes spontaneously *in vitro* and drive the fusion of reconstituted lipid bilayer vesicles in liposome/liposome fusion assays (Weber et al., 1998). Additional *in vitro* studies have also shown that SNARE proteins can facilitate the fusion of small vesicles to flat lipid bilayer membranes, which is more physiologically relevant for many intracellular fusion steps (Fix et al., 2004; Kiessling et al., 2010; Ramakrishnan et al., 2018). Consequently, SNAREs constitute the minimal machinery required for membrane fusion (Weber et al., 1998). Initially, SNARE proteins themselves were thought to provide the necessary specificity for their various

compartments, however, later studies were able form stable SNARE complexes with the mixing of SNAREs that do not reside in the same trafficking pathways or compartments (Fasshauer et al., 1999; Yang et al., 1999). As such, the specificity of SNARE complex formation is also mediated by spatial and regulatory components.

These regulatory components include the tethering complexes and Rab-GTPases. Although formation of SNARE complexes drives membrane fusion, they are not responsible for the initial interaction of a vesicle with its target membrane. Instead, this function is performed by tethering complexes. Different tethering complexes are involved in various aspects of endocytosis, exocytosis and vacuolar protein sorting pathways and include: TRAPPI (ER to Golgi traffic), Dsl1 (Golgi to ER), TRAPPII (intra-Golgi and endosome to late Golgi), COG (endosome to *cis*-Golgi), GARP/VFT (endosome to *trans*-Golgi), CORVET (*trans*-Golgi to endosome), HOPS (endosome to vacuole) and exocyst (Golgi/endosome to plasma membrane) (Cai et al., 2007). Rab-GTPases move between GDP and GTP bound states, which determine their function and localisation. GDP-bound Rab-GTPases are found in the cytosol in complex with GDI (guanine nucleotide dissociation inhibitor) (Dirac-Svejstrup, 1997). Switching of Rabs to membranes involves a GDF (GDI displacement factor), where they are then bound to the membrane via a prenyl group and activated by the exchanging of GDP for GTP (Ullrich et al., 1994). The GTP-bound Rabs are involved in vesicle tethering and interact with tethering complexes by recruiting them to specific locations (Cai et al., 2007; Cao et al., 1998; Munson & Novick, 2006). Consequently, both Rab-GTPases and tethering complexes work upstream of SNARE proteins in mediating membrane fusion.

Perhaps the best studied of the SNARE regulators are the Sec1/Munc18 (SM) proteins. SMs are a small family of hydrophilic proteins, ~60 – 70 kDa in size, that do not form any recognisable motifs or domains. However, the relative sequence similarity and structural conservation of the proteins across trafficking steps and organisms suggests a conservation of function. SM proteins can be categorised into four subfamilies, based on the trafficking pathway they're involved in: exocytosis, endocytosis, protein biosynthesis and degradation (Sec1, Vps45, Sly1 and Vps33, respectively). SM proteins form an arch shape that is comprised of domains 1, 2 and 3. Domain 3 can be further subdivided into 3a and 3b. An arch cavity is formed between domains 1 and 3, with an additional hydrophobic pocket located on the outer surface of domain 1 (Carr & Rizo, 2010).

SM proteins have been demonstrated to bind to their cognate SNAREs via three distinct modes. The first described binding between a syntaxin and its regulatory SM partner was that of the neuronal Stx1a and Munc18a. Munc18a was demonstrated to bind to the closed conformation of

Stx1a via its arch cavity. As this binding mode stabilised the closed conformation of the syntaxin, it was believed to play an inhibitory role in Stx1a assembly into SNARE complexes (Dulubova et al., 1999; Misura et al., 2000; Pevsner et al., 1994). However, this was at odds with the requirement of Munc18-1 for neurotransmitter release in mice (Verhage et al., 2000). Subsequent discovery of a second binding site helped to shed light on this apparent contradiction. The N-terminal motif of Stx1a was found to bind to a hydrophobic pocket on domain 1 of Munc18a, alongside the closed conformation of binding. The presence of both binding modes blocked Stx1a from entering SNARE complexes. However, removal of the N-terminal motif allowed Stx1a to readily form SNARE complexes, even when still apparently bound to Munc18a via the arch cavity (Burkhardt et al., 2008). This finding suggested that Munc18a was able to regulate its cognate SNARE's entry into complexes through modulation of the two binding sites.

Additional SM:SNARE complexes have been shown to only require the N-terminal motif for binding. Studies with the SM Sly1 and its cognate SNARE Sed5 demonstrated that the first 40aa of Sed5 were required for binding to the Sly1 hydrophobic pocket (Yamaguchi et al., 2002a). Similarly, Stx4 also utilises the first 29aa to bind to Munc18c. In a manner distinct from what is seen with Stx1a and Munc18c, this binding mode appears to positively regulate Stx4's entry into SNARE complexes (Latham et al., 2006). A third binding mode involves SM proteins binding to SNARE complexes. Although the structural mechanisms behind this have not yet been elucidated, experimental data has provided evidence for various SM proteins binding to assembled SNARE complexes in addition to the other binding modes. These include Sly1, Munc18-1 and Munc18c (Carr & Rizo, 2010; Gallwitz & Jahn, 2003). The SM protein Sec1 is distinct from the previously mentioned SM proteins in that it does not appear to bind directly to its monomeric syntaxin (Sso1) in any conformation, but instead exclusively interacts with the assembled SNARE complex (Togneri et al., 2006). Taken together, the evidence of multiple modes of binding for various SM proteins and their cognate SNAREs suggests that SM proteins may regulate various stages of SNARE complex formation and also potentially prevent premature disassembly prior to membrane fusion (in the case of SNARE complex binding).

1.4.3 The SNARE complex and membrane fusion

The energy constraints of spontaneous membrane fusion make it unfeasible in a biologically relevant timescale. As such, SNARE protein complexes act to bridge the energy barrier and catalyse the fusion of vesicles and target membranes (Fig. 4). Q-SNAREs are typically located on the target membrane and, as such, they form together in an intermediary step known as the Qabc complex (Jahn & Scheller, 2006). Completion of the four helical SNARE complex occurs

through association with the R-SNARE, which is contributed by the vesicle membrane, becoming the QabcR complex. The formation of SNARE complexes occurs in a 'zippering' manner, in which the SNARE interactions begin at the N-terminal end of the SNARE motif and 'zip' together towards the C-terminal TMD and results in a tightly bound *trans*-SNARE complex (Hanson et al., 1997; Jahn & Scheller, 2006; Lin & Scheller, 1997). This mechanism brings the two membranes into nanometre proximity and facilitates a point of contact known as the fusion stalk. This stalk then undergoes hemifusion, whereby the outer membrane leaflets of the target and vesicle conjoin, but the inner leaflets and aqueous content remain separate. Finally, pore formation in the hemifusion region completes the fusion of the two membranes (Chernomordik & Kozlov, 2003). This in turns transitions the *trans*-SNARE complex into the *cis*-SNARE complex, where disassembly and recycling of the individual SNARE proteins can occur.

Disassembly of *cis*-SNARE complexes requires the actions of N-ethylmaleimide-sensitive factor (NSF) proteins and soluble NSF attachment proteins (SNAPs). As NSF proteins do not bind directly with the SNARE complex, they utilise SNAPs as a cofactor. Three SNAP molecules are required to bind to the centre of the SNARE complex. Studies have demonstrated that the hydrophilic '0' layer appears to be this site of binding and is therefore crucial for SNARE disassembly (Marz et al., 2003). The role of the bound SNAPs is then to recruit the NSF proteins. The exact mechanisms for how NSF proteins monomerise the SNARE proteins are not known but are thought to involve ATP hydrolysis via the protein's ATP binding sites (Hanson & Whiteheart, 2005; Jahn & Scheller, 2006).

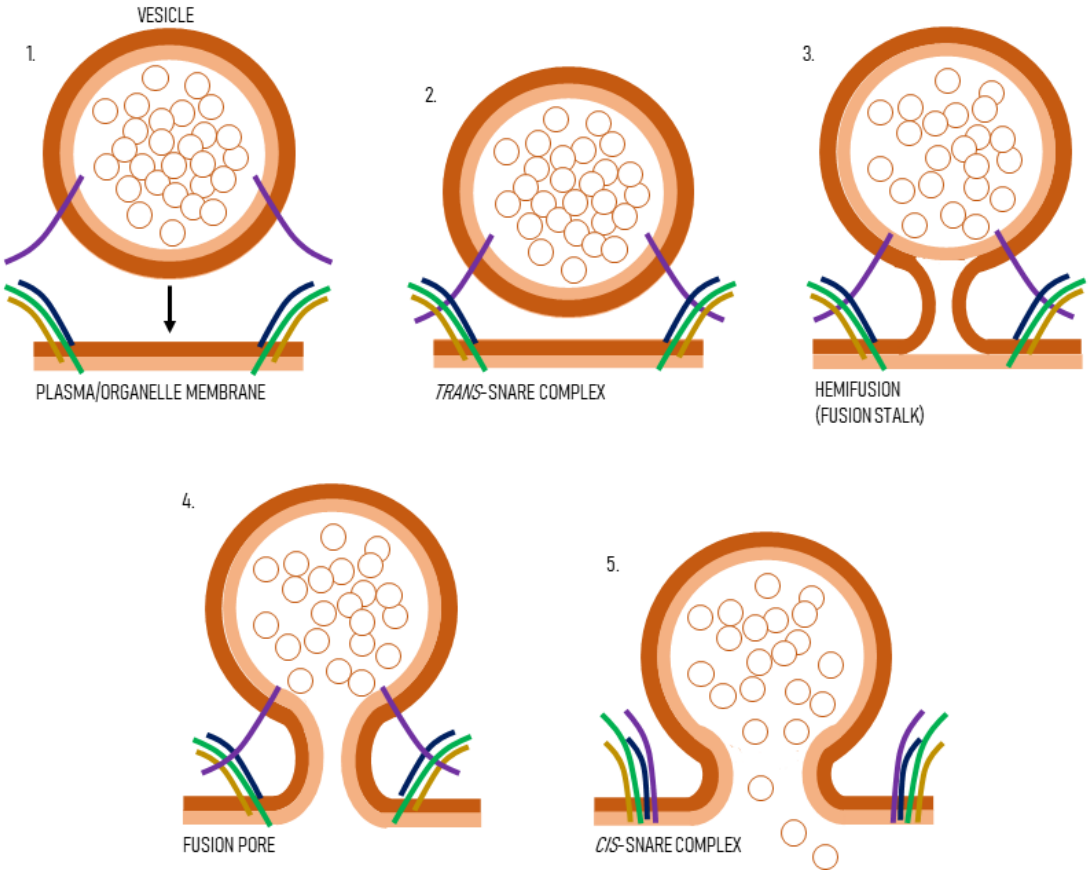

Figure 4. *Schematic depicting the steps of SNARE-mediated membrane fusion*. Formation of *trans*-SNARE complexes bring membranes into close proximity. Hemifusion fuses the outer leaflets together, before a fusion pore forms and expands. When the SNARE complex is all on one membrane it become the *cis*-SNARE complex, ready for disassembly and recycling.

1.4.4 Binding modes of Tlg2 and Vps45

In yeast, Tlg2 is a Qa-SNARE that mediates membrane fusion events within the endosomal system and localises to the TGN and endosomes (Abeliovich et al., 1998). Tlg2 forms SNARE complexes with the Qb-SNARE Vti1, the Qc-SNARE Tlg1 and the R-SNAREs Snc1 and Snc2 (Abeliovich et al., 1998; Coe et al., 1999; Paumet et al., 2001). The SM protein Vps45 has been shown to bind to both Tlg2 and Snc2 and regulates the cellular levels of these SNAREs (Shanks et al., 2012). In the absence of Vps45, Tlg2 is rapidly degraded by the proteosome. Interestingly, when proteasome activity was ablated in *vps45*Δ yeast the cellular levels of Tlg2 were rescued but the protein appeared non-functional (Bryant & James, 2001). This demonstrates the important role that SM proteins can play both in stabilising their cognate syntaxins and promoting their entry into SNARE complexes.

In a manner analogous to Munc18a, Vps45 can bind to Tlg2 via multiple modes. Initially, it was believed that the N-terminal/hydrophobic pocket mode of binding was both necessary and the only mode of binding between these two proteins (Dulubova et al., 2002). However, later research demonstrated that Vps45 could also interact with the Tlg2-containing SNARE complexes independently of the N-terminal motif (Carpp et al., 2006). In addition, experiments by Furgason et al. (2009) highlighted that Vps45 could bind to free Tlg2 lacking the first 36 N-terminal residues ($Tlg2^{37-318}$). It was therefore postulated that Vps45 also binds to a closed conformation of Tlg2 via the SM arch cavity, as had previously been described for Munc18a and Stx1a. In support of this, mutations of key residues in $Tlg2^{37-318}$ that promoted an open conformation showed no binding between the SNARE and Vps45. A surprising finding from this research was that the two modes of binding appeared to be mutually exclusive, as a $Tlg2^{1-33}$ N-peptide was able to strongly compete for binding to Vps45 against $Tlg2^{37-318}$ (Furgason et al., 2009). This data indicates that the Tlg2 N-terminal motif is able modulate the affinity for closed conformation binding to Vps45 and act to regulate the entry of Tlg2 into SNARE complexes. Although neither binding mode appears to be essential for Tlg2 function, disruption of the high affinity pocket-mode of binding leads to a significant downregulation of Tlg2, demonstrating the importance of this binding mode for Vps45's stabilisation of Tlg2 cellular levels (Carpp et al., 2007).

1.4.5 The function of Tlg2

As previously mentioned, Tlg2 functions within the endosomal pathway. In yeast, cells lacking Tlg2 or Vps45 are still viable, which demonstrate that the proteins are non-essential, but display phenotypes characteristic of defects in endocytosis. Yeast with disrupted Tlg2 have an increased sensitivity to osmotic stress and display abnormally fragmented vacuoles (Abeliovich et al., 1998; Holthuis et al., 1998). In addition, they are defective in vacuolar protein sorting, as demonstrated by the missorting of carboxypeptidase Y (CPY). CPY is processed from the ER, through the Golgi complex and into the vacuole. Post-translational modifications of CPY gives rise to various forms, including the ER residing p1 CPY, the late Golgi p2 form and the mature mCPY found in the vacuole. *tlg2*Δ yeast secrete ~20% of the cells CPY, in the p2 form, which demonstrates that whilst the maturation of CPY was not blocked, it was missorted for secretion instead of being delivered to the vacuole (Abeliovich et al., 1998). Other *tlg2*Δ phenotypes that denote defects in endocytosis include deficiency in the uptake and trafficking of fluorescently labelled dyes, such as Lucifer Yellow, and a reduction in the turnover of an a-factor receptor (Ste3) by the vacuole (Abeliovich et al., 1998). Tlg2 is also essential for the Cvt pathway in yeast, a selective autophagy pathway that is responsible for delivering aminopeptidase I (API) hydrolase to the vacuole, with *tlg2*Δ displaying almost a complete block in API maturation

(Abeliovich et al., 1999). *vps45*Δ yeast also display many similar phenotypes as *tlg2*Δ, which is indicative of their shared role in endocytosis, and are also slower to grow and display temperature sensitivity in growth (Cowles et al., 1994; Piper et al., 1994; Shanks et al., 2012). Mutations in Vps45 in humans have also been linked to congenital neutropenia, bone marrow fibrosis and nephromegaly in infants, potentially as a result of increased apoptosis in neutrophils and bone marrow due to defects in the endosomal-lysosomal pathway (Stepensky et al., 2013; Vilboux et al., 2013).

Additionally, Tlg2 appears to play a role in autophagy. In the absence of Tlg2, yeast display a significant reduction in autophagy and have a disruption in the anterograde transport of Atg9, which is required for the delivery of membranes to the expanding phagophore in autophagy initiation (Nair et al., 2011). A similar mechanism has been postulated to occur with Stx16 (the mammalian homologue of Tlg2), whereby Stx16 forms SNARE complexes with VAMP7 and SNAP-42 to mediate autophagosome formation through the trafficking of Atg9+ vesicles (Aoyagi et al., 2018; Tang, 2019). Tlg2 deletion in mice cells also resulted in a decrease in LC3-PE (mammalian homologue of Atg8-PE) positive puncta as well as mitochondrial dysfunction, which are phenotypes associated with a defect in autophagy (Aoyagi et al., 2018).

1.4.6 SNAREs in *Leishmania*

The SNARE family of proteins and other aspects of membrane trafficking are an understudied area of research in *Leishmania* and other trypanosomatids. To date, there has been one known study that has attempted to classify SNARE proteins in *Leishmania.* Besteiro et al., (2006) were able to identify 27 SNARE domain-containing proteins in *L. major*, which, based on sequence homology, were allocated to each of the four Q- or R-SNARE subfamilies and included a Tlg2 Qa-SNARE homologue. Additionally, five SM proteins were discovered, with two Vps45 homologues. Localisation analysis of the *L. major* Tlg2 revealed a cytosolic punctate distribution with a strong signal next to the kinetoplast. This was predicted to relate to the Golgi apparatus and endosomal compartments, as is seen in yeast (Abeliovich et al., 1998). However, use of a *T. brucei*-derived Rab1 Golgi marker did not co-localise with the Tlg2, although was directly adjacent to the stronger signalling punctate. In addition, the remaining puncta did not appear to co-localise with endocytic vesicles stained with the lipophilic FM4-64 probe (Besteiro et al., 2006). However, no further research was conducted, so the nature of these puncta remains unknown. A similar study was also conducted for *Trypanosoma*, with 26 SNAREs identified for *T. brucei*. In contrast to what was seen in *L. major*, the *T. brucei* Tlg2 homologue did co-localise with the Golgi apparatus, which may be indicative of a conservation of function (Murungi et al., 2014).

1.5 Aims

The work presented in this thesis aimed to identify and characterise the *L. mexicana* homologues of Tlg2 and Vps45. Initially, this would be achieved by the *in silico* analysis of the *L. mexicana* genome to discover the gene identities of Tlg2, Vps45 and their SNARE complex partners. Generation of *L. mexicana* promastigotes either overexpressing ectopic wild-type Tlg2 ($Tlg2^{WT}$) or with Tlg2 knocked out would allow for characterisation of any resulting phenotypes as well as being utilised to determine protein expression patterns and localisation. In addition, inclusion of a Tlg2 with mutations in the N-terminal motif ($Tlg2^{FL}$) that were predicted to disrupt the high-affinity pocket-mode of binding to Vps45 would highlight the necessity of this binding mode and determine whether there was a conservation of function from what is witnessed in yeast. Following this, the role of Tlg2 in differentiation would be assessed, with a focus on infectivity/virulence and autophagy. Finally, the identification of *in vivo* binding partners for Tlg2 would be attempted through the use of immunoprecipitation assays. This thesis constitutes the first study to functionally characterise a SNARE protein in *Leishmania*. As such, completion of these aims would help to expand the field of study of SNARE proteins in *Leishmania* and provide valuable insight into the role of Tlg2 in these parasites.

Chapter 2 – Materials and methods

2.1 Bioinformatics

2.1.1 Protein identification and domain searches

To identify homologues of proteins of interest in *Leishmania mexicana*, *Saccharomyces cerevisiae* and *Homo sapiens* protein sequences were obtained from the Saccharomyces Genome Database (SGD) (https://www.yeastgenome.org/) and UniProt (https://www.uniprot.org/). Protein sequences were then submitted to a BLASTP search against the *L. mexicana* (MHOM/GT/2001/U1103 strain) protein database in TriTrypDB (https://tritrypdb.org/tritrypdb/app/search/transcript/UnifiedBlast). The *L. mexicana* proteins identified with the highest scores and E values were inputted into InterPro (Blum et al., 2021) and SMART (Letunic et al., 2021) softwares to determine predicted SNARE, transmembrane, Habc and longin domains. The predicted molecular weights of each protein were also calculated by inputting protein sequences into the ExPASy ProtParam online tool (Gasteiger et al., 2005).

2.1.2 Protein alignments

To ascertain percentage identities between protein homologues, sequences were inputted into Clustal Omega (Sievers et al., 2011) and Percent Identity Matrixes were generated. Protein alignments were performed using T-Coffee (Notredame et al., 2000) to identify conserved residues in protein homologues.

2.2 Molecular cloning

2.2.1 Plasmid design

Plasmids were designed using SnapGene software (version 5.1). Sequences from laboratory stock plasmids were imported into the software, whereby *in silico* cloning was undertaken to identify appropriate restriction digestion and ligation sites for input of desired DNA sequences. SnapGene primer tools were also used to identify optimal primer binding sites for amplification of relevant DNA sequences from plasmids.

2.2.2 Polymerase chain reaction (PCR)

Primers for PCR were designed using either SnapGene or Primer-BLAST online tool (https://www.ncbi.nlm.nih.gov/tools/primer-blast/) and synthesised by Integrated DNA Technologies (IDT). Primer melting temperatures were calculated using the New England

Biolabs (NEB) online Tm Calculator (https://tmcalculator.neb.com). All PCRs were performed with either Q5® High-Fidelity DNA Polymerase (NEB) or *Taq* DNA Polymerase (NEB), following the manufacturer's recommended protocols. When using the Q5® High-Fidelity DNA Polymerase the reaction recipe was as follows: 1x Q5 reaction buffer (NEB), 200 µM deoxynucleotide triphosphates (dNTPs), 0.5 µM of both forward and reverse primers, <1,000 ng template DNA, 0.02 U/µL Q5 high-fidelity polymerase (NEB) and nuclease-free water up to 25 or 50 µL. For a standard PCR run, the steps were: 30 sec initial denaturation at 98°C, then 25-35 cycles of 98°C for 10 sec, 50-72°C (based on primer melting temperature) for 30 sec and 72°C for 30 sec / kb of amplified DNA. There was then a final extension step of 72°C for 2 min.

For PCRs using *Taq* DNA Polymerase the reaction recipe was: 1x concentration of standard *Taq* reaction buffer (NEB), 200 µM dNTPs, 0.2µM of both forward and reverse primers, <1,000 ng template DNA, 0.025 U/µL *Taq* polymerase (NEB) and nuclease-free water up to 25 or 50 µL. PCRs were then run with an initial 30 sec denaturation step at 95°C, followed by 30 cycles of 95°C for 30 sec, 45-68°C (primer melting temperature dependant) for 30 sec and 68°C for 1 min / kb amplified DNA. A final extension step of 68°C for 5 min then followed. For colony PCRs or for amplification from genomic DNA (gDNA), using either Q5 or *Taq* polymerase, the initial denaturation step was increased to 5 min. For touchdown PCRs, 10 cycles were included after the initial denaturation whereby the annealing temperature was set 5-10°C above the primer melting temperature and then decreased by 0.5-1°C per cycle. Subsequent cycles then followed the standard PCR format, but the number was reduced by 10.

2.2.3 Restriction digestion

Restriction digests of plasmid and PCR products were performed using enzymes and buffers obtained from NEB. Protocols were available at NEBcloner® Restriction Enzyme Single/Double Digestion (https://nebcloner.neb.com/#!/redigest). Most restriction digests were undertaken using CutSmart Buffer (NEB), with a standard reaction made up of 1 µg DNA, 1 x CutSmart Buffer, 5 – 10 U of each restriction enzyme and nuclease-free water up to 50 µL. Reactions were then incubated at 37°C for a minimum of 15 min, but more typically for 1-2 hours.

2.2.4 Agarose gel electrophoresis

Gels were prepared at 1%, 1.5% or 2% w/v agarose concentrations in 1x TAE buffer (40 mM Tris, 20 mM acetic acid and 1 mM EDTA, pH 8). Solutions were heated in the microwave until the agarose had dissolved, then left to cool slightly before adding 1 x SYBR Safe DNA Gel Stain (Invitrogen) to allow DNA visualisation. Gel solutions were poured into plastic moulds

with combs to make the appropriate number of wells and allowed to set. DNA samples were mixed with 1x Purple Gel Loading Dye (NEB) before loading into gel wells. 5-10 µL of either GeneRuler 1 kb Plus DNA Ladder (Thermo Fisher Scientific) or Quick-Load® 100 bp DNA Ladder (NEB) were run alongside samples to allow size determination of DNA fragments. Gels were immersed in 1 x TAE buffer in agarose gel tanks and samples run at 80 V for 30-60 min. Visualisation and image capture of DNA fragments was performed using the SYBR Safe UV setting on a Chemidoc Imaging System with Image Lab Touch Software (Bio-Rad).

2.2.5 DNA purification

PCR products or DNA extracted from agarose gels were purified using the NucleoSpin Gel and PCR Clean-up kit (Macherey-Nagel), following the manufacturer's protocol. For plasmids designated for parasite transfections, purification was achieved though ethanol precipitation. Briefly, 10% v/v 3 M sodium acetate and 200% v/v ice-cold ethanol were added to DNA samples, then left on ice to incubate for 30 min. Samples were then centrifuged at >10,000 g for 15 min before the supernatant was removed and the DNA resuspended in 1ml ice-cold 70% ethanol. A further 15 min centrifugation was followed by removal of supernatant. The DNA was left to air-dry in a sterile environment, before being resuspended in 10 µL sterile, nuclease-free water.

2.2.6 DNA ligation

DNA fragments were ligated together using T4 DNA ligase (NEB). A typical reaction was made up of 1x T4 DNA ligase buffer (NEB), DNA at 1:3-1:7 vector to insert ratio (for DNA insertion into a plasmid) or 1:1 ratio for PCR products, 1 µL T4 DNA ligase and nuclease-free water up to 20 µL. Samples were incubated either overnight at 16°C or for 2 hours at room temperature.

For blue-white screening, DNA inserts were ligated into a pGEM®-T Easy Vector system (Promega) using the supplied T4 DNA ligase and Rapid Ligation Buffer. Reactions contained: 1x Rapid Ligation Buffer, 50 ng of pGEM®-T Easy Vector, DNA insert (typically at a 1:3 vector to insert ratio), 1 µL (3 Weiss U) T4 DNA ligase and nuclease-free water up to 10 µL. Samples were incubated at room temperature for 1 hour.

2.2.7 Bacterial transformations and DNA extraction

All bacterial transformations were performed in XL1-Blue competent cells (Agilent Technologies). Cells were stored at -80°C and thawed on ice when required. For

transformations, 0.1–50 ng of experimental DNA was added to 50-100 µL of cells and gently mixed. Cells were incubated on ice for 30 min, then heat shocked at 42°C for 45 sec. A further 2 min incubation on ice was performed before 450 – 900 µL of Luria-Bertani (LB) media was added. Cells were then incubated at 37°C with shaking at 225-250 rpm for 1 hour, followed by plating onto LB agar supplemented with 100 µg/mL ampicillin. Plates were incubated at 37°C overnight to promote colony formation. For blue-white screening, 20 µL X-gal (50 mg/mL) and 40µL IPTG (100mM) were spread on the surface of the LB agar ampicillin plates and allowed to dry in a laminar flow hood, prior to the addition of the transformed cells.

For DNA extraction, colonies were picked from the LB agar plates and grown overnight in 5 mL LB media with 100 µg/mL ampicillin at 37°C with shaking. For blue-white screening, white colonies were expected to contain plasmids with the correct DNA inserts, whereas blue colonies would contain plasmids without inserts. DNA was extracted from the overnight cultures using the NucleoSpin® Plasmid DNA Purification kit (Macherey-Nagel), following the manufacturer's protocol. DNA concentration and purity were ascertained using a NanoDrop™ 1000 Spectrophotometer (Thermo Fisher Scientific).

2.2.8 DNA sequencing

DNA sequencing was performed by Eurofins Genomics using their Mix2Seq service. DNA was sequenced using a modified Sangar sequencing method (known as cycle sequencing) on ABI 3730XL instruments. Primers for sequencing were ordered through IDT.

2.3 *Leishmania* cell culture

2.3.1 Cell maintenance

L. mexicana (MNYC/BZ/62/M379) promatigotes were grown at 26°C in Medium 199 (M199) with Hanks' Salts (Gibco), supplemented with 10% v/v heat-inactivated Fetal Bovine Serum (FBS) (Gibco), 40 mM HEPES, pH 7.4 (Sigma-Aldrich), 100 µM Adenine hemisulfate salt (Sigma-Aldrich), 1% v/v Penicillin/Streptomycin (Sigma-Aldrich) and 0.0005% Hemin (from a stock of 0.25% dissolved in 50% triethanolamine) (Sigma-Aldrich). Where appropriate, drugs were added to the medium to aid selection: 10 µg/mL Blasticidin (InvivoGen), 40 µg/mL Puromycin (InvivoGen) and 40 µg/mL Hygromycin B Gold (InvivoGen). Cells were passaged 1-2x per week.

For generation of stabilates, 1 mL of cell culture was mixed with 1 mL freezing solution (supplemented M199 with additional 30% FBS and 10% DMSO) and then stored at -80°C or in

liquid nitrogen. To recover after freezing, stabilates were thawed at room temperature before adding to supplemented M199 and then left at 26°C overnight before addition of any selection drugs.

2.3.2 Cell counting

To determine cell density per mL, 100 µL of promastigote culture was diluted in 10 mL of filtered ISOTON™ II Diluent (Beckman Coulter®) and counted with the Z1 Particle Counter (Beckman Coulter®), set with a 100 µm C aperture size and aperture Kd of 60, and a minimum detected particle size of 3 µm.

2.3.3 Transfections and cell selection

For transfections, 8 x 10^6 log phase promastigotes were harvested via centrifugation (1000 g for 10 min), washed in 1 x Phosphate Buffered Saline (PBS), then resuspended in either 210 µL 1 x cytomix (66.7 mM Na_2HPO_4, 23.3 mM NaH_2PO_4, 5 mM KCl, 50 mM HEPES and 150 µM $CaCl_2$, pH 7.3) or 200 µL 1 x Tb-BSF buffer (90mM Na_3PO_4, 5mM KCl, 0.15mM $CaCl_2$, 50mM HEPES, pH 7.3), containing the DNA to be transfected. Cell suspensions were then transferred to electroporation cuvettes and transfected using one pulse of the X-001 programme on the Nucleofector™ 2b Device (Lonza). As a transfection negative control, water was used in place of DNA. Transfected cells were left to recover overnight at 26°C in 10 mL of supplemented M199.

Transfectants were selected for at either the population level, by the addition of appropriate antibiotics (see section 2.3.1 for drug concentrations), or by diluting the cell culture at 1:8 in supplemented M199 and cloning onto a 96-well plate, along with selection antibiotics.

2.3.4 Null mutant generation using CRISPR-Cas9

Null mutants were generated in *L. mexicana* cell lines that expressed Cas9 and T7 RNAP, using a CRISPR-Cas9 based strategy (Beneke et al., 2017). Primers to amplify single guide RNAs (sgRNAs) and knockout cassettes were designed using an online tool (http://www.leishgedit.net/Home.html). sgRNA primers were engineered to contain a T7 RNA polymerase promotor, a complimentary 20 nt sequence to introduce double-strand breaks to the target DNA and a 20 nt CRISPR-Cas9 backbone overlap (for PCR amplification). To replace the gene of interest with the knockout cassette two sgRNAs were required, to direct the Cas9 enzyme to the gene's 5' and 3'UTRs respectively. The knockout cassette consisted of a drug resistance gene (either blasticidin or puromycin resistance), flanked by *L. mexicana* 5' and

3’UTRs to drive expression. Primers to amplify knockout cassettes included 30 nt sequences homologous to regions upstream and downstream of the sgRNA targets, to facilitate homologous recombination of the cassette. The plasmids used for cassette amplification were pTBlast_v1 and pTPuro_v1, sequences of which can be found at http://www.leishgedit.net/Home.html. Transfections of sgRNAs and cassettes were as described in section 2.3.3 and selection was done at both the population and clonal level.

PCRs for the CRISPR-Cas9 strategy differed from those described in section 2.2.2. PCR reactions for the sgRNAs contained 1 x Q5 reaction buffer (NEB), 2 µM OL6137 (standard reverse primer for all sgRNAs), 2 µM forward primer, 1 U Q5® High-Fidelity DNA Polymerase (NEB), 0.2 mM dNTPs and nuclease-free water up to 20 µL. PCRs were then run with an initial denaturation of 98°C for 30 sec, followed by 35 cycles of 98°C for 10 sec, 60°C for 30 sec and 72°C for 15 sec. The final extension step was 72°C for 10 min. For the knockout cassettes, the PCR reactions were made up of 1 x Q5 reaction buffer, 2 µM of forward and reverse primers, 30 ng of plasmid DNA (either pTBlast_v1 or pTPuro_v1), 1 U Q5® High-Fidelity DNA Polymerase (NEB), 0.2 mM dNTPs and nuclease-free water up to 40 µL. The PCR protocol included: initial denaturation at 94°C for 5 min, then 45 cycles of 94°C for 30 sec, 65°C for 30 sec and 72°C for 2 min 15 sec, with a final extension of 72°C for 7 min.

2.3.5 DNA extraction

Two methods were utilised for gDNA extraction. For cleaner and purer extracted gDNA (e.g. for amplifying sequences for cloning purposes) 5 x 10^6 cells were harvested by centrifugation (1000 g for 10 min) and washed in 1 x PBS. gDNA was then extracted from cell pellets using the E.Z.N.A.® Tissue DNA Kit (Omega Bio-Tek), following the manufacturer’s protocol. For a quicker, less pure extraction, 2 mL of cell culture was centrifuged, then washed in 1 x PBS and the cell pellets left to dry in a sterile environment for several minutes. gDNA extraction was then carried out using the PCRBIO Rapid Extract PCR Kit (PCR Biosystems), according to the manufacturer’s protocol. PCR reactions from extracted supernatant were also set up using the manufacturer’s supplied PCRBIO HS Taq Mix Red master mix and protocol. DNA samples were stored at -20°C.

2.3.6 RNA extraction

To harvest RNA from *Leishmania* cells, 5-10 mL of promastigote cell culture was centrifuged (1000g for 10 min) and the cell pellet resuspended in 500 µL of TRIzol™ (Invitrogen). RNA was then extracted using the Direct-zol™ RNA Miniprep kit (Zymo Research). The manufacturer’s protocol was followed, except for step 3, where the provided DNase I treatment

was disregarded in favour of a more stringent DNase after RNA extraction was completed (see section 2.5.2). RNA samples were stored at -80°C.

2.3.7 Protein extraction

For protein extraction, 0.5-3 x 10^7 cells were harvested, and the cell pellet resuspended in 40-60 µL of 1 x Laemmli buffer (2% w/v SDS, 10% v/v glycerol, 0.002% w/v bromophenol blue, 62.5 mM Tris-Cl, pH 6.8 and 5% v/v 2-mercaptoethanol), before incubating at 95°C for 5 min. Protein samples were stored at -20°C.

2.4 Protein assays

2.4.1 SDS-PAGE

SDS-PAGE gels were made at 12%, 15% or 18% according to established recipes (Harlow & Lane, 1988). Protein samples in 1 x Laemmli buffer were loaded alongside Precision Plus Protein™ Dual Color or All Blue Prestained Standards (Bio-Rad) to allow molecular weight estimations for proteins of interest. Samples were run at 120-150 V in 1 x Running Buffer (25 mM Tris, pH 8.3, 190 mM glycine and 0.1% w/v SDS).

2.4.2 Western blotting

To perform western blots, Immun-Blot® PVDF membranes (Bio-Rad) were incubated in methanol for 30 sec, before being washed in purified water for 2 min. The PVDF membranes and SDS-PAGE gels were then sandwiched between two layers of gel blotting paper soaked in 1 x Transfer Buffer (25 mM Tris, 190 mM glycine, 20% methanol and 0.1% w/v SDS) and semi-dry transfer performed using a Novex™ Semi-Dry Blotter (Invitrogen) at 20 V for 1 hour.

For blocking, membranes were incubated overnight at 4°C, with shaking, in 1 x PBS with 0.05% v/v Tween 20 (PBS-T) and 5% w/v milk. Membranes were then incubated for 3 hours at room temperature, with shaking, in 1 x PBS-T and 1% milk, with appropriately diluted primary antibodies. Washing of the membranes was then performed 3x in PBS-T, before incubating for 1 hour at room temperature, with shaking, with the secondary antibody diluted in PBS-T and 1% milk. The membrane was then washed a further 3x in PBS-T. For HRP-conjugated secondary antibodies, Amersham™ ECL™ Prime Western Blotting Detection Reagent (Cytiva) or Clarity™ Western ECL Substrate (Bio-Rad) was applied and the membranes incubated for 2 min. Visualisation was achieved using the colorimetric and chemiluminescent settings on the Chemidoc Imaging System (Bio-Rad).

To strip the membranes for re-probing with additional antibodies, membranes were washed in PBS-T for 5 min, then incubated in Western BLoT Stripping Buffer (TaKaRa) for 30 min at room temperature, with shaking, before being washed again in PBS-T for 5 min.

2.4.3 Ponceau S staining

Staining was performed after transfer of proteins from the SDS-PAGE gel to the PVDF membrane, as described in section 2.4.3. Ponceau S stain (0.4% w/v Ponceau S and 3% w/v Trichloroacetic acid) was applied to the membrane and left to incubate for 5 min, with manual agitation. The membrane was then washed with purified water until all non-bound stain was removed and protein bands were visible. Images were captured using the Ponceau S setting on the Chemidoc Imaging System (Bio-Rad).

2.4.4 Protein quantification

Western blot images were uploaded into Fiji software (ImageJ). The ‘Rectangle’ tool was then used to select and draw around the first protein bands of interest. The ‘Area’ and ‘Mean grey value’ measurements in the ‘Analyse’ tab were selected. The ‘Analyse’ -> ‘Gels’ -> ‘Select First Lane’ were then chosen. The rectangle was then moved to the next band of interest and the ‘Analyse’ -> ‘Gels’ -> ‘Select Next Lane’ selected. This process was repeated for all protein bands to be analysed and was then followed by ‘Analyse’ -> ‘Gels’ -> ‘Plot Lanes’, whereby a curve should appear. In the case of lots of background, to try and minimise this ‘Process’ -> ‘Subtract background’ was selected, making sure that ‘Light background’ and ‘Disable smoothing’ boxes were checked, with a ‘Rolling ball radius’ set at 50 pixels. To further remove any background a line was drawn from the bottom of each side of the curve. The ‘Wand’ tool was then selected and used to choose the ‘Area wanted’ between the line drawn and the curve, with a resultant signal.

The same process was then repeated for the loading control protein bands and the protein of interest signals normalised against these. To do this, the loading control with the highest signal was identified and the remaining loading controls divided by this to get the relative values. The signals for each protein band of interest were then divided by their corresponding relative loading control signals.

2.5 qPCRs

2.5.1 DNase treatment

The concentration of purified RNA extracted from *L. mexicana* promastigotes (section 2.3.8) was measured using the NanoDrop™ 1000 Spectrophotometer (Thermo Fisher Scientific). Samples were diluted to 10 µg in 44 µL and then processed to remove any contaminating double-stranded DNA using the TURBO DNA-*free*™ Kit (Invitrogen), following the manufacturer's protocol for a routine DNase treatment. An additional centrifugation step was included at the end of the protocol to ensure complete removal of DNase Inactivation Reagent.

2.5.2 Reverse transcription

To convert RNA to non-specific cDNA, SuperScript™ II Reverse Transcriptase (Invitrogen) was used. The reverse transcriptase reaction was initially made up with 0.2 µg Random Hexamer primers (Thermo Fisher Scientific), 500 ng of RNA, 1 µL of 10 mM dNTPs and nuclease-free water up to 12 µL. The mixture was heated to 65°C for 5 min, before placing on ice. 1 x First Strand Buffer, 2 µL of 0.1 M DTT and 40 U of RNaseOUT™ (Invitrogen) were then added and the mixture incubated at 25°C for 2 min. A final addition of 200 U of SuperScript™ II RT was followed by incubations at 25°C for 10 min and 42°C for 50 min. The reaction was inactivated by heating to 70°C for 15 min. cDNA samples were stored at -20°C.

2.5.3 qPCR protocol

Primers for quantitative PCR (qPCR) amplification were designed using the Primer-BLAST online tool and ordered through IDT. qPCR protocols were designed using the Thermo Fisher Connect™ Design and Analysis online tool (https://apps.thermofisher.com/apps/da2/#/home/welcome) and run in 96-well plates on the QuantStudio™ 3 Real-Time PCR System (Applied Biosystems). To determine the efficiency and melting temperature (Tm) of the primers for each mRNA target, a 5 point 1:10 serial dilution of cDNA from a control cell line was used to create a standard curve. A 20 µL qPCR reaction was set up using 1 x Fast SYBR® Green Master Mix (Applied Biosystems), 1 µL of cDNA and 7 µM of forward and reverse primers. The qPCR was run using the Relative Standard Curve protocol, selected on the Thermo Fisher Connect™ Design and Analysis tool. The cycling parameters consisted of an initial denaturation of 95°C for 20 sec, then 40 cycles of 95°C for 1 sec and 60°C for 20 sec, followed by the standard melt curve protocol. To ascertain primer efficiencies, the dilutions were converted into log values and the slope of regression calculated in Microsoft Excel using the equation '=SLOPE(Average Ct value range, log

quantity range)'. Efficiency values were then converted into a percentage using the Excel equation '=(10^(-1/The Slope Value)-1)*100'. Acceptable primer efficiencies fell within the range of 90-110%. Primer Tms were calculated by averaging the supplied values across dilutions for each gene target. Additional amplicons seen in melt curves were determined to be primer-dimers.

For qPCRs to ascertain relative quantification of target genes against a housekeeping gene, 20 µL reactions were set up with 1 x Fast SYBR® Green Master Mix (Applied Biosystems), 1 µL of cDNA (at 2.5 ng/µL) and 7 µM of forward and reverse primers. The qPCR was run using the Relative Quantification protocol on the Thermo Fisher Connect™ Design and Analysis tool. The parameters consisted of an initial denaturation of 95°C for 20 sec, then 40 cycles of 95°C for 1 sec, 60°C for 20 sec and 77°C for 3 sec (temperature set halfway between highest primer-dimer Tm and lowest gene amplicon Tm, to allow capture of fluorescent reporter from desired amplicons). This was followed by the standard melt curve protocol.

2.5.4 qPCR data analysis

To undertake analysis of the qPCR data, firstly, ΔCts for individual cell lines were determined by subtracting the Ct of the housekeeping gene from the Ct of the target genes. The ΔΔCts for experimental cell lines were then calculated by subtracting the ΔCt of each gene in the control cell line from the ΔCt of the same gene in the experimental cell lines. Finally, gene expression fold change was calculated using the formula $2^{-\Delta\Delta Ct}$ and the results log transformed for statistical analysis.

2.6 Flow cytometry

2.6.1 Sample preparation

To analyse the cell cycle of *L. mexicana* promastigotes, 3 x 10^6 cells were harvested by centrifugation (1000g for 10 min), then washed in PBS. For fixation, cells were incubated in 70% methanol at 4°C overnight. The fixed cells were pelleted and then incubated in PBS containing 10 µg/mL propidium iodide (PI) and 10 µg/mL RNase A (both Invitrogen) for 30 min at room temperature. Cells were analysed on a Beckman Coulter CyAn ADP flow cytometer.

2.6.2 Flow cytometry data analysis

Only single events were recorded for all experiments. Using the FlowJo™ software (version 10.5.3, BD Biosciences), cellular debris, doublets and other anomalous materials were excluded

after gating on the forward scatter (FSC) plotted against the side scatter (SSC). Data was converted into histograms on the Linear PE-Texas Red channel and analysed using the in-built Cell Cycle algorithms to calculate the percentages of cells in G0/G1, S and G2 phases.

2.7 Fluorescence microscopy

2.7.1 Sample preparation and imaging

To prepare *L. mexicana* promastigotes for fluorescence imaging, 2 x 10^6 cells were pelleted by centrifugation (1000g for 10 min) and the cells fixed in 4% paraformaldehyde (PFA) for 20 min at room temperature. Cells were washed twice in 1 x PBS, then incubated in 1 x PBS with 2% v/v Triton X-100 and 0.1M glycine for 20 min at room temperature, before being pelleted and resuspended in 100 µL of 1 x PBS. On Superfrost® Plus microscope slides (Thermo Fisher Scientific) a 5 mm circle was marked out with a PAP pen and 10 µL of the cell suspension was placed in the middle. The cells were left to adhere to the slides for 15-20 min and were then blocked with 1 x PBS with 1% w/v bovine serum albumin (BSA) (Sigma) for 10 min at room temperature. The blocking was repeated 3x before incubating the cells on the slide with the primary antibody, diluted appropriately in 1 x PBS with 0.1% Triton X-100 (PBT) and 1% BSA, for 1 hour in a humidity chamber. The cells were then washed thrice in 1 x PBT and once in 1 x PBS. The relevant Alexa Fluor® secondary antibodies (Invitrogen) were diluted in 1 x PBT and 1% BSA and incubated with the cells in a humidity chamber for 1 hour. Cells were washed twice in 1 x PBT and once in 1 x PBS and then covered in a drop of VECTASHIELD® Antifade Mounting Medium with DAPI (Vector Laboratories) and a coverslip. The slides were sealed with nail varnish and left to dry in a dark environment. For all cell lines visualised, a 'secondary antibody only' control was made, where the primary antibody incubation step was not included. Slides were stored at 4°C. Images were captured on a Zeiss Axio Observer with the 63x and 100x oil objectives, using excitation and emission settings suitable for the secondary Alexa Fluor® antibodies used.

2.7.2 Image analysis

Images captured on the Zeiss Axio Observer were processed using Fiji software (ImageJ). To determine what was the signal of antibody bound to the target protein versus background signal, the image intensity of the 'secondary antibody only' control samples were manipulated using the *Brightness and Contrast* window until no fluorescent signal was present. These setting were then applied to the images from the experimental samples.

2.8 Macrophage infection assay

The macrophage infection assay was performed by Dr Natalia Teles, Walrad laboratory, according to the following protocol.

Peritoneal macrophages were harvested from CD-1 mice 24 hours after intraperitoneal starch induction (2% starch, aq). The macrophages were then washed and resuspended in RPMI-1640 mammalian cell culture media (Gibco) supplemented with 10% v/v heat-inactivated FBS (Gibco), to a density of 5 x 10^5 cells/mL. 100 µL of this suspension was then added to each well on a 16-well Nunc™ Lab-Tek™ II Chamber Slide™ (Thermo Fisher Scientific) and left to adhere at 37°C and 5% CO_2. After 24 hours, stationary phase *L. mexicana* promastigotes were added to each well at a 1:1 macrophage to promastigote ratio. For each *L. mexicana* promastigote cell line to be analysed, eight wells were allocated; four to ascertain infection status after 24 hours, and four for infection status after 72 hours. At the designated time points (24 or 72 hours post-infection), the supernatant was removed from the wells and the cells fixed with 100% methanol for 30 sec, then stained in a 10% Giemsa solution (Sigma-Aldrich) for 3 min. The cells were then washed in ultra-pure water and left to dry at room temperature. The wells were divided into quadrants and the infected status of 25 macrophages determined per quadrant (100 macrophages per well) using a light microscope with a 20x objective. The percentage of infection was calculated for the 24- and 72-hour post-infection time points and averaged across the four replicates.

2.9 Co-immunoprecipitation

2.9.1 Sample preparation

To undertake co-immunoprecipitation experiments, *L. mexicana* promastigotes were passaged to a density of 2 x 10^5 cells/mL in 250mL of supplemented M199 media (as stated in section 2.3.1), along with antibiotics where appropriate. Cells were incubated at 26°C and left to grow until reaching a density between 2 – 6 x 10^6 (logarithmic growth phase). 5 x 10^8 cells were harvested from each culture and washed in 50 mL of sterile ice-cold PBS before being suspended in 250 µL of filter-sterilised IP lysis buffer (10mM Tris, pH 8.0, 0.05mM EDTA, 150mM NaCl and 1 Roche cOmplete™ EDTA-free Protease Inhibitor Cocktail tablet/15 mL of buffer). Cell suspensions were flash frozen and stored in 1.5 mL Protein LoBind® Tubes (Eppendorf) at -80°C.

To lyse the harvested cells, cell suspensions were defrosted on ice and placed in a sonicating water bath for an initial 3 min. Lysis stasis was determined by placing 10 µL of cell suspensions

on a glass slide and observing them under the light microscope at 40x objective. If any whole cells were observed the suspensions were subjected to further 1 min sonication bursts until only cellular debris, and no whole cells, could be visualised. The cell lysates were then centrifuged at 10,000 g for 4 min before the supernatant (S10) was removed into new Protein LoBind® Tubes. 30 µL of each S10 was collected for mass spectrometry analysis by mixing with an equal volume of 2x Laemmli buffer and then incubating at 95°C for 5 min.

For protein immunoprecipitations, 5 mL of Pierce™ Anti-HA Magnetic Beads (Thermo Fisher Scientific) were washed 3x in 15 mL of IP lysis buffer using magnetic separation racks, before being resuspended in 5 mL of IP lysis buffer. 250 µL of the anti-HA bead slurry was then added to the S10 samples before incubated for 1 hour at 4°C, using a rotating wheel. The magnetic separation racks were used to isolate the beads and the supernatant was removed and stored as 'flow through' for western blot analysis. The anti-HA beads were then washed 6x in 1 mL of IP lysis buffer, with the wash supernatants collected and stored for western blot analysis. To elute the immunoprecipitated protein complexes, the anti-HA beads were moved to fresh Protein LoBind® Tubes and mixed with 100 µL of 1 x Laemmli buffer, before incubating at 95°C for 5 min. 20 µL of the elutions were collected for western blot analysis and the remaining solutions used for mass spectrometry to identify co-immunoprecipitated proteins.

2.9.2 Mass spectrometry and data analysis

Mass spectrometry was performed by the Metabolomics & Proteomics laboratory within the department of Biology's Technology Facility at the University of York, according to the following protocol.

Protein elution and S10 samples were run 1 cm into an SDS-Page gel before being visualised with SafeBLUE Protein Stain (NBS Biologicals). Stained gel sections were excised and subjected to trypsin digestion, post reduction with 1,4-Dithioerythritol and alkylation with iodoacetamide. Resulting extracted peptides were analysed by LC-MS/MS. Briefly, peptides were eluted from a 50 cm EN C18 PepMap column (Thermo Fisher Scienfitic) driven by a mClass UPLC (Waters), over a 1 hour acquisition, onto an Orbitrap Fusion Tribrid mass spectrometer (Thermo Fisher Scientific) operated in DDA mode. MS1 spectra were acquired at high resolution in the Orbitrap mass analyser with product ion spectra acquired in parallel in the linear ion trap.

LC-MS chromatograms were aligned and peak picked using Progenesis QI software (Nonlinear Dynamics) with a concatenated MS spectrum exported for database searching. Database searching was run using Mascot software (Matrix Science) against version 54 of the *L.*

mexicana subset of the TriTrypDB database, appended with common proteomic contaminants. Identifications were filtered through the percolator algorithm to achieve a 5% false discovery rate as assessed empirically against a reverse database. Accepted identifications were mapped back onto the LC-MS chromatograms in Progenesis QI and identifications mapped between runs. Areas under non-conflicting precursor ions were integrated and compared for relative quantification between samples, following normalisation to total peptide signal. Relative protein quantification was inferred from peptide-level measurements. A multi-way ANOVA was applied between all sample groups with the null hypothesis that protein abundance was equal between all samples. P-values were converted to q-values by applying the Hochberg and Benjamini multiple test correction.

Chapter 3 – Overexpression of Tlg2 in *Leishmania* and introduction of the N-peptide

3.1 Introduction

3.1.1 SNAREs and SMs in *Leishmania*

The intracellular membrane trafficking machinery is highly conserved across eukaryotes (Dacks & Field, 2018). SNAREs and SMs, protein families that are essential for membrane fusion, have already been identified in *Leishmania major* and the related parasite *Trypanosoma brucei* (Besteiro et al., 2006; Murungi et al., 2014). SNARE proteins are classified as either Q- or R-SNAREs, based on the residue at the ionic layer of the synaptic fusion complex (Fasshauer et al., 1998). Q-SNAREs are further subdivided into Qa-, Qb- and Qc-SNAREs, depending on the homology of the N-terminal domain, and one each of the four SNARE subfamilies typically come together to form a parallel four-helical "QabcR complex" during membrane fusion (Bock et al., 2001; Kloepper et al., 2007). Q-SNAREs are often found on target membranes and the R-SNARE on vesicle membranes. 27 SNAREs from all four subfamilies, along with five SM proteins, were identified in *L. major* (Besteiro et al., 2006), so *Leishmania mexicana* is predicted to possess a similar complement of proteins.

Tlg2 is a Qa-SNARE that mediates membrane fusion events between the endosome and the late Golgi and forms part of the endocytic pathway within the *trans*-Golgi network (TGN) (Abeliovich et al., 1998). Tlg2 forms a SNARE complex with the Qb-SNARE Vti1, the Qc-SNARE Tlg1 and the R-SNAREs Snc1 and Snc2 (Paumet et al., 2001). The SM protein, Vps45, stabilises Tlg2 cellular levels and regulates Tlg2's entry into SNARE complexes (Bryant & James, 2001). Although SNAREs have been identified in trypanosomatid parasites, including homologs of Tlg2 and Vps45, there is little-to-no functional data available. To try and remedy this deficiency, this chapter covers the bioinformatic analysis to identify Tlg2 and its interacting proteins in *L. mexicana* and begins to characterise some of the phenotypic effects of Tlg2 overexpression and the expression of a Tlg2 N-peptide.

3.1.2 The N-peptide of Tlg2

A common feature of several Qa-SNAREs is an N-terminal peptide motif, which has been shown to bind with high-affinity to a hydrophobic pocket on domain I of their SM regulatory protein (Burkhardt et al., 2008; Peng & Gallwitz, 2002; Yamaguchi et al., 2002). This binding mode has been demonstrated to be critical in several Qa-SNARE:SM interactions (Johnson et al., 2009; McEwen & Kaplan, 2008; Shen et al., 2018). Tlg2 and Vps45 utilise multiple modes

of binding, one of which is via the Tlg2 N-terminal motif (Carpp et al., 2006; Dulubova et al., 2002). Studies in yeast reveal that Tlg2 N-terminal binding to Vps45 plays an important role in stabilising the cellular levels of Tlg2 and promotes Tlg2's entry into SNARE complexes (Carpp et al., 2007; Furgason et al., 2009). Mutations of key residues in the N-terminus, such as F9A and L10A, are able to disrupt this high-affinity binding mode (Dulubova et al., 2002). However, unlike what has been demonstrated in humans, the N-terminus of Tlg2 does not appear to be crucial for the protein's function, as Tlg2 with deletions or F9A/L10A mutations within the N-terminal motif can still bind to Vps45 and rescue *tlg2*Δ cell phenotypes (Dulubova et al., 2002; Furgason et al., 2009).

An interesting observation of Furgason et al., was that the Tlg2 N-peptide ($Tlg2^{1-33}$) strongly competed with a Tlg2 mutant lacking the N-terminus ($Tlg2^{37-318}$) for binding to Vps45. This was surprising to the authors, as there was no expected overlap in the modes of interaction. $Tlg2^{1-33}$ binds to the hydrophobic pocket on the outside of Vps45 domain I, and $Tlg2^{37-318}$, due to its lack of the N-terminal motif, relies on its C-terminus to bind to the arch cavity of Vps45. This data was suggestive of these two binding modes being mutually exclusive. It was therefore predicted that, if the interaction between Tlg2 and Vps45 is conserved in *L. mexicana*, expression of a Tlg2 N-peptide in *L. mexicana* would disrupt the interaction between the parasite's endogenous Tlg2 and Vps45 and lead to growth phenotypes. In contrast, expression of a Tlg2 N-peptide containing the double alanine mutation should be unable to compete with endogenous Tlg2 for binding to Vps45 and, consequently, would not be expected to produce a phenotype.

3.1.3 Aims

This chapter aims to provide an overview of the identification of Tlg2, Vps45 and the interacting SNARE complex proteins in *L. mexicana*. As Tlg2 is predicted to play a role in autophagy, and consequently parasite differentiation, it was hypothesised that overexpression in *L. mexicana* would result in logarithmic promastigotes undergoing an earlier differentiation into the stationary metacyclic promastigotes. In contrast, ectopic expression of a wild-type Tlg2 N-peptide was hypothesised to disrupt endogenous Tlg2 protein function by competing for binding to the Vps45 hydrophobic pocket. This chapter will therefore also describe the generation and validation of Tlg2 overexpression and ectopic N-peptide expression in *L. mexicana* promastigotes, alongside characterisation of cellular growth and differentiation phenotypes. Additionally, the expression profile of Tlg2 in *L. mexicana* promastigotes will be detailed, which, due to the predicted role of Tlg2 in autophagy and differentiation, was hypothesised to peak during metacyclogenesis.

3.2 Results

3.2.1 Identification of Tlg2 and related proteins

To identify the Tlg2 Qa-SNARE, along with its SM protein partner Vps45 and interacting SNAREs (Vti1, Tlg1 and Snc1/Snc2) in *L. mexicana*, a BLASTP search was conducted in TriTrypDB (https://tritrypdb.org/tritrypdb/app/search/transcript/UnifiedBlast). Sequences for the *S. cerevisiae* and *H. sapiens* protein homologues were obtained from the Saccharomyces Genome Database (SGD, www.yeastgenome.org) and UniProt (www.uniprot.org) and inputted against the *L. mexicana* (MHOM/GT/2001/U1103 strain) protein database to find those with the highest sequence similarity (Table 1). For Tlg2/Stx16, LmxM.34.2720 was highlighted as having the most similarity. Two homologues of Vps45 were identified for *L. mexicana*: LmxM.36.2230 and LmxM.36.0460. LmxM.36.2230 was thereafter designated as Vps45a, due to having the higher similarity, and LmxM.36.0460 as Vps45b. Vti1/Vti1a both returned the most similarity with LmxM.23.1750. The *L. mexicana* Tlg1/Stx6 homologue was less clear, as searches with the yeast or human sequences yielded different results, with LmxM.07.0520 the most similar for yeast Tlg1, albeit with a relatively low score and E value, and LmxM.26.0690 for human Stx6. Yeast Snc2 had the highest similarity to LmxM.21.1290, whereas human VAMP proteins (VAMP1/VAMP2/VAMP3/VAMP4/VAMP5) showed most sequence homology to LmxM.08.0030, with LmxM.21.1290 also demonstrating high homology. The yeast Snc1 sequence was also inputted into BLASTP, and this returned LmxM.08.0030 as having the highest similarity, with LmxM.21.1290 the second most similar.

S. cerevisiae SNARE & SM proteins	*H. sapiens* homologues	BLASTP search results against the *L. mexicana* protein database				
		ID	Similarity score for *S. cerevisiae* protein	E value for *S. cerevisiae* protein	Similarity score for *H. sapien* protein	E value for *H. sapien* protein
Tlg2	Stx16	LmxM.34.2720	60.8	$1e^{-10}$	87.8	$3e^{-20}$
Vti1	Vti1a	LmxM.23.1750	57.8	$2e^{-10}$	62.8	$3e^{-12}$
Tlg1	Stx6	LmxM.07.0520	36.2	$4e^{-3}$	-	-
		LmxM.26.0690	-	-	54.3	$5e^{-9}$
Snc1	VAMPs	LmxM.08.0030	59.3	$4e^{-12}$	47 - 77.8	$9e^{-8}$ - $2e^{-18}$
Snc2		LmxM.21.1290	64.3	$8e^{-14}$	37.7 - 65.9	$2e^{-4}$ - $4e^{-14}$
Vps45	Vps45	LmxM.36.2230	250	$6e^{-75}$	290	$4e^{-90}$
		LmxM.36.0460	220	$2e^{-63}$	247	$4e^{-73}$

Table 1. *Results of BLASTP searches for* L. mexicana *homologues of Tlg2 and the related SM and SNARE proteins.* The IDs for highest rated homologues for searches run with either the *S. cerevisiae* or *H. sapien* protein sequences are presented, along with the similarity scores and E values. The human VAMP proteins include VAMP1, VAMP2, VAMP3, VAMP4 and VAMP5, with a resulting range of scores and E values.

The result of these BLASTP searches was then compared against what is already known about SNAREs and SMs in *L. major* and *T. brucei* (Besteiro et al., 2006; Murungi et al., 2014), to ascertain whether similar proteins were identified in more closely related organisms. *S. cerevisiae, H. sapiens, T. brucei, L. major* and *L. mexicana* sequences for each of the SNAREs and SMs were aligned in Clustal Omega (Sievers et al., 2011) and Percent Identity Matrices were generated (Table 2). The two *L. mexicana* Vps45 homologues were also aligned, and their overall percentage identity was determined to be 31.93. A similar alignment was performed with *L. mexicana* Snc1 and Snc2 and their total percentage identity was 20.63, with the highest conservation seen at the C-terminus.

Domain searches were performed for the *L. mexicana* SNAREs identified by the BLASTP analysis. Sequences were inputted into InterPro (Blum et al., 2021) and SMART (Letunic et al., 2021) softwares to determine the presence of known domains. All the identified SNARE proteins contained SNARE and C-terminal transmembrane domains. For Tlg2 (LmxM.34.2720) and Vti1 (LmxM.23.1750), an N-terminal helical region was also identified, which possibly corresponds to the Habc domain that is characteristic of Qa-SNAREs, as well as some Qb- and Qc-SNAREs (Antonin et al., 2002; Misura et al., 2002). The Snc1/VAMP (LmxM.08.0030) also

had a predicted N-terminal longin domain, which is characteristic of the Longin family of R-SNAREs that is conserved across eukaryotes (Rossi et al., 2004b). InterPro was also able to successfully match the orthology of the protein families to what was already predicted with the BLASTP searches. The molecular weight of each protein was estimated using the ExPASy ProtParam tool (Gasteiger et al., 2005) (Fig. 5).

A partial alignment of the first 34aa of *L. mexicana* and *S. cerevisiae* Tlg2 and *H. sapiens* Stx16 using T-Coffee (Notredame et al., 2000) revealed high levels of sequence conservation across the first 15aa. There were seven identical residues, four of which have previously been demonstrated to be essential for the N-terminal binding of Tlg2 to Vps45 (Dulubova et al., 2002) (Fig. 6).

S. cerevisiae SNARE & SM proteins	*H. sapiens* homologues	*L. mexicana* homologues	*L. major* homologues	*T. brucei* homologues	Percentage Identity Matrix					
					S. cerevisiae	*H. sapiens*	*L. mexicana*	*L. major*	*T. brucei*	
Tlg2	Stx16	LmxM.34.2720	LmjF.35.2720	Tb927.9.13030		22.98	23.15	23.15	22.59	*S. cerevisiae*
					22.98		26.99	27.34	26.80	*H. sapiens*
					23.15	26.99		97.68	61.26	*L. mexicana*
					23.15	27.34	97.68		61.92	*L. major*
					22.59	26.80	61.26	61.92		*T. brucei*
Vti1	Vti1a	LmxM.23.1750	LmjF.23.1750	Tb427.08.3470		31.60	24.77	25.23	22.97	*S. cerevisiae*
					31.60		25.46	25.93	20.95	*H. sapiens*
					24.77	25.46		89.01	35.78	*L. mexicana*
					25.23	25.93	89.01		36.21	*L. major*
					22.97	20.95	35.78	36.21		*T. brucei*
Tlg1	Stx6	LmxM.26.0690	LmjF.26.0690	Tb427.07.1260		21.03	21.36	20.87	10.20	*S. cerevisiae*
					21.03		27.75	28.19	12.38	*H. sapiens*
					21.36	27.75		90.00	29.03	*L. mexicana*
					20.87	28.19	90.00		29.95	*L. major*
					10.20	12.38	29.03	29.95		*T. brucei*
Snc1	VAMPs	LmxM.08.0030	LmjF.08.0030	Tb427.05.3560		31.00	29.57	27.83	29.00	*S. cerevisiae*
					31.00		25.00	27.00	29.00	*H. sapiens*
					29.57	25.00		98.14	79.07	*L. mexicana*
					27.83	27.00	98.14		79.53	*L. major*
					29.00	29.00	79.07	79.53		*T. brucei*
Snc2		LmxM.21.1290	LmjF.21.1290	Tb427.10.790		31.00	25.44	25.44	25.23	*S. cerevisiae*
					31.00		21.21	22.22	27.08	*H. sapiens*
					25.44	21.21		92.61	50.84	*L. mexicana*
					25.44	22.22	92.61		50.63	*L. major*
					25.23	27.08	50.84	50.63		*T. brucei*
Vps45	Vps45	LmxM.36.2230	LmjF.36.2230	Tb427.10.6780		37.59	29.68	30.06	26.16	*S. cerevisiae*
					37.59		33.72	33.08	32.83	*H. sapiens*
					29.68	33.72		95.53	51.72	*L. mexicana*
					30.06	33.08	95.53		51.58	*L. major*
					26.16	32.83	51.72	51.58		*T. brucei*
		LmxM.36.0460	LmjF.36.0460			37.59	26.44	25.54	26.16	*S. cerevisiae*
					37.59		29.54	28.62	32.83	*H. sapiens*
					26.44	29.54		96.43	31.44	*L. mexicana*
					25.54	28.62	96.43		31.79	*L. major*
					26.16	32.83	31.44	31.79		*T. brucei*

Table 2. *Summary of* S. cerevisiae *Tlg2 and interacting SNARE and SM proteins, with the identities of homologous proteins in* H. sapiens, L. mexicana, L. major *and* T. brucei *organisms.* Percentage Identity Matrices were generated using Clustal Omega. The human VAMP proteins

include VAMP1, VAMP2, VAMP3, VAMP4 and VAMP5, with VAMP1 (as the most similar) being used for the Percent Identity Matrix.

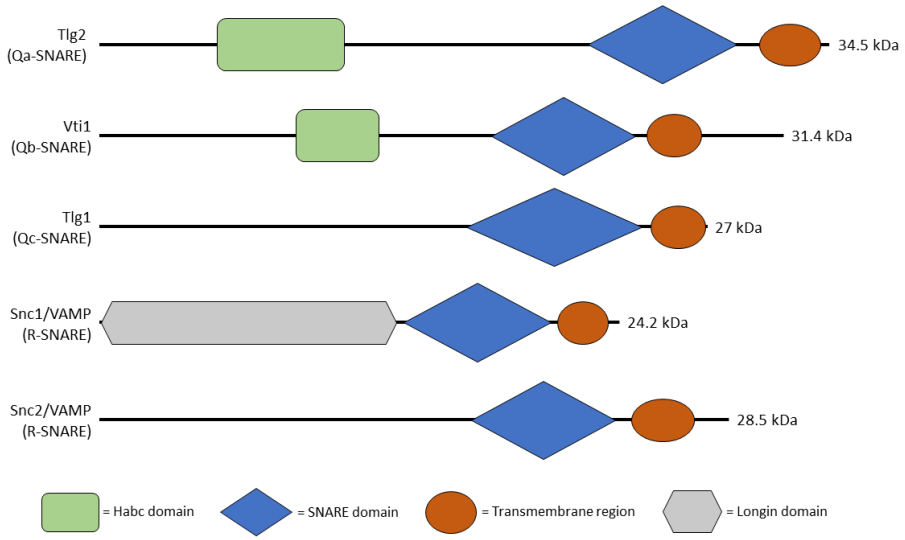

Figure 5. *Domain structures of* L. mexicana *SNARE proteins*. InterPro and SMART were used to identify domains and regions in protein sequences of Tlg2 (LmxM.34.2720), Vti1 (LmxM.23.1750), Tlg1 (LmxM.26.0690), Snc1/VAMP (LmxM.08.0030) and Snc2/VAMP (LmxM.21.1290), with predicted molecular weights indicated (calculated using ExPASy Protparam).

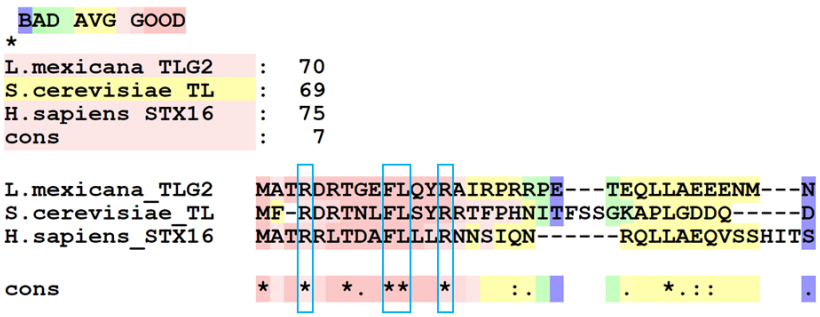

Figure 6. *Alignments of the Tlg2/Stx16 N-terminal regions from* L. mexicana, S.cerevisiae *and* H. sapiens. Sequences were obtained from TriTrypDB (*L. mexicana)*, SGD (*S. cerevisiae*) and UniProt (*H. sapiens*) and aligned using T-Coffee. Colour-coding relates to the level of consistency between the sequences from a score out of 100. The * symbol denotes those residues that are identical. The blue boxed residues are those that have been identified as essential for the binding of the *S.cerevisiae* Tlg2 N-peptide to Vps45.

3.2.2. Generation of Tlg2 overexpression cell lines

In order to investigate whether overexpression of $Tlg2^{WT}$, or a Tlg2 F10A/L11A double mutant ($Tlg2^{FL}$) designed to disrupt N-terminal binding to Vps45, had any effect on *L. mexicana* promastigotes, a pSSU-GFP-*sherp* vector previously generated by Luis de Pablos was modified. Briefly, the *GFP* was replaced by either $TLG2^{WT}$ or $TLG2^{FL}$ gene sequences, and the *sherp* 3'UTR was replaced with the first 1000bp of the *tlg2* 3'UTR, or 800bp of the *nmt* 3'UTR, which is a constitutively expressed gene in *Leishmania* (Price et al., 2003). The length of the 3'UTR sequences was determined by ascertaining the likely polyA site in the closely related *L. major* parasite using TriTrypDB. The $TLG^{WT}/TLG2^{FL}$ genes also included a C-terminal 3 x *HA* epitope sequence, to allow detection of the protein via western blot. C-terminal tagging was deemed the best strategy, so as not to have a negative impact on the N-terminal Habc domain or the interaction of the Tlg2 N-terminus with Vps45. For a drug resistance-only control vector, the *GFP-sherp* sequences were replaced with a multiple cloning site, leaving the hygromycin phosphotransferase gene (*HYG*) in place. Sequencing of the vectors confirmed that the cloning had been successful and they were then transfected into early log-phase promastigotes. After being grown under hygromycin selection, several clones for each transfection were chosen to be validated via anti-HA western blot against the C-terminal HA-tags (Fig. 7). All clones, bar the pSSU HYG^{R} control lines, were demonstrated to express $Tlg2^{WT}$-HA or $Tlg2^{FL}$-HA, although the expression levels appeared to vary.

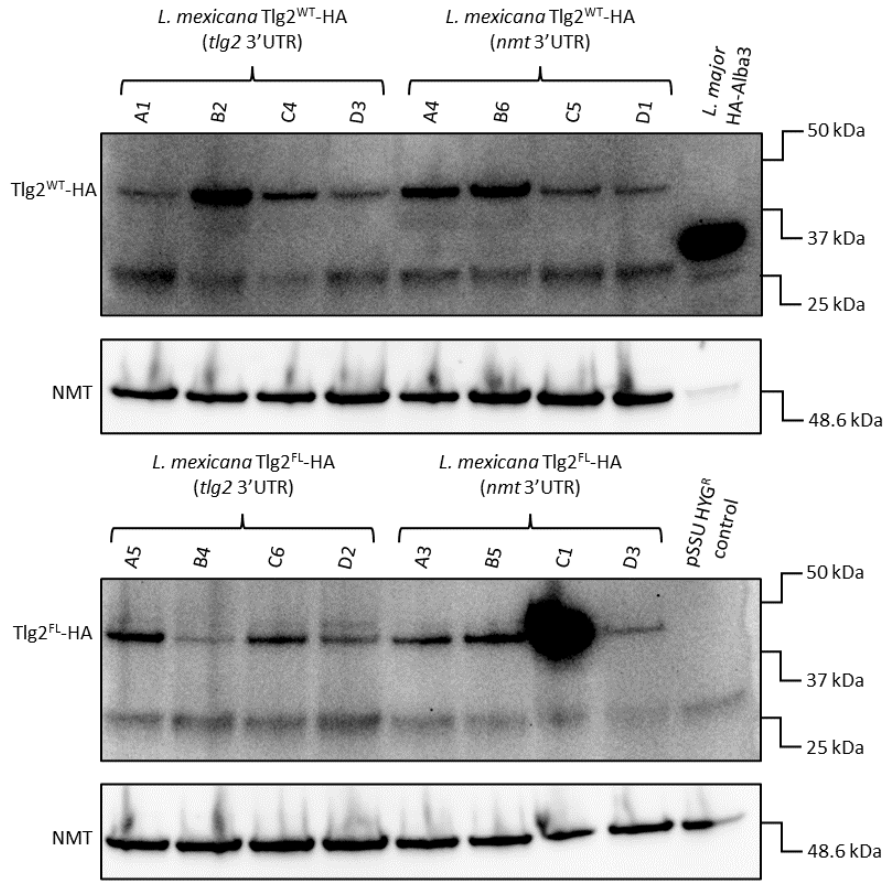

Figure 7. *Validation of Tlg2^{WT} and Tlg2^{FL} overexpression clones*. Anti-HA western blots were performed to visualise the Tlg2^{WT}-HA and Tlg2^{FL}-HA episomally expressed using the modified pSSU vector. *L. major* HA-Alba3 was used as an HA expressing positive control. Anti-NMT was used as a sample loading control. Clones are denoted by an alphanumeric sequence that corresponds to the well they were sampled from.

3.2.3 Phenotypes of Tlg2 overexpression

To determine whether overexpression of Tlg2^{WT} or Tlg2^{FL} led to any growth phenotypes, *L. mexicana* expressing Tlg2^{WT}-HA-*tlg2* (clone B2), Tlg2^{WT}-HA-*nmt* (clone B6), Tlg2^{FL}-HA-*tlg2* (clone A5) and Tlg2^{FL}-HA-*nmt* (clone B5) were selected for further validation. These clones were chosen due to having the strongest protein signals. Clone C1 of the Tlg2^{FL}-HA-*nmt* transfection was not chosen due to doubt over whether the overloaded signal was true or an artifact of the blot. A pSSU HYG^{R} control clone was also selected. To construct a growth curve, promastigotes in logarithmic growth were diluted to an initial density of 2 x 10^5 cells/mL and then counted daily (Fig. 8A). The cell counts were inputted into GraphPad Prism (version 9.3.0, www.graphpad.com) and tested for normality using the Shapiro-Wilk method. All returned a confirmation of normal distribution. To determine whether there were significant differences in

the densities between the cell lines, the samples were compared against the pSSU HYG^{R} control using an unpaired t-test. Examination of the growth curves as a whole failed to highlight significant differences. However, at individual timepoints there were some significant differences for each of the overexpression clones when compared to the pSSU HYG^{R} (Fig. 8B).

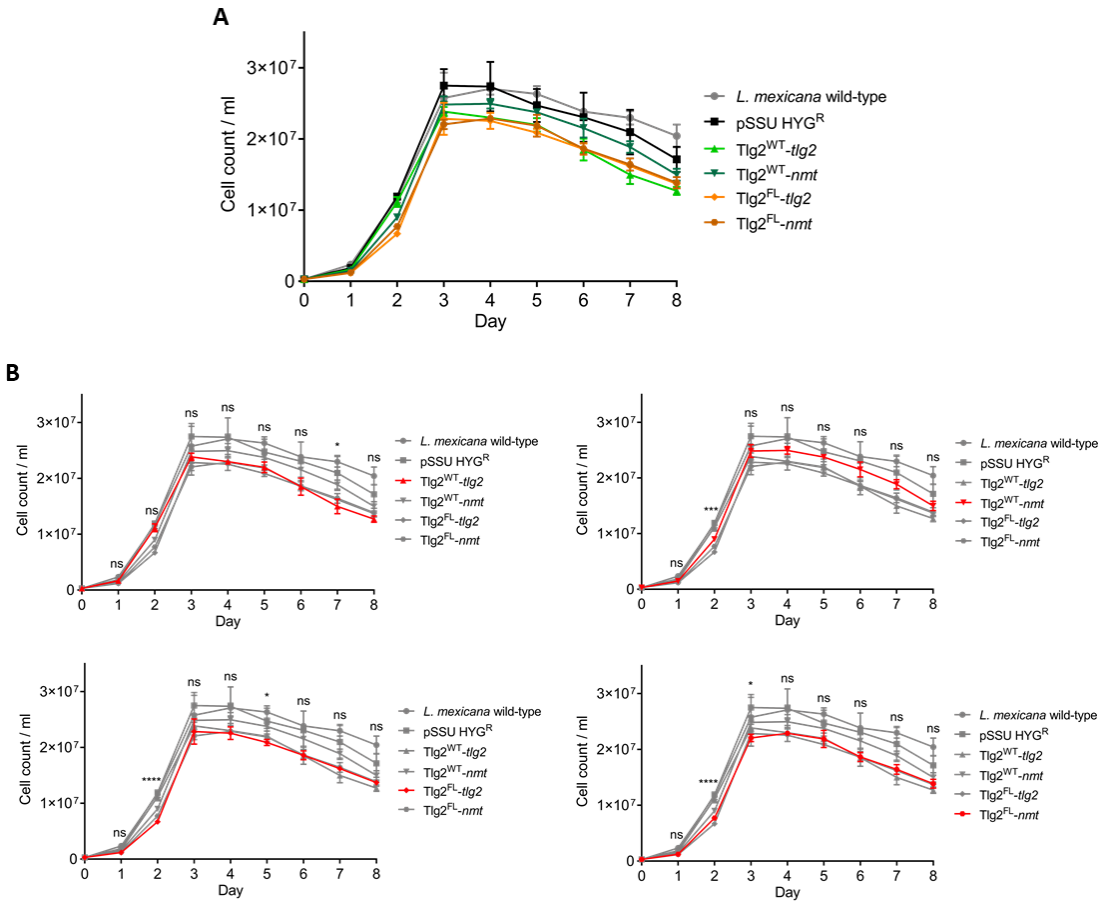

Figure 8. *Growth curves of Tlg2^{WT}-HA and Tlg2^{FL}-HA overexpression cell lines. L. mexicana* promatigotes for each clone were diluted to an initial density of 2 x 10^{5}, then counted daily. **A.** Growth curves constructed from the cell count data (n = 3, error bars = std dev from mean). **B.** Unpaired t-tests of individual timepoints were performed for each overexpression line against the pSSU HYG^{R} control. ns = not significant (P > 0.05), * = P < 0.05, *** = P < 0.001 and **** = P < 0.0001.

As the growth curves were being constructed, cells were harvested daily and fixed in methanol before being incubated with propidium iodide (PI), which stains the cellular DNA. Flow cytometry was performed on the fixed cells to examine DNA content and cell cycle (G0/G1, S or G2/M phase). FlowJo software (version 10.5.3, BD Biosciences) was utilised to plot cell

cycle histograms and the percentage of cells in each phase. The cell cycle histograms (Fig. 9A) overlap very closely for all the cell lines and there are no significant differences in the percentages in G0/G1, S and G2/M phases (Fig. 9B). This demonstrates that overexpression of either the mutant or wild-type versions of Tlg2, whether under their own or the *nmt* 3'UTR, had no effect on the cell cycle of the parasites. It is also worth noting that when viewing the parasites under a light microscope, no phenotypic differences were observed between the overexpression clones and the *L. mexicana* wild-type and pSSU HYG^R control cell lines (data not shown).

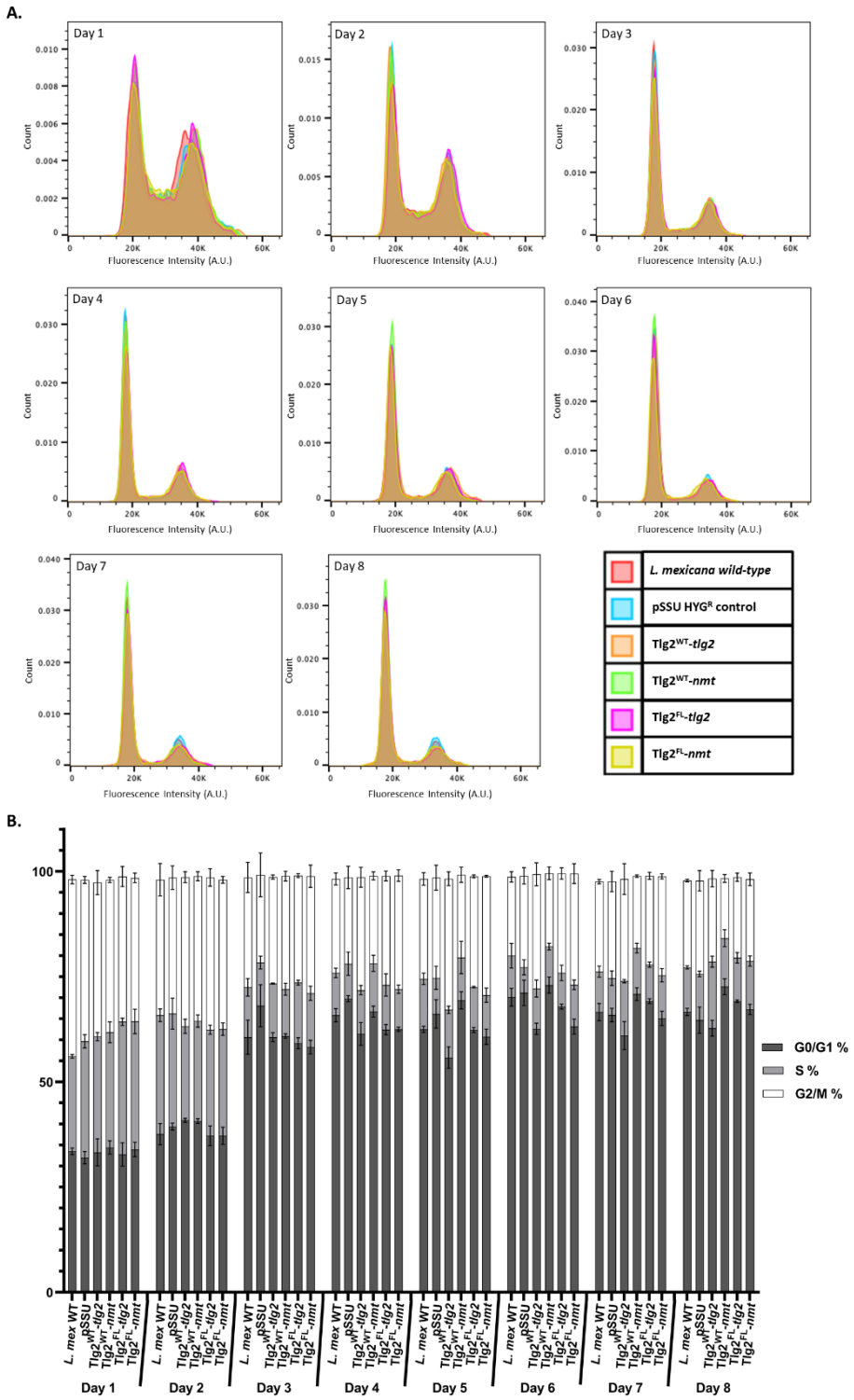

Figure 9. *Flow cytometry data for $Tlg2^{WT}$ and $Tlg2^{FL}$ overexpression cell lines.* Cells were harvested daily, fixed with methanol and incubated with propidium iodide before being analysed by flow cytometry. **A.** Data were gated to only include single events and cell cycle histograms generated in FlowJo using the PE-Texas Red channel. The first peak corresponds to cells in the G0/G1 phase, the second peak to G2/M phase and the area in between the two peaks to the S phase. **B.** Percentage of cells in each cell cycle phase. n = 3, error bars = std dev from mean.

3.2.4 Expression of Tlg2^{WT} and Tlg2^{FL}

To isolate when *Leishmania* expresses Tlg2 during the promastigote phase of its lifecycle, protein samples were extracted daily from the Tlg2^{WT}-HA and Tlg2^{FL}-HA overexpression cell lines. Anti-HA western blots against the C-terminal HA tags were performed. Fig. 10 demonstrates that both Tlg2^{WT}-HA and Tlg2^{FL}-HA were expressed on Days 1 & 2, which corresponds to when the promatigotes were in logarithmic growth. The signal then dropped off dramatically from Day 3 onwards, which was when the cells entered the stationary phase of their growth. Importantly, a similar pattern is also seen irrespective of which 3'UTR was used, indicative of tight post-translational regulation

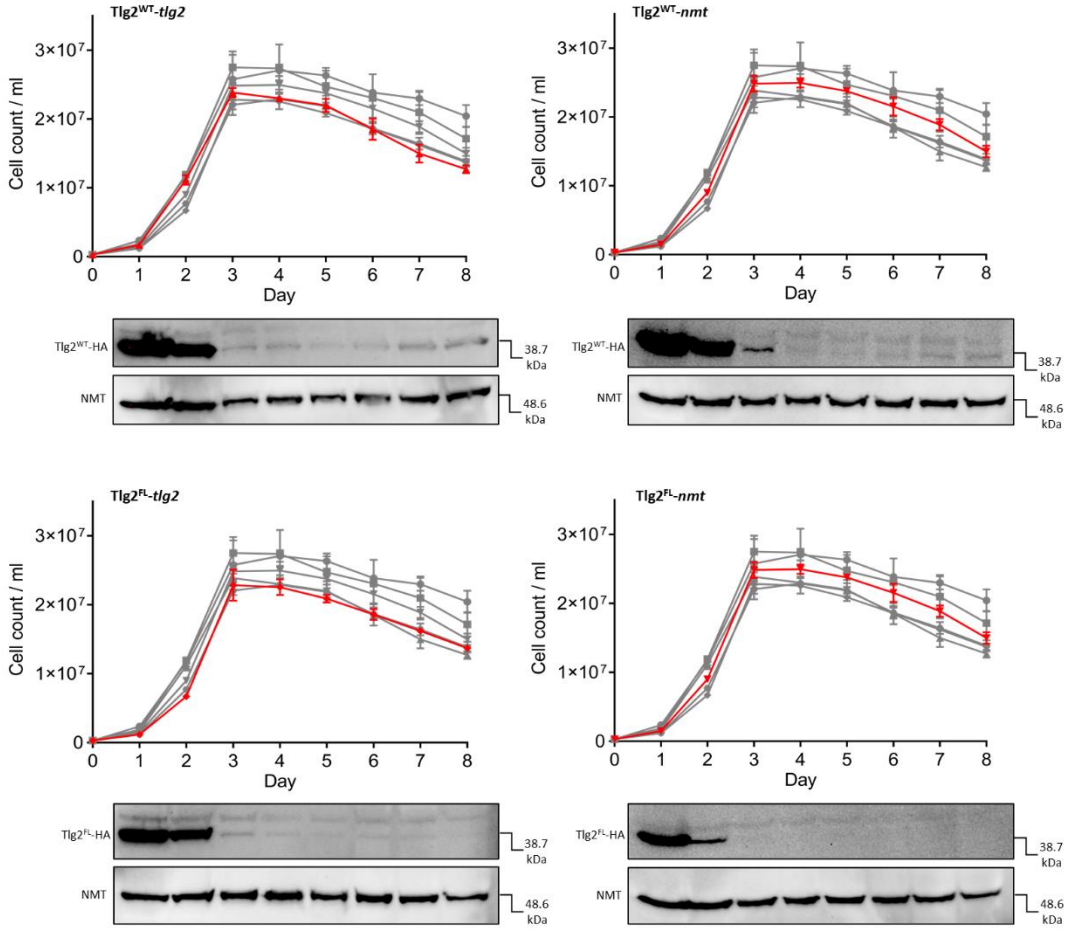

Figure 10. *Expression patterns of Tlg2^{WT}-HA and Tlg2^{FL}-HA.* Protein samples were extracted from *L. mexicana* promastigotes and an anti-HA western blot performed to detect the C-terminal HA-tags of the overexpression cell lines. Growth curves demonstrate what stage of growth the cells were at when the protein samples were collected. Anti-NMT was used as a sample loading control.

Comparing levels of expression for each of the cell lines, observable differences were evident between these samples (Fig. 11A). Tlg2^{WT}-HA appears to have higher levels of expression for all days versus Tlg2^{FL}-HA. For Tlg2^{FL}-HA, the *nmt* 3'UTR seems to lower the protein expression levels compared to the *tlg2* 3'UTR. To determine whether there were any statistically significant differences, the signal for each cell line was normalised against an NMT loading control. The normalised signal was then converted into a percentage against the highest value for each set of replicates across days 1 – 3 (Fig. 11B). When analysing the data in GraphPad Prism (version 9.3.0, www.graphpad.com) a Kruskal-Wallis test was performed, due to the data being non-normal. A significant difference was detected for protein expression levels on day 1 ($P = 0.0013$). Multiple comparisons with a Dunn's post-test revealed that the difference on day 1 between Tlg2^{WT}-HA-*tlg2* and Tlg2^{FL} -HA-*nmt* was significant ($P = 0.0372$). Importantly, the Tlg2^{WT}-HA expression is slight, but present, on the third day, while the Tlg2^{FL}-HA protein is negligible.

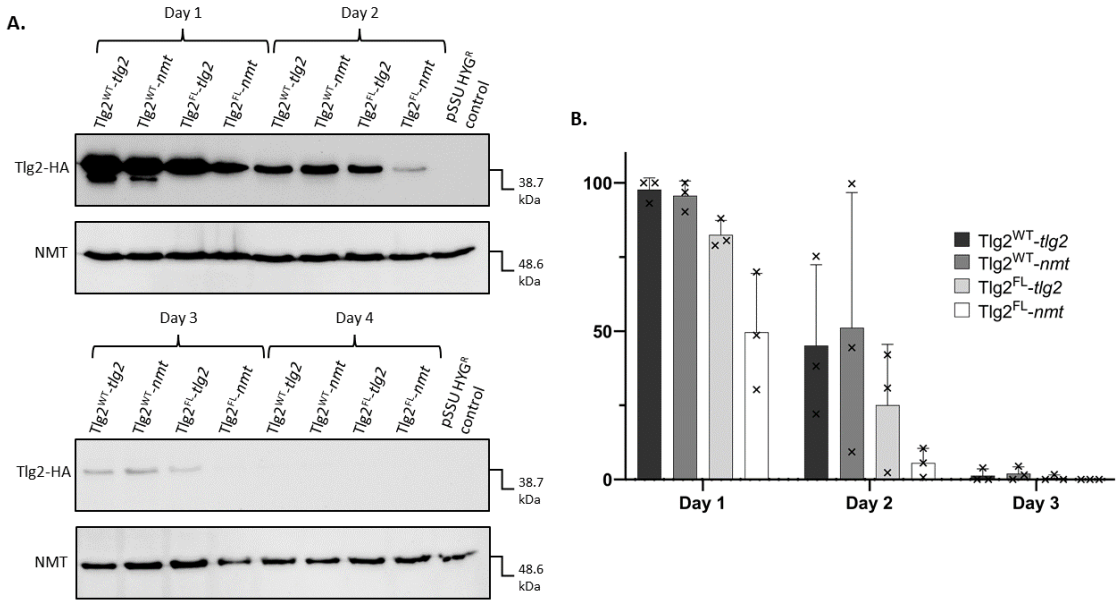

Figure 11. *Comparison of Tlg2^{WT}-HA and Tlg2^{FL} -HA protein expression levels.* **A.** Representative anti-HA western blots against the C-terminal HA-tag to allow visualisation of differences in the levels of protein expression. Anti-NMT was used as a sample loading control. **B.** Quantitative graph of (**A**.) showing ectopic Tlg2 expression from western blots, normalised against the loading control and converted into a percentage against the highest signal across all days, for each replicate set. n = 3, error bars = std dev from mean, X symbol denotes individual replicate percentages.

3.2.5 The effect of N-peptide expression on *L. mexicana* growth

An N-terminal (1-33aa) peptide of yeast Tlg2 has shown to strongly compete against full length Tlg2 for binding to Vps45, via the hydrophobic pocket on domain I of Vps45 (Furgason et al., 2009). Therefore *L. mexicana* promastigotes were engineered to express a 34aa N-peptide of either $Tlg2^{WT}$ ($Tlg2^{1-34}$) or $Tlg2^{FL}$ ($Tlg2^{FL1-34}$) to determine whether this led to growth defects by a possible disruption of the Tlg2:Vps45 binding. The pSSU-Tlg2-*tlg2* plasmid vector was modified to replace the full-length Tlg2 with either $Tlg2^{1-34}$ or $Tlg2^{FL1-34}$ and then sequenced to confirm the cloning was successful. The vectors were then transfected, alongside the pSSU HYG^R control vector, into early log-phase promastigotes and positive clones were selected using hygromycin. Two clones of each N-peptide expression transfection, along with the pSSU HYG^R control, were diluted to an initial density of 2×10^5 cells/mL and then counted daily (Fig. 12A). This growth curve data was inputted into GraphPad Prism (version 9.3.0, www.graphpad.com) and was confirmed as normally distributed using the Shapiro-Wilk method. Significant differences were observed when comparing the individual timepoints of the N-peptide expressing clones against the control, using an unpaired t-test, as is shown in Fig. 12B.

To ascertain if variation in the expression levels of the N-peptides could account for differences in observed growth curves, western blots were attempted. However, visualisation of the N-peptides using anti-HA antibody were unsuccessful. To maximise the likelihood of visualising the N-peptides, an alternative strategy was employed. Samples were loaded onto an SDS-PAGE gel and only run for a couple of centimetres, to prevent the protein bands from separating. Initially, to test whether or not the strategy would work, protein samples from only one of the two clones from each transfection were selected and days 1- 6 run. Fig. 13A shows that anti-HA western blots were able to successfully visualise the $Tlg2^{1-34}$-HA and $Tlg2^{FL1-34}$ -HA N-peptides, with bands seen on days 1, 2 and 5. As day 1 showed the strongest signal for both clones, this day was selected for further analysis. Day 1 protein samples for both clones of $Tlg2^{1-34}$ and $Tlg2^{FL1-34}$ were visualised by an anti-HA western blot, after following the alternative short-run SDS-PAGE gel strategy (Fig. 13B). An alternative anti-EF1α loading control was used, after the poor visualisation of the anti-NMT loading control seen in Fig. 9A. The signal for each cell line was then normalised against the EF1α before being converted into a percentage against a Tlg2-HA overexpressing positive control (Fig. 9C). Differences in the expression were observed, however, no statistical analysis could be performed due to a lack of replicates.

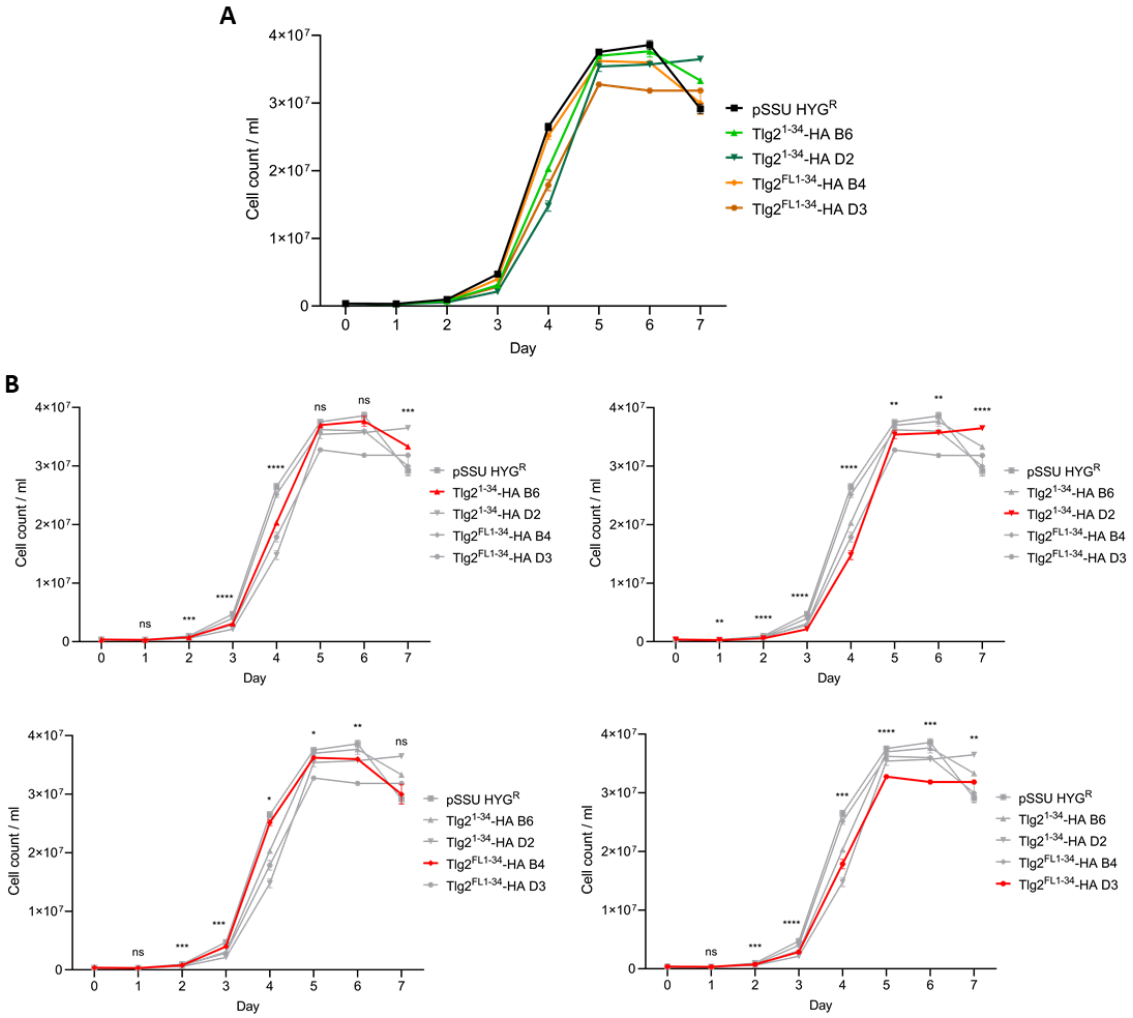

Figure 12. *Growth curves of Tlg2$^{1-34}$-HA and Tlg2^{FL1-34}-HA expressing cell lines. L. mexicana* promastigotes were diluted to an initial density of 2 x 10^5, then counted daily. **A.** Growth curves constructed from the cell count data (n = 3, error bars = std dev from mean). **B.** Unpaired t-tests of individual timepoints were performed for each overexpression line against the pSSU HYG^R control. ns = not significant (P > 0.05), * = P < 0.05, ** = P < 0.01, *** = P < 0.001 and **** = P < 0.0001.

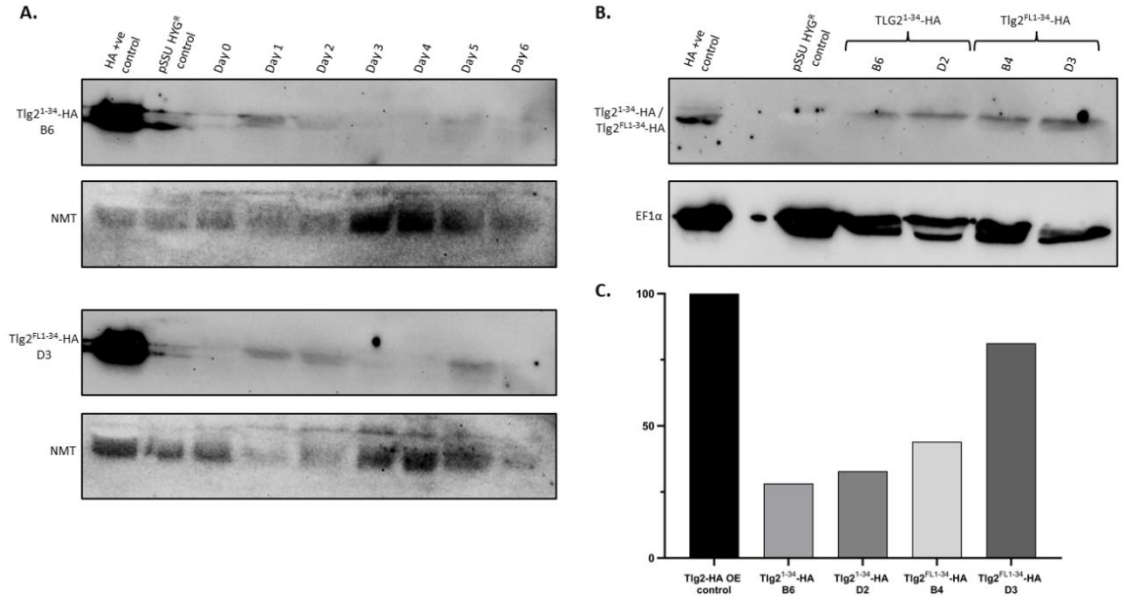

Figure 13. *Expression and quantification of Tlg2$^{1-34}$-HA and Tlg2^{FL1-34}-HA.* **A.** Protein samples for Tlg2$^{1-34}$-HA (clone B6) and Tlg2^{FL1-34}-HA (clone D2) were run for two centimetres into an SDS-PAGE gel and then anti-HA western blots were performed to visualise the episomally expressed HA-tagged N-peptides. Anti-NMT was used as a sample loading control. **B.** Anti-HA western blot against day 1 samples for both clones of Tlg2$^{1-34}$-HA and Tlg2^{FL1-34}-HA, with anti-EF1α as a loading control. **C.** Peptide signals were normalised against EF1α and then converted into a percentage against a full length Tlg2^{WT}-HA overexpressing positive control (n = 1).

3.3 Discussion

3.3.1 SNARE and SM genes in *L. mexicana*

Membrane trafficking is one of the most highly conserved systems in eukaryotes and has been studied in diverse organisms such as yeast, flies, plants, nematodes and humans. However, in trypanosomatid parasites, the machinery involved in membrane trafficking is relatively understudied. Although studies have identified SNARE and SM proteins in *L. major*, *T. brucei* and *T. cruzi*, this has largely relied on bioinformatic and protein localisation data, with no phenotypic analysis (Besteiro et al., 2006; Murungi et al., 2014). To date, there have been no studies investigating SNARE or SM proteins in *L. mexicana*. However, due to the general conservation of *L. major* SNAREs and SMs, it was predicted that *L. mexicana* would possess a similar complement of proteins.

To test this theory, protein sequences for *S. cerevisiae* and *H. sapiens* Tlg2/Stx16, Vps45, Vti1/Vti1a, Tlg1/Stx6 and Snc1/Snc2/VAMP were inputted into BLASTP against the *L. mexicana* proteome. Homologues for each protein were identified in *L. mexicana*, although the

yeast and human sequences did not always return the same results, as was the case with Tlg1/Stx6. *S. cerevisiae* Tlg1 identified LmxM.07.0520 as the most similar, but as the score and E value were relatively low, this was discarded in favour of the homologue identified when using the *H. sapiens* Stx6 sequence (LmxM.26.0690). Snc1 and Snc2 are paralogues that resulted via genome duplication (Byrne & Wolfe, 2005), both of which can form SNARE complexes with Tlg2 (Paumet et al., 2001). Homologues of Snc1/Snc2 in humans are the synaptobrevins/vesicle-associated membrane proteins (VAMPs) (Gerst, 1997). Searches using the *S. cerevisiae* Snc1 and Snc2 sequences resulted in two proteins being identified in *L. mexicana*: LmxM.08.0030 and LmxM.21.1290 respectively. Interestingly, *H. sapiens* VAMP proteins (VAMPs 1-5) all had higher sequence similarity to LmxM.08.0030, although LmxM.21.1290 was always the second most similar, which suggests that they are more homologous to Snc1 than Snc2 (Table 1).

Encouragingly, when comparing the proteins identified in *L. mexicana* against those previously identified in *L. major* (Besteiro et al., 2006), they were all orthologous, with percentage identities above 89% (Table 2). Each protein also fell into the same SNARE subfamilies that had been outlined by Besteiro et al., with Tlg2/LmxM.34.2720 as a Qa-SNARE, Vti1/LmxM.23.1750 as a Qb-SNARE, Tlg1/LmxM.26.0690 as a Qc-SNARE and both Snc1/LmxM.08.0030 and Snc2/LmxM.21.1290 as R-SNAREs. Unlike in yeast and humans, *L. mexicana* appear to have two Vps45 homologues, which is also the case for *L. major*, although the reasons for why are unclear. As *T. brucei* only appears to have one Vps45 homologue, this may indicate that the duplication event took place after these trypanosomatid species diverged.

Domain searches revealed that the identified *L. mexicana* SNARE proteins all contained a C-terminal SNARE domain (Fig. 5). In the case of Tlg2 and Vti1, a helical region was also predicted upstream of the SNARE domain, which is likely to correspond to the three-helical Habc domain that is characteristic of Qa-SNAREs and some Qb- and Qc-SNAREs (including Vti1) (Antonin et al., 2002; Misura et al., 2002). In concurrence with *L. major*, the R-SNARE Snc1 has a predicted longin domain, which are the only R-SNARE domains conserved across all eukaryotes (Besteiro et al., 2006). However, for the Snc2, unlike with *L. major*, no longin domain could be identified. When performing an alignment of these two proteins, the most conservation is at the C-terminus. This could suggest that either Snc1 has lost its N-terminal longin domain in *L. mexicana* or that the sequence has diverged to the point where the homology cannot be recognised. Due to the extended N-terminal region of the Snc2 homologue it is unlikely to be a Brevin R-SNARE, as these characteristically have a short, variable N-terminal region (Jahn & Scheller, 2006).

The N-terminal peptide motif of Tlg2/Stx16 plays an important role in binding to Vps45. In yeast and humans, several residues were identified that were key to this binding: R3, R13, F9 and L10 (Dulubova et al., 2002). To ascertain whether the N-peptide of *L. mexicana* Tlg2 also contained these key residues, an alignment of the first 34aa was performed. Fig. 6 demonstrates that there is a high level of conservation in the first 15aa of the N-peptide sequences across all three organisms and that the four key residues for N-terminal binding are also present in *L. mexicana.* This data is indicative of the importance of these residues for *L. mexicana* Tlg2 and suggests that there is conservation in the method of binding to Vps45. By introducing mutations such as the F9A/L10A double mutant, this binding mode of Tlg2:Vps45 could potentially be disrupted as well in this organism.

3.3.2 Overexpression of Tlg2 in *L. mexicana*

In order to characterise any phenotypes that arise from manipulation of cellular Tlg2 levels, *L. mexicana* promastigotes were engineered to episomally overexpress $Tlg2^{WT}$ or the $Tlg2^{FL}$ double mutant, with a C-terminal HA tag. As the expression profile of Tlg2 had not yet been characterised in *L. mexicana*, as well as using the *tlg2* 3'UTR, an alternative *nmt* 3'UTR was also utilised to try and maintain constitutive expression of the protein (Price et al., 2003). Although Fig. 7 shows that all the clones that were analysed by western blot expressed the protein, the level of expression within each transfection group varied. This could be due to there being variability in the number of plasmids taken up by each clonal cell line. Another potential explanation is that the clonal populations were not synchronised, and if the Tlg2 protein is expressed at specific developmental stages of the promastigote lifecycle (i.e. procyclic, nectomonad, leptomonad or metacyclic), then differing proportions of the clonal populations could have been expressing the proteins when samples were collected.

Growth curves of $Tlg2^{WT}$ and $Tlg2^{FL}$ overexpression clones demonstrate significant growth decreases compared to the control on individual days. This is particularly apparent on day 2 (Fig. 8), which corresponds to when $Tlg2^{WT}$ and $Tlg2^{FL}$ ectopic expression is highest (Fig. 10). Interestingly, the $Tlg2^{FL}$ clones had a more significant decrease in growth than the $Tlg2^{WT}$ overexpressing cells on day 2. As the F10A/L11A mutation within the N-terminus was predicted to disrupt Tlg2:Vps45 high-affinity binding, overexpression of the $Tlg2^{FL}$ was therefore expected to result in less of a phenotype than overexpression of $Tlg2^{WT}$. However, as yeast *tlg2*Δ CPY sorting phenotype can be rescued by ectopically expressed Tlg2 containing the F9A/L10A mutant (Furgason et al., 2009), this suggests that *L. mexicana* $Tlg2^{FL}$ may still be functionally viable and able to form SNARE complexes, with a resultant overexpression phenotype.

It is important to note that the overall picture for the growth curves is that there are no significant differences compared to the control cell line and therefore any potential effects from the overexpression of $Tlg2^{WT}$ or $Tlg2^{FL}$ are short-lived. This is also reflected in the cell cycle data, as the proportion of cells in G0/G1, S or G2/M phases remain unchanged across the cell lines (Fig. 9). Taken together, this data shows that overexpression of $Tlg2^{WT}$ or $Tlg2^{FL}$ has little effect on the growth of *L. mexicana* promastigotes. The lack of morphological changes when viewing these promastigotes under a light microscope also supports this observation. The absence of significant growth phenotypes could potentially be due to the levels of protein overexpression being insufficient to induce a phenotype, but given the tightly controlled expression, independent of the 3'UTR, it is likely the cells will not tolerate higher levels of Tlg2 protein expression. There are also pathway and interaction components that could limit the usable levels of Tlg2 in the cell, thereby negating any potential impacts of overexpression. For example, it is known in yeast that Vps45 regulates the cellular levels of Tlg2 and *vps45*Δ results in decreases in Tlg2 levels (Shanks et al., 2012). A similar interaction could exist in *L. mexicana*, whereby the endogenous levels of Vps45 are a rate limiting step in the cellular levels and functionality of Tlg2.

The expression profile of $Tlg2^{WT}$ and $Tlg2^{FL}$ shows clear and strong expression on days 1 and 2, which correspond to when promastigotes are in the logarithmic phase of growth (Fig. 10). Interestingly, both the *tlg2* and *nmt* 3'UTRs result in similar expression profiles, which suggests that Tlg2 is regulated on a post-translational level. As Tlg2 is believed to play a role in autophagy (Nair et al., 2011), this expression profile was unexpected. As the autophagy pathway in *Leishmania* peaks upon initiation of metacyclogenesis, which occurs after the cells have entered the stationary phase (Besteiro et al., 2006), Tlg2 expression was predicted to mirror this. A potential explanation for the distinct expression of Tlg2 during promastigote logarithmic growth could be linked to the protein's role in endocytosis. Evidence suggests that endocytosis plays a crucial role in cell division, by regulating the cell surface of dividing cells (Boucrot & Kirchhausen, 2007; Schweitzer et al., 2005; Fürthauer & González-Gaitán, 2009). It is therefore possible that endocytosis, and consequently Tlg2, is upregulated during *L. mexicana* logarithmic growth to aid the dividing cells in regulating the changes in cell surface area.

Fig. 11 demonstrates that $Tlg2^{WT}$ protein levels are, on average, higher than those for $Tlg2^{FL}$. The *nmt* 3'UTR also appears to result in a more drastic decrease in protein levels for $Tlg2^{FL}$. Unfortunately, the variability between the replicates led to large error bars and made interpreting the data difficult. Significant differential expression of $Tlg2^{WT}$-*tlg2* and $Tlg2^{FL}$-*nmt* on day 1 is observed but discerning between RNA and protein regulation is challenging. $Tlg2^{WT}$ appears as a doublet on day 1, which may be indicative of modification. Studies have shown

that dephosphorylation of Tlg2 promotes the protein's entry into SNARE complexes in yeast (Gurunathan et al., 2002) and a similar process may be taking place in *L. mexicana*.

3.3.3 The N-peptide of Tlg2

In vitro studies have highlighted how a yeast $Tlg2^{1-33}$ N-peptide has the ability to strongly compete for binding to Vps45 against a Tlg2 deletion construct lacking the first 36 residues (Furgason et al., 2009). This result was surprising to the authors, as the two Tlg2:Vps45 binding modes are distinct from each other yet appear to be mutually exclusive. It was also demonstrated that inclusion of the F9A/L10A double mutant ablated the N-peptide's ability to strongly compete for binding to Vps45, highlighting the importance of these residues for high affinity binding to the hydrophobic pocket of Vps45.

The introduction of vectors ectopically expressing either the $Tlg2^{1-34}$ or the $Tlg2^{FL1-34}$ into *L. mexicana* promastigotes led to significant defects in cell growth (Fig. 12). This result was unexpected, as $Tlg2^{FL1-34}$ was not predicted to be able to compete with the endogenous full-length Tlg2 for binding to Vps45 and was therefore not expected to produce a growth defect. To try and determine a possible explanation for this phenotype, the expression levels of the N-peptides were calculated. Fig. 13C demonstrates that $Tlg2^{FL1-34}$ clone D3 had more than 2x the level of expression than $Tlg2^{1-34}$ clones B6 and D2 on day 1. $Tlg2^{FL1-34}$ clone D3 also had almost 2x the peptide levels than $Tlg2^{FL1-34}$ clone B4. This variation in peptide expression levels could account for the highly significant difference in growth curves seen for $Tlg2^{FL1-34}$ clone D3 in comparison to $Tlg2^{FL1-34}$ clone B4. Although F10A/L11A abrogates high-affinity binding to Vps45, *in vitro* competition assays from yeast show that the double mutant $Tlg2^{FL1-33}$ binds to Vps45 with a similar apparent affinity as both full length cytosolic Tlg2 ($Tlg2^{1-318}$) and $Tlg2^{37-318}$ (Furgason et al., 2009). The higher peptide levels in $Tlg2^{FL1-34}$ clone D3 could therefore potentially be enough to compete with the endogenous Tlg2 for Vps45 binding, in a way that the $Tlg2^{FL1-34}$ clone B4 could not. Encouragingly, despite the lower peptide levels seen in the $Tlg2^{1-34}$ clones, both had a significant growth phenotype, in particular the $Tlg2^{1-34}$ clone D2 (Fig. 12B). This could reflect the non-mutated Tlg2 peptide's higher affinity for binding to Vps45, and therefore demonstrate that lower levels of peptide expression are sufficient to compete with the endogenous Tlg2. An alternative explanation could be that Tlg2:Vps45 binding mechanisms may vary between the yeast and *L. mexicana* homologues, with the F10/L11 residues playing a less essential role in the interaction between the Tlg2 N-peptide and the Vps45 domain I hydrophobic pocket in *L. mexicana.* In this scenario, $Tlg2^{FL1-34}$ may still have a stronger affinity for binding than the endogenous Tlg2, leading to the resultant growth defects.

Chapter 4 – Phenotypes of *tlg2* null mutants

4.1 Introduction

4.1.1 The role of Tlg2

Tlg2 is a Qa-SNARE protein involved in endocytosis and forms part of the *trans*-Golgi network; mediating fusion events between endosome-derived vesicles and the late Golgi. Although it is a non-essential protein, yeast cells with depleted Tlg2 display fragmented vacuoles, defects in endocytosis and growth defects on high-salt media (Abeliovich et al., 1998; Holthuis et al., 1998). Delays in the delivery of lipophilic dyes to the vacuole membranes in *tlg2*Δ yeast also indicate defects in endosomal-vacuolar trafficking (Struthers et al., 2009). In addition to its endocytic capabilities, Tlg2 has been shown to be involved in autophagy. Cells lacking Tlg2 display a 50% reduction in autophagy and Tlg2 appears to play a role in regulating the anterograde transport of the autophagy-related Atg9 protein; thus affecting the formation of autophagosomes (Nair et al., 2011). This insight was further supported by a study in mice, which demonstrated that knockdown of Stx16 (the mammalian homologue of Tlg2) resulted in defective autophagosome formation and the accumulation of damaged mitochondria (these being usually cleared by autophagy) (Aoyagi et al., 2018).

In *Leishmania*, autophagy plays an integral role in the parasite's ability to differentiate into its mammalian infective forms (Besteiro et al., 2006). As Tlg2 is involved in autophagy it was hypothesised that knocking out this gene might result in a reduced ability to differentiate, or display growth inhibitions associated with endocytic defects. This chapter describes the design, creation and validation of null mutants using a CRISPR/Cas9 strategy (Beneke et al., 2017) and attempts to characterise the resultant phenotypes.

4.1.2 Utilising an addback strategy

A common method to validate that any phenotypes arising in null mutant cell lines are a result of the deletion of the gene-of-interest (GOI) and not that of off target modifications is to reintroduce a wild-type ectopic copy of the gene and determine whether this can suppress associated null phenotypes and restore cells to wild-type conditions. This strategy of GOI replacement into a null background is known widely as gene 'addback' and has been successfully used across a wide range of organisms, including *L. mexicana* (Garami & Ilg, 2001; Shrivastava et al., 2019). An extension of this strategy is to reintroduce a mutated version of the GOI, to determine whether or not the mutation is functionally viable and can rescue the null mutant phenotypes. This approach has already been used for the Tlg2 harbouring the

F9A/L10A mutation in yeast, whereby it was demonstrated to be able to successfully rescue the CPY trafficking defect in *tlg2*Δ cells (Furgason et al., 2009). A similar strategy is described in this chapter for the attempted rescue of *L. mexicana tlg2*Δ promastigotes, with pSSU plasmid vectors expressing either $Tlg2^{WT}$ or the equivalent $Tlg2^{FL}$ mutant.

4.1.3 Lifecycle markers for *Leishmania*

Leishmania, like other kinetoplastids, have a strong reliance upon post-transcriptional gene regulation due to constitutive production of polycistronic gene arrays. Although it is believed that the majority of the *Leishmania* genome is constitutively expressed, studies have demonstrated that 30–40% of the transcriptome may be differentially expressed (Dillon et al., 2015; Fiebig et al., 2015). Previous research has highlighted several differentially expressed genes within *Leishmania* that can be used as markers of specific lifecycle stages. A recent study demonstrated that *Histone H4* can be used as a marker for procyclic promastigotes in *L. mexicana* (de Pablos et al., 2019), whereas for metacyclic promastigotes *SHERP* is a well characterised marker (de Pablos et al., 2019; Giraud et al., 2019; Knuepfer et al., 2001; Leifso et al., 2007). As well as being used to identify what stage of the lifecycle a promastigote cell is in, these markers can be utilised to highlight any defect in growth or differentiation in null mutants, by measuring the gene expression levels against the parental control cell line (Alcoforado Diniz et al., 2021).

4.1.4 Aims

In the previous chapter, overexpression of Tlg2 was demonstrated to have little effect on the growth or cell cycle of *L. mexicana* promastigotes. In contrast to this, deletion of Tlg2 or Vps45 was hypothesised to disrupt endocytosis and autophagy and result in parasites with growth and differentiation defects, as is seen in yeast studies. This chapter will therefore explore whether or not removal of Tlg2 or Vps45a via CRISPR/Cas9 leads to any growth phenotypes. The use of an addback strategy will also clarify the success of the CRISPR/Cas9 method for targeted deletion of Tlg2 and help to demonstrate the functionality of the $Tlg2^{FL}$ mutant. Finally, this chapter aims to highlight the use of *Leishmania* lifecycle markers to identify variations in *Histone H4* and *SHERP* gene expression levels in *tlg2*Δ and addback cell lines that may indicate defects in differentiation specific to Tlg2 depletion. It was predicted that *tlg2*Δ promastigotes would undergo delayed metacylogenesis due to a disruption in autophagy, and consequently display a delay in *SHERP* expression.

4.2 Results

4.2.1 Generation of null mutants

To investigate the role of Tlg2 and Vps45a (LmxM.36.2230) in the lifecycle of *Leishmania*, a CRISPR-Cas9 method was utilised for targeted deletion of these genes in *L. mexicana* promastigotes (Beneke et al., 2017). sgRNAs engineered to match the 5'- and 3'- UTRs of the genes were transfected into early log-phase promastigotes, along with two knockout cassettes encoding either blasticidin or puromycin resistance. Selection was undertaken at the population and clonal levels by growing up the cells in either blasticidin or puromycin, or a combination of both antibiotics. Null mutants were validated by PCRs designed to detect the removal of the GOI (by amplifying a ~500bp region from the middle of the GOI) as well as correct integration of the knockout cassettes (amplification of a ~100bp region encompassing the end of the 5'UTR of the gene and the start of the knockout cassette) (Fig. 14A).

The initial round of transfections was unsuccessful in generating a *tlg2* null mutant, but on the second round of transfections, a single clone was recovered, along with several drug resistant clones that still retained at least one copy of the gene of interest (partial knockouts) (Fig. 14B). Null mutants for *vps45a* were successfully selected during the first round of transfections, as well as several partial knockouts (Fig. 14C). The ability to generate null mutants for both *tlg2* and *vps45a* demonstrates that these genes are non-essential for *L. mexicana* promastigote survival. However, the fact that only one null mutant clone was able to be recovered for *tlg2* was a notable and unexpected outcome that could be indicative of compensatory mutations to promote cell survival.

To try and highlight whether the *tlg2*Δ clone that was recovered had undergone any off-target mutations, genomic DNA was extracted and subjected to Illumina next-generation sequencing. Analysis of the results was undertaken by Dr. Cooper Grace (Jeffares Laboratory, University of York). Briefly, sequences were mapped to the *L. mexicana* reference genome (v52; TriTrypDB-52_LmexicanaMHOMGT2001U1103_Genome.fasta) using bwa v0.7.17-r1188 with default parameters (Li & Durbin, 2009). Sequence variants were identified with Freebayes v1.3.2 with default parameters (Garrison & Marth, 2012) and compared against sequences from the T7/Cas9 parental cell line to identify unique mutations. The Illumina sequencing was able to confirm that the CRISPR/Cas9 method had successfully knocked out the *Tlg2* gene (Fig. 15). A total number of 3414 SNPs were identified in the *tlg2*Δ clone, of which 1165 were within CDS regions, affecting 134 genes. SNPs in 78 of these genes there then deemed to be of a moderate effect, according to annotation using the snpEff programme (Cingolani et al., 2012) (Appendix 3).

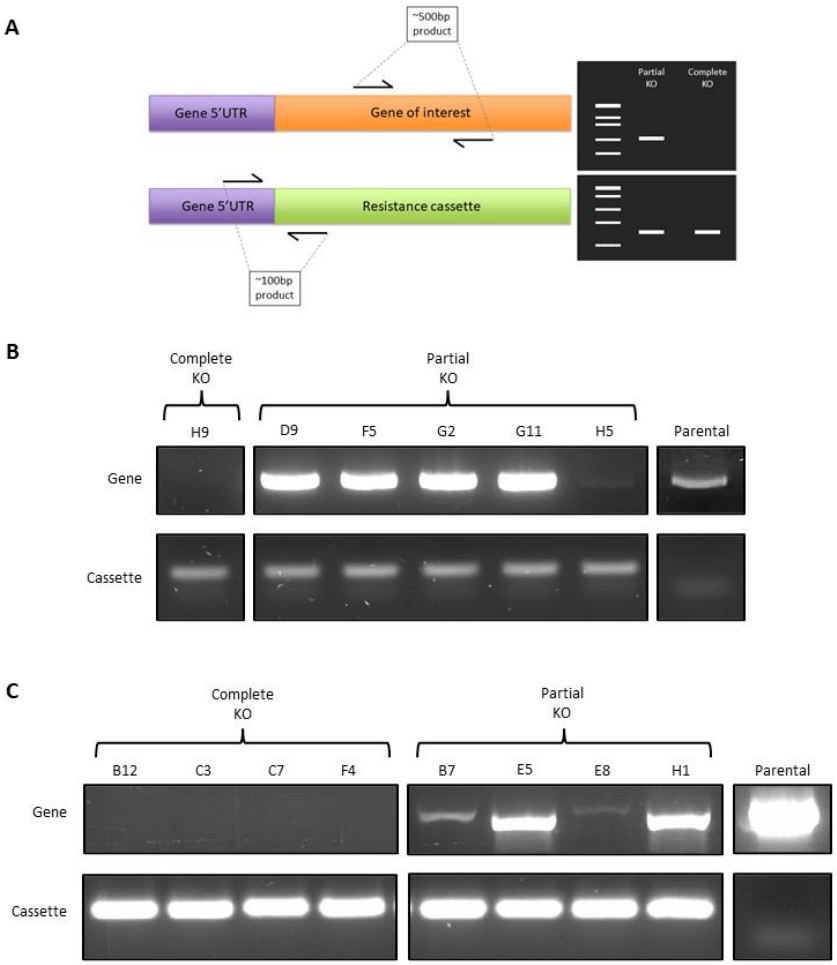

Figure 14. *Generation of* tlg2 *and* vps45a *null mutants.* **A.** Schematic to represent diagnostic PCRs to identify null mutants. Primers were designed to amplify an internal portion of the GOI (orange section) and a section spanning the end of the gene's 5'UTR and the beginning of the resistance cassette (purple and green sections). Representatives of expected PCR bands are also shown for partial KO (where both the knockout resistance cassette and at least one copy of the gene is still present) and complete KO (null mutants). **B.** PCRs were performed on genomic DNA extracted from parental cells and clones where *Tlg2* was targeted for deletion. H9 is here verified as a knockout clone with H5 a potential heterozygote (+/-) clone. **C.** PCRs were performed on genomic DNA extracted from parental cells and clones where *Vps45a* was targeted for deletion.

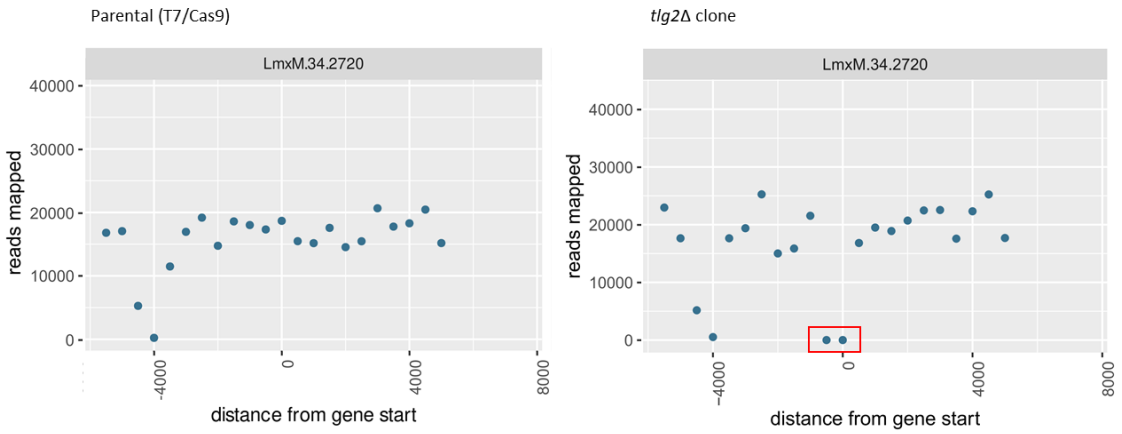

Figure 15. *Raw read counts for parental and* tlg2Δ *cell lines to identify gene knock out.* Counts were conducted over a 10kb region spanning the *TLG2* gene locus (LmxM.34.2720) and confirmed the absence of the gene in the *tlg2*Δ clone when compared to the parental cell line (red boxed area). Graphs provided by Dr Cooper Grace, Jeffares lab, University of York.

4.2.2 Null mutant phenotypes

To determine whether deletion of the *TLG2* or *VPS45a* genes in *L. mexicana* promastigotes resulted in any phenotypes, growth curves were constructed with the null mutant clones. Promastigotes in logarithmic growth were diluted to an initial density of 2 x 10^5 cells/mL and then counted daily (Fig. 16A). The cell counts were inputted into GraphPad Prism (version 9.3.0, www.graphpad.com) and tested for normality using the Shapiro-Wilk method. All returned a confirmation of normal distribution. To ascertain whether there were significant differences between the cell lines, the samples were compared against the T7/Cas9 parental cell line using an unpaired t-test. Examining the whole of the growth curves, *tlg2*Δ returned a significant difference (P = 0.0412), with no significant difference for *vps45a*Δ. Individual timepoints display highly significant differences between parental cells and *tlg2*Δ cells, particularly on days 1, 2, 3, 5 and 8 (Fig. 16B). Several specific timepoints for *vps45a*Δ also demonstrated statistical difference, though the significance was lower than for *tlg2*Δ, and multiple days displayed no significance (Fig. 16C). This data suggests that whilst *vps45a*Δ has a slight impact on the growth of *L. mexicana* promastigotes, the impact on growth caused by the absence of Tlg2 in *tlg2*Δ cells is more severe.

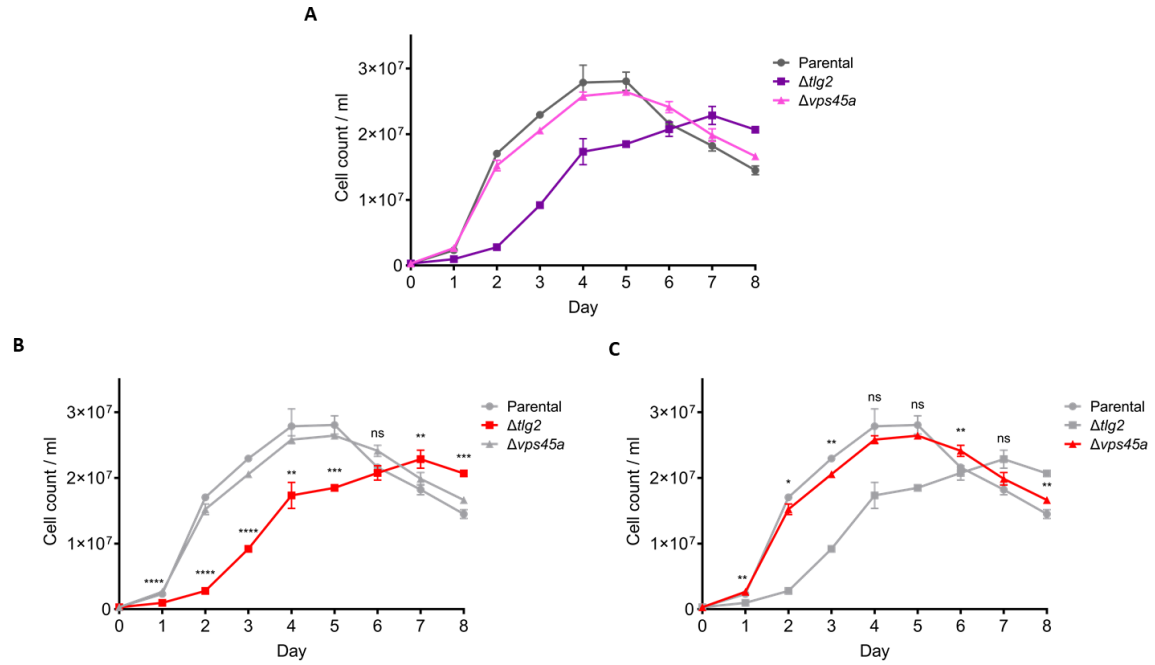

Figure 16. *Growth curves of* tlg2Δ *and* vps45aΔ *cell lines. L. mexicana* promatigotes for each clone were diluted to an initial density of 2 x 10^5, then counted daily. **A.** Growth curves constructed from the cell count data (n = 3, error bars = std dev from mean). **B** Unpaired t-tests of individual timepoints were performed for *tlg2*Δ and **C.** *vps45a*Δ against the T7/Cas9 parental cell line. ns = not significant (P > 0.05), * = P < 0.05, ** = P < 0.01, *** = P < 0.001 and **** = P < 0.0001.

To investigate whether the inhibited *tlg2*Δ and *vps45a*Δ growth rates were also reflected in the cell cycle of the *L. mexicana* promastigotes, cells were harvested daily and methanol fixed. To measure the percentage of cells in each stage of the cell cycle, the fixed promastigotes were incubated with PI and then flow cytometry was performed to measure the cellular DNA content. FlowJo software (version 10.5.3, BD Biosciences) was utilised to plot cell cycle histograms, using the PE-Texas Red channel, and calculate the percentage of cells in G0/G1, S and G2/M phases. Fig. 17 demonstrates that, like the growth curves, *tlg2*Δ had a marked effect on the cell cycle of the promastigotes, which was not apparent in the *vps45a*Δ. The effect of *tlg2*Δ can be particularly noted on days 2 – 4, whereby the percentage of cells in the G0/G1 was significantly lower than the T7/Cas9 parental and *vsp45a*Δ cell lines (Fig. 17B). Conversely, the G2/M percentages were significantly higher for *tlg2*Δ, which, in combination with the growth curve data (Fig. 16B), indicates that the cells were delayed in their entry into the stationary phase.

Promastigotes from the *tlg2*Δ, *vps45*Δ and T7/Cas9 parental populations were also collected on days 4 and 8, fixed with paraformaldehyde (PFA) to maintain morphology and stained with DAPI (to fluorescently label the nuclei and kinetoplasts). The fixed *tlg2*Δ promastigotes on day

4 were morphologically distinct from both *vps45a*Δ and the parental lines. The *tlg2*Δ cells displayed a more rounded and shorter cell body, in contrast to the longer and more slender cell bodies seen for the *vps45a*Δ and parental populations (Fig. 18A). By day 8, the morphology of the *tlg2*Δ promastigotes was indistinguishable from that of either *vps45a*Δ or parental cell populations and the cell cycle was nearly recovered as well (Fig. 18B).

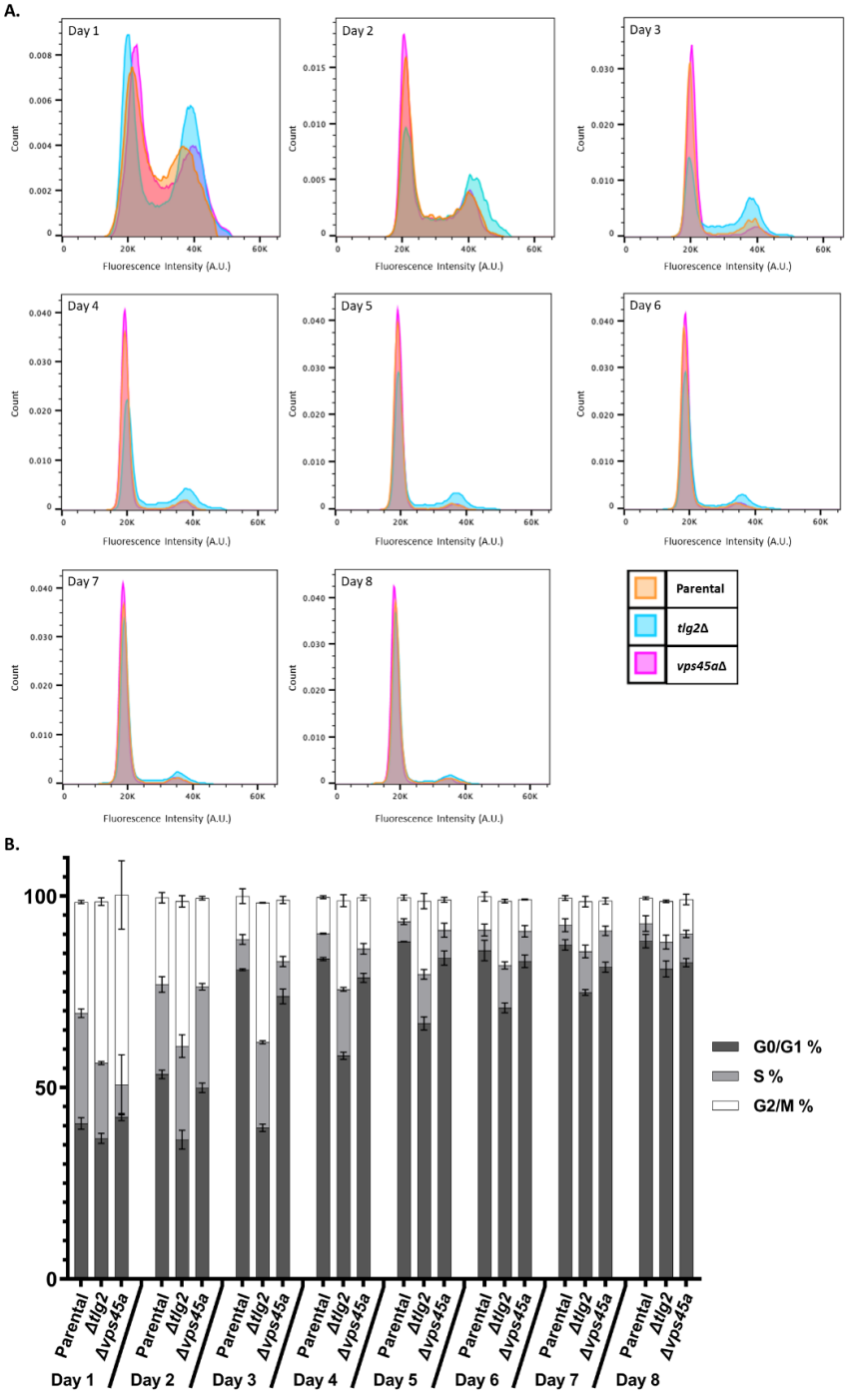

Figure 17. *Flow cytometry data for* tlg2Δ *and* vps45aΔ *cell lines.* Cells were harvested daily, fixed with methanol and incubated with PI before being analysed by flow cytometry. **A.** Data were gated to only include single events and cell cycle histograms generated in FlowJo using the PE-Texas Red channel. The first peak corresponds to cells in the G0/G1 phase, the second peak to G2/M phase and the area in between the two peaks to the S phase. **B.** Percentage of cells in each cell cycle phase. n = 3, error bars = std dev from mean.

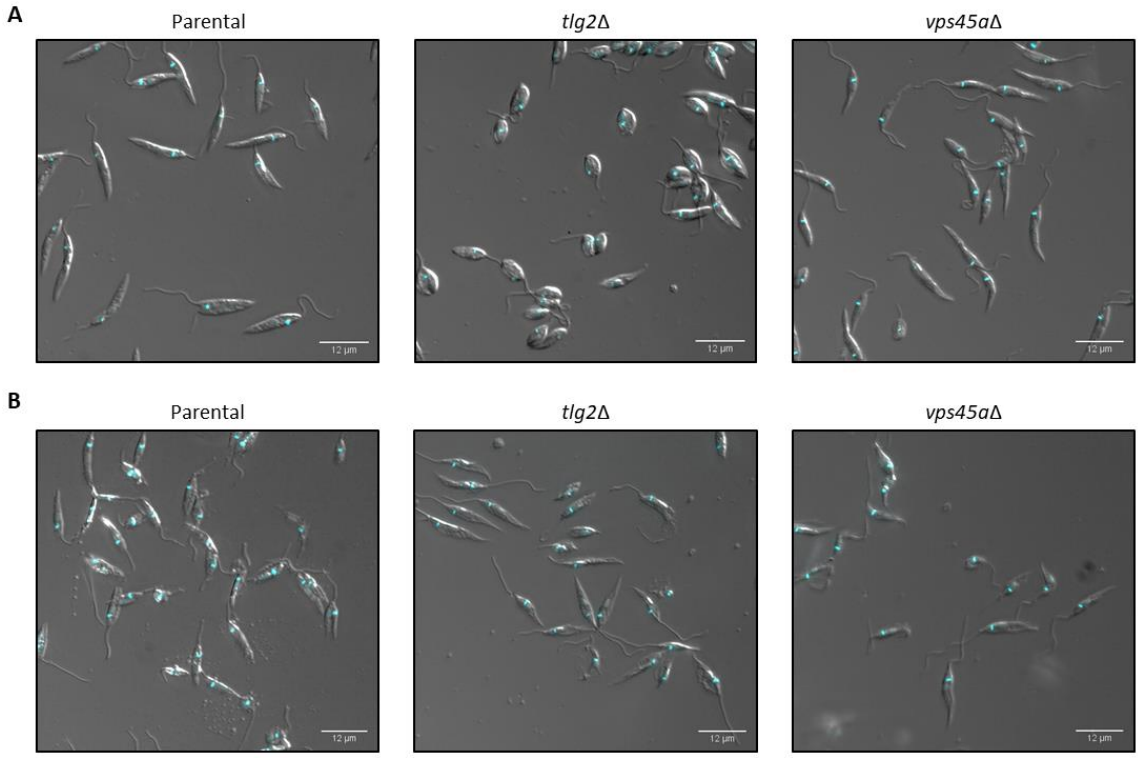

Figure 18. *Morphology of parental,* tlg2Δ *and* vps45aΔ *promastigotes.* Cells were harvested, fixed with PFA and then incubated with DAPI to stain nuclei and kinetoplasts. **A.** Panels represent promastigotes collected on day 4 **B.** Promastigotes collected on day 8.

4.2.3 Addback for rescue of null mutant phenotypes

Due to the fact that only a single clone was recovered from the *tlg2*Δ transfections, it was important to ascertain whether the phenotypes witnessed were caused by the loss of the *TLG2* gene or because of some unknown, off target effects. Consequently, an addback strategy was employed. The pSSU plasmid vectors designed to express C-terminal HA-tagged Tlg2^{WT} or the Tlg2^{FL} mutant, with the *tlg2* 3'UTR, were modified to replace the *HYG* with a blasticidin S deaminase (*BSD*) gene. The pSSU HYG^{R} control vector was also similarly modified to become a pSSU blasticidin-resistant (BLA^{R}) plasmid. All the vectors were sequenced to confirm the

cloning had been successful and they were then transfected into early log-phase *tlg2*Δ promastigotes. After being grown under blasticidin selection two clones each from the $Tlg2^{WT}$ and $Tlg2^{FL}$ addback transfections were chosen for further analysis, along with a pSSU BLA^R control.

To determine whether introduction of episomally expressed $Tlg2^{WT}$ or $Tlg2^{FL}$ was sufficient to rescue the growth phenotype of *tlg2*Δ promastigotes, growth curves were constructed by diluting the cells to an initial density of 2×10^5 cells/mL and then conducting daily cell counts (Fig. 19A). Fig. 19B shows that, as expected, introduction of the pSSU BLA^R control vector alone was not sufficient to rescue the *tlg2*Δ growth phenotype, with the cell counts mirroring those of the *tlg2*Δ. In contrast, both of the $Tlg2^{WT}$ addback clones resulted in growth curves that more closely resembled the parental population (Fig. 19C), which demonstrates that addback of wild-type Tlg2 is able to rescue the null mutant growth phenotype. Interestingly, the two $Tlg2^{FL}$ addback clones were less successful in rescuing the null mutant phenotype than ectopic $Tlg2^{WT}$ was (Fig. 19D). It is also worth noting that there appeared to be more variability in the cell counts of the two $Tlg2^{FL}$ addback populations than was observed for the wild-type addbacks, which could perhaps be due to differences in the expression levels of the mutant protein between the clones.

As the *tlg2*Δ promastigotes displayed defects in their cell cycle, the ability of the ectopic $Tlg2^{WT}$ and $Tlg2^{FL}$ to rescue this phenotype was also investigated. Cells were harvested daily, fixed in methanol and analysed by flow cytometry to measure their DNA content (via PI staining). Cell cycle histograms in the PE-Cy5 channel were plotted and analysed using FlowJo software (version 10.5.3, BD Biosciences) to determine the percentage of cells in the G0/G1, S and G2/M phases. As was the case with the growth curves, Fig. 20 demonstrates that addback of $Tlg2^{WT}$ was able to rescue the null mutant cell cycle phenotype. This is particularly apparent from day 3, where there is a marked shift of cells into the G0/G1 phase for both $Tlg2^{WT}$ addback clones, which reflects what is also seen with the parental cell line. Conversely, ectopic $Tlg2^{FL}$ expression was unable to rescue the cell cycle phenotype, with the G0/G1, S and G2/M proportions mirroring those of the *tlg2*Δ and the empty vector (pSSU BLA^R) populations.

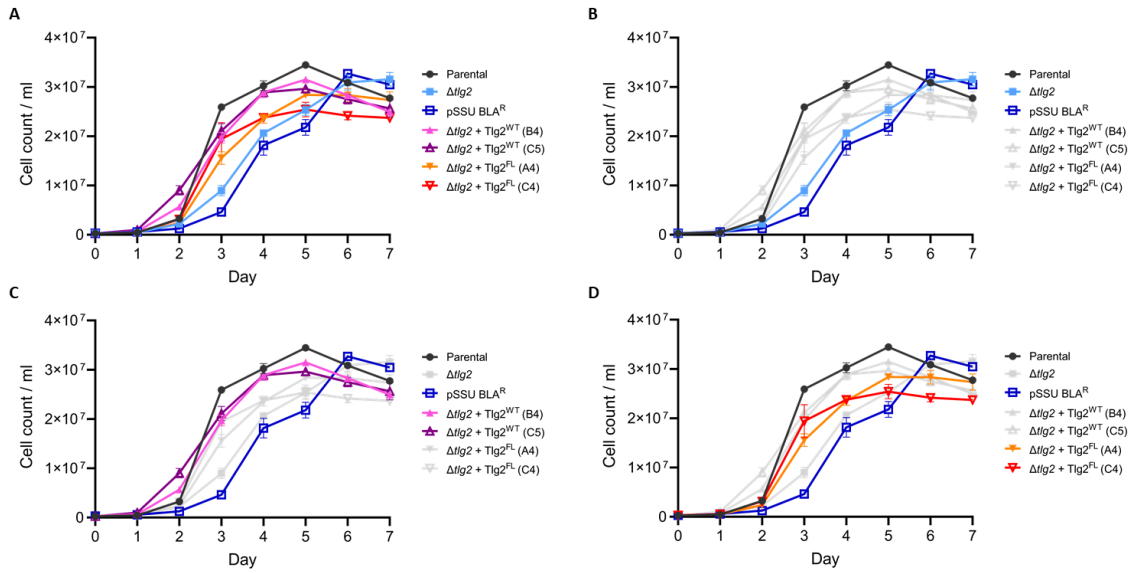

Figure 19. *Growth curves of Tlg2^{WT} and Tlg2^{FL} ectopic expression addback cell lines. L. mexicana* promatigotes for each clone were diluted to an initial density of 2 x 10^5, then counted daily. Growth curves constructed from the cell count data (n = 3, error bars = std dev from mean) showing **A.** All cell lines **B** Parental and null mutant cell lines (*tlg2*Δ and pSSU BLA^R). **C.** and **D.** Growth curves of Tlg2^{WT} and Tlg2^{FL} addback clones compared to the parental and empty vector expressing (pSSU BLA^R) cell lines.

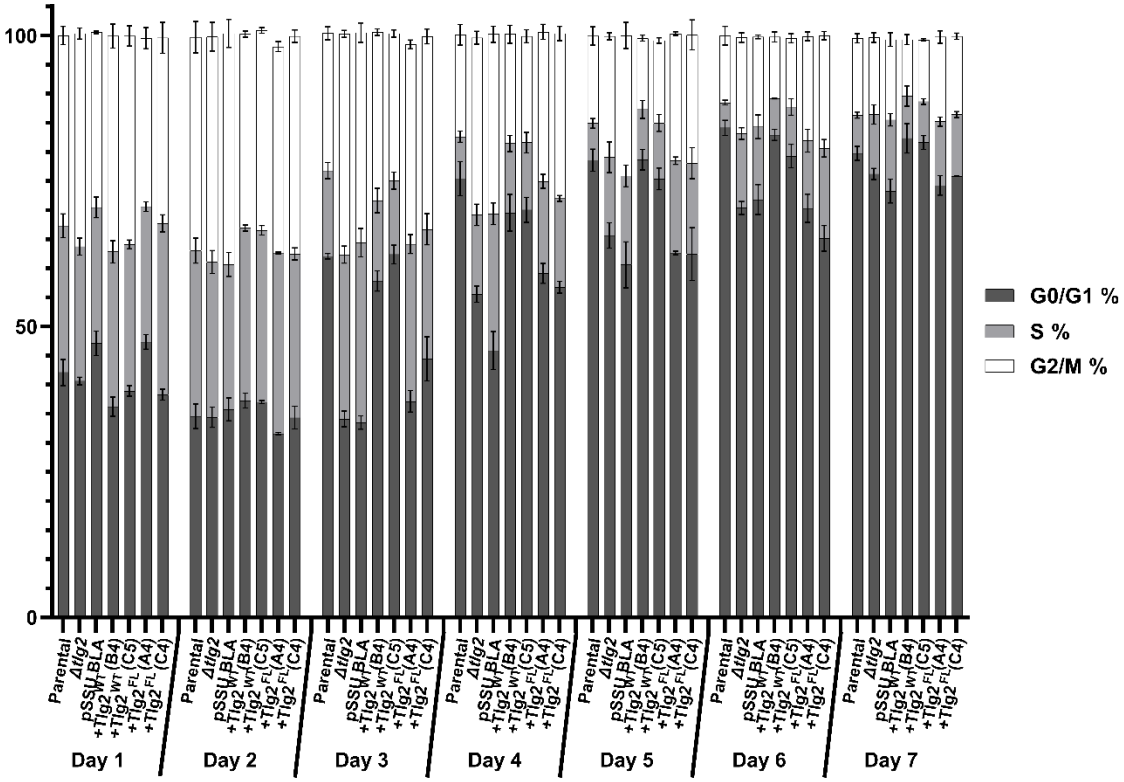

Figure 20. *Cell cycle proportions of the Tlg2^{WT} and Tlg2^{FL} addback cell lines.* Cells were harvested daily, fixed with methanol and incubated with PI before being analysed by flow cytometry. Data were gated to only include single events and cell cycle histograms analysed using the PE-Cy5 channel to determine the percentage of cells in G0/G1, S and G2/M phases. n = 3, error bars = std dev from mean.

4.2.4 Expression of the Tlg2^{WT} and Tlg2^{FL} addback proteins

As the addback proteins had been engineered to include a C-terminal HA tag, this was utilised to determine the levels and pattern of protein expression, to ascertain whether there were any differences that could account for why the wild-type but not the F10A/L11A mutant was able to rescue the *tlg2*Δ phenotype. Protein samples were collected daily and anti-HA western blots were performed. Fig. 21 clearly demonstrates that the expression of Tlg2^{WT} was substantially stronger than Tlg2^{FL}, a factor that may have played a role in the apparent inability of tlg2$_{F10A/L11A}$ to rescue the null mutant phenotypes. As was the case with the *L. mexicana* promastigotes that overexpressed Tlg2^{WT} in a wild-type background (section 3.2.4), the ectopic expression of Tlg2^{WT} in a null mutant background was most strong when the promastigotes were in logarithmic growth, with a subsequent decrease when cells entered the stationary phase.

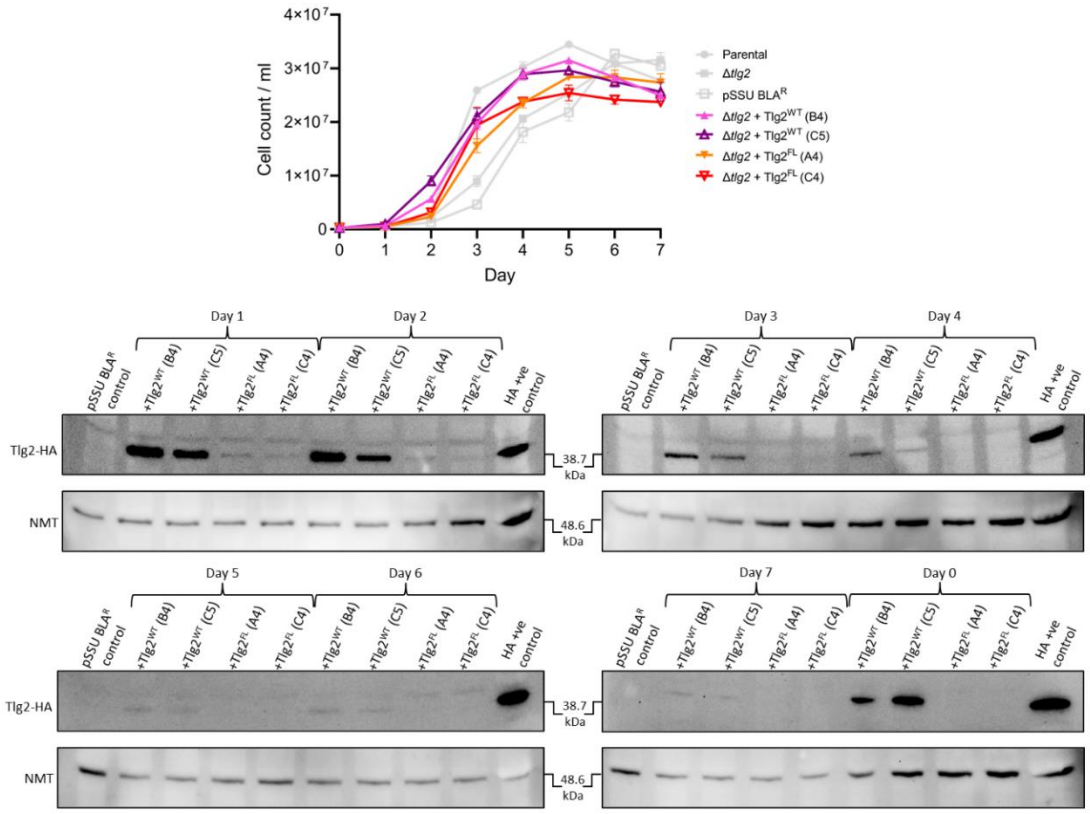

Figure 21. *Expression patterns of Tlg2^{WT}-HA and Tlg2^{FL}-HA addbacks into tlg2Δ promastigotes.* Protein samples were collected from *L. mexicana tlg2*Δ promastigotes that had been transfected with a plasmid vector expressing either Tlg2^{WT}-HA or the Tlg2^{FL}-HA mutant. An anti-HA western blot against the C-terminal HA tag was performed. Two control cell lines were also run alongside the addbacks; the *L. mexicana* pSSU BLA^{R} was used as an HA-negative control and *L. mexicana* ectopically overexpressing Tlg2^{WT}-HA as an HA-positive control. Anti-NMT was used as a sample loading control. The growth curve represents what stage of growth the cells were at when the protein samples were collected.

4.2.5 Quantitative PCR analysis of *TLG2* and the procyclic/metacyclic markers

As Fig. 21 demonstrated the variable levels of protein expression between the Tlg2^{WT} and Tlg2^{FL} addback cell lines, a quantitative PCR (qPCR) strategy was employed to ascertain if there were any differences in the relative *TLG2* mRNA levels. This was also an opportunity to investigate markers of the procyclic and metacyclic stages of the promastigote lifecycle, to determine whether changes in Tlg2 availability have an impact on differentiation. Primers were designed to amplify a short internal section (70 – 100bp) of *TLG2*, *Histone H4* (a procyclic promastigote marker (de Pablos et al., 2019)) and *SHERP* (a metacyclic promastigote marker (Giraud et al., 2019; Knuepfer et al., 2001)), along with a constitutively expressed *NMT* reference gene (Price et al., 2003). To test the primer efficiencies, a qPCR was run using a serial 10-fold dilution of an *L. mexicana* positive control cDNA sample and the percentage efficiencies calculated. All fell within the acceptable range of 90 – 110%. The specificity of the primers was then determined by running a melt curve analysis. All primers had a clear main peak, however *Histone H4*, *SHERP* and *NMT* had a small second peak that was likely to be the result of primer-dimers. To counter this issue, an additional step was included in the qPCR protocol, whereby fluorescence capture of the DNA-binding dye was performed at a temperature above the primer-dimer peaks, but below that of the main amplicon peaks.

To perform the qPCRs, RNA was harvested from *L. mexicana* promastigotes on a daily basis, purified, DNase treated and then converted into cDNA via random hexamer reverse transcription. The optimised qPCR assay was then run on the samples and the relative levels of *TLG2*, *Histone H4* and *SHERP* were calculated against the *NMT* reference gene (ΔC_t). The $\Delta\Delta C_t$ and expression fold change ($2^{-\Delta\Delta Ct}$) for the genes was then calculated for individual cell lines, using the T7/Cas9 parental as the reference control line, along with the pSSU BLA^{R} and *tlg2*Δ where appropriate. ΔC_t data demonstrate that the levels of *Histone H4* and *TLG2* mRNA remain relatively consistent for all cell lines through days 1 – 5. In contrast, *SHERP* mRNA levels increase over time for all cell lines, although the *tlg2*Δ and pSSU BLA^{R} cell lines show a 24 hour delay (Fig, 22).

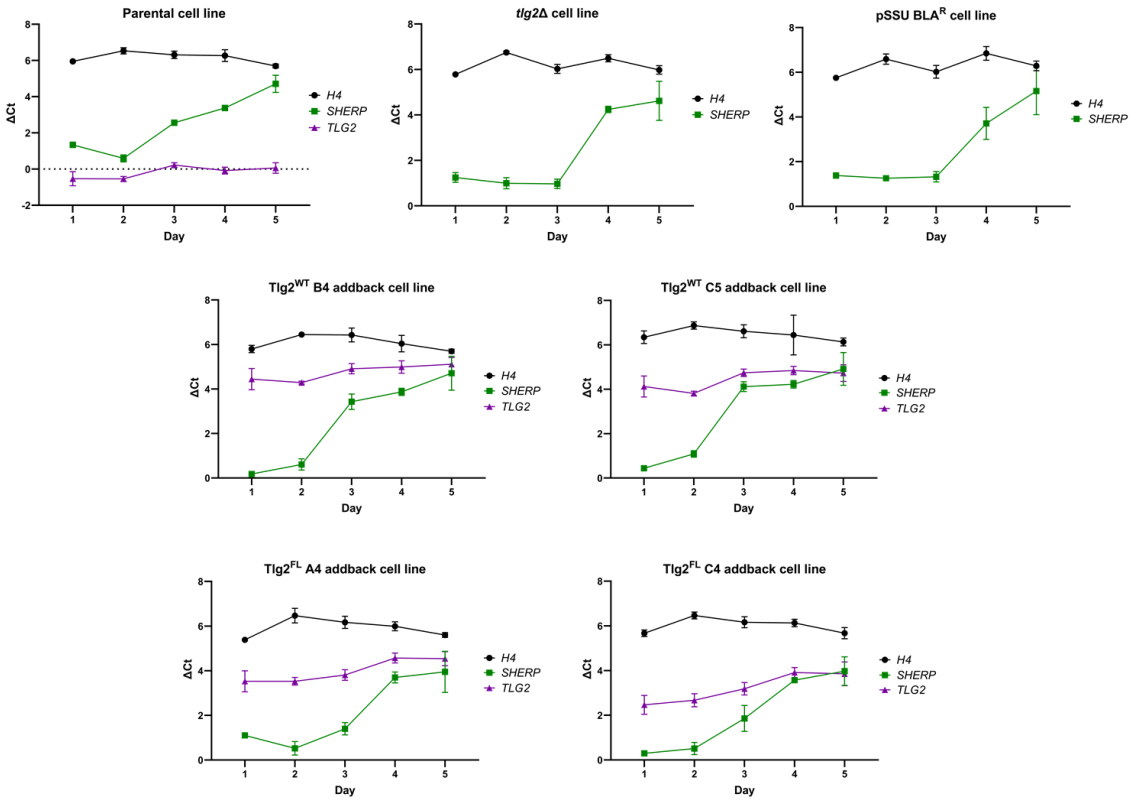

Figure 22. *ΔCt analysis of qPCR data from* L. mexicana *promastigotes.* RNA was extracted from *L. mexicana* promastigotes, Turbo DNase treated and reverse transcribed into cDNA, before being analysed by qPCR. The ΔCt for the parental, *tlg2*Δ, pSSU BLA^{R}, Tlg2^{WT} addback and Tlg2^{FL} addback cell lines was calculated for *Histone H4 (H4)*, *SHERP* and *TLG2* genes against an *NMT* reference gene. For all graphs n = 3, error bars = std dev from mean.

Fig. 23A shows the *TLG2* log fold gene change for the addback cells lines, using the parental as the reference cell line. All the addback cell lines demonstrate greater levels of *TLG2* mRNA than the parental cell line (with fold gene changes ranging from 800 – 3300%). The highest levels of *TLG2* expression were seen in the Tlg2^{WT} B4 clone addback. Statistical analysis across days 1 – 5, using a one-way ANOVA and Tukey's multiple comparisons test, revealed that there was no statistically significant difference in the *TLG2* levels between the two Tlg2^{WT} addback clones (P = 0.0918). However, there were significant differences in *TLG2* levels between the wild-type addback clones and the two Tlg2^{FL} addback clones. In particular, when comparing Tlg2^{WT} B4 clone and Tlg2^{FL} C4 clone, the log fold gene change for *TLG2* was significantly higher for Tlg2^{WT} B4 (P = <0.0001). In contrast, the difference in the *TLG2* log fold gene changes between Tlg2^{WT} C5 clone and Tlg2^{FL} A4 clones was only moderately significant, with a P value of 0.008.

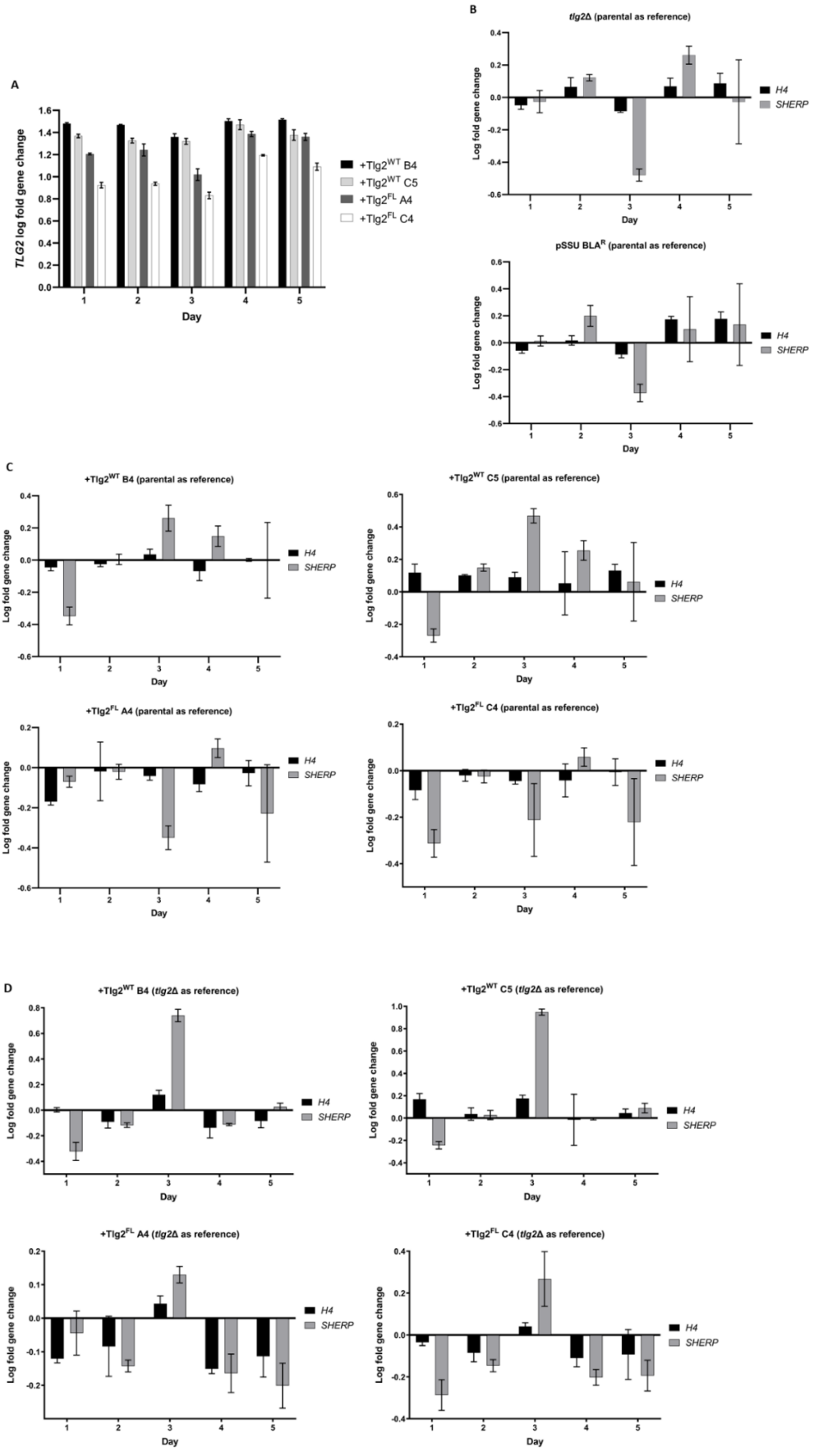
A
TLG2 log fold gene change
Day
+Tlg2WT B4
+Tlg2WT C5
+Tlg2FL A4
+Tlg2FL C4
B
tlg2Δ (parental as reference)
pSSU BLAR (parental as reference)
Log fold gene change
H4
SHERP
C
+Tlg2WT B4 (parental as reference)
+Tlg2WT C5 (parental as reference)
+Tlg2FL A4 (parental as reference)
+Tlg2FL C4 (parental as reference)
D
+Tlg2WT B4 (tlg2Δ as reference)
+Tlg2WT C5 (tlg2Δ as reference)
+Tlg2FL A4 (tlg2Δ as reference)
+Tlg2FL C4 (tlg2Δ as reference)

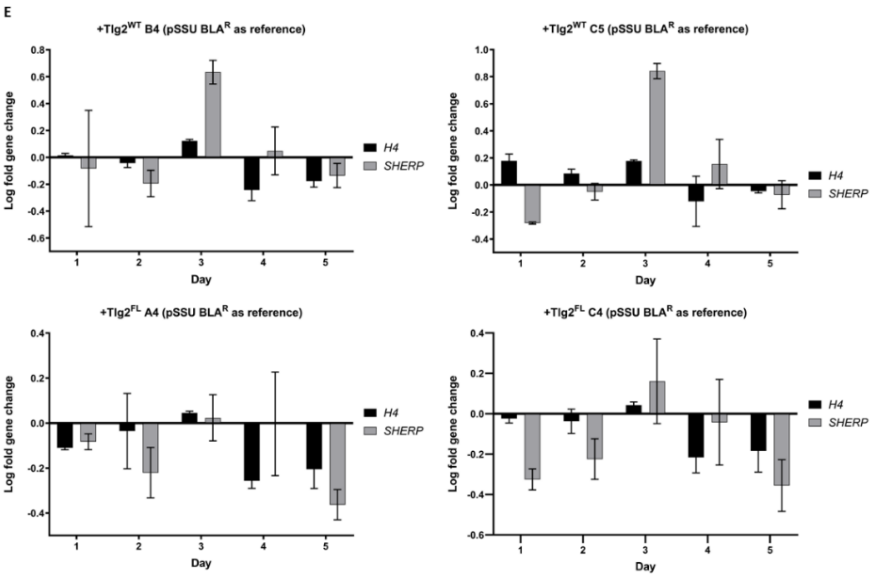

Figure 23. *qPCR gene expression analysis for* TLG2, Histone H4 *(*H4*) and* SHERP *in null mutant and addback* L. mexicana *promastigotes.* **A.** Log fold gene change for *TLG2* transcripts in addback cell lines, using the parental (T7/Cas9) as the reference control line. **B.** Log fold gene change for *H4* and *SHERP* in null mutant cell lines (*tlg2*Δ and pSSU BLA^R) with the parental as the reference control line. **C.** Log fold gene change for *H4* and *SHERP* in addback cell lines, compared to the parental cell line. **D.** Log fold gene change for *H4* and *SHERP* in addback cell lines, compared to the *tlg2*Δ cell line. **E.** Log fold gene change for *H4* and *SHERP* in addback cell lines, compared to the pSSU BLA^R cell line. For all graphs n = 3, error bars = std dev from mean.

When looking at the procyclic and metacyclic markers across the different cell lines, an interesting pattern emerges. Fig. 23B demonstrates that when Tlg2 is not present in *L. mexicana* promastigotes, there is a decrease in *SHERP* mRNA expression on day 3, with log fold gene changes of -0.479 and -0.373 for the *tlg2*Δ and pSSU BLA^R populations (which equates to decreases of 66% and 57% respectively). In contrast, addback of the Tlg2^{WT} results in greater expression (200 – 300%) of *SHERP* compared to the parental line on day 3 (Fig. 23C). As the mRNA levels of *TLG2* are higher in the addbacks than the parental population (as evidenced in Fig. 23A), this could suggest that ectopic overexpression of Tlg2^{WT} leads to increases in *SHERP* mRNA levels. This phenomenon is not witnessed with addback of the Tlg2^{FL}, which instead appears similar to the null mutants in that *SHERP* levels are lower than the parental cell line on day 3 (Fig. 23C).

Statistical analysis (one-way ANOVA) of *SHERP* log fold gene changes (when measured against the parental cell line) on day 3 reveal highly significant differences between cell lines (P = <0.0001). More comprehensive analysis using Tukey's multiple comparisons test showed that there were highly significant differences in *SHERP* levels for the Tlg2^{WT} addbacks versus the

Tlg2^{FL} addbacks and the *tlg2*Δ and pSSU BLA^{R} null mutants (P = <0.0002). Overall, the null mutants and Tlg2^{FL} addbacks showed no significant differences in *SHERP* levels, except for a moderately significant difference between *tlg2Δ* and the Tlg2^{FL} C4 addback clone (P = 0.0197).

When measuring the log fold gene change in *SHERP* in the Tlg2^{WT} addback clones against the *tlg2*Δ and pSSU BLA^{R} empty vector control cell lines, the differences on day 3 are even more apparent. Ectopic expression of Tlg2^{WT} led to *SHERP* log fold gene changes between 0.740 and 0.948 (550 – 880% increases) compared to *tlg2*Δ (Fig. 23D) and 0.634 and 0.842 (430 – 690% increases) compared to the pSSU BLA^{R} (Fig 23E). There was a moderate increase in *SHERP* for the Tlg2^{FL} addback clones compared to the *tlg2*Δ cell line, with log fold gene changes between 0.130 and 0.267 (135 – 190% increases) (Fig. 23D). No such difference was seen when comparing Tlg2^{FL} addback clones to the pSSU BLA^{R} empty vector null mutant (Fig 23E).

4.3 Discussion

4.3.1 Generation of null mutants and the resultant phenotypes

The fact that null mutants for both Tlg2 and Vps45a were able to be generated using CRISPR/Cas9 demonstrates that these genes are non-essential for *L. mexicana* promastigotes. However, the initial round of transfections for Tlg2 failed and the subsequent round only resulted in one null mutant clone (Fig. 14). In contrast, several null mutant clones were recovered for Vps45a on the first round of transfection. This raises question marks over how the *tlg2*Δ clone was able to survive, and with only moderately severe phenotypes, and suggests that compensatory mutations may have taken place to promote cell viability. Analysis of the Illumina sequencing of the *tlg2*Δ clone was able to confirm that the CRISPR/Cas9 method had been successful in targeting and knocking out the *TLG2* gene (Fig. 15). It also highlighted the presence of almost 80 SNPs in CDS gene region that were deemed could have a moderate effect (Appendix 3). Although some of these SNPS may be the product of random mutagenesis, it is also possible that they arose as a result of *tlg2* deletion to try and compensate for any loss of fitness. Although these mutations may be, at best, only partially compensatory, as *tlg2*Δ promastigotes still display growth and morphological phenotypes, future investigation might lend insight into relevant pathways to promote parasite survival when there is an absence of Tlg2.

Subsequent analysis of the *tlg2*Δ and *vps45a*Δ clones revealed that, whilst deletion of *vps45a* had a slight impact on the growth of *L. mexicana* promastigotes, removal of *tlg2* lead to a much more significant replication phenotype (Fig. 16). This result was somewhat surprising, as in yeast removal of Vps45 leads to defects in vacuolar protein sorting, slower growth rates and

ablation of growth at temperatures above 38°C (Cowles et al., 1994; Piper et al., 1994; Shanks et al., 2012). In humans, mutations in Vps45 disrupt endosomal intracellular protein trafficking, increase apoptosis and can lead to congenital neutropenia, bone marrow fibrosis and nephromegaly in infants (Stepensky et al., 2013; Vilboux et al., 2013). Additionally, Vps45 is known to stabilise the levels of Tlg2 in yeast (Bryant & James, 2001). Knockout of Vps45 would therefore be expected to result in a concomitant decrease in cellular Tlg2 levels (Shanks et al., 2012), and all associated phenotypes. A potential explanation for why this was not the case in *L. mexicana* is that the presence of two Vps45 homologues may result in some functional redundancy, whereby either or both are able to fulfil the vacuolar protein sorting and Tlg2-stabilising roles. Development of *vps45b*Δ and *vps45a*Δ*/vps45b*Δ mutants would help to identify whether one protein plays a more important role or if knockout of both is required to ablate protein function.

The growth curve of *tlg2*Δ (Fig. 16B) demonstrates that the promastigotes grow significantly more slowly than both the T7/Cas9 parental and *vps45a*Δ cell lines. This is particularly apparent on days 1 – 3, where the difference in cell counts is highly significant. Interestingly, this correlates to when the wild-type Tlg2 protein is most highly expressed, according to the expression profiles of the Tlg2 addback clones (Fig. 21). In addition to growth phenotypes, *tlg2*Δ promastigotes show defects in their cell cycle, with the population maintaining a profile that is akin to parasites in the early log-phase of growth (a high percentage of cells in the G2/M stage) beyond what is witnessed for the parental cell line (Fig. 17). *tlg2*Δ promastigotes are also morphologically distinct from both parental and *vps45a*Δ populations on day 4, with shorter and rounder cells bodies (Fig. 18). This morphology more closely resembles early log-phase promastigotes and those cells that are undergoing the S and G2/M stages of the cell cycle (Wheeler et al., 2011). Taken together this data suggests that deletion of Tlg2 leads to a prolonged and slower growing procyclic promastigote stage and delayed entry into the stationary phase, demonstrated by the eventual plateau of the *tlg2*Δ growth curve on day 7 and the morphology of the cells being indistinguishable from the parental cell line on day 8. These results are consistent with what is witnessed in other organisms, with deletion of Tlg2 and Vps45 leading to slow growth (Shanks et al., 2012; Struthers et al., 2009), and could be due to disruptions in the endocytic and autophagy pathways caused by loss of Tlg2. Unfortunately, attempts to use the lipophilic marker FM4-64 as an endocytic tracer were unsuccessful and so qualification of any endocytic defects in the null mutants cannot be presented here. This would therefore be an interesting area for future study, to confirm whether the endocytic defects witnessed in other organisms in the absence of Tlg2 are also present in *Leishmania.*

An alternative explanation for the reduced cell counts of *tlg2*Δ could be due to increased levels of cell death, with the more rounded and shorter morphology occurring due to an apoptosis-like response (Paris et al., 2004; van Zandbergen et al., 2006). Contradicting this argument, the flow cytometry data presented in Fig. 17A does not support this theory as there was no evidence of DNA fragmentation occurring, a hallmark of apoptosis-like cell death in *Leishmania* (Basmaciyan & Casanova, 2019). Further research could help to elucidate whether Tlg2 deletion plays a role in cell death, with use of viability stains such as trypan blue or measurement of apoptosis/necrosis markers, such as calcein and PI, via flow cytometry (Basmaciyan et al., 2017).

4.3.2 The rescue of *tlg2*Δ using an addback strategy

To try and address whether the phenotypes witnessed in the single *tlg2*Δ clone were the result of targeted deletion of Tlg2 or due to off-target events, an addback strategy was conceived. This strategy would serve dual purposes; firstly, to confirm the specificity of the CRISPR/Cas9 method with wild-type Tlg2 rescue and secondly, to determine whether a Tlg2 containing a double mutation (F10A/L11A) in the N-terminus rescues the null mutant phenotypes. Data from Fig. 19C and Fig. 20 demonstrate that ectopic expression of $Tlg2^{WT}$ into the null mutant cells resulted in a restoration of the growth curve and cell cycle to levels comparable to the parental cell line. The slight difference between the growth curves of the $Tlg2^{WT}$ addback clones and the parental cell line could be due to the fact that the addback clones, but not the parental line, were grown under drug selection to prevent loss of the addback plasmid, which may confer a small loss of fitness. A similar difference is also observed between *tlg2*Δ and the pSSU BLA^R null mutant control line (Fig. 19B), with pSSU BLA^R, which was grown under drug selection, displaying a slightly slower growth rate. Evidence has demonstrated that development of resistance against certain drugs, such as miltefosine, can have a negative impact on parasite fitness in the *L. infantum* species (Hendrickx et al., 2016; van Bockstal et al., 2019). It is therefore possible that the presence of an ectopically expressed drug resistance gene could partially impair promastigote cell growth.

The ability of $Tlg2^{WT}$ addback to rescue the null mutant supports the conclusion that the phenotypes were a result of Tlg2 deletion and not because of off-target genetic modifications. In contrast to wild-type Tlg2, addback of $Tlg2^{FL}$ is unable to rescue the null mutant. Although there appears to be a slight improvement in the growth curve compared to the pSSU BLA^R (Fig. 19D), which suggests that $Tlg2^{FL}$ has some functionality in restoring the growth phenotype, when looking at the cell cycle data the $Tlg2^{FL}$ addback clones fare no better than the null mutants (Fig. 20). A possibility for why $Tlg2^{FL}$ appears incapable of rescuing the null mutant

can be seen in Fig. 21. Western blots against the C-terminal HA tags of the Tlg2^{WT} addback proteins demonstrate strong levels of expression for both clones whilst the cells are logarithmic. The mutant addback clones, on the other hand, show much lower levels of ectopic Tlg2^{FL} expression, with the protein becoming undetectable from day 4 onwards. This difference in expression levels could potentially account for the apparent inability of Tlg2^{FL} to rescue the null mutant. Perhaps the cellular levels of the Tlg2^{FL} protein may be insufficient to fully rescue functionality.

To try and understand this distinction in Tlg2^{WT} and Tlg2^{FL} ectopic expression further, the relative *TLG2* mRNA levels for the addback cell lines were measured against the parental cell line using qPCR. Fig. 23A shows that the log fold gene changes for *TLG2* were highest for the addback cell lines ectopically expressing Tlg2^{WT} and were, when taken as a whole, significantly higher than the relative *TLG2* levels in the Tlg2^{FL} addback clones. This could, in turn, be reflected in the protein levels. However, when looking at the individual clonal cell lines, the relative expression of *TLG2* mRNA in the Tlg2^{FL} A4 clone more closely matches the relative expression of *TLG2* in the Tlg2^{WT} C5 clone (Fig. 23A). This is particularly apparent on days 2, 4 and 5 and suggests that an additional mechanism is regulating the expression of the Tlg2^{FL} protein.

For all the ectopic Tlg2 addback cell lines, gene expression levels of *TLG2* mRNA are several magnitudes higher than the endogenous levels seen in the parental cell line. If translation is non-selective, this would provide the cells with more than sufficient amounts of protein to restore functionality. This may suggest that the F10A/L11A mutations themselves abrogate the expression or function of Tlg2. This could happen either through post-transcriptional regulation preventing Tlg2^{FL} protein translation, or, as is seen in other organisms, by the F10A/L11A mutations disrupting high-affinity binding to Vps45 (Dulubova et al., 2002). Although studies in yeast have demonstrated that Tlg2 lacking the N-terminus are still functionally viable and able to bind to Vps45 through alternative sites (Furgason et al., 2009), the N-terminus is important in stabilising cellular levels of Tlg2. Disruption of the high-affinity binding between the Tlg2 N-terminus and the hydrophobic pocket on domain I of the Vps45 prevents Vps45 from stabilising Tlg2 and leads to a decrease in protein levels within the cell (Carpp et al., 2007; Shanks et al., 2012). The presence of the F10/L11 residues and overall high conservation of the N-terminal motif in *L. mexicana* Tlg2 suggests a potential conservation of function and an equivalent N-terminal mode of binding to Vps45. The inability of endogenous Vps45 to stabilise Tlg2^{FL} could potentially explain why protein levels in the addback clones are lower than Tlg2^{WT} (Fig. 21) and why only a partial rescue of the growth defect was achieved. In future studies, *in vitro* binding assays and structural analysis using recombinantly expressed proteins could help to solve the

interactions between Tlg2 and Vps45 and demonstrate whether, like in yeast, multiple modes of binding exist. The differences in protein expression levels between $Tlg2^{WT}$ and $Tlg2^{FL}$ addback cell lines also have the potential to impact downstream experiments. For example, changes in protein localisation as a result of functional disruption may be difficult to detect when protein expression is low. With the low protein levels seen in $Tlg2^{FL}$, this could make localisation comparisons to $Tlg2^{WT}$ difficult. The low levels of $Tlg2^{FL}$ could also present difficulties in experiments where significant amounts of protein is required, such as for immunoprecipitation and *in vivo* binding assays, due to the need to produce, store and harvest large volumes of cellular culture.

4.3.3 Tlg2 and the molecular lifecycle markers

qPCR analysis of procyclic and metacyclic molecular markers in null mutant and addback cell lines demonstrated an interesting pattern. The levels of *SHERP* (a metacyclic marker) varied on day 3 in a Tlg2-level dependant manner. In the *tlg2*Δ, pSSU BLA^{R} and $Tlg2^{FL}$ addback populations there was a decrease in the *SHERP* expression levels compared to the parental line (Fig. 23B & 23C). In contrast, the $Tlg2^{WT}$ addback clones, which had higher-than-endogenous levels of *TLG2* mRNA, displayed an increase in *SHERP* on day 3. This data potentially demonstrates that cellular levels of Tlg2 are able to impact gene expression markers of metacyclogenesis. This may point to a possible role for Tlg2 in parasite differentiation, whereby overexpression of the wild-type protein prompts the promastigotes to undergo earlier metacyclogenesis, therefore stimulating earlier expression of the *SHERP* gene. In contrast, reduction of Tlg2 appears to delay the expression of *SHERP* (Fig. 22) and may subsequently impact initiation of metacyclogenesis. Although SHERP is known as a marker of metacyclic promastigotes, previous research has demonstrated that expression of this protein can be seen at low levels from day 3 in *L. major* promastigotes (Sádlová et al., 2010), so changes to the gene expression could also be reflected at the protein level. As Tlg2 is known to be involved in autophagy, this result is not unexpected, as autophagy plays a key role in the ability of *Leishmania* parasites to differentiate into the mammalian infective metacyclic form (Besteiro et al., 2006). Deletion of Tlg2 could lead to a subsequent decrease in autophagy and consequently delay or reduce the ability of promastigotes to differentiate.

As there may not be a direct correlation between the amount of *TLG2* and *SHERP* mRNA and the levels of protein expression, caution should be taken when interpreting these results. Previous research has highlighted that there is a low correlation between mRNA transcripts and corresponding protein expression in *L. mexicana* (de Pablos et al., 2019). This has already been demonstrated by Tlg2, where the mRNA *TLG2* levels remain relatively consistent in the $Tlg2^{WT}$

addback cell lines across days 1 – 5 (Fig. 22) yet display a very distinct expression pattern in logarithmic promastigotes (Fig. 21). Although it is encouraging that variations in *SHERP* on day 3 appear to be Tlg2-level dependant and that *SHERP* transcript levels increase as the cells grow towards the stationary phase, it is important not to conflate the mRNA transcript levels with protein expression levels. Additionally, as the function of SHERP is not yet known, caution should be taken when it is being utilised as a measure of metacyclogenesis, as it is possible that changes in transcription or expression could be due to disruption of pathways unrelated to autophagy or differentiation. A better understanding of the impact of modifying cellular Tlg2 levels on parasite differentiation could therefore be achieved by the analysis of SHERP protein levels alongside other markers of metacyclogenesis, such as sensitivity to complement killing in human serum and morphological measurements (Franke et al., 1985; Giraud et al., 2019; Sádlová et al., 2010).

Chapter 5 – Further investigation of Tlg2 and identification of *in vivo* binding partners

5.1 Introduction

5.1.1 The localisation of Tlg2

Tlg2 is known to be an endosomal SNARE and part of the TGN. Tlg2 mediates fusion between the late Golgi and endosomes and can localise to both membranes. When visualising GFP-Tlg2 with fluorescence microscopy in yeast, there is typically a punctate distribution that corresponds to the endocytic structures (Abeliovich et al., 1998). A similar pattern is seen in kinetoplastids. The *T. brucei* Tlg2 homologue (Tb927.9.13030) was tagged as part of a TrypTag online resource to determine the localisation of all proteins expressed by *T. brucei* and shows a punctate distribution, much like what has been observed in the related *L. major* parasite (Dean et al., 2017; Besteiro et al., 2006). One aspect of the Tlg2 localisation in *L. major* is that there was a strong protein signal at the anterior end of the cell, close to the kinetoplast, which is also where the Golgi apparatus resides (Halliday et al., 2019). Interestingly, co-localisation with a *T. brucei* derived Rab1 Golgi apparatus marker displayed a close, but not-overlapping signal, which suggests that either the Tlg2 was not localised to the Golgi, or that the Rab1 marker used did not encompass the entire organelle (Besteiro et al., 2006). In contrast, a similar study in *T. brucei* did show Tlg2 co-localising with the Golgi apparatus, which indicates a possible conservation of function (Murungi et al., 2014). This chapter describes the use of fluorescent antibodies to visualise the HA-tagged Tlg2 protein within the *L. mexicana* promastigotes to ascertain its localisation within the cell.

5.1.2 Differentiation and autophagy in *Leishmania*

Due to their digenetic lifecycle, differentiation plays a vital role in *Leishmania* parasites and their ability to adapt their morphology and function to survive in the extracellular sandfly or intracellular mammalian environments (de Pablos et al., 2016; Gossage et al., 2003). In the promastigote sandfly stages of the lifecycle, differentiation is essential for the parasites to morph into the mammalian-infective metacyclic promastigote form. Autophagy is one of the processes that controls differentiation. It has been demonstrated that disruption of autophagy prevents *Leishmania* promastigotes from undergoing metacyclogenesis and, consequently, the parasites are less infective and virulent (Besteiro et al., 2006). As deletion of Tlg2 results in a significant reduction in autophagy in yeast (Nair et al., 2011), it was predicted that *tlg2*Δ *L. mexicana* might also display reduced autophagy, which would in turn impact parasite

differentiation, infectivity and virulence. A commonly used marker for autophagy is the Atg8 protein. Atg8 is typically detected via western blot in two forms, an unconjugated and a phosphatidylethanolamine (PE) conjugated form that is reliably associated with completed autophagosomes (Giri & Shaha, 2019; Klionsky et al., 2008). This chapter describes a macrophage infectivity assay utilising the T7/Cas9 parental, *tlg2*Δ and ectopic expression 'addback' cell lines. Additionally, this chapter details testing of an *L. major* anti-Atg8 antibody to highlight any differences in expression between the parental and *tlg2*Δ cell lines.

5.1.3 The use of co-immunoprecipitation to determine binding partners

Co-immunoprecipitation (Co-IP) assays are commonly used to identify protein associations *in vivo*. Traditionally, Co-IPs were performed by incubating cell lysates with an antibody raised against a specific protein or tag, which is then captured by antibody-binding proteins, such as Protein G or A, immobilised to beads. Washing of these beads removes any proteins not bound and elution of the target protein from the beads then allows identification of any proteins that co-elute, and thus associate, with the target protein (Phizicky & Fields, 1995). These interactions can be via direct or indirect binding with the targeted protein, or as a result of a protein complex. A more streamlined approach to Co-IP utilises the addition of an epitope tag, such as 3 x HA, to the N- or C-terminus of the target protein, which, along with its interacting proteins, can be directly immunoprecipitated by magnetic beads coated in anti-HA antibodies (Lim et al., 2021). This chapter covers the use of the Tlg2^{WT}-HA and Tlg2^{FL}-HA ectopic *L. mexicana* promastigotes to perform a Co-IP and the resulting analysis to identify interacting partners.

5.1.4 Aims

This chapter aims to visualise the subcellular localisation of Tlg2 in log-phase *L. mexicana* promastigotes via fluorescence microscopy and determine whether, as predicted, there is a similar pattern to what is witnessed in yeast and related kinetoplastids. Furthermore, it was hypothesised that deletion of *tlg2* in *L. mexicana* would lead to reduced infectivity or virulence of the promastigotes, due to Tlg2's predicted role in autophagy and differentiation. This chapter aims to test this hypothesis by using a macrophage infection assay. Furthermore, expression of either Tlg2^{WT} or Tlg2^{FL} ectopic protein in *tlg2* null cell lines will lend insight into whether either protein can rescue phenotypes of the null mutant. Western blots using an *L. major*-derived anti-Atg8 antibody will allow examination of whether Atg8 protein levels respond to Tlg2 levels and determine if both the conjugated and unconjugated forms of Atg8 can be detected. Finally, Co-IP experiments aim to characterise the *in vivo* interactors of Tlg2 and establish if different

proteins associate with the Tlg2^{WT} versus Tlg2^{FL} proteins, which may be expected, given the reduced functionality of Tlg2^{FL}.

5.2 Results

5.2.1 Localisation of Tlg2^{WT} and Tlg2^{FL} in *L. mexicana*

To try and characterise the proteins *in vivo*, the localisation of Tlg2^{WT}-HA and Tlg2^{FL}-HA were determined by fluorescence microscopy. Briefly, *tlg2*Δ *L. mexicana* promastigotes transfected with the Tlg2^{WT}-HA or Tlg2^{FL} encoding plasmids were harvested two days after dilution to an initial density of 2 x 10^5, as this is when the Tlg2 protein has been shown to be most expressed. These cells were fixed in PFA and then treated with Triton X-100 and glycine (to permeabilise the cell membranes and quench autofluorescing aldehydes, respectively). The cells were then incubated with an anti-HA monoclonal primary antibody (Sigma), to visualise the C-terminal HA tag of the ectopic Tlg2 proteins, followed by an Alexa Fluor 488 secondary antibody (Thermo Fisher Scientific). Finally, the cells were mounted in VECTASHIELD® Antifade Mounting Medium with DAPI (Vector Laboratories) to stain the nucleus and kinetoplast and examine the subcellular localisation of Tlg2^{WT} and Tlg2^{FL}.

In line with protein expression of the addback clones (Section 4.2.4), the fluorescence signal for Tlg2^{FL} was noticeably weaker than the wild-type Tlg2 (Fig. 24). Both proteins display a distinct signal close to the kinetoplast, which, as Tlg2 is known to be a Golgi-associated Qa-SNARE, could therefore correspond to this organelle. Fig. 24A demonstrates that for Tlg2^{WT}, as well as the strong signal close to the kinetoplast, there often appeared to be a diffuse pattern throughout the rest of the cytoplasm. When looking at the cells under a confocal microscope (Fig. 24D), this pattern appeared dotted, with varying numbers of puncta throughout the cytosol, which may represent Tlg2 on the membrane of vesicles within the endocytic pathway. In line with the fluorescent microscopy images, the strongest signal was frequently located next to the kinetoplast. In contrast, the Tlg2^{FL} did not appear dotted throughout the cells, with only a single detectable punctum next to the kinetoplast (Fig. 24B & Fig. 24E). To ensure that non-specific binding of the anti-HA antibody could not account for the apparent distributions of Tlg2^{WT}-HA or Tlg2^{FL}-HA proteins, the parental cell line was also incubated with the anti-HA primary and Alexa Fluor 488 secondary antibodies. Additional controls included Tlg2^{WT}-HA or Tlg2^{FL}-HA expressing promastigotes incubated with only the Alexa Fluor 488 secondary, which would highlight if the secondary antibody induced non-specific binding. All controls demonstrated very low background signals (Fig. 24C) that did not correspond to the distributions of Tlg2^{WT}-HA or Tlg2^{FL}-HA seen in Fig. 24A or 24B.

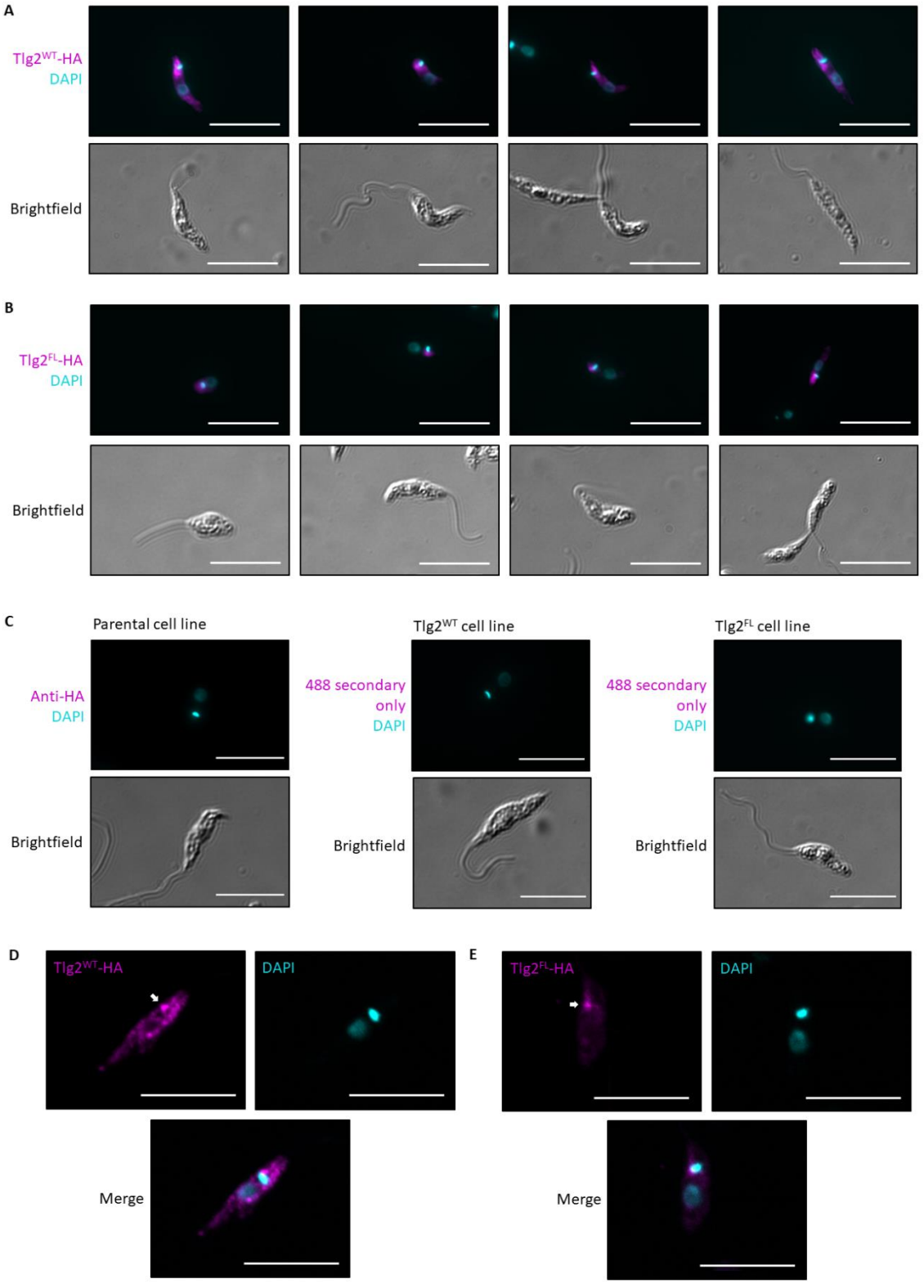

Figure 24. *Localisation of Tlg2^{WT} and Tlg2^{FL} in* L. mexicana *promastigotes.* Cells were diluted to a density of 2 x 10^5 and left to grow for two days before harvesting and fixing. Cells were incubated with an anti-HA primary monoclonal antibody, followed by an Alexa Fluor 488

secondary antibody, with the nucleus and kinetoplast stained by DAPI. **A.** Panels display various promastigotes expressing the Tlg2^{WT}-HA protein, visualised under a fluorescent microscope at x1000 magnification. **B.** Panels display various promastigotes expressing the Tlg2^{FL}-HA protein, visualised under a fluorescent microscope at x1000 magnification. **C.** Images for parental control cell line incubated with anti-HA primary and Alexa Fluor 488 secondary antibodies, along with Tlg2^{WT} and Tlg2^{FL} expressing promastigotes incubated only with Alexa Fluor 488 secondary antibody. **D.** A representative promastigote of the Tlg2^{WT}-HA expression pattern visualised using confocal microscopy. **E.** A representative promastigote of the Tlg2^{FL}-HA expression pattern visualised using confocal microscopy. Scale bars represent 10µm. The white arrows point to the predominant fluorescent signal located close to the kinetoplast.

5.2.2 The role of Tlg2 in *Leishmania* infectivity and virulence

To investigate whether the deletion of Tlg2 had any impact on the infectivity and virulence of *L. mexicana* promastigotes, a macrophage infectivity assay was conducted by Dr. Natalia Teles, of the Walrad laboratory, using the *tlg2*Δ cell line. The ectopic Tlg2^{WT} and Tlg2^{FL} addback cell lines were also included to see if they were able to rescue any potential phenotypes of the null mutant. The parental T7/Cas9 *L. mexicana* cell line was used as the control cell line. To summarise, peritoneal macrophages were harvested from CD-1 mice, resuspended in mammalian cell culture media and left to adhere to wells in a chamber slide for 24 hours. Stationary phase (10 days post-split) *L. mexicana* promastigotes were added to the wells at a 1:1 ratio and left to infect the macrophages over 24 or 72 hours. To visualise the infection status of the macrophages the cells were fixed and stained with Giemsa for the two timepoints. The cells were observed under a light microscope and the infection status of 100 macrophages per well determined.

Fig. 25 demonstrates that at 24 hours post-infection (P.I), there was a high level of infection across all four of the *L. mexicana* cell lines, with the average percentage of infected macrophages ranging from 74 – 86%. When analysing the data using a one-way ANOVA the difference between the cell lines was slightly significant (P = 0.0117). Further analysis using a Dunnett's multiple comparisons test revealed that there was a slight significant difference between the parental cell line and the ectopic Tlg2^{WT}-expressing B4 clone (P = 0.0378). Importantly, after 72 hours P.I only the parental control cell line had maintained the infection. All remaining cell lines had a significant reduction in the levels of macrophage infection (P = <0.0001). This data demonstrates that, although *tlg2*Δ promastigotes are initially able to infect macrophages, they are not able to maintain this infection and display reduced virulence in comparison to the parental promastigotes. Remarkably, both the Tlg2^{WT} and Tlg2^{FL} ectopic 'addback' cell line also displayed the same phenotype as the null mutant at 72 hours P.I. This

suggests an inability to rescue the null mutant in terms of parasite virulence. To try and find a possible explanation for why addback of Tlg2^{WT} did not rescue the virulence phenotype displayed by *tlg2*Δ promastigotes, GO analysis of the 78 moderate effect SNPs identified in the sequencing of *tlg2*Δ clone was conducted (Appendix 4). This analysis identified several proteins with roles in microtubule-based movement, microtubule binding, flagellar motility, flagellar assembly and the ciliary pocket that had undergone moderate missense mutations. Moderate missense mutations were also found in a proteophosphoglycan protein, three amastin-like proteins and an Atg8 protein. The presence of missense mutations has the potential to affect the functionality of these proteins and, consequently, may impact the ability of parasites to infect macrophages, regardless of the presence of Tlg2.

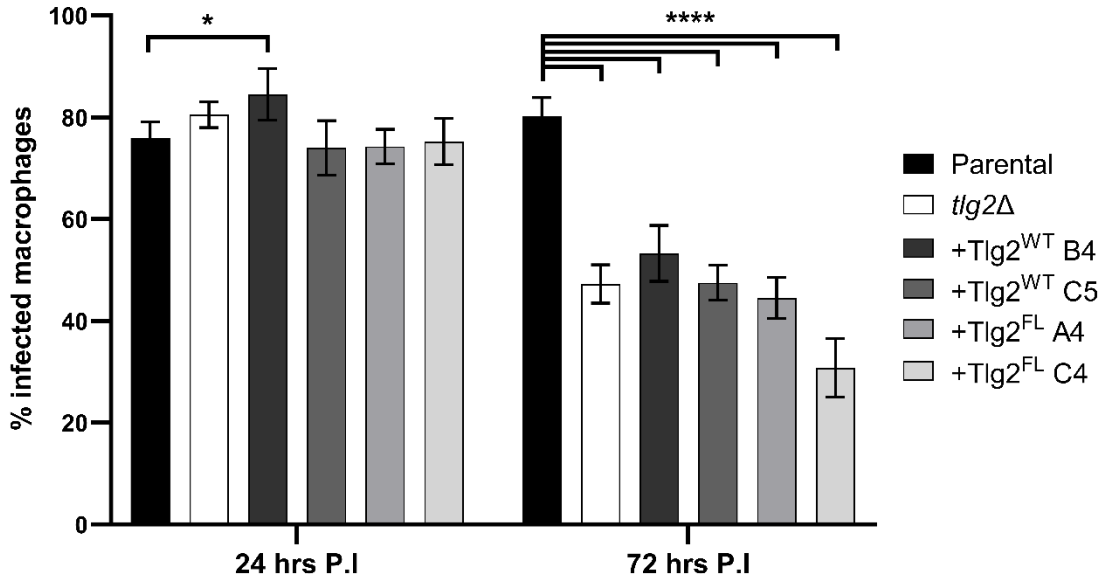

Figure 25. *Macrophage infection assay for* L. mexicana *promastigotes.* Stationary phase promastigotes for parental, *tlg2*Δ, Tlg2^{WT} and Tlg2^{FL} ectopic addback clones were incubated with peritoneal macrophages harvested from mice. The percentage of infected macrophages was calculated at 24 or 72 hours post-infection (P.I). n = 4, error bars = std dev from mean. * = P < 0.05, and **** = P < 0.0001, with the statistical analysis conducted against the parental line.

5.2.3 Detection of Atg8 in *L. mexicana* promastigotes

Given the implicit connection between Tlg2 function and Atg8 expression in other systems, upon discovery of an antibody raised against *L. major* Atg8, we tested its capacity to detect Atg8 in *L. mexicana*. Atg8 expression was examined by western blot using protein samples previously harvested for parental and *tlg2*Δ cell lines across an eight-day time period. Fig. 26

demonstrates that putative Atg8 protein bands were detected for all timepoints at varying levels. In contrast to what has previously been noted in the literature for *Leishmania* species, only one band was visualised for Atg8 between the 10 and 15 kDa size markers, which is in the correct range for predicted sizes of Atg8 protein in *L. mexicana* (~14 kDa). Two bands were seen in *L. donovani* and *L. mexicana* species that correspond to a non-cleaved form of Atg8 (Atg8-I) and a cleaved form, conjugated to phosphatidylethanolamine (Atg8-PE) (Giri & Shaha, 2019; Williams et al., 2012). When the protein expression signals were normalised against the NMT loading control, the increase seen in Atg8 levels on days 1 and 2 for *tlg2*Δ were between 3.5 – 4x higher than the parental cell line. Additionally, on day 7, *tlg2*Δ has more than twice the Atg8 expression of the parental cell line. In contrast, the expression of Atg8 in the parental cell line is consistent across all days.

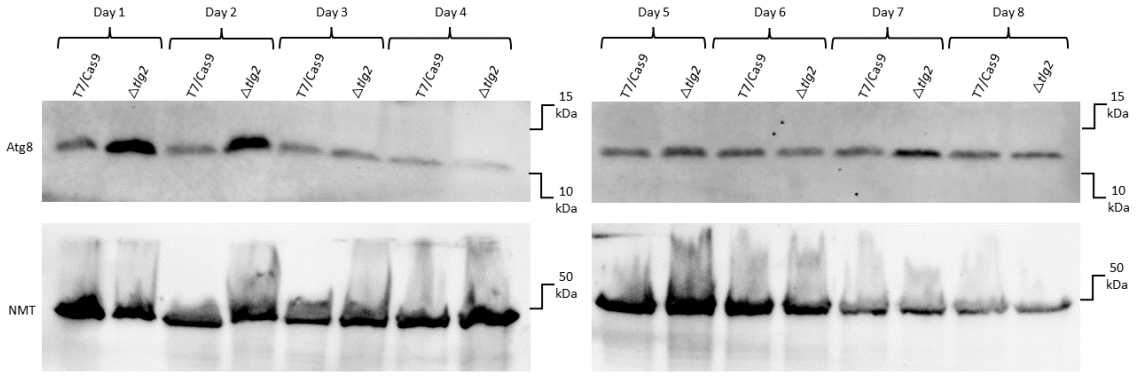

Figure 26. *Expression patterns of Atg8 in parental and* tlg2Δ *promastigotes. L. mexicana* promastigotes were diluted to an initial density of 2 x 10^5 and left to grow over an eight-day time period, with protein samples collected daily. Western blots using an *L. major* anti-Atg8 antibody were performed. Anti-NMT was used as a sample loading control.

5.2.4 Interacting partners of Tlg2

To identify *in vivo* interacting partners of Tlg2, an IP experiment followed by mass spectrometry analysis was conducted using ectopic $Tlg2^{WT}$-HA and $Tlg2^{FL}$-HA in *tlg2*Δ log-phase promastigotes. The C-terminal 3 x HA tag was used to precipitate the ectopic Tlg2-HA and associating proteins. The parental cell line and an HA-tagged RNA-binding protein (LmxM.25.0290, courtesy of Ewan Parry, Walrad lab) not expected to be functionally linked to Tlg2, were used as negative controls. Briefly, samples for IP were prepared by harvesting early log-phase promastigote cells and gently lysing them by water-bath sonication in protease-inhibitor buffer. Pierce™ Anti-HA Magnetic Beads (Thermo Fisher Scientific) were used to

isolate the target and interacting proteins, which were then eluted via boiling of the beads in Laemmli buffer.

To check the successful isolation of HA-tagged Tlg2^{WT} and Tlg2^{FL}, samples from successive stages of the protocol were run on an SDS-Page gel and an anti-HA western blot was performed. Fig. 27 demonstrates that, when using a Ponceau S stain, there were four bands in the elute for all the cell lines, which likely correspond to the anti-HA IgG. When looking at the western blots, the parental cell line shows two bands in both the S10 and flow through samples (Fig. 27A). These could be due to unrelated proteins that have cross-reactivity with the anti-rabbit secondary antibody. That the bands are also present in the RBP control cell lines supports this theory. Importantly, bands were visualised in the elute at the expected protein size specific to the ectopic Tlg2^{WT} and Tlg2^{FL} expression cell line clones, indicating that these Tlg2-HA isolations were successful (Fig. 27C – F). Protein bands in the anti-HA IP elute were the correct size for the HA-RBP product (Fig. 27B).

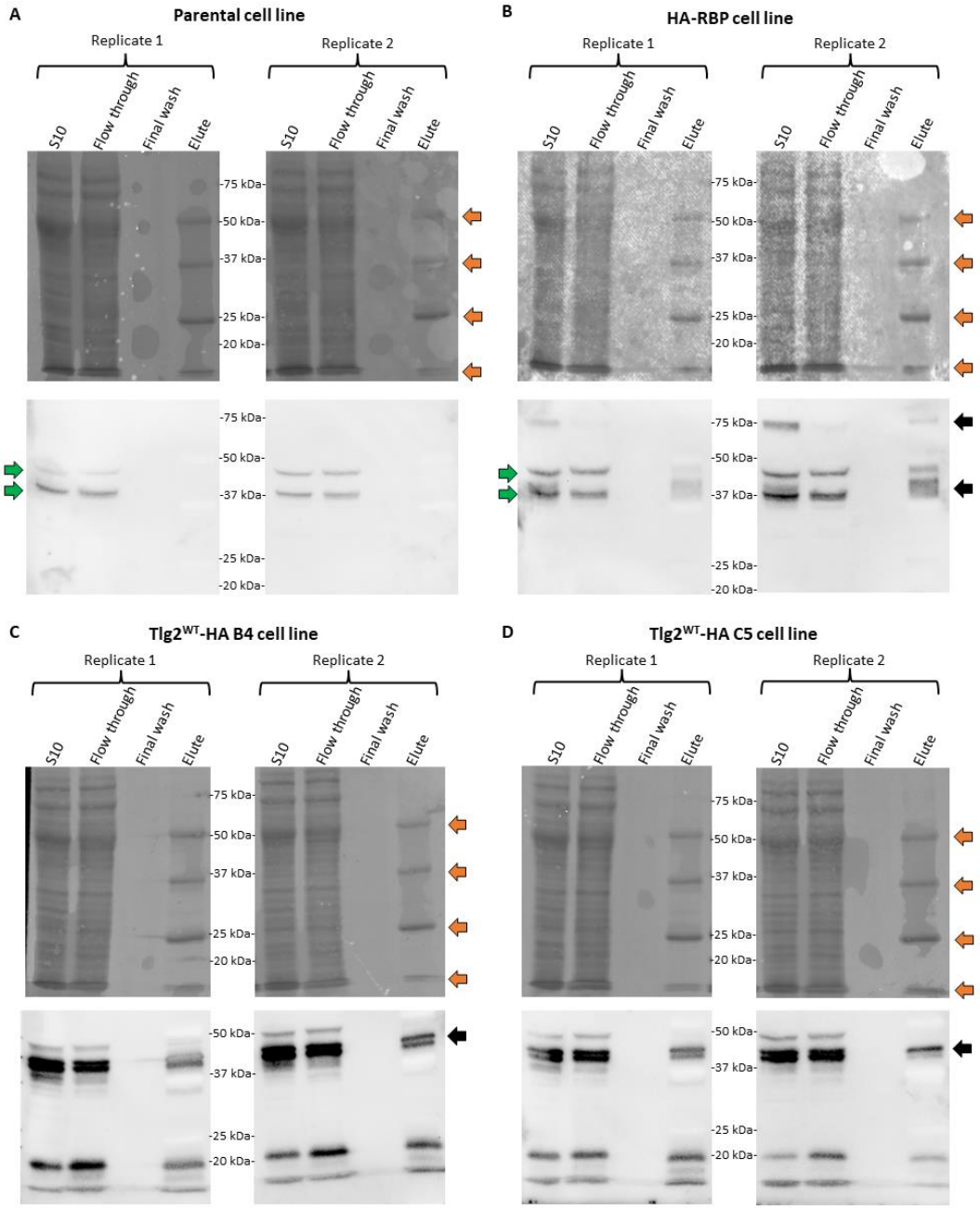
A
Parental cell line
Replicate 1
Replicate 2
S10
Flow through
Final wash
Elute
75 kDa
50 kDa
37 kDa
25 kDa
20 kDa
B
HA-RBP cell line
C
Tlg2WT-HA B4 cell line
D
Tlg2WT-HA C5 cell line

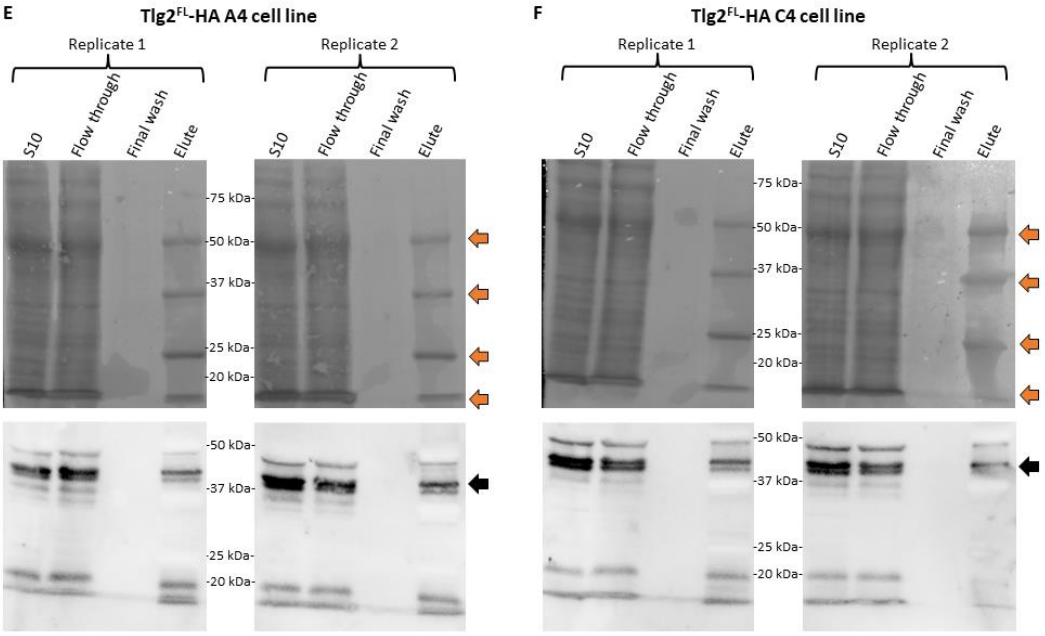

Figure 27. *Ponceau S and western blot analysis of protein immunoprecipitations. L. mexicana* promastigotes were harvested, lysed and the supernatant (S10) incubated with anti-HA magnetic beads. The protein-bound beads were then extracted from the S10, leaving the flow through. The beads were then washed several times and the bound proteins eluted. **A – E.** Samples from each stage were collected and run on an SDS-Page gel, then transferred to a membrane, which was stained with Ponceau S to visualise all the transferred proteins (upper panels), followed by an anti-HA western blot (lower panels). **A.** Parental **(**T7/Cas9) **B.** HA-RBP (LmxM.25.0290) **C.** Tlg2^{WT}-HA addback clone B4 **D.** Tlg2^{WT}-HA addback clone C5 **E.** Tlg2^{FL}-HA addback clone A4 **F.** Tlg2^{FL}-HA addback clone C4. Orange arrows indicate predicted heady and light chains of anti-HA IgG antibody. Green arrows indicate non-specific anti-rabbit cross-reactive bands. Black arrows indicate isolated protein of interest (HA-RBP appears as multiple bands, in accordance with data from Ewan Parry, Walrad lab).

Eluted protein samples were passed to the Metabolomics & Proteomics laboratory (Biological Technology Facility, University of York), where they were subjected to trypsin digestion to produce peptides for analysis by LC-MS/MS. LC-MS chromatograms and peaks were searched against version 54 of the *L. mexicana* subset of the TriTrypDB database to map the peptides to identified proteins, with inclusion of single peptides and a 5% false discovery rate. Relative protein quantification was inferred from peptide-level measurements, with statistical analysis undertaken using a multi-way ANOVA and a Hochberg and Benjamini multiple test correction. Taking the whole dataset of identified proteins within the eluted samples, a principal component analysis (PCA) revealed a lot of variability, with little evidence of grouping between cell line types or replicates (Fig. 28A). The same held true even when the data was clustered by relative protein abundance in the cell lines (Fig. 28B).

Out of 1000 proteins identified in the eluted samples, 46 were determined as differently abundant (at $q < 0.05$) between the Tlg2-expressing cell lines and the controls. PCA and cluster dendrogram analyses clarify appropriate groupings of these HA-tagged protein complexes (Fig. 29). On the PCA (Fig. 29A), both the control cell lines, parental and the RBP-associating complex, were more closely grouped with each other than the Tlg2-associating complexes. Interestingly, whilst all the replicates for the $Tlg2^{WT}$ B4 clone formed a distinct group, all but one of the replicates of the C5 clone were more dispersed and did not group with the B4 clone. In contrast, all the replicates of the $Tlg2^{FL}$ clones were closely clustered. Fig. 29B shows a similar pattern, with the cluster dendrogram for relative protein abundance demonstrating that complexes derived from the parental and RBP cell lines more closely matched. The mutant $Tlg2^{FL}$ clones all clustered together and the $Tlg2^{WT}$ B4 replicates formed their own cluster. Again, the $Tlg2^{WT}$ C5 replicates were the outliers, with one more closely grouped with $Tlg2^{FL}$ and the other two clustering with the RBP control cell line.

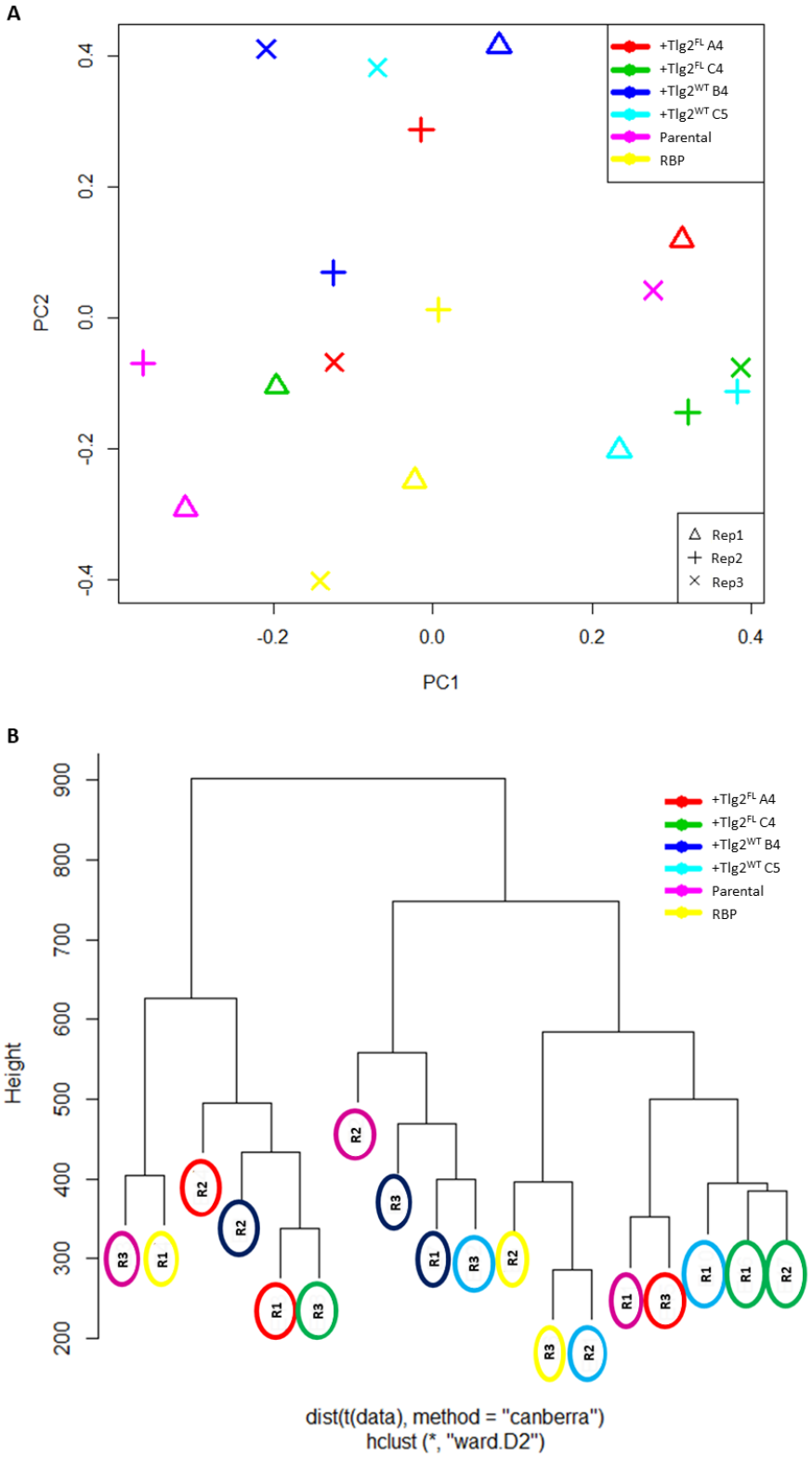

Figure 28. *Analysis of LC-MS/MS protein identities and relative protein abundance.* Peptides from Co-IP eluted proteins were acquired by LC-MS/MS. Peptide identities were mapped back to the *L. mexicana* genome. **A.** Principal component analysis (PCA) of all proteins identified, to determine grouping between cell types and replicates. **B.** Cluster dendrogram of relative protein

abundance. Each cell line had three replicates (R1 – 3). Graphs produced by Dr Adam Dowle, MAP lab, TF, University of York.

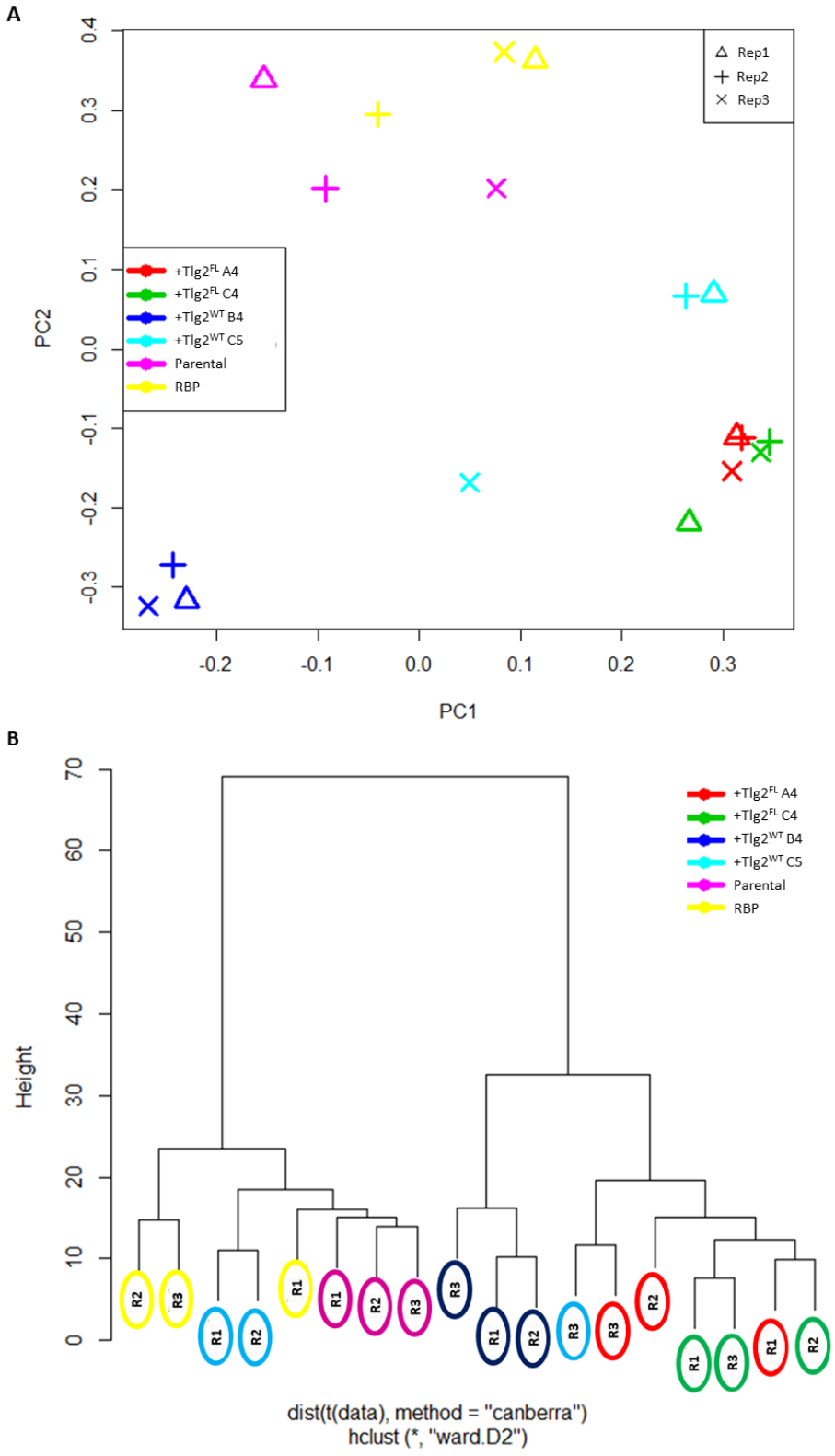

Figure 29. *Analysis of proteins that were differentially abundant in Tlg2^{WT} and Tlg2^{FL} expressing cell lines.* Proteins that had been identified in the LC-MS/MS analysis were classified as differentially abundant in the Tlg2-ectopic expressing cell lines when $q < 0.05$. **A.** Principal component analysis (PCA) of proteins identified, to determine grouping between cell types and replicates. **B.** Cluster dendrogram of relative protein abundance. Each cell line had three replicates (R1 – 3). Graphs produced by Dr Adam Dowle, MAP lab, TF, University of York.

A heat map of the differentially abundant proteins revealed that 23 proteins were more abundant in the Tlg2^{WT} expressing B4 clone and 21 more abundant in the Tlg2^{FL} expressing clones (Fig. 30). As evidenced by the PCA and cluster dendrogram of Fig. 29, the Tlg2^{WT} C5 clone did not behave in the same manner as the B4 clone, with two of the three replicates appearing more like the negative control cell lines. This may suggest the Co-IP was less successful for these samples. Table 3 demonstrates that, of the 23 proteins identified as more abundant in the Tlg2^{WT} B4 clone, there were several involved in fatty acid and very long chain fatty acid (VLCFA) elongation. Using GO term localisations for each protein from TriTrypDB, several proteins were also identified as being Golgi and/or lysosomal associating proteins (Ashburner et al., 2000; Carbon et al., 2021). Additionally, there are proteins that have a generic 'membrane' localisation, which could include the Golgi or endosomal membrane. An example of this is the LmxM.23.0640 hypothetical protein, whose closest human homologue, when conducting a BLASTP, is a golgin subfamily A member 6-like protein 2, which localises to the Golgi. Interestingly, another protein, the Golgi-associated SNARE proteins (LmxM.28.0710), has a designated GO term localisation of the nucleus, nuclear envelope and membrane (Ashburner et al., 2000; Carbon et al., 2021). However, investigation of Interpro Domains on TriTrypDB for LmxM.28.0710 revealed an Interpro ID of IPR032816, which relates to a family of SNARE associated Golgi proteins (Inadome et al., 2005, 2007). LmxM.28.0710 also shows homology to the human vacuole membrane protein 1 (VMP1) when conducting a BLASTP. Phosphatidylinositol 3- and 4-kinase (PI(3)K/PI(4)K) was also more abundant in the Tlg2^{WT} complex than the Tlg2^{FL} mutant complex. PI(3)P and PI(4)P, substrates of PI3K and PI4K are known to be enriched in early endosomes and the Golgi in organisms such as yeast and mammals (Matteis & Godi, 2004; Roth, 2004).

Table 4 shows the 21 proteins that were identified as enriched in the Tlg2^{FL} protein complexes relative to Tlg2^{WT}. Only one Tlg2^{FL}-associated protein was shown to be Golgi-associated (LmxM.05.1140), which was a V-type proton ATPase subunit, a protein that transports protons across membranes and is important for acidifying endosomal vesicles and lysosomes (Lafourcade et al., 2008; Song et al., 2020). The majority of the proteins found in complex with Tlg2^{FL} had nuclear, cytoplasmic or membrane GO terms (Ashburner et al., 2000; Carbon et al.,

2021) and several appear to play a role in mRNA translation or regulation. Additionally, there were two heat shock proteins identified, which are molecular chaperones upregulated during stress to aid protein refolding (Georgopoulos & Welch, 1993; Shan et al., 2020). One of the heat shock proteins identified is a Hsp70 (LmxM.28.2770/LmxM.28.2780). The other heat shock protein (LmxM.32.2390) was not designated in *L. mexicana*, but when searching in TritrypDB was orthologous to Hsp84 or Hsp90 in related *Leishmania* and *Trypanosoma* species. A polyubiquitin was also identified (LmxM.09.0891/LmxM.36.3530partial), which is orthologous to either trypanosomatid Ubiquitin-2 like Rad60 SUMO-like or Ubiquitin-60S ribosomal protein L40.

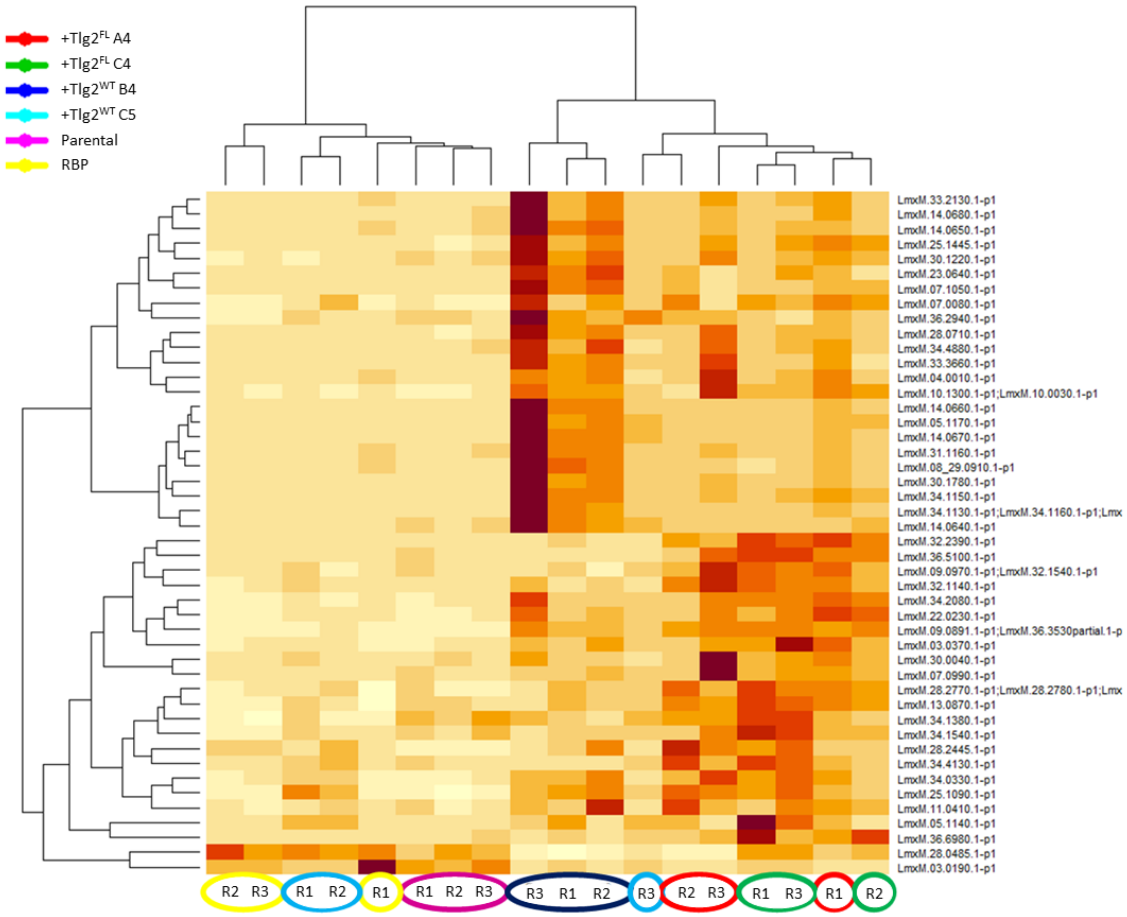

Figure 30. Heat map of raw protein abundance in Tlg2^{WT} B4 addback clone and the Tlg2^{FL} for proteins that were identified as differentially expressed. The top half of the map represents those proteins that were enriched in the Tlg2^{WT} B4 expressing addback clone replicates and the bottom half (excepting the final two rows) those proteins that were enriched in the Tlg2^{FL} expressing addback clonal replicates, when compared to the parental and RBP control cell lines. Map produced by Dr Adam Dowle, MAP lab, TF, University of York.

Tlg2 peptides were detected in all cell line IPs, despite the absence of an HA tag for endogenous Tlg2 in the parental and HA-RBP populations (Fig. 31). Surprisingly, although abundance was higher in those samples with ectopic Tlg2-HA, the difference was not significantly different from the parental and HA-RBP negative control cell lines (q = 0.545). Several of *L. mexicana* Tlg2's predicted SM and SNARE binding partners were also identified within the mass spectrometry analysis. There were hits for the *L. mexicana* Tlg1, Snc1 and Snc2 homologues (LmxM.26.0690, LmxM.08.0030 and LmxM.21.1290), but only one unique peptide was identified for each protein and there was no significant difference between the Tlg2-HA protein complexes and the negative controls. Interestingly, when looking at the raw abundance for Snc1 there were very low levels in the control IP samples (0 – 1% range and 0.16% average) and in complex with ectopic $Tlg2^{WT}$-HA (0 – 6% range and 1.6% average), whereas for ectopic $Tlg2^{FL}$-HA protein complexes there was an average raw abundance of 14.83% (with a range of 3 – 31%). For Snc2 there were very low levels in all cell lines (0 – 8%), except for one replicate of the $Tlg2^{FL}$ C4 clone, which had a raw abundance of 87%. Finally, no peptides were identified for Vps45a (LmxM.36.2230). For Vps45b (LmxM.36.0460), there was a very weak single spectrum match, but no abundance differences were observed in the IP samples for each cell line.

Accession	Unique peptides	q value	Max. fold change	Description	GO term localisations
LmxM.33.2130	2	0.047	13.02	hypothetical protein	membrane
LmxM.14.0680	3	0.024	10.38	fatty acid elongase	nucleus, endoplasmic reticulum
LmxM.14.0650	4	0.017	6.68	fatty acid elongase	membrane
LmxM.25.1445	2	0.018	8.41	Present in the outer mitochondrial membrane proteome 23 (POMP23)	mitochondrion
LmxM.30.1220	10	0.017	5.70	Pyrophosphate-energized vacuolar membrane proton pump 1 (VP1)	Golgi membrane, contractile vacuole, membrane, acidocalcisome
LmxM.23.0640	8	0.027	12.36	hypothetical protein	membrane
LmxM.07.1050	5	0.021	16.33	cation-transporting ATPase	endoplasmic reticulum
LmxM.07.0080	1	0.045	19.05	Golgi/lysosome glycoprotein 1 (GLP1)	lysosome, lysosomal membrane, Golgi apparatus
LmxM.36.2940	1	0.047	4.20	phosphatidylinositol 3- and 4-kinase (PI3K/PI4K)	no localisation given
LmxM.28.0710	2	0.049	11.04	SNARE associated Golgi protein	Nucleus, nuclear envelope, membrane
LmxM.34.4880	2	0.038	12.85	TPR repeat	Endoplasmic reticulum
LmxM.33.3660	4	0.017	36.38	transmembrane/endomembrane-like protein	membrane
LmxM.04.0010	2	0.048	12.77	organelle-type calcium ATPase	membrane
LmxM.10.1300/ LmxM.10.0030	2	0.023	14.95	phosphate-Repressible Phosphate Permease-like protein	membrane
LmxM.14.0660	5	0.017	13.30	fatty acid elongase	membrane
LmxM.05.1170	1	0.027	16.98	elongation of very long chain fatty acids protein	membrane
LmxM.14.0670	7	0.017	10.67	fatty acid elongase	nucleus, endoplasmic reticulum
LmxM.31.1160	2	0.047	11.20	long chain polyunsaturated fatty acid elongation enzyme-like protein	membrane
LmxM.08_29.0910	1	0.016	10.80	signal peptide peptidase	membrane
LmxM.30.1780	2	0.016	38.00	Sphingosine N-acyltransferase (DHCS)	nucleus, cytoplasm, nuclear lumen, ciliary plasm
LmxM.34.1150	1	0.047	127140.99	oligosaccharyl transferase-like protein	nuclear envelope, endplasmic reticulum, membrane
LmxM.34.1130/ LmxM.34.1160	3	0.016	77.37	oligosaccharyl transferase-like protein	nuclear envelope, endplasmic reticulum, membrane
LmxM.14.0640	1	0.027	32.74	fatty acid elongase	nucleus, cytoplasm, membrane

Table 3. *Proteins enriched in Tlg2^{WT}-HA protein complexes relative to parental and HA-RBP controls.* A q value of 0.05 was used as the cut-off, with q values obtained using a multi-way ANOVA and a Hochberg and Benjamini multiple test correction. The max. fold change was determined by calculating ratio of the maximum and minimum mean from all sample groups for each protein. GO term searches were conducted in TriTrypDB.

Accession	Unique peptides	q value	Max. fold change	Description	GO term localisations
LmxM.32.2390	4	0.016	10.47	heat shock protein	Mitochondrion, kinetoplast
LmxM.36.5100	5	0.001	30.13	hypothetical protein	cytoplasm
LmxM.09.0970/ LmxM.32.1540	3	0.048	4.45	elongation factor-1 gamma	nucleus
LmxM.32.1140	2	0.001	54.15	hypothetical protein	cytoplasm, membrane, nuclear lumen, ciliary plasm
LmxM.34.2080	7	0.047	11.83	calcium motive p-type ATPase	membrane
LmxM.22.0230	1	0.050	30.96	amino acid permease	membrane
LmxM.09.0891/ LmxM.36.3530partial	1	0.001	14.76	polyubiquitin	nucleus, cytoplasm, ribosome
LmxM.03.0370	1	0.017	14.77	GPR1/FUN34/yaaH family	membrane
LmxM.30.0040	1	0.018	36.48	MFS/sugar transport protein	membrane
LmxM.07.0990	3	0.012	16.51	nucleolar RNA-binding protein	nucleus, nucleolus
LmxM.28.2770/ LmxM.28.2780	19	0.050	5.22	heat-shock protein hsp70	glycosome
LmxM.13.0870	3	0.001	5.21	mitochondrial processing peptidase, alpha subunit	mitochondrion
LmxM.34.1380	10	0.048	2.68	mitochondrial processing peptidase, beta subunit	cytoplasm, mitochondrion
LmxM.34.1540	3	0.047	7.76	rieske iron-sulfur protein, mitochondrial precursor (RISP)	mitochondrion, membrane, kinetoplast
LmxM.28.2445	1	0.014	333.64	Putative serine esterase (DUF676)	no localisation given
LmxM.34.4130	4	0.039	8.57	polyadenylate-binding protein 2 (PABP2)	cytoplasm, cytoplasmic stress granule, nuclear stress granule
LmxM.34.0330	3	0.017	6.14	short chain dehydrogenase	nuclear envelope, endoplasmic reticulum
LmxM.25.1090	3	0.009	4.87	magnesium transporter protein 2 (MGT2)	membrane
LmxM.11.0410	2	0.045	8.18	Nucleolar protein 89 (NOP89)	nucleus, nucleoplasm, nucleolus
LmxM.05.1140	1	0.017	Infinity	V-type proton ATPase subunit D (VAd)	cytoplasm, lysosome, Golgi apparatus, acidocalcisome
LmxM.36.6980	3	0.018	33.33	eukaryotic translation initiation factor 3 subunit c (EIF3C)	cytoplasm

Table 4. *Proteins enriched in Tlg2^{FL}-HA protein complexes relative to parental and HA-RBP controls.* A q value of 0.05 was used as the cut-off, with q values obtained using a multi-way ANOVA and a Hochberg and Benjamini multiple test correction. The max. fold change was determined by calculating ratio of the maximum and minimum mean from all sample groups for each protein. GO term searches were conducted in TriTrypDB.

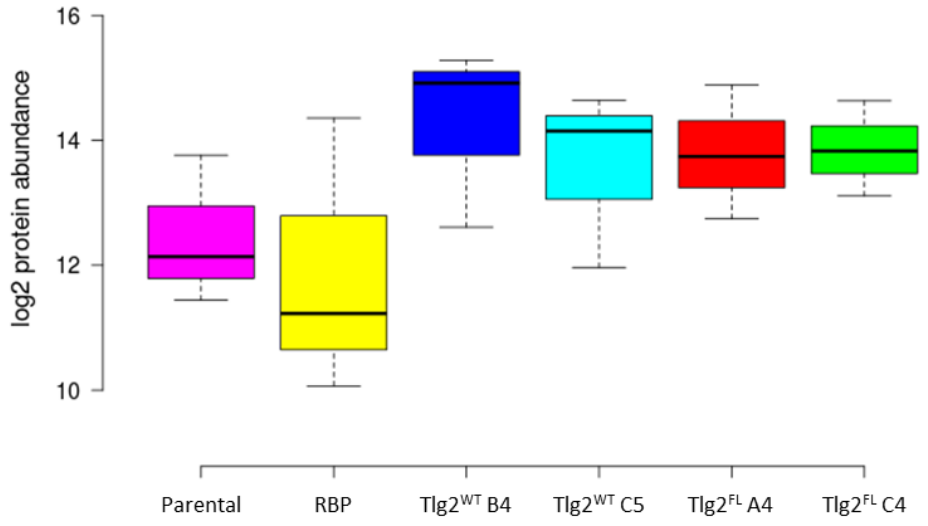

Figure 31. *Abundance of the Tlg2 protein in the eluted protein samples from anti-HA Co-IPs.* Box and whisker plot demonstrates the median (thick black line), interquartile range (filled box) and the minimum (low whisker) and maximum (high whisker) log protein abundances. Plot produced by Dr Adam Dowle, MAP lab, TF, University of York.

5.3 Discussion

5.3.1 Tlg2 localisation in *L. mexicana*

Tlg2 was successfully visualised by fluorescence microscopy in early log-phase *L. mexicana* promastigotes via the C-terminal HA-tag (Fig. 24). As the *tlg2*Δ promastigotes transfected with either the $Tlg2^{WT}$ or $Tlg2^{FL}$ addback plasmids were used, this allowed comparison of expression patterns between the wild-type and mutant versions of the protein. The $Tlg2^{WT}$ addback promastigotes displayed a similar pattern to what has previously been visualised in yeast and the related kinetoplasts *L. major* and *T. brucei*; a cytosolic punctate distribution with a particularly strong signal near the kinetoplast (Abeliovich et al., 1998; Besteiro et al., 2006; Dean et al., 2017). Based on what has been demonstrated in yeast, these signals are predicted to correspond to the *trans*-Golgi apparatus (the distinct signal near the kinetoplast) and endocytic structures (the cytosolic puncta). Curiously, when performing co-localisation assays in *L. major*, researchers were not able to confirm that the kinetoplast-adjacent signal originated on the Golgi apparatus, as the GFP-tagged Tlg2 did not co-localise with a *T. brucei* derived Rab1 Golgi marker. As endocytosis takes place exclusively at the flagellar pocket, which is also in the vicinity of the Golgi and kinetoplast (Halliday et al., 2019), it is possible that the Tlg2 signal corresponds to an endocytic structure that is distinct from the *trans*-Golgi apparatus. Alternatively, Rab1 may not localise to the entirety of the Golgi apparatus, hence appearing distinct from the Tlg2 signal in *L. major* studies. In support of this theory, a study in *T. brucei* was able to demonstrate co-localisation of Tlg2 to the Golgi apparatus (Murungi et al., 2014). Furthermore, an alternative Golgi marker (LPG2-HA) was used in *L. donovani*, which co-localised with Rab1, but appeared to bind to a greater area of the Golgi apparatus, which suggests that Rab1 does not bind to the entire organelle (Bahl et al., 2015). Future experiments could therefore utilise both the Rab1 and LPG2-HA markers to determine whether Tlg2 in *L. mexicana* co-localises with the Golgi, as is witnessed in yeast and *T. brucei*, or, as in *L. major*, it displays a distinct signal adjacent to the Golgi. Additionally, utilisation of the FM4-64 lipophilic marker to track endocytic structures could help determine the nature of the cytosolic Tlg2 puncta by seeing if the two co-localise.

In contrast to Tlg2^{WT}, the Tlg2^{FL} did not display a punctate cytosolic distribution. When the protein was detected in the promastigotes, the cells displayed a single Tlg2 signal close to the kinetoplast. It has already been demonstrated that Tlg2^{FL} ectopic protein is expressed at significantly lower levels than the ectopic Tlg2^{WT} in *L. mexicana* promastigote cells despite more-than-endogenous RNA levels (Fig. 23A; Section 4.2.4). This difference in ectopic protein expression levels may be due to stabilisation via the F10/L11 N-terminal amino acid interactions, as in yeast. Reduced protein stability and resultant expression could contribute to, but not fully account for, the observed difference in Tlg2 subcellular distribution between the two cell lines. Considering that the signal close to the kinetoplast was noticeably weaker in the Tlg2^{Fl} expressing cells compared to the Tlg2^{WT}, it could be that any remaining Tlg2^{FL} localising to cytosolic puncta are at too low a level to be detected. Alternatively, the introduction of the F10A/L11A mutation could result in altered protein distribution, due to a functional disruption.

5.3.2 How Tlg2 impacts *Leishmania* infectivity and virulence

A macrophage infection assay demonstrated that *tlg2*Δ *L. mexicana* stationary stage promastigotes appeared as infective as the parental cell line at 24 hours P.I (Fig. 25). Importantly, the Tlg2^{WT} and Tlg2^{FL} ectopic expression cell lines also showed similar levels of infection at this time point. However, after 72 hours a different picture emerged in the capacity of parasites to maintain a macrophage infection in the absence of endogenous Tlg2 levels. Only the parental cell line had maintained a high level of infection, with all other cell lines examined displaying a significant reduction in the number of macrophages that were infected at 72 hours P.I. Although this result was encouraging in terms of the *tlg2*Δ displaying a phenotype, it was also somewhat unexpected, as ectopic Tlg2^{WT} addback had been predicted to rescue the null mutant, as it had replicative efficiency and increased *SHERP* mRNA expression.

There are several potential explanations for why this may have occurred. Firstly, unlike the parental and *tlg2*Δ stationary promastigote cells, the ectopic Tlg2 ‘addback’ cell lines were grown in cell culture media containing antibiotics. Although the antibiotics were removed prior to macrophage infection, it is possible that the presence of additional antibiotic-resistance genes may have had a negative impact on parasite fitness and the ability to maintain infections within macrophages, as has been seen in *Leishmania* who develop resistance to miltefosine (Hendrickx et al., 2016; van Bockstal et al., 2019). To address this question, a repeat of the macrophage infection assay could be performed with the inclusion of an additional control cell line; the T7/Cas9 parental transfected with the pSSU BLA^{R}. This would help to highlight whether the additional antibiotic-resistance genes are detrimental for *Leishmania* virulence.

An alternative explanation is that removal of the antibiotics prior to macrophage infection removed the selection pressure and led to loss of the ectopic Tlg2-expressing plasmids, effectively rendering the cells as null mutants. A study in yeast demonstrated that Tlg2 has a half-life of 7.5 hours, so if *L. mexicana* Tlg2 have a similar half-life it is possible all the ectopic Tlg2 may have been degraded after 72 hours P.I, if the plasmids were lost (Christiano et al., 2014). Integration of the Tlg2 addback genes into the genome of the *tlg2*Δ *L. mexicana* would combat this issue and simultaneously remove the need for antibiotic selection beyond the initial transfection event.

Finally, it is possible that, although able to rescue the growth and cell cycle deficiencies displayed by the null mutant, the $Tlg2^{WT}$ addback is not sufficient to rescue the macrophage infection phenotype. This could be due to off-target mutations that resulted from the initial generation of the *tlg2*Δ cell line or, potentially, the proximity of the C-terminal HA tag to the Tlg2 transmembrane domain could interfere with membrane binding and affect the protein's function. To explore the potential role off-target mutations may have had on the $Tlg2^{WT}$ addback, GO analysis of the 78 moderate SNP mutations identified through sequencing of the *tlg2*Δ was conducted. This analysis revealed several proteins with a role in microtubule motility, motor activity, binding and ciliary pocket and a flagellar protein involved in cilium assembly and motility. Disruption of the function of these proteins could have the potential to affect the motility of the parasites, which may be less critical for parasite survival in culture but could potentially impact their ability to find and infect macrophages. In addition, the flagellar pocket (FP) and flagellum attachment zone (FAZ) have been demonstrated to play an important role in *Leishmania* pathogenicity. Parasites with mutations in FP and FAZ proteins have a reduced ability to proliferate in sandflies and mouse hosts (Sunter et al., 2019). SNP missense mutations in proteins involved in flagellar assembly and the ciliary (flagellar) pocket may therefore affect the $Tlg2^{WT}$ addback clones' ability to survive and proliferate in macrophages. Moderate missense mutations were also found in three amastin-like proteins. Amastins are a group of glycoproteins found on the surface of *Leishmania* amastigotes that are essential for parasite growth in macrophages (both *in vitro* and *in vivo*) (de Paiva et al., 2015). In the *tlg2*Δ clone, three amastin-like proteins had missense SNPs, which may not have had an impact on promastigote growth in the $Tlg2^{WT}$ addback clones, but could potentially have impaired the ability of $Tlg2^{WT}$ addback amastigotes to survive and replicate in macrophages. There was also a missense SNP in a proteophosphoglycan (PPG). Research has shown that expression of PPGs by *Leishmania* promastigotes can aid with macrophage infection both *in vivo* and *in vitro* by promoting the alternative activation and arginase production of macrophages (Rogers et al., 2009; Rogers, 2012). Potential disruption of function in PPG production could reduce the ability

of Tlg2^{WT} addback parasites to induce increased arginase activity in macrophages and, consequently, may not promote intracellular parasite growth to the same degree as the parental cell line. Finally, a missense SNP in one of the *L. mexicana* Atg8 proteins could also have contributed to the inability of the Tlg2^{WT} addback to rescue the virulence phenotype. As there are 25 Atg8 proteins in *Leishmania* (Williams et al., 2009), it's possible that this Atg8 protein was not essential for promastigote differentiation events but plays a role in amastigogenesis, resulting in decreased survival and virulence compared to the parental cell line.

Because the cell lines were not grown up in identical conditions, it is hard to draw direct comparisons for the parental and *tlg2*Δ against the ectopic Tlg2 'addback' cell lines. However, comparisons between parental and *tlg2*Δ cell lines can be drawn, and the data is indicative of a defect in the ability of the null mutants to survive within macrophages after 24 hours P.I. That the *tlg2*Δ promastigotes are initially able to infect macrophages at a rate similar to the parental line is suggestive of their ability to undergo metacyclogenesis (da Silva et al., 2015). This data is supported by the fact that, although *tlg2*Δ promastigotes grow more slowly, they do eventually appear to reach a stationary phase of growth, with a cell cycle profile and morphology that is indistinguishable from parental cell line counterparts on day 8 (Section 4.2.2). As the *L. mexicana* promastigotes were left to grow for 10 days after being split, this may have been enough time for *tlg2*Δ cells to have differentiated into the macrophage infective metacyclic form. In contrast, at 72 hours P.I *tlg2*Δ display a highly significant decrease in the number of macrophages infected compared to the parental *L. mexicana*. As *Leishmania* metacyclic promastigotes typically require longer than 24 hours to complete their differentiation into amastigotes after macrophage internalisation (Sarkar et al., 2018), this data could be suggestive of *tlg2*Δ parasites having a reduced ability to undergo amastigogenesis and thus displaying reduced virulence at the 72 hour P.I timepoint. Future experiments could therefore utilise visualisation of metacyclic and amastigote-specific markers, such as SHERP and amastin (Knuepfer et al., 2001; Wu et al., 2000), to quantify the proportions of each cell type within the macrophages at 24 and 72 hours P.I. An extension of this assay would be to count the number of individual parasites in a given number of macrophages (i.e. number of parasites / 100 macrophages) at 24, 72 and 120 hours P.I. to determine the parasites' ability to not only infect and survive in the macrophages, but to divide and multiply (Besteiro et al., 2006).

5.3.3 *tlg2*Δ and Atg8 expression

Given the paucity of available antibodies and lack of sequence conservation rendering antibodies from other systems unusable, we sought out potentially useful antibodies from related systems. An *L. major* derived anti-Atg8 provided some inspiration. Atg8 levels are

commonly used as an autophagy marker because the PE-conjugated protein reliable associates with mature autophagosomes (Klionsky et al., 2008; Mizushima & Yoshimori, 2007). As *tlg2*Δ has been demonstrated to reduce autophagy in other systems (Nair et al., 2011), the anti-Atg8 antibody could be a useful tool in identifying any *tlg2*Δ-dependant changes to autophagy in *L. mexicana*. Due to the high level of sequence conservation for Atg8 proteins between the two species, it was predicted that the anti-Atg8 antibody would successfully detect the *L. mexicana* homologue. Western blot analysis across days 1 – 8 demonstrated a clear protein band within the expected size range of Atg8 (~14 kDa) (Fig. 26). Interestingly, unlike what has previously been witnessed in *L. major* and *L. donovani*, where the unconjugated and PE-conjugated forms of Atg8 were visualised, only a single band was apparent for *L. mexicana* (Besteiro et al., 2006; Giri & Shaha, 2019; Williams et al., 2013). Although larger than 14 kDa, Atg8-PE tends to run on an SDS-Page gel in concurrence with that size marker, due to the lipidation and hydrophobicity of the protein (Mizushima & Yoshimori, 2007; Zens et al., 2015). In contrast, unconjugated Atg8 (Atg8-I) runs at around the 18 kDa marker (Giri & Shaha, 2019). Because of this, it is assumed that the band that was visualised in Fig. 26 corresponds to the conjugated Atg8-PE. Atg8-I is more likely to be degraded in samples that have been subjected to freeze-thawing or have been stored in SDS sample buffer (Klionsky et al., 2008), which could explain why it was not detected for these *L. mexicana* samples. Additionally, anti-Atg8 antibodies often show higher affinities for Atg8-PE than Atg8-I (Mizushima & Yoshimori, 2007), which could further explain why only one band was visualised.

The conversion of Atg8-I to Atg8-PE moves the protein from the cytosol onto autophagosome membranes. Atg8-PE levels therefore correlate with the number of completed autophagosomes, making it a commonly used autophagy marker for this purpose (Mizushima & Yoshimori, 2007). On days 1 and 2, Atg8-PE appears more highly expressed in *tlg2*Δ. There are a couple of possible causal explanations for this. Firstly, Tlg2 has previously been shown to be expressed most strongly in the early stages of promastigote logarithmic growth (Sections 3.2.4 and 4.2.4). Cells lacking Tlg2 could therefore be under greater stress during days 1 and 2, when Tlg2 is usually highly expressed. This could lead to an increase in autophagy and, consequently, a concomitant increase in autophagosomes (and consequently the Atg8-PE protein). Alternatively, the increase in Atg8-PE could indicate a defect in the autophagy pathway, with an accumulation of autophagosomes that are unable to complete the pathway and fuse to the lysosome (Klionsky et al., 2008; Mizushima & Yoshimori, 2007; Williams et al., 2013). Interestingly, Stx16 (the mammalian Tlg2 homologue) has been demonstrated to be involved in the correct shuttling of Atg9+ membranes to a developing autophagosome in mice cells, with knockdown of Stx16 resulting in a decrease in LC3-PE (the mammalian homologue of Atg8-PE) (Aoyagi et al.,

2018). This apparently contrasts to what is seen in Fig. 26, however, further analysis is needed to tease apart what is happening in the *L. mexicana tlg2*Δ cells. Additional controls could be utilised to help confirm whether the single band visualised is representative of Atg8-PE and reflects differences in autophagy. For example, use of an *atg1*Δ cell line, in which autophagy has been ablated, would allow comparison of protein expression patterns across the promastigote lifecycle. Culturing of parasites in conditions that induce autophagy, such as nitrogen starvation, removal of FBS from the culture, or addition of rapamycin, could also be used to ascertain how *tlg2*Δ parasites respond in stress conditions and highlight any differences in Atg8 expression compared to the parental cell line.

Using the anti-Atg8 antibody in immunofluorescence assays would allow quantification of Atg8-PE+ autophagosomes in cells and highlight any accumulation issues. Additionally, measurement of autophagic flux using an mRFP-GFP-Atg8 fluorescent protein quenching assay could highlight defects at different stages of the autophagy pathway. When mRFP-GFP-Atg8 is localised to autophagosome membranes a yellow fluorescence is detected (red and green signal). Fusion of autophagosomes to the lysosome results in quenching of GFP in the acidic environment, so only the mRFP signal is detected. An increase in yellow-fluorescing puncta and decrease in red fluorescence would therefore indicate a defect in autophagosome maturation or formation of autophagolysosomes (Klionsky et al., 2016; Yoshii & Mizushima, 2017). A lack of yellow or red fluorescent signal could also indicate defects in phagophore initiation and expansion. Unfortunately, attempts to clone an mCherry-GFP-Atg8 expressing plasmid vector were unsuccessful, so future experiments could complete this plasmid and utilise it for measuring autophagic flux in *tlg2*Δ promastigotes.

5.3.4 The interacting partners of Tlg2

Co-IP assays are used to identify *in vivo* interacting partners for target proteins. The inclusion of both the ectopic $Tlg2^{WT}$ and $Tlg2^{FL}$ expressing cell lines for the *L. mexicana* Co-IP presented the opportunity to identify any differences in interacting partners that may have resulted from the F10A/L11A mutation. Fig. 27 demonstrates that both the $Tlg2^{WT}$-HA and $Tlg2^{FL}$-HA were able to be successfully immunoprecipitated using the anti-HA magnetic beads. Ponceau staining visualisation of bands in the elution samples are likely to correspond to the heavy and light chains of the anti-HA IgG antibody and is indicative of the protein elution method used. Boiling of beads in Laemmli buffer to elute target protein complexes also disrupts the binding of the antibodies to the beads.

In total, 1000 proteins were identified in the eluted samples from all cell lines. When analysing this data by PCA and cluster dendrogram (Fig. 28) there were no clear distinctions between the cell types or even between replicates of the same cell line. This variability is indicative of a background contamination within the samples. However, the multi-way ANOVA and a Hochberg and Benjamini multiple test correction did identify 46 proteins that were differentially abundant at $q < 0.05$; 23 more abundant in the ectopic $Tlg2^{WT}$-expressing B4 clone and 21 more abundant in both the $Tlg2^{FL}$-expressing clones (Fig. 30). These proteins showed much clearer groupings when analysed by PCA and cluster dendogram (Fig. 29), with the $Tlg2^{FL}$ samples clustering together particularly closely. The grouping was less successful for the $Tlg2^{WT}$-expressing clones. Although the $Tlg2^{WT}$ B4 replicates displayed strong similarity to each other, two of the $Tlg2^{WT}$ C5 replicates were more dispersed and did not cluster with the B4 replicates. As $Tlg2^{WT}$ C5 addback promastigotes displayed the same apparent ability to rescue *tlg2*Δ growth and cell cycle phenotypes as $Tlg2^{WT}$ B4 addback promastigotes this variability was unexpected. It is possible that the Co-IPs for $Tlg2^{WT}$ C5 were less successful and hence presented closer to the RBP and parental control cell lines.

When looking at the identities and descriptions of the differentially abundant proteins it is encouraging to note that for the ectopic $Tlg2^{WT}$-expressing samples, several interactors are associated with the Golgi, lysosome and endomembranes (Table 3). As Tlg2 is a membrane-bound SNARE protein within the *trans*-Golgi and endocytic network (Abeliovich et al., 1998), it is likely to be in close proximity to and come into contact with other proteins bound to the same membranes, potentially resulting in direct or indirect binding. Additionally, some of these proteins have also been indicated as playing a role in autophagy. For example, the PI(3)K class of kinases, as well as being required for traffic between the *trans*-Golgi network and endosomes (Bryant & Stevens, 1998), have been identified as key regulators and components of autophagy. PI(3)Ks can either exert a negative regulation of autophagy (via interaction with mTORC1), or act in complex to initiate membrane recruitment to the phagophore assembly site as well as facilitating autophagosome to lysosome fusion (Yu et al., 2015). Another protein, LmxM.28.0710, had an Interpro domain identity of IPR032816, which relates to a family of SNARE associated Golgi proteins . Interestingly, the yeast member of this family, Tvp38, has been shown to localise with Tlg2-containing Golgi-associated membranes (Inadome et al., 2005, 2007). Further to this, BLASTP of LmxM.28.0710 against the human proteome revealed VMP1 as a homologue. VMP1 is also believed to be involved in autophagy, and may play a role in autophagosome formation, by providing essential components for maturing autophagosomes or via the recruitment of Beclin-1 and components of the PI(3)K complex I (Itakura & Mizushima, 2010; Longatti & Tooze, 2009). One of the methods by which Tlg2 is proposed to

be involved in autophagy is by facilitating the normal anterograde transport of Atg9 (Nair et al., 2011). This is in turn coordinated by the Beclin-1-PI(3)KC3 complex, to translocate Atg9 for autophagosome formation (He et al., 2013), which could further explain the presence of the PI(3)K/PI(4)K (LmxM.36.2940) in the $Tlg2^{WT}$ IPs. $Tlg2^{WT}$ also appears to interact with several fatty acid elongase and elongation of very long chain fatty acid (VLCFA) proteins (LmxM.14.0680, LmxM.14.0650, LmxM.14.0670, LmxM.14.0640 and LmxM.05.1170). These proteins are often associated with the endoplasmic reticulum (Jakobsson et al., 2006). However, VLCFAs may also be required for endosomal trafficking pathways, which could explain the presence of the fatty acid elongase and long chain elongation proteins (Obara et al., 2013).

In contrast to the ectopic $Tlg2^{WT}$, the $Tlg2^{FL}$ mutant appears to have only one interacting partner with a defined Golgi localisation, the V-type proton ATPase subunit (LmxM.05.1140) (Table 4). Notably, two heat-shock proteins had elevated abundance in the $Tlg2^{FL}$ Co-IPs (Hsp70 and a Hsp83/90 orthologue). Heat shock proteins are molecular chaperones or proteases that are characteristically upregulated during times of cellular stress. They help to maintain protein homeostasis by preventing or refolding misfolded proteins, or alternatively targeting them for degradation (Georgopoulos & Welch, 1993; Jolly, 2000). There is also the presence of a polyubiquitin, albeit with only one unique peptide, which tags proteins with ubiquitin chains for degradation by the proteosome (Nguyen et al., 2014). In yeast, Vps45 stabilises the cellular levels of Tlg2 SNARE proteins by binding to the N-terminus. Mutations that disrupted this binding resulted in reduced levels of Tlg2 due to rapid targeting of the protein for degradation by the proteosome (Bryant & James, 2001; Carpp et al., 2007). The presence of the heat shock proteins and polyubiquitin in the $Tlg2^{FL}$ protein complexes could therefore be due to the F10A/L11A mutation in the Tlg2 disrupting the N-terminal binding to Vps45, subsequently targeting the $Tlg2^{FL}$ for degradation. $Tlg2^{FL}$ also appears to interact with several proteins involved in RNA binding or translation. A possible explanation for this is that the presence of the F10A/L11A mutation causes stalling of the protein translation by ribosomes, thus maintaining an interaction with translational and RNA-binding machinery and the potential formation of stress granules (Karamyshev & Karamysheva, 2018). The increased abundance of polyadenylate-binding protein 2 (PABP2) (LmxM.34.4130) lends credence to this theory, as this protein regulates mRNA translation but is also found in stress granules of many organisms, including plants and trypanosomatids (Gray et al., 2015; Kramer et al., 2013). Additionally, the enrichment of Hsp70 and Hsp83/90-like proteins in the ectopic $Tlg2^{FL}$-expressing complexes again suggests a stress response. Hsp70 and Hsp90 are found within the endoplasmic reticulum, cytoplasm or mitochondria and are involved in maintaining protein homeostasis through the refolding of denatured proteins or by promoting the degradation of such proteins (Ellgaard et

al., 2016). Hsp70 also plays a role in the disassembly of stress granules, to release sequestered mRNAs for translation or for entry into the autophagic degradation pathway (Walters & Parker, 2015).

Surprisingly, Vps45 and Tlg2's SNARE complex partners from other systems were either not detected in the Tlg2 IPs, or, if they were, displayed no significant difference in abundance compared to the control cell lines. This could in part be explained by the fact that the Tlg2 bait proteins levels, although higher in the Tlg2-HA Co-IPs (Fig. 31), were also not significantly more abundant than the control cell lines. It is possible that the methods used to lyse, pull-down or elute the samples resulted in protein degradation or disruption of the protein-protein interactions, particularly if the binding was weak or transient. Of those SNARE proteins that were identified, Tlg1 (LmxM.26.0690) levels did not appear different even when looking at the raw abundance figures. In contrast, when looking at the raw abundance levels of Snc1 (LmxM.08.0030), there appeared to be consistently higher levels in the $Tlg2^{FL}$-expressing protein complexes compared to the $Tlg2^{WT}$, the parental or the RBP control cell lines, despite the difference not being deemed significant. This could potentially be due to only one unique peptide being identified for Snc1, therefore lowering the confidence of the identity being true and not the result of false positives (S. Carr et al., 2004). If the identity and raw abundance truly reflect the *in vivo* interactions, the increase seen in the $Tlg2^{FL}$ protein complexes compared to the $Tlg2^{WT}$ could be due to the F10A/L11A mutation negating Vps45's role in regulating Tlg2's entry into SNARE complexes. In yeast, it is known that Tlg2 lacking the N-terminus are still able to form SNARE complexes (Furgason et al., 2009), thus, $Tlg2^{FL}$ may be in an open conformation that can freely bind to its SNARE complex partners, in a manner analogous to Stx1a in the absence of its N-terminal peptide (Burkhardt et al., 2008).

Future IP experiments could benefit from using alternative lysing and eluting methods to help reduce background noise and preserve low-affinity or transient binding partners. Lysing cells by sonication may disrupt protein-protein interactions, as well as promote formation of protein aggregates (Stathopulos et al., 2008). Non-ionic detergent-based cell lysis could therefore be used as an alternative method, as it generally more gentle than physical disruption methods, does not denature proteins, and can be useful for solubilising membrane-bound proteins (Lim et al., 2021; Thermo Fisher Scientific, 2022). A common issue with eluting proteins through use of denaturing SDS sample buffers is the high levels of non-specific background proteins and macromolecules. As well as the intended target protein complexes, any proteins that have bound to the Fc region of the anti-HA antibodies, or to the beads themselves, will be eluted, increasing the likelihood of false-positive signals and complicating downstream analysis (Lim et al., 2021). An alternative elution strategy is to utilise an HA peptide that would out-compete the target

complexes for the antigen binding region of the anti-HA antibodies, thus displacing and eluting them whilst leaving the non-specific contaminants bound to the beads and antibody Fc regions (Lim et al., 2021; Tomomori-Sato et al., 2013). Finally, to increase the likelihood of co-precipitating low-affinity or transient interacting partners, crosslinking of the samples could be performed to stabilise the interactions and prevent loss of such proteins (Wang et al., 2019).

Chapter 6 – General Discussion

SNAREs are a highly conserved family of proteins that mediate intracellular membrane fusion events. Although the presence of SNAREs has been verified in the *L. major* species of *Leishmania*, and also in the related trypanosomatids *T. brucei* and *T. cruzi*, to date, no functional studies have been undertaken for these parasites (Besteiro et al., 2006; Dacks & Doolittle, 2002; Murungi et al., 2014). The data contained in this thesis therefore constitutes the first functional analysis of a SNARE protein in *Leishmania*. Encouragingly, genome searches of *L. mexicana* were able to identify homologues of Tlg2 and its SNARE complex partners when searches were conducted with yeast and human sequences, along with two Vps45 SM protein homologues. These identities were in concurrence with what had previously been described for *L. major* and showed a high level of sequence conservation between the two species (Besteiro et al., 2006).

Neither Tlg2 nor the Vps45a homologue appear to be essential in *L. mexicana* promastigotes, as null mutants for both of these proteins were still viable. Interestingly, whilst *tlg2*Δ promastigotes displayed several growth-related defects, the same was not seen in the *vps45a*Δ, which is in contrast to what is witnessed in yeast (Cowles et al., 1994; Piper et al., 1994; Shanks et al., 2012). This could potentially be explained by the presence of two Vps45 homologues in *L. mexicana*, as opposed to the one Vps45 found in yeast, which may provide some level of functional redundancy. Future research could therefore aim to characterise both of these homologues, with CRISPR/Cas9 mediated knockout of Vps45b, and well as engineering a *vps45a/vps45b* double null mutant. Epitope protein tagging strategies and immunofluorescence studies could also be utilised to determine whether or not the two proteins are 1) expressed 2) display the same expression profile as each other 3) display the same expression profile as Tlg2 (which would support the assumption that these proteins are interacting partners) and 4) co-localise with each other to the same subcellular localisations (which would suggest a conservation of function). As yeast cells display a concomitant increase or decrease in Tlg2 levels when Vps45 is overexpressed or deleted, respectively, measurement of Tlg2 expression levels to see if they mirror those of Vps45 in *L. mexicana vps45* null mutants or overexpression cell lines could also be undertaken. If expression of Tlg2 is shown to be Vps45-dependant, this would point to a conservation of function whereby either one or both of the Vps45s stabilises and positively promotes the cellular levels of Tlg2 (Bryant & James, 2001; Carpp et al., 2007; Shanks et al., 2012).

The growth-related defects of *tlg2*Δ are consistent with yeast studies, where deletion of Tlg2 and Vps45 led to slower growth (Abeliovich et al., 1998; Shanks et al., 2012). Notably, *tlg2*Δ in

L. mexicana promastigotes causes a delay in cell growth and division, but eventually appears to 'catch-up' with the parental cell line. However, this may have biologically relevant implications for the transmission potential of *L. mexicana* promastigotes lacking Tlg2. In sand flies, *L. mexicana* metacyclic promastigotes are detected in the midgut from day 4 post-blood meal, with the number steadily increasing on subsequent days (Gossage et al., 2003). The gonotrophic cycle of sand flies is ~5 – 6 days, with intake of a fresh blood meal starting a new cycle (Falcão de Oliveira et al., 2017; Moraes et al., 2018). In this scenario, metacyclic promastigotes are present in the sand fly and are ready to be transmitted to a mammalian host when the sand fly takes a blood meal. As *tlg2*Δ causes proliferative defects in promastigotes, it is possible that the differentiation to metacyclic promastigotes would no longer correlate with when the sand fly blood feeds and therefore cause a reduction in transmission potential. qPCR evidence also supports a possible delay in metacyclogenesis, with *tlg2* null mutants expressing *SHERP* transcripts 24 hours later than the parental or ectopic $Tlg2^{WT}$-expressing 'addback' cell lines. Future studies could test this theory by infecting sand flies with *tlg2*Δ promastigotes and tracking the progress of proliferation and differentiation through the sand fly midgut, to determine if the appearance of metacyclic promastigotes is able to coincide with when sand flies take a blood meal (Gossage et al., 2003).

Tlg2 deletion also appears to play a role in parasite virulence, as macrophage infection assays show that, whilst *tlg2*Δ stationary-phase promastigotes are initially able to infect macrophages to the same apparent levels as the parental cell line, they cannot sustain this infection after 24 hours P.I. This could be indicative of a defect in the *tlg2* null mutant's ability to undergo amastigogenesis. A repeat of this experiment could examine the morphology of the parasites within the macrophages to determine whether they are more promastigote-like or amastigote-like in appearance at the different timepoints. Additionally, use of life cycle markers such as SHERP (for metacyclic promastigotes) or amastin (for amastigotes) would allow quantification of the proportions found of each form. An extension of this research would be to conduct mice infections with *tlg2*Δ stationary phase promastigotes and measure the appearance, growth rate and size of cutaneous leishmaniasis lesions in comparison to those produced by infection with the parental cell lines (Alexander et al., 1998). This would help to determine any differences for *in vivo* virulence in *Leishmania* parasites caused by an absence of Tlg2 and would shed greater light on the role of Tlg2 in parasite differentiation and survival within a mammalian host.

Although the addback of ectopic $Tlg2^{WT}$ into the null mutants was not apparently sufficient to rescue the virulence phenotype the difference in cell culturing methods make it difficult to compare the cell lines and draw any meaningful conclusions. This issue could be remedied by integrating the gene into the *L. mexicana* genome, thus removing the need for drug selection. It

is, however, encouraging that the Tlg2^{WT} 'addback' was able to rescue the null mutant growth and cell cycle defects, which is indicative of the null mutant phenotypes being due to the absence of Tlg2 and not to off-target effects. Although SNPs were identified in the *tlg2*Δ cell line that were unique from the parental population, time constraints meant that analysis of the genes affected was not possible. Future studies could therefore utilise this dataset to highlight any gene/protein pathways that could contribute to parasite survival in the absence of Tlg2.

In contrast to Tlg2^{WT}, addback of ectopic Tlg2^{FL} was unable to rescue the null mutant growth phenotypes. Western blots demonstrate very low levels of expression for Tlg2^{FL} in the addback cell lines, in contrast to Tlg2^{WT}, despite the higher-than-endogenous levels of Tlg2 mRNA. This raises the question of whether the mRNA is being modified post-transcriptionally to prevent translation of the mutant protein, or whether post-translation degradation of the Tlg2^{FL} protein is occurring. As yeast Vps45 stabilises its cognate Tlg2 via the N-terminal motif (Carpp et al., 2007), inclusion of the F10A/L11A mutation in the *L. mexicana* Tlg2, which is predicted to abrogate this N-terminal pocket-mode of binding, could target the protein for rapid proteasomal degradation. This proposed degradation pathway is analogous to what is seen for Tlg2 in yeast *vps45*Δ cells (Bryant & James, 2001). To test this hypothesis, proteosome inhibitors, such as MG132, could be used to block this degradation pathway to see if this stabilises the levels of cellular Tlg2^{FL}. This would help to clarify whether *TLG2^{FL}* mRNA is being translated and subsequently degraded or if an alternative process is occurring.

Tlg2 demonstrated a distinct expression pattern in *L. mexicana*, whereby the protein was highly expressed during logarithmic growth and then dramatically dropped off when the promastigotes entered the stationary phase. In contrast, *TLG2* mRNA levels remained relatively stable up to Day 5 for the Tlg2 addback cell lines, along with the parental cell line, which would suggest that Tlg2 protein levels are regulated post-transcriptionally. Consequently, when promastigotes enter stationary phase, Tlg2 could be undergoing post-transcriptional regulation to prevent translation, or post-translational regulation such as rapid proteasomal degradation. An extension of the proteasome inhibition experiment could therefore be utilised to see if Tlg2^{WT} is also being degraded via the proteasome, once the promatigotes have reached the stationary phase.

An interesting result of the immunoprecipitation assays to determine Tlg2 binding partners was the absence of Vps45 and the predicted SNARE complex partners in the list of proteins that were classified as differentially expressed. In fact, identifiable peptides for some of these proteins, such as Vps45a, were completely absent from the immunoprecipitations, which raises questions over whether these proteins do bind to Tlg2 in *L. mexicana* or if alternative pathways and complexes are formed. *In vitro* binding assays, such as pulldowns, could therefore be used

to try and address these questions. In addition, detailed illustration of the interactions between *L. mexicana* Tlg2 and Vps45 could be achieved through x-ray crystallography and structural analysis of recombinantly expressed forms of these protein, as has previously been demonstrated for the Sec1–Stx1a complex (Misura et al., 2000). This would serve several purposes. Firstly, it would demonstrate whether or not the structure of *L. mexicana* Tlg2 and the two Vps45s are homologous to what is seen in other organisms and for other syntaxin-SM complexes. Secondly, it would also allow characterisation of the mode of binding employed when Tlg2 and Vps45 are in complex, as well as identify key residues for these interactions. Thirdly, analysis of the crystal structures could be used to see if there are any differences in the methods of binding to Tlg2 for the two Vps45 homologues. Finally, inclusion of the $Tlg2^{FL}$ protein would highlight whether mutation of the F10 and L11 residues disrupt any or all binding to Vps45. Size exclusion chromatography (SEC) could also be performed using these recombinantly expressed proteins to show whether they form complexes, characterised by a shift in the molecular weight of individual components to larger complexes in the protein peaks (Mayer et al., 2009). This method could also be used to see if Tlg2 is able to bind to any of its predicted SNARE partners, either individually or as part of a QabcR SNARE complex. In addition, mixing of Vps45 and the Tlg2 1-34aa WT or FL N-peptides would demonstrate whether either, or both, is able to bind to the SM protein and potentially highlight any differences from what has been demonstrated in yeast (namely, that the FL N-peptide cannot bind the hydrophobic pocket on domain 1 of Vps45) (Furgason et al., 2009).

An alternative approach to try and confirm N-peptide binding to Vps45 and resolve the importance of the F10/L11 residues could include *in vitro* direct binding assays such as fluorescence polarisation (FP). This method utilises a phenomenon whereby a fluorescently labelled peptide, when excited by polarised light, in turn emits light that is either polarised or depolarised depending on the degree of molecular rotation. When in solution with a recombinantly expressed protein of interest, binding of the fluorescently labelled peptide to this protein reduces its molecular rotations and increases the level of polarised light emitted. The fraction of bound peptide is therefore proportional to the levels of observed polarisation and can be used to calculate binding affinities (Moerke, 2009). An extension of this method is the competitive binding assay, whereby an unlabelled peptide (such as $Tlg2^{FL1-34}$) is introduced to the solution containing the labelled peptide and target protein (i.e. $Tlg2^{1-34}$ and Vps45). The ability of the unlabelled peptide to competitively displace the labelled peptide can then be determined by measuring any decreases in the emitted polarised signal. The use of FP, or similar techniques, could also determine any differences in the binding capacity of the two *L.*

mexicana Vps45s and highlight whether both are capable of the hydrophobic pocket mode of binding to the Tlg2 N-peptide.

The functionality of Tlg2 in endocytosis and autophagy in *L. mexicana* has not yet been clearly identified. Although the growth phenotypes of *tlg2*Δ may point to an underlying defect in endocytosis, further investigation is required. Attempts to utilise the FM4-64 lipophilic dye to track endocytosis were unsuccessful for this study. However, the use of alternative markers, such as dextran pHrodo dyes (Thermo Fisher Scientific), that fluoresce more brightly as pH decreases, could be used to track internalisation and trafficking through the endocytic pathway. An alternative strategy to determine the functionality of *L. mexicana* Tlg2 would be to see whether its expression could complement mutant phenotypes in yeast *tlg2*Δ cell lines (Struthers et al., 2009). If expression of *Lmx*Tlg2 is able to rescue the phenotypes of *tlg2*Δ mutant yeast, then this would infer functional homology for these proteins. Conversely, if *Lmx*Tlg2 is unable to rescue the yeast phenotypes then this could be indicative of a functional divergence between the organisms. Future research could also focus on the role of Tlg2 in autophagy for these parasites. Although the data presented in this thesis highlight changes in *SHERP* expression and decreased virulence that point to defects in differentiation, further research would shed a greater light on this. In yeast, cells lacking Tlg2 show significant reductions in autophagy and it is known that autophagy plays a crucial role in differentiation in *Leishmania* (Besteiro et al., 2006; Nair et al., 2011; Williams et al., 2006). Consequently, *tlg2* deletion in *L. mexicana* may lead to a decrease in autophagy and, in turn, this may impact the ability of the promastigote parasites to differentiate. More direct analysis of autophagy will help to tease this apart. Use of an mCherry-GFP-Atg8 tandem probe can be used to measure autophagic flux and the Atg8 antibody could be utilised in immunofluorescence assays to monitor autophagosome accumulation (Klionsky et al., 2016). Subjecting the *tlg2*Δ promastigotes to starvation would be a useful way to induce autophagy in these cells and allow comparisons to parental cells lines in a controlled environment. It would also be useful to help ascertain whether or not *tlg2*Δ promastigotes are more susceptible to such stressors. Finally, undertaking localisation studies of Atg9 would help to determine if a similar mislocalisation occurs in *tlg2*Δ *L. mexicana* to what is seen in yeast (Nair et al., 2011). As Atg9 containing membranes are important for the expansion of the phagophore membrane, mislocalisation of this protein may indicate a defect in the anterograde trafficking of these membranes in a Tlg2-dependant manner, with a subsequent impact on autophagosome maturation and autophagy.

In summary, this work presents the first functional characterisation of a SNARE protein in *Leishmania* and offers an excellent starting point for future study. Although the SNAREs are highly conserved across eukaryotes, the functional homology of *Leishmania* is assumed based

on sequence conservation, without any supporting functional data. As such it would be interesting to characterise further *Leishmania* SNARE proteins to see if any have a divergent or unique role within these parasites that could be exploited for therapeutic intervention. Besteiro et al. (2006) were able to identify 27 SNARE-domain containing proteins in *L. major*, some of which appeared to be novel and may therefore present an attractive target for future analysis. In addition, it would to also be useful to identify SNARE null mutants that have a lethal phenotype, as this could help to highlight critical membrane trafficking pathways within these disease-causing parasites.

Appendices

Plasmid	Description	Drug Resistance	Source
pSSU-GFP-*sherp*	For expression of ectopic GFP under control of *sherp* 3'UTR	Hygromycin	Dr Luis de Pablos, Walrad lab
pSSU-Tlg2^{WT}-*tlg2*	For expression of ectopic Tlg2^{WT}-HA under control of *tlg2* 3'UTR	Hygromycin	This study
pSSU-Tlg2^{FL}-*tlg2*	For expression of ectopic Tlg2^{FL}-HA under control of *tlg2* 3'UTR	Hygromycin	This study
pSSU-Tlg2^{WT}-*nmt*	For expression of ectopic Tlg2^{WT}-HA under control of *nmt* 3'UTR	Hygromycin	This study
pSSU-Tlg2^{FL}-*nmt*	For expression of ectopic Tlg2^{FL}-HA under control of *nmt* 3'UTR	Hygromycin	This study
pSSU HYG^{R}	Plasmid containing a multiple cloning site	Hygromycin	This study
pSSU-Tlg2$^{1-34}$	For expression of Tlg2^{WT}-HA N-peptide under control of *tlg2* 3'UTR	Hygromycin	This study
pSSU-Tlg2^{FL1-34}	For expression of Tlg2^{FL1-34}-HA N-peptide under control of *tlg2* 3'UTR	Hygromycin	This study
pSSU-Tlg2^{WT}	For expression of ectopic Tlg2^{WT}-HA under control of *tlg2* 3'UTR	Blasticidin	This study
pSSU-Tlg2^{FL}	For expression of ectopic Tlg2^{FL}-HA under control of *tlg2* 3'UTR	Blasticidin	This study
pSSU BLA^{R}	Plasmid containing a multiple cloning site	Blasticidin	This study
pTBlast_v1	Plasmid for amplification of resistance cassette for CRISPR/Cas9 mediated knockout	Blasticidin	Beneke et al. 2017
pTPuro_v1	Plasmid for amplification of resistance cassette for CRISPR/Cas9 mediated knockout	Blasticidin	Beneke et al. 2017
pGEM®-T Easy	PCR cloning vector	Ampicillin	Promega

Appendix 1. *List of plasmids used in this study.*

Antibody	Description	Concentration used	Source
mouse anti-HA	monoclonal antibody used for Western blot	1:10,000	Thermo Fisher Scienfitic
rabbit anti-HA	monoclonal antibody used for Western blot	1:2,000	Thermo Fisher Scientific
rabbit anti-NMT	polyclonal antibody used for Western blot	1:2,000 - 1:10,000	Price et al. 2002 (Eurogentec)
mouse anti-EF1α	monoclonal antibody used for Western blot (clone CBP-KK1)	1:10,000	Merck-Millipore
Anti-*Lm* Atg8	Rabbit derived antibody against *L. major* Atg8	1:2,000	Smith lab, University of York
mouse anti-HA	monoclonal antibody used for immunofluorescence	1:500	Sigma
Alexa-fluor 488	goat anti-mouse secondary antibody for immunofluorescence assays	1:2,000	Thermo Fisher Scientific

Appendix 2. *List of antibodies used in this study.*

Appendix 3. *List of oligos used in study*. Provided as a supplemental .csv file.

Appendix 4. *List of SNPs that are unique in* tlg2Δ *compared to T7/Cas9 parental cell line*. Data and table provided by Dr Cooper Grace, Jeffares lab, University of York. Provided as a supplemental .csv file.

Abbreviations

aa	amino acid
A	alanine
AIDs	acquired immunodeficiency syndrome
AmB	amphotericin B
AMPK	AMP-activated protein kinase
API	aminopeptidase I
ATG/Atg	autophagy-related
ATP	adenosine triphosphate
base J	β-D-glucosyl-hydroxymethyluracil
BLA	blasticidin
BLAST	basic local alignment search tool
BSA	bovine serum albumin
Cas9	CRISPR-associated protein 9
cDNA	complementary DNA
CDS	coding Sequence
CL	cutaneous leishmaniasis
CMA	chaperone-mediated autophagy
COG	conserved oligomeric Golgi
CORVET	class C core vacuole/endosome tethering
CPY	carboxypeptidase Y
CRISPR	clustered regularly interspaced short palindromic repeats
Cvt	cytoplasm-to-vacuole targeting
DCL	diffuse cutaneous leishmaniasis
DIC	differential interference contrast
DMSO	dimethyl sulfoxide
DNA	deoxyribonucleic acid
dNTPs	deoxynucleotide triphosphates

E	glutamic acid
EDTA	ethylenediaminetetraacetic acid
EF1α	elongation factor 1 α
ER	endoplasmic reticulum
F	phenylalanine
FBS	fetal bovine serum
FP	fluorescence polarisation
FSC	forward scatter
GARP	Golgi associated retrograde protein complex
GDI	guanine nucleotide dissociation inhibitor
gDNA	genomic DNA
GDF	GDI displacement factor
GDP	guanosine diphosphate
GOI	gene-of-interest
GFP	green fluorescent protein
GTP	guanosine triphosphate
HIV	human immunodeficiency virus
HOPS	homotypic fusion and protein sorting
HYG	hygromycin
IP	immunoprecipitation
IPTG	isopropyl ß-D-1-thiogalactopyranoside
K	lysine
kDa	kilodalton
kDNA	kinetoplast DNA
L	leucine
LB	Luria-Bertani
LAmB	liposomal amphotericin B
LC3	microtubule-associated protein 1A/1B-light chain 3

LC-MS/MS	liquid chromatography with tandem mass spectrometry
MA	meglumine antimoniate
MCL	mucocutaneous leishmaniasis
MF	miltefosine
mRNA	messenger RNA
mTOR	mechanistic target of rapamycin
MVB	multivesicular bodies
NMT	N-myristoyltransferase
NSF	N-ethylmaleimide-sensitive factor
PCA	principle component analysis
PCR	polymerase chain reaction
PBS	phosphate buffered saline
PAS	phagophore assembly site
PE	phosphatidylethanolamine
PFA	paraformaldehyde
PI	propidium iodide
P.I	post-infection
PKA	cAMP-dependent protein kinase
PM	paromomycin or peritrophic matrix (context dependant)
PKDL	post-kala-azar dermal leishmaniasis
PSG	promastigote secretory gel
PI(3)K	phosphatidylinositol 3-kinase
PI(3)P	phosphatidylinositol-3-phosphate
PTU	polycistronic transcriptions units
PVDF	polyvinylidene difluoride
Q	glutamine
R	arginine
RBP	RNA binding protein

RFP	red fluorescent protein
RNA	ribonucleic acid
SDS-PAGE	sodium dodecyl sulphate-polyacrylamide gel electrophoresis
SGD	Saccharomyces Genome Database
sgRNA	single guide RNA
SHERP	small hydrophilic endoplasmic reticulum-associated protein
SM	Sec1/Munc18
SNAP	soluble NSF attachment proteins
SNARE	soluble *N*-ethylmaleimide-sensitive factor adaptor proteins receptors
Snc	synaptobrevin homolog
SNP	single nucleotide polymorphism
SSC	side scatter
SSG	sodium stibogluconate
Stx	syntaxin
T7 RNAP	T7 RNA polymerase
TAE	Tris-acetate-EDTA
TGN	*trans*-Golgi network
Tlg	t-SNARE affecting a late Golgi compartment
TMD	transmembrane domain
TRAPP	transport protein particle
UTR	untranslated region
VAMP	vesicle-associated membrane protein
VMP	vacuole membrane protein
VFT	Vps fifty-three
VL	visceral leishmaniasis
VLCFA	very long chain fatty acid
Vps45	vacuolar protein sorting-associated protein 45
Vti	vesicle transport through interaction with t-SNAREs

References

Abeliovich, H., Darsow, T., & Emr, S. D. (1999). Cytoplasm to vacuole trafficking of aminopeptidase I requires a t-SNARE-Sec1p complex composed of Tlg2p and Vps45p. *The EMBO Journal*, *18*(21), 6005–6016. https://doi.org/10.1093/emboj/18.21.6005

Abeliovich, H., Grote, E., Novick, P., & Ferro-Novick, S. (1998). Tlg2p, a Yeast Syntaxin Homolog That Resides on the Golgi and Endocytic Structures. *Journal of Biological Chemistry*, *273*(19), 11719–11727. https://doi.org/10.1074/jbc.273.19.11719

Alcoforado Diniz, J., Chaves, M. M., Vaselek, S., Miserani Magalhães, R. D., Ricci-Azevedo, R., de Carvalho, R. V. H., Lorenzon, L. B., Ferreira, T. R., Zamboni, D., Walrad, P. B., Volf, P., Sacks, D. L., & Cruz, A. K. (2021). Protein methyltransferase 7 deficiency in Leishmania major increases neutrophil associated pathology in murine model. *PLOS Neglected Tropical Diseases*, *15*(3), e0009230. https://doi.org/10.1371/journal.pntd.0009230

Alcolea, P. J., Alonso, A., Molina, R., Jiménez, M., Myler, P. J., & Larraga, V. (2019). Functional genomics in sand fly–derived Leishmania promastigotes. *PLOS Neglected Tropical Diseases*, *13*(5), e0007288. https://doi.org/10.1371/journal.pntd.0007288

Alexander, J., Coombs, G. H., & Mottram, J. C. (1998). Leishmania mexicana cysteine proteinase-deficient mutants have attenuated virulence for mice and potentiate a Th1 response. *Journal of Immunology (Baltimore, Md. : 1950)*, *161*(12), 6794–6801.

Alvar, J., Vélez, I. D., Bern, C., Herrero, M., Desjeux, P., Cano, J., Jannin, J., & Boer, M. den. (2012). Leishmaniasis Worldwide and Global Estimates of Its Incidence. *PLoS ONE*, *7*(5), e35671. https://doi.org/10.1371/journal.pone.0035671

Anderson, B. A., Wong, I. L. K., Baugh, L., Ramasamy, G., Myler, P. J., & Beverley, S. M. (2013). Kinetoplastid-specific histone variant functions are conserved in Leishmania major. *Molecular and Biochemical Parasitology*, *191*(2), 53–57. https://doi.org/10.1016/j.molbiopara.2013.09.005

Antonin, W., Dulubova, I., Araç, D., Pabst, S., Plitzner, J., Rizo, J., & Jahn, R. (2002). The N-terminal Domains of Syntaxin 7 and vti1b Form Three-helix Bundles That Differ in Their Ability to Regulate SNARE Complex Assembly. *Journal of Biological Chemistry*, *277*(39), 36449–36456. https://doi.org/10.1074/jbc.M204369200

Antonin, W., Fasshauer, D., Becker, S., Jahn, R., & Schneider, T. R. (2002). Crystal structure of the endosomal SNARE complex reveals common structural principles of all SNAREs. *Nature Structural Biology*, *9*(2), 107–111. https://doi.org/10.1038/nsb746

Aoyagi, K., Itakura, M., Fukutomi, T., Nishiwaki, C., Nakamichi, Y., Torii, S., Makiyama, T., Harada, A., & Ohara-Imaizumi, M. (2018). VAMP7 Regulates Autophagosome Formation by Supporting Atg9a Functions in Pancreatic β-Cells From Male Mice. *Endocrinology*, *159*(11), 3674–3688. https://doi.org/10.1210/en.2018-00447

Arias, E., & Cuervo, A. M. (2011). Chaperone-mediated autophagy in protein quality control. *Current Opinion in Cell Biology*, *23*(2), 184–189. https://doi.org/10.1016/j.ceb.2010.10.009

Ashburner, M., Ball, C. A., Blake, J. A., Botstein, D., Butler, H., Cherry, J. M., Davis, A. P., Dolinski, K., Dwight, S. S., Eppig, J. T., Harris, M. A., Hill, D. P., Issel-Tarver, L., Kasarskis, A., Lewis, S., Matese, J. C., Richardson, J. E., Ringwald, M., Rubin, G. M., & Sherlock, G. (2000). Gene Ontology: tool for the unification of biology. *Nature Genetics*, *25*(1), 25–29. https://doi.org/10.1038/75556

Bahl, S., Parashar, S., Malhotra, H., Raje, M., & Mukhopadhyay, A. (2015). Functional Characterization of Monomeric GTPase Rab1 in the Secretory Pathway of Leishmania. *Journal of Biological Chemistry*, *290*(50), 29993–30005. https://doi.org/10.1074/jbc.M115.670018

Balaska, S., Fotakis, E. A., Chaskopoulou, A., & Vontas, J. (2021). Chemical control and insecticide resistance status of sand fly vectors worldwide. *PLOS Neglected Tropical Diseases*, *15*(8), e0009586. https://doi.org/10.1371/journal.pntd.0009586

Balderhaar, H. J. kleine, & Ungermann, C. (2013). CORVET and HOPS tethering complexes – coordinators of endosome and lysosome fusion. *Journal of Cell Science*, *126*(6), 1307–1316. https://doi.org/10.1242/jcs.107805

Barak, E., Amin-Spector, S., Gerliak, E., Goyard, S., Holland, N., & Zilberstein, D. (2005). Differentiation of Leishmania donovani in host-free system: analysis of signal perception and response. *Molecular and Biochemical Parasitology*, *141*(1), 99–108. https://doi.org/10.1016/j.molbiopara.2005.02.004

Basmaciyan, L., Azas, N., & Casanova, M. (2017). Calcein+/PI- as an early apoptotic feature in Leishmania. *PLOS ONE*, *12*(11), e0187756. https://doi.org/10.1371/journal.pone.0187756

Basmaciyan, L., & Casanova, M. (2019). Cell death in *Leishmania*. *Parasite*, *26*, 71. https://doi.org/10.1051/parasite/2019071

Bates, P. A. (2008). Leishmania sand fly interaction: progress and challenges. *Current Opinion in Microbiology*, *11*(4), 340–344. https://doi.org/10.1016/j.mib.2008.06.003

Beattie, L., & Kaye, P. M. (2011). Leishmania-host interactions: what has imaging taught us? *Cellular Microbiology*, *13*(11), 1659–1667. https://doi.org/10.1111/j.1462-5822.2011.01658.x

Beneke, T., Madden, R., Makin, L., Valli, J., Sunter, J., & Gluenz, E. (2017). A CRISPR Cas9 high-throughput genome editing toolkit for kinetoplastids. *Royal Society Open Science*, *4*(5), 170095. https://doi.org/10.1098/rsos.170095

Berg, T. O., Fengsrud, M., Strømhaug, P. E., Berg, T., & Seglen, P. O. (1998). Isolation and Characterization of Rat Liver Amphisomes. *Journal of Biological Chemistry*, *273*(34), 21883–21892. https://doi.org/10.1074/jbc.273.34.21883

Besteiro, S., Coombs, G. H., & Mottram, J. C. (2006). The SNARE protein family of Leishmania major. *BMC Genomics*, *7*(1), 250. https://doi.org/10.1186/1471-2164-7-250

Besteiro, S., Williams, R. A. M., Morrison, L. S., Coombs, G. H., & Mottram, J. C. (2006). Endosome Sorting and Autophagy Are Essential for Differentiation and Virulence of Leishmania major. *Journal of Biological Chemistry*, *281*(16), 11384–11396. https://doi.org/10.1074/jbc.M512307200

Blum, M., Chang, H.-Y., Chuguransky, S., Grego, T., Kandasaamy, S., Mitchell, A., Nuka, G., Paysan-Lafosse, T., Qureshi, M., Raj, S., Richardson, L., Salazar, G. A., Williams, L., Bork, P., Bridge, A., Gough, J., Haft, D. H., Letunic, I., Marchler-Bauer, A., … Finn, R. D. (2021). The InterPro protein families and domains database: 20 years on. *Nucleic Acids Research*, *49*(D1), D344–D354. https://doi.org/10.1093/nar/gkaa977

Bock, J. B., Matern, H. T., Peden, A. A., & Scheller, R. H. (2001). A genomic perspective on membrane compartment organization. *Nature*, *409*(6822), 839–841. https://doi.org/10.1038/35057024

Boucrot, E., Kirchhausen, T. (2007) Endosomal recycling controls plasma membrane area during mitosis. *Proceedings of the National Academy of Sciences*, *104*(19), 7939–7944. https://doi.org/10.1073/pnas.0702511104

Brennand, A., Rico, E., & Michels, P. A. M. (2012). Autophagy in Trypanosomatids. *Cells*, *1*(3), 346–371. https://doi.org/10.3390/cells1030346

Britch, S. C., Linthicum, K. J., Walker, T. W., Farooq, M., Gordon, S. W., Clark, J. W., Ngere, F., Ngonga, D., & Chepchieng, C. (2011). Evaluation of ULV Applications Against Old World Sand Fly (Diptera: Psychodidae) Species in Equatorial Kenya. *Journal of Medical Entomology*, *48*(6), 1145–1159. https://doi.org/10.1603/ME11025

Bryant, N. J., & James, D. E. (2001). Vps45p stabilizes the syntaxin homologue Tlg2p and positively regulates SNARE complex formation. *EMBO Journal*, *20*(13), 3380–3388. https://doi.org/10.1093/emboj/20.13.3380

Bryant, N. J., & Stevens, T. H. (1998). Vacuole biogenesis in Saccharomyces cerevisiae: protein transport pathways to the yeast vacuole. *Microbiology and Molecular Biology Reviews : MMBR*, *62*(1), 230–247. https://doi.org/10.1128/MMBR.62.1.230-247.1998

Burkhardt, P., Hattendorf, D. A., Weis, W. I., & Fasshauer, D. (2008). Munc18a controls SNARE assembly through its interaction with the syntaxin N-peptide. *The EMBO Journal*, *27*(7), 923–933. https://doi.org/10.1038/emboj.2008.37

Burman, C., & Ktistakis, N. T. (2010). Regulation of autophagy by phosphatidylinositol 3-phosphate. *FEBS Letters*, *584*(7), 1302–1312. https://doi.org/10.1016/j.febslet.2010.01.011

Burza, S., Croft, S. L., & Boelaert, M. (2018). Leishmaniasis. *The Lancet*, *392*(10151), 951–970. https://doi.org/10.1016/S0140-6736(18)31204-2

Byrne, K. P., & Wolfe, K. H. (2005). The Yeast Gene Order Browser: Combining curated homology and syntenic context reveals gene fate in polyploid species. *Genome Research*, *15*(10), 1456–1461. https://doi.org/10.1101/gr.3672305

Cai, H., Reinisch, K., & Ferro-Novick, S. (2007). Coats, Tethers, Rabs, and SNAREs Work Together to Mediate the Intracellular Destination of a Transport Vesicle. *Developmental Cell*, *12*(5), 671–682. https://doi.org/10.1016/j.devcel.2007.04.005

Cao, X., Ballew, N., & Barlowe, C. (1998). Initial docking of ER-derived vesicles requires Uso1p and Ypt1p but is independent of SNARE proteins. *The EMBO Journal*, *17*(8), 2156–2165. https://doi.org/10.1093/emboj/17.8.2156

Carbon, S., Douglass, E., Good, B. M., Unni, D. R., Harris, N. L., Mungall, C. J., Basu, S., Chisholm, R. L., Dodson, R. J., Hartline, E., Fey, P., Thomas, P. D., Albou, L.-P., Ebert, D., Kesling, M. J., Mi, H., Muruganujan, A., Huang, X., Mushayahama, T., … Elser, J. (2021). The Gene Ontology resource: enriching a GOld mine. *Nucleic Acids Research*, *49*(D1), D325–D334. https://doi.org/10.1093/nar/gkaa1113

Carpp, L. N., Ciufo, L. F., Shanks, S. G., Boyd, A., & Bryant, N. J. (2006). The Sec1p/Munc18 protein Vps45p binds its cognate SNARE proteins via two distinct modes. *Journal of Cell Biology*, *173*(6), 927–936. https://doi.org/10.1083/jcb.200512024

Carpp, L. N., Shanks, S. G., Struthers, M. S., & Bryant, N. J. (2007). Cellular levels of the syntaxin Tlg2p are regulated by a single mode of binding to Vps45p. *Biochemical and Biophysical Research Communications*, *363*(3), 857–860. https://doi.org/10.1016/j.bbrc.2007.09.067

Carr, C. M., & Rizo, J. (2010). At the junction of SNARE and SM protein function. *Current Opinion in Cell Biology*, *22*(4), 488–495. https://doi.org/10.1016/j.ceb.2010.04.006

Carr, S., Aebersold, R., Baldwin, M., Burlingame, A., Clauser, K., & Nesvizhskii, A. (2004). The Need for Guidelines in Publication of Peptide and Protein Identification Data. *Molecular & Cellular Proteomics*, *3*(6), 531–533. https://doi.org/10.1074/mcp.T400006-MCP200

Castro, R., Scott, K., Jordan, T., Evans, B., Craig, J., Peters, E. L., & Swier, K. (2006). The ultrastructure of the parasitophorous vacuole formed by Leishmania major. *Journal of Parasitology*, *92*(6), 1162–1170. https://doi.org/10.1645/GE-841R.1

Chappuis, F., Sundar, S., Hailu, A., Ghalib, H., Rijal, S., Peeling, R. W., Alvar, J., & Boelaert, M. (2007). Visceral leishmaniasis: what are the needs for diagnosis, treatment and control? *Nature Reviews Microbiology*, *5*(11), 873–882. https://doi.org/10.1038/nrmicro1748

Chernomordik, L. v., & Kozlov, M. M. (2003). Protein-Lipid Interplay in Fusion and Fission of Biological Membranes. *Annual Review of Biochemistry*, *72*(1), 175–207. https://doi.org/10.1146/annurev.biochem.72.121801.161504

Chowdhury, R., Huda, M. M., Kumar, V., Das, P., Joshi, A. B., Banjara, M. R., Akhter, S., Kroeger, A., Krishnakumari, B., Petzold, M., Mondal, D., & Das, M. L. (2011). The Indian and Nepalese programmes of indoor residual spraying for the elimination of

visceral leishmaniasis: performance and effectiveness. *Annals of Tropical Medicine & Parasitology*, *105*(1), 31–35. https://doi.org/10.1179/136485911X12899838683124

Christiano, R., Nagaraj, N., Fröhlich, F., & Walther, T. C. (2014). Global Proteome Turnover Analyses of the Yeasts S. cerevisiae and S. pombe. *Cell Reports*, *9*(5), 1959–1965. https://doi.org/10.1016/j.celrep.2014.10.065

Cingolani, P., Platts, A., Wang, L. L., Coon, M., Nguyen, T., Wang, L., Land, S. J., Lu, X., & Ruden, D. M. (2012). A program for annotating and predicting the effects of single nucleotide polymorphisms, SnpEff. *Fly*, *6*(2), 80–92. https://doi.org/10.4161/fly.19695

Clayton, C. (2016). Gene expression in Kinetoplastids. *Current Opinion in Microbiology*, *32*, 46–51. https://doi.org/10.1016/j.mib.2016.04.018

Coe, J. G. S., Lim, A. C. B., Xu, J., & Hong, W. (1999). A Role for Tlg1p in the Transport of Proteins within the Golgi Apparatus of *Saccharomyces cerevisiae*. *Molecular Biology of the Cell*, *10*(7), 2407–2423. https://doi.org/10.1091/mbc.10.7.2407

Cowles, C. R., Emr, S. D., & Horazdovsky, B. F. (1994). Mutations in the VPS45 gene, a SEC1 homologue, result in vacuolar protein sorting defects and accumulation of membrane vesicles. *Journal of Cell Science*, *107 (Pt 12)*, 3449–3459.

da Silva, I. A., Morato, C. I., Quixabeira, V. B. L., Pereira, L. I. de A., Dorta, M. L., de Oliveira, M. A. P., Horta, M. F., & Ribeiro-Dias, F. (2015). *In Vitro* Metacyclogenesis of *Leishmania (Viannia) braziliensis* and *Leishmania (Leishmania) amazonensis* Clinical Field Isolates, as Evaluated by Morphology, Complement Resistance, and Infectivity to Human Macrophages. *BioMed Research International*, *2015*, 1–15. https://doi.org/10.1155/2015/393049

Dacks, J. B., & Doolittle, W. F. (2002). Novel syntaxin gene sequences from Giardia, Trypanosoma and algae: implications for the ancient evolution of the eukaryotic endomembrane system. *Journal of Cell Science*, *115*(Pt 8), 1635–1642.

Dacks, J. B., & Field, M. C. (2018). Evolutionary origins and specialisation of membrane transport. *Current Opinion in Cell Biology*, *53*, 70–76. https://doi.org/10.1016/j.ceb.2018.06.001

Das, V. N. R., Ranjan, A., Bimal, S., Siddique, N. A., Pandey, K., Kumar, N., Verma, N., Singh, V. P., Sinha, P. K., & Bhattacharya, S. K. (n.d.). Magnitude of unresponsiveness to

sodium stibogluconate in the treatment of visceral leishmaniasis in Bihar. *The National Medical Journal of India*, *18*(3), 131–133.

Daste, F., Galli, T., & Tareste, D. (2015). Structure and function of longin SNAREs. *Journal of Cell Science*. https://doi.org/10.1242/jcs.178574

de Pablos, L., Ferreira, T., & Walrad, P. (2016). Developmental differentiation in Leishmania lifecycle progression: post-transcriptional control conducts the orchestra. *Current Opinion in Microbiology*, *34*, 82–89. https://doi.org/10.1016/j.mib.2016.08.004

de Pablos, L. M., Ferreira, T. R., Dowle, A. A., Forrester, S., Parry, E., Newling, K., & Walrad, P. B. (2019). The mRNA-bound Proteome of Leishmania mexicana: Novel Genetic Insight into an Ancient Parasite. *Molecular & Cellular Proteomics*, *18*(7), 1271–1284. https://doi.org/10.1074/mcp.RA118.001307

de Paiva, R. M. C., Grazielle-Silva, V., Cardoso, M. S., Nakagaki, B. N., Mendonça-Neto, R. P., Canavaci, A. M. C., Melo, N. S., Martinelli, P. M., Fernandes, A. P., daRocha, W. D., Teixeira, S. M. R. (2015) Amastin Knockdown in *Leishmania braziliensis* Affects Parasite-Macrophage Interaction and Results in Impaired Viability of Intracellular Amastigotes. *PLOS Pathogens*, *11*(12) e1005296. https://doi.org/10.1371/journal.ppat.1005296

de Pina Carvalho, J., de Assis, T. M., Simões, T. C., & Cota, G. (2021). Estimating direct costs of the treatment for mucosal leishmaniasis in Brazil. *Revista da Sociedade Brasileira de Medicina Tropical*, *54*, e04542020. https://doi.org/10.1590/0037-8682-0454-2020

de Vries, H. J. C., Reedijk, S. H., & Schallig, H. D. F. H. (2015). Cutaneous Leishmaniasis: Recent Developments in Diagnosis and Management. *American Journal of Clinical Dermatology*, *16*(2), 99–109. https://doi.org/10.1007/s40257-015-0114-z

Dean, S., Sunter, J. D., & Wheeler, R. J. (2017). TrypTag.org: A Trypanosome Genome-wide Protein Localisation Resource. *Trends in Parasitology*, *33*(2), 80–82. https://doi.org/10.1016/j.pt.2016.10.009

Dietrich, L. E. P., Boeddinghaus, C., LaGrassa, T. J., & Ungermann, C. (2003). Control of eukaryotic membrane fusion by N-terminal domains of SNARE proteins. *Biochimica et Biophysica Acta (BBA) - Molecular Cell Research*, *1641*(2–3), 111–119. https://doi.org/10.1016/S0167-4889(03)00094-6

Dillon, L. A. L., Okrah, K., Hughitt, V. K., Suresh, R., Li, Y., Fernandes, M. C., Belew, A. T., Corrada Bravo, H., Mosser, D. M., & El-Sayed, N. M. (2015). Transcriptomic profiling of gene expression and RNA processing during *Leishmania major* differentiation. *Nucleic Acids Research*, *43*(14), 6799–6813. https://doi.org/10.1093/nar/gkv656

Dirac-Svejstrup, A. B. (1997). Identification of a GDI displacement factor that releases endosomal Rab GTPases from Rab-GDI. *The EMBO Journal*, *16*(3), 465–472. https://doi.org/10.1093/emboj/16.3.465

Doehl, J. S. P., Sádlová, J., Aslan, H., Pružinová, K., Metangmo, S., Votýpka, J., Kamhawi, S., Volf, P., & Smith, D. F. (2017). Leishmania HASP and SHERP Genes Are Required for In Vivo Differentiation, Parasite Transmission and Virulence Attenuation in the Host. *PLOS Pathogens*, *13*(1), e1006130. https://doi.org/10.1371/journal.ppat.1006130

Domínguez, M., & Toraño, A. (1999). Immune adherence-mediated opsonophagocytosis: the mechanism of Leishmania infection. *Journal of Experimental Medicine 189*(1), 25-35. doi: 10.1084/jem.189.1.25

Dorlo, T. P. C., Balasegaram, M., Beijnen, J. H., & de Vries, P. J. (2012). Miltefosine: a review of its pharmacology and therapeutic efficacy in the treatment of leishmaniasis. *Journal of Antimicrobial Chemotherapy*, *67*(11), 2576–2597. https://doi.org/10.1093/jac/dks275

Dulubova, I., Sugita, S., Hill, S., Hosaka, M., Fernandez, I., Südhof, T. C., & Rizo, J. (1999). A conformational switch in syntaxin during exocytosis: role of munc18. *The EMBO Journal*, *18*(16), 4372–4382. https://doi.org/10.1093/emboj/18.16.4372

Dulubova, I., Yamaguchi, T., Gao, Y., Min, SW., Huryeva, I., Südhof, T., & Rizo, J. (2002). How Tlg2p/syntaxin 16 “snares” Vps45. *The EMBO Journal*, *21*(14), 3620–3631. https://doi.org/10.1093/emboj/cdf381

Dunlop, E. A., & Tee, A. R. (2014). mTOR and autophagy: A dynamic relationship governed by nutrients and energy. *Seminars in Cell & Developmental Biology*, *36*, 121–129. https://doi.org/10.1016/j.semcdb.2014.08.006

Ellgaard, L., McCaul, N., Chatsisvili, A., & Braakman, I. (2016). Co- and Post-Translational Protein Folding in the ER. *Traffic*, *17*(6), 615–638. https://doi.org/10.1111/tra.12392

Epple, U. D., Suriapranata, I., Eskelinen, E.-L., & Thumm, M. (2001). Aut5/Cvt17p, a Putative Lipase Essential for Disintegration of Autophagic Bodies inside the Vacuole. *Journal of Bacteriology*, *183*(20), 5942–5955. https://doi.org/10.1128/JB.183.20.5942-5955.2001

Falcão de Oliveira, E., Oshiro, E. T., Fernandes, W. de S., Murat, P. G., Medeiros, M. J. de, Souza, A. I., Oliveira, A. G. de, & Galati, E. A. B. (2017). Experimental infection and transmission of Leishmania by Lutzomyia cruzi (Diptera: Psychodidae): Aspects of the ecology of parasite-vector interactions. *PLOS Neglected Tropical Diseases*, *11*(2), e0005401. https://doi.org/10.1371/journal.pntd.0005401

Fasshauer, D., Antonin, W., Margittai, M., Pabst, S., & Jahn, R. (1999). Mixed and Non-cognate SNARE Complexes. *Journal of Biological Chemistry*, *274*(22), 15440–15446. https://doi.org/10.1074/jbc.274.22.15440

Fasshauer, D., Sutton, R. B., Brunger, A. T., & Jahn, R. (1998). Conserved structural features of the synaptic fusion complex: SNARE proteins reclassified as Q- and R-SNAREs. *Proceedings of the National Academy of Sciences*, *95*(26), 15781–15786. https://doi.org/10.1073/pnas.95.26.15781

Fernandez, I., Ubach, J., Dulubova, I., Zhang, X., Südhof, T. C., & Rizo, J. (1998). Three-Dimensional Structure of an Evolutionarily Conserved N-Terminal Domain of Syntaxin 1A. *Cell*, *94*(6), 841–849. https://doi.org/10.1016/S0092-8674(00)81742-0

Fidalgo, L. M., & Gille, L. (2011). Mitochondria and Trypanosomatids: Targets and Drugs. *Pharmaceutical Research*, *28*(11), 2758–2770. https://doi.org/10.1007/s11095-011-0586-3

Fiebig, M., Kelly, S., & Gluenz, E. (2015). Comparative Life Cycle Transcriptomics Revises Leishmania mexicana Genome Annotation and Links a Chromosome Duplication with Parasitism of Vertebrates. *PLOS Pathogens*, *11*(10), e1005186. https://doi.org/10.1371/journal.ppat.1005186

Field, M. C., & Carrington, M. (2009). The trypanosome flagellar pocket. *Nature Reviews Microbiology*, *7*(11), 775–786. https://doi.org/10.1038/nrmicro2221

Fix, M., Melia, T. J., Jaiswal, J. K., Rappoport, J. Z., You, D., Sollner, T. H., Rothman, J. E., Simon, S. M. (2004). Imaging single membrane fusion events mediated by SNARE proteins. *Proceedings of the National Academy of Sciences of the United States of America*, *101*(19), 7311–7316. https://doi.org/10.1073/pnas.0401779101

Franke, E. D., McGreevy, P. B., Katz, S. P., & Sacks, D. L. (1985). Growth cycle-dependent generation of complement-resistant Leishmania promastigotes. *Journal of Immunology (Baltimore, Md. : 1950)*, *134*(4), 2713–2718.

Fukasawa, M., Varlamov, O., Eng, W. S., Sollner, T. H., & Rothman, J. E. (2004). Localization and activity of the SNARE Ykt6 determined by its regulatory domain and palmitoylation. *Proceedings of the National Academy of Sciences*, *101*(14), 4815–4820. https://doi.org/10.1073/pnas.0401183101

Furgason, M. L. M., Macdonald, C., Shanks, S. G., Ryder, S. P., Bryant, N. J., & Munson, M. (2009). The N-terminal peptide of the syntaxin Tlg2p modulates binding of its closed conformation to Vps45p. *Proceedings of the National Academy of Sciences USA106*(34), 14303–14308. https://doi.org/10.1073/pnas.0902976106

Fürthauer, M., González-Gaitán, M. (2009) Endocytosis and mitosis: A two-way relationship. *Cell Cycle*, *8*(20), 3311–3318. https://doi.org/10.4161/cc.8.20.9700

Gallwitz, D., & Jahn, R. (2003). The riddle of the Sec1/Munc-18 proteins – new twists added to their interactions with SNAREs. *Trends in Biochemical Sciences*, *28*(3), 113–116. https://doi.org/10.1016/S0968-0004(03)00028-8

Gálvez, R., Montoya, A., Fontal, F., Martínez De Murguía, L., & Miró, G. (2018). Controlling phlebotomine sand flies to prevent canine Leishmania infantum infection: A case of knowing your enemy. *Research in Veterinary Science*, *121*, 94–103. https://doi.org/10.1016/j.rvsc.2018.10.008

Ganesan, D., & Cai, Q. (2021). Understanding amphisomes. *Biochemical Journal*, *478*(10), 1959–1976. https://doi.org/10.1042/BCJ20200917

Garami, A., & Ilg, T. (2001). Disruption of mannose activation in Leishmania mexicana: GDP-mannose pyrophosphorylase is required for virulence, but not for viability. *The EMBO Journal*, *20*(14), 3657–3666. https://doi.org/10.1093/emboj/20.14.3657

Garrison, E., & Marth, G. (2012). *Haplotype-based variant detection from short-read sequencing*.

Gasteiger, E., Hoogland, C., Gattiker, A., Duvaud, S., Wilkins, M., Appel, R., & Bairoch, A. (2005). Protein Identification and Analysis Tools on the ExPASy Server. In J. Walker (Ed.), *The Proteomics Protocols Handbook* (pp. 571–607). Humana Press.

Georgopoulos, C., & Welch, W. J. (1993). Role of the Major Heat Shock Proteins as Molecular Chaperones. *Annual Review of Cell Biology*, *9*(1), 601–634. https://doi.org/10.1146/annurev.cb.09.110193.003125

Gerst, J. E. (1997). Conserved α-Helical Segments on Yeast Homologs of the Synaptobrevin/VAMP Family of v-SNAREs Mediate Exocytic Function. *Journal of Biological Chemistry*, *272*(26), 16591–16598. https://doi.org/10.1074/jbc.272.26.16591

Giraud, E., Martin, O., Yakob, L., & Rogers, M. (2019). Quantifying Leishmania Metacyclic Promastigotes from Individual Sandfly Bites Reveals the Efficiency of Vector Transmission. *Communications Biology*, *2*(1), 84. https://doi.org/10.1038/s42003-019-0323-8

Giri, S., & Shaha, C. (2019). Leishmania donovani parasite requires Atg8 protein for infectivity and survival under stress. *Cell Death & Disease*, *10*(11), 808. https://doi.org/10.1038/s41419-019-2038-7

Gluenz, E., Höög, J. L., Smith, A. E., Dawe, H. R., Shaw, M. K., & Gull, K. (2010). Beyond 9+0: noncanonical axoneme structures characterize sensory cilia from protists to humans. *The FASEB Journal*, *24*(9), 3117–3121. https://doi.org/10.1096/fj.09-151381

Gluenz, E., Wheeler, R. J., Hughes, L., & Vaughan, S. (2015). *Scanning and three-dimensional electron microscopy methods for the study of Trypanosoma brucei and Leishmania mexicana flagella* (pp. 509–542). https://doi.org/10.1016/bs.mcb.2014.12.011

Gossage, S. M., Rogers, M. E., & Bates, P. A. (2003). Two separate growth phases during the development of Leishmania in sand flies: implications for understanding the life cycle. *International Journal for Parasitology*, *33*(10), 1027–1034. https://doi.org/10.1016/s0020-7519(03)00142-5

Gray, N. K., Hrabálková, L., Scanlon, J. P., & Smith, R. W. P. (2015). Poly(A)-binding proteins and mRNA localization: who rules the roost? *Biochemical Society Transactions*, *43*(6), 1277–1284. https://doi.org/10.1042/BST20150171

Gurunathan, S., Marash, M., Weinberger, A., & Gerst, J. E. (2002). t-SNARE Phosphorylation Regulates Endocytosis in Yeast. *Molecular Biology of the Cell*, *13*(5), 1594–1607. https://doi.org/10.1091/mbc.01-11-0541

Hailey, D. W., Rambold, A. S., Satpute-Krishnan, P., Mitra, K., Sougrat, R., Kim, P. K., & Lippincott-Schwartz, J. (2010). Mitochondria Supply Membranes for Autophagosome Biogenesis during Starvation. *Cell*, *141*(4), 656–667. https://doi.org/10.1016/j.cell.2010.04.009

Halliday, C., Billington, K., Wang, Z., Madden, R., Dean, S., Sunter, J. D., & Wheeler, R. J. (2019). Cellular landmarks of Trypanosoma brucei and Leishmania mexicana. *Molecular and Biochemical Parasitology*, *230*, 24–36. https://doi.org/10.1016/j.molbiopara.2018.12.003

Halliday, C., de Castro-Neto, A., Alcantara, C. L., Cunha-e-Silva, N. L., Vaughan, S., & Sunter, J. D. (2021). Trypanosomatid Flagellar Pocket from Structure to Function. *Trends in Parasitology*, *37*(4), 317–329. https://doi.org/10.1016/j.pt.2020.11.005

Hannaert, V., Bringaud, F., Opperdoes, F. R., & Michels, P. A. (2003). Evolution of energy metabolism and its compartmentation in Kinetoplastida. *Kinetoplastid Biology and Disease*, *2*(1), 11. https://doi.org/10.1186/1475-9292-2-11

Hanson, P. I., Roth, R., Morisaki, H., Jahn, R., & Heuser, J. E. (1997). Structure and Conformational Changes in NSF and Its Membrane Receptor Complexes Visualized by Quick-Freeze/Deep-Etch Electron Microscopy. *Cell*, *90*(3), 523–535. https://doi.org/10.1016/S0092-8674(00)80512-7

Hanson, P. I., & Whiteheart, S. W. (2005). AAA+ proteins: have engine, will work. *Nature Reviews Molecular Cell Biology*, *6*(7), 519–529. https://doi.org/10.1038/nrm1684

Harlow, E., & Lane, D. (1988). *Antibodies: A Laboratory Manual*. Cold Spring Harbour Laboratories Press.

Hayashi-Nishino, M., Fujita, N., Noda, T., Yamaguchi, A., Yoshimori, T., & Yamamoto, A. (2009). A subdomain of the endoplasmic reticulum forms a cradle for autophagosome formation. *Nature Cell Biology*, *11*(12), 1433–1437. https://doi.org/10.1038/ncb1991

He, S., Ni, D., Ma, B., Lee, J.-H., Zhang, T., Ghozalli, I., Pirooz, S. D., Zhao, Z., Bharatham, N., Li, B., Oh, S., Lee, W.-H., Takahashi, Y., Wang, H.-G., Minassian, A., Feng, P., Deretic, V., Pepperkok, R., Tagaya, M., … Liang, C. (2013). PtdIns(3)P-bound UVRAG coordinates Golgi–ER retrograde and Atg9 transport by differential interactions with the ER tether and the beclin 1 complex. *Nature Cell Biology*, *15*(10), 1206–1219. https://doi.org/10.1038/ncb2848

Hendrickx, S., Beyers, J., Mondelaers, A., Eberhardt, E., Lachaud, L., Delputte, P., Cos, P., & Maes, L. (2016). Evidence of a drug-specific impact of experimentally selected paromomycin and miltefosine resistance on parasite fitness in *Leishmania infantum*. *Journal of Antimicrobial Chemotherapy*, *71*(7), 1914–1921. https://doi.org/10.1093/jac/dkw096

Hendry, K. A. K., & Vickerman, K. (1988). The requirement for epimastigote attachment during division and metacyclogenesis in Trypanosoma congolense. *Parasitology Research*, *74*(5), 403–408. https://doi.org/10.1007/BF00535138

Herman, M., Gillies, S., Michels, P. A., & Rigden, D. J. (2006). Autophagy and Related processes in Trypanosomatids: Insights from Genomic and Bioinformatic Analyses. *Autophagy*, *2*(2), 107–118. https://doi.org/10.4161/auto.2.2.2369

Holthuis, J. C. M., Nichols, B. J., Dhruvakumar, S., & Pelham, H. R. (1998). Two syntaxin homologues in the TGN/endosomal system of yeast. *The EMBO Journal*, *17*(1), 113–126. https://doi.org/10.1093/emboj/17.1.113

Hosokawa, N., Hara, T., Kaizuka, T., Kishi, C., Takamura, A., Miura, Y., Iemura, S., Natsume, T., Takehana, K., Yamada, N., Guan, J.-L., Oshiro, N., & Mizushima, N. (2009). Nutrient-dependent mTORC1 Association with the ULK1–Atg13–FIP200 Complex Required for Autophagy. *Molecular Biology of the Cell*, *20*(7), 1981–1991. https://doi.org/10.1091/mbc.e08-12-1248

Hughson, F. M., Munson, M., Chen, X., Cocina, A. E., & Schultz, S. M. (2000). Interactions within the yeast t-SNARE Sso1p that control SNARE complex assembly. *Nature Structural Biology*, *7*(10), 894–902. https://doi.org/10.1038/79659

Inadome, H., Noda, Y., Adachi, H., & Yoda, K. (2005). Immunoisolaton of the yeast Golgi subcompartments and characterization of a novel membrane protein, Svp26, discovered in the Sed5-containing compartments. *Molecular and Cellular Biology*, *25*(17), 7696–7710. https://doi.org/10.1128/MCB.25.17.7696-7710.2005

Inadome, H., Noda, Y., Kamimura, Y., Adachi, H., & Yoda, K. (2007). Tvp38, Tvp23, Tvp18 and Tvp15: novel membrane proteins in the Tlg2-containing Golgi/endosome compartments of Saccharomyces cerevisiae. *Experimental Cell Research*, *313*(4), 688–697. https://doi.org/10.1016/j.yexcr.2006.11.008

Inbar, E., Hughitt, V. K., Dillon, L. A. L., Ghosh, K., El-Sayed, N. M., & Sacks, D. L. (2017). The Transcriptome of *Leishmania major* Developmental Stages in Their Natural Sand Fly Vector. *MBio*, *8*(2). https://doi.org/10.1128/mBio.00029-17

Itakura, E., & Mizushima, N. (2010). Characterization of autophagosome formation site by a hierarchical analysis of mammalian Atg proteins. *Autophagy*, *6*(6), 764–776. https://doi.org/10.4161/auto.6.6.12709

Jahn, R., & Scheller, R. H. (2006). SNAREs — engines for membrane fusion. *Nature Reviews Molecular Cell Biology*, *7*(9), 631–643. https://doi.org/10.1038/nrm2002

Jakobsson, A., Westerberg, R., & Jacobsson, A. (2006). Fatty acid elongases in mammals: Their regulation and roles in metabolism. *Progress in Lipid Research*, *45*(3), 237–249. https://doi.org/10.1016/j.plipres.2006.01.004

Jiang, P., Nishimura, T., Sakamaki, Y., Itakura, E., Hatta, T., Natsume, T., & Mizushima, N. (2014). The HOPS complex mediates autophagosome–lysosome fusion through interaction with syntaxin 17. *Molecular Biology of the Cell*, *25*(8), 1327–1337. https://doi.org/10.1091/mbc.e13-08-0447

Johnson, J. R., Ferdek, P., Lian, L.-Y., Barclay, J. W., Burgoyne, R. D., & Morgan, A. (2009). Binding of UNC-18 to the N-terminus of syntaxin is essential for neurotransmission in *Caenorhabditis elegans*. *Biochemical Journal*, *418*(1), 73–80. https://doi.org/10.1042/BJ20081956

Johnson, P. J., Kooter, J. M., Borst, P. (1987). Inactivation of transcription by UV irradiation of T. brucei provides evidence for a multicistronic transcription unit including a VSG gene. *Cell*, *51*(2), 273–281. https://doi.org/10.1016/0092-8674(87)90154-1

Jolly, C. (2000). Role of the Heat Shock Response and Molecular Chaperones in Oncogenesis and Cell Death. *Journal of the National Cancer Institute*, *92*(19), 1564–1572. https://doi.org/10.1093/jnci/92.19.1564

Joshi, A. B., Das, M. L., Akhter, S., Chowdhury, R., Mondal, D., Kumar, V., Das, P., Kroeger, A., Boelaert, M., & Petzold, M. (2009). Chemical and environmental vector control as a contribution to the elimination of visceral leishmaniasis on the Indian subcontinent: cluster randomized controlled trials in Bangladesh, India and Nepal. *BMC Medicine*, *7*(1), 54. https://doi.org/10.1186/1741-7015-7-54

Kamada, Y., Yoshino, K., Kondo, C., Kawamata, T., Oshiro, N., Yonezawa, K., & Ohsumi, Y. (2010). Tor Directly Controls the Atg1 Kinase Complex To Regulate Autophagy. *Molecular and Cellular Biology*, *30*(4), 1049–1058. https://doi.org/10.1128/MCB.01344-09

Karamyshev, A. L., & Karamysheva, Z. N. (2018). Lost in Translation: Ribosome-Associated mRNA and Protein Quality Controls. *Frontiers in Genetics*, *9*. https://doi.org/10.3389/fgene.2018.00431

Kiessling, V., Domanska, M. K., Tamm, L. K. (2010). Single SNARE mediated vesicle fusion observed in vitro by polarized TIRFM. *Biophysical Journal*, *99*(12), 4047–4055. https://doi.org/10.1016/j.bpj.2010.10.022

Killick-Kendrick, R. (1999). The biology and control of Phlebotomine sand flies. *Clinics in Dermatology*, *17*(3), 279–289. https://doi.org/10.1016/S0738-081X(99)00046-2

Killick-Kendrick, R., Molyneux, D. H., & Ashford, R. W. (1974). *Leishmania* in phlebotomid sandflies I. Modifications of the flagellum associated with attachment to the mid-gut and oesophageal valve of the sandfly. *Proceedings of the Royal Society of London. Series B. Biological Sciences*, *187*(1089), 409–419. https://doi.org/10.1098/rspb.1974.0085

Kim, D. H., Chung, H. J., Bleys, J., & Ghohestani, R. F. (2009). Is Paromomycin an Effective and Safe Treatment against Cutaneous Leishmaniasis? A Meta-Analysis of 14 Randomized Controlled Trials. *PLoS Neglected Tropical Diseases*, *3*(2), e381. https://doi.org/10.1371/journal.pntd.0000381

Kim, D.-H., Sarbassov, D. D., Ali, S. M., Latek, R. R., Guntur, K. V. P., Erdjument-Bromage, H., Tempst, P., & Sabatini, D. M. (2003). GβL, a Positive Regulator of the Rapamycin-Sensitive Pathway Required for the Nutrient-Sensitive Interaction between Raptor and mTOR. *Molecular Cell*, *11*(4), 895–904. https://doi.org/10.1016/S1097-2765(03)00114-X

Kimblin, N., Peters, N., Debrabant, A., Secundino, N., Egen, J., Lawyer, P., Fay, M. P., Kamhawi, S., & Sacks, D. (2008). Quantification of the infectious dose of Leishmania major transmitted to the skin by single sand flies. *Proceedings of the National Academy of Sciences*, *105*(29), 10125–10130. https://doi.org/10.1073/pnas.0802331105

Klionsky, D. J., Abdelmohsen, K., Abe, A., Abedin, M. J., Abeliovich, H., Acevedo Arozena, A., Adachi, H., Adams, C. M., Adams, P. D., Adeli, K., Adhihetty, P. J., Adler, S. G., Agam, G., Agarwal, R., Aghi, M. K., Agnello, M., Agostinis, P., Aguilar, P. v, Aguirre-

Ghiso, J., … Zughaier, S. M. (2016). Guidelines for the use and interpretation of assays for monitoring autophagy (3rd edition). *Autophagy*, *12*(1), 1–222. https://doi.org/10.1080/15548627.2015.1100356

Klionsky, D. J., Abeliovich, H., Agostinis, P., Agrawal, D. K., Aliev, G., Askew, D. S., Baba, M., Baehrecke, E. H., Bahr, B. A., Ballabio, A., Bamber, B. A., Bassham, D. C., Bergamini, E., Bi, X., Biard-Piechaczyk, M., Blum, J. S., Bredesen, D. E., Brodsky, J. L., Brumell, J. H., … Deter, R. L. (2008). Guidelines for the use and interpretation of assays for monitoring autophagy in higher eukaryotes. *Autophagy*, *4*(2), 151–175. https://doi.org/10.4161/auto.5338

Klionsky, D. J., Cregg, J. M., Dunn, W. A., Emr, S. D., Sakai, Y., Sandoval, I. v, Sibirny, A., Subramani, S., Thumm, M., Veenhuis, M., & Ohsumi, Y. (2003). A Unified Nomenclature for Yeast Autophagy-Related Genes. *Developmental Cell*, *5*(4), 539–545. https://doi.org/10.1016/S1534-5807(03)00296-X

Kloepper, T. H., Kienle, C. N., & Fasshauer, D. (2007). An Elaborate Classification of SNARE Proteins Sheds Light on the Conservation of the Eukaryotic Endomembrane System. *Molecular Biology of the Cell*, *18*(9), 3463–3471. https://doi.org/10.1091/mbc.e07-03-0193

Knuepfer, E., Stierhof, Y.-D., McKean, P. G., & Smith, D. F. (2001). Characterization of a differentially expressed protein that shows an unusual localization to intracellular membranes in Leishmania major. *Biochemical Journal*, *356*(2), 335. https://doi.org/10.1042/0264-6021:3560335

Kramer, S., Bannerman-Chukualim, B., Ellis, L., Boulden, E. A., Kelly, S., Field, M. C., & Carrington, M. (2013). Differential Localization of the Two T. brucei Poly(A) Binding Proteins to the Nucleus and RNP Granules Suggests Binding to Distinct mRNA Pools. *PLoS ONE*, *8*(1), e54004. https://doi.org/10.1371/journal.pone.0054004

Lafourcade, C., Sobo, K., Kieffer-Jaquinod, S., Garin, J., & van der Goot, F. G. (2008). Regulation of the V-ATPase along the Endocytic Pathway Occurs through Reversible Subunit Association and Membrane Localization. *PLoS ONE*, *3*(7), e2758. https://doi.org/10.1371/journal.pone.0002758

Laplante, M., & Sabatini, D. M. (2012). mTOR Signaling in Growth Control and Disease. *Cell*, *149*(2), 274–293. https://doi.org/10.1016/j.cell.2012.03.017

Latham, C. F., Lopez, J. A., Hu, S.-H., Gee, C. L., Westbury, E., Blair, D. H., Armishaw, C. J., Alewood, P. F., Bryant, N. J., James, D. E., & Martin, J. L. (2006). Molecular Dissection of the Munc18c/Syntaxin4 Interaction: Implications for Regulation of Membrane Trafficking. *Traffic*, *7*(10), 1408–1419. https://doi.org/10.1111/j.1600-0854.2006.00474.x

Laufs, H., Müller, K., Fleischer, J., Reiling, N., Jahnke, N., Jensenius, J. C., Solbach, W., & Laskay, T. (2002). Intracellular Survival of *Leishmania major* in Neutrophil Granulocytes after Uptake in the Absence of Heat-Labile Serum Factors. *Infection and Immunity*, *70*(2), 826–835. https://doi.org/10.1128/IAI.70.2.826-835.2002

le Rutte, E. A., Zijlstra, E. E., & de Vlas, S. J. (2019). Post-Kala-Azar Dermal Leishmaniasis as a Reservoir for Visceral Leishmaniasis Transmission. *Trends in Parasitology*, *35*(8), 590–592. https://doi.org/10.1016/j.pt.2019.06.007

LeBowitz, J. H., Smith, H. Q., Rusche, L., Beverley, S. M. (1993). Coupling of poly(A) site selection and trans-splicing in Leishmania. *Genes & Development*, *7*(6), 996–1007. https://doi.org/10.1101/gad.7.6.996

Lehane, M. J. (1997). PERITROPHIC MATRIX STRUCTURE AND FUNCTION. *Annual Review of Entomology*, *42*(1), 525–550. https://doi.org/10.1146/annurev.ento.42.1.525

Leifso, K., Cohen-Freue, G., Dogra, N., Murray, A., & McMaster, W. R. (2007). Genomic and proteomic expression analysis of Leishmania promastigote and amastigote life stages: The Leishmania genome is constitutively expressed. *Molecular and Biochemical Parasitology*, *152*(1), 35–46. https://doi.org/10.1016/j.molbiopara.2006.11.009

Letunic, I., Khedkar, S., & Bork, P. (2021). SMART: recent updates, new developments and status in 2020. *Nucleic Acids Research*, *49*(D1), D458–D460. https://doi.org/10.1093/nar/gkaa937

Li, H., & Durbin, R. (2009). Fast and accurate short read alignment with Burrows-Wheeler transform. *Bioinformatics (Oxford, England)*, *25*(14), 1754–1760. https://doi.org/10.1093/bioinformatics/btp324

Lim, J., Iftner, T., & Simon, C. (2021). Native Isolation of 3×HA-Tagged Protein Complexes to Characterize Protein-Protein Interactions. *Current Protocols*, *1*(2). https://doi.org/10.1002/cpz1.29

Lin, R. C., & Scheller, R. H. (1997). Structural Organization of the Synaptic Exocytosis Core Complex. *Neuron*, *19*(5), 1087–1094. https://doi.org/10.1016/S0896-6273(00)80399-2

Lindoso, J., Moreira, C., Cunha, M., & Queiroz, I. T. (2018). Visceral leishmaniasis and HIV coinfection: current perspectives. *HIV/AIDS - Research and Palliative Care*, *Volume 10*, 193–201. https://doi.org/10.2147/HIV.S143929

Liu D. & Uzonna J. E. (2012). The early interaction of Leishmania with macrophages and dendritic cells and its influence on the host immune response. *Frontiers in Cellular Infection Microbiology*, *2*(83). https://doi.org/10.3389/fcimb.2012.00083

Longatti, A., & Tooze, S. A. (2009). Vesicular trafficking and autophagosome formation. *Cell Death & Differentiation*, *16*(7), 956–965. https://doi.org/10.1038/cdd.2009.39

Lu, J., Garcia, J., Dulubova, I., Südhof, T. C., & Rizo, J. (2002). Solution Structure of the Vam7p PX Domain. *Biochemistry*, *41*(19), 5956–5962. https://doi.org/10.1021/bi020050b

Maintz, E. M., Hassan, M., Huda, M. M., Ghosh, D., Hossain, M. S., Alim, A., Kroeger, A., Arana, B., & Mondal, D. (2014). Introducing single dose liposomal amphotericin B for the treatment of visceral leishmaniasis in rural bangladesh: feasibility and acceptance to patients and health staff. *Journal of Tropical Medicine*, 676817. https://doi.org/10.1155/2014/676817

Martínez-Calvillo, S., Yan, S., Nguyen, D., Fox, M., Stuart, K., Myler, P. J. (2003). Transcription of *Leishmania major Friedlin* chromosome 1 initiates in both directions within a single region. *Molecular Cell*, *11*(5), 1291–1299. https://doi.org/ 10.1016/s1097-2765(03)00143-6

Marz, K. E., Lauer, J. M., & Hanson, P. I. (2003). Defining the SNARE Complex Binding Surface of α-SNAP. *Journal of Biological Chemistry*, *278*(29), 27000–27008. https://doi.org/10.1074/jbc.M302003200

Matteis, M. A. de, & Godi, A. (2004). PI-loting membrane traffic. *Nature Cell Biology*, *6*(6), 487–492. https://doi.org/10.1038/ncb0604-487

Mayer, C. L., Snyder, W. K., Swietlicka, M. A., VanSchoiack, A. D., Austin, C. R., & McFarland, B. J. (2009). Size-exclusion chromatography can identify faster-associating protein complexes and evaluate design strategies. *BMC Research Notes*, *2*(1), 135. https://doi.org/10.1186/1756-0500-2-135

McEwen, J. M., & Kaplan, J. M. (2008). UNC-18 Promotes Both the Anterograde Trafficking and Synaptic Function of Syntaxin. *Molecular Biology of the Cell*, *19*(9), 3836–3846. https://doi.org/10.1091/mbc.e08-02-0160

Michels, P. A. M., Bringaud, F., Herman, M., & Hannaert, V. (2006). Metabolic functions of glycosomes in trypanosomatids. *Biochimica et Biophysica Acta (BBA) - Molecular Cell Research*, *1763*(12), 1463–1477. https://doi.org/10.1016/j.bbamcr.2006.08.019

Mijaljica, D., Prescott, M., & Devenish, R. J. (2011). Microautophagy in mammalian cells: Revisiting a 40-year-old conundrum. *Autophagy*, *7*(7), 673–682. https://doi.org/10.4161/auto.7.7.14733

Misura, K. M. S., Bock, J. B., Gonzalez, L. C., Scheller, R. H., & Weis, W. I. (2002). Three-dimensional structure of the amino-terminal domain of syntaxin 6, a SNAP-25 C homolog. *Proceedings of the National Academy of Sciences*, *99*(14), 9184–9189. https://doi.org/10.1073/pnas.132274599

Misura, K. M. S., Scheller, R. H., & Weis, W. I. (2000). Three-dimensional structure of the neuronal-Sec1–syntaxin 1a complex. *Nature*, *404*(6776), 355–362. https://doi.org/10.1038/35006120

Mizushima, N., & Yoshimori, T. (2007). How to Interpret LC3 Immunoblotting. *Autophagy*, *3*(6), 542–545. https://doi.org/10.4161/auto.4600

Moerke, N. J. (2009). Fluorescence Polarization (FP) Assays for Monitoring Peptide-Protein or Nucleic Acid-Protein Binding. *Current Protocols in Chemical Biology*, *1*(1), 1–15. https://doi.org/10.1002/9780470559277.ch090102

Moore, E. M., & Lockwood, D. N. (2010). Treatment of visceral leishmaniasis. *Journal of Global Infectious Diseases*, *2*(2), 151–158. https://doi.org/10.4103/0974-777X.62883

Moraes, C. S., Aguiar-Martins, K., Costa, S. G., Bates, P. A., Dillon, R. J., & Genta, F. A. (2018). Second Blood Meal by Female *Lutzomyia longipalpis*: Enhancement by Oviposition and Its Effects on Digestion, Longevity, and *Leishmania* Infection. *BioMed Research International*, *2018*, 1–10. https://doi.org/10.1155/2018/2472508

Munson, M., & Novick, P. (2006). The exocyst defrocked, a framework of rods revealed. *Nature Structural & Molecular Biology*, *13*(7), 577–581. https://doi.org/10.1038/nsmb1097

Munstermann, L. E. (2019). Phlebotomine Sand Flies and Moth Flies (Psychodidae). In *Medical and Veterinary Entomology* (pp. 191–211). Elsevier. https://doi.org/10.1016/B978-0-12-814043-7.00012-1

Murungi, E., Barlow, L. D., Venkatesh, D., Adung'a, V. O., Dacks, J. B., Field, M. C., & Christoffels, A. (2014). A comparative analysis of trypanosomatid SNARE proteins. *Parasitology International*, *63*(2), 341–348. https://doi.org/10.1016/j.parint.2013.11.002

Nair, U., Jotwani, A., Geng, J., Gammoh, N., Richerson, D., Yen, W.-L., Griffith, J., Nag, S., Wang, K., Moss, T., Baba, M., McNew, J. A., Jiang, X., Reggiori, F., Melia, T. J., & Klionsky, D. J. (2011). SNARE Proteins Are Required for Macroautophagy. *Cell*, *146*(2), 290–302. https://doi.org/10.1016/j.cell.2011.06.022

Nair, U., Yen, W.-L., Mari, M., Cao, Y., Xie, Z., Baba, M., Reggiori, F., & Klionsky, D. J. (2012). A role for Atg8–PE deconjugation in autophagosome biogenesis. *Autophagy*, *8*(5), 780–793. https://doi.org/10.4161/auto.19385

Nguyen, L. K., Dobrzyński, M., Fey, D., & Kholodenko, B. N. (2014). Polyubiquitin chain assembly and organization determine the dynamics of protein activation and degradation. *Frontiers in Physiology*, *5*. https://doi.org/10.3389/fphys.2014.00004

Notredame, C., Higgins, D. G., & Heringa, J. (2000). T-coffee: a novel method for fast and accurate multiple sequence alignment 1 1Edited by J. Thornton. *Journal of Molecular Biology*, *302*(1), 205–217. https://doi.org/10.1006/jmbi.2000.4042

Obara, K., Kojima, R., & Kihara, A. (2013). Effects on vesicular transport pathways at the late endosome in cells with limited very long-chain fatty acids. *Journal of Lipid Research*, *54*(3), 831–842. https://doi.org/10.1194/jlr.M034678

Olivier, M., Badaró, R., Medrano, F. J., & Moreno, J. (2003). The pathogenesis of Leishmania/HIV co-infection: cellular and immunological mechanisms. *Annals of Tropical Medicine & Parasitology*, *97*(sup1), 79–98. https://doi.org/10.1179/000349803225002561

Ossig, R., Schmitt, H. D., de Groot, B., Riedel, D., Keränen, S., Ronne, H., Grubmüller, H., & Jahn, R. (2000). Exocytosis requires asymmetry in the central layer of the SNARE complex. *The EMBO Journal*, *19*(22), 6000–6010. https://doi.org/10.1093/emboj/19.22.6000

Papinski, D., Schuschnig, M., Reiter, W., Wilhelm, L., Barnes, C. A., Maiolica, A., Hansmann, I., Pfaffenwimmer, T., Kijanska, M., Stoffel, I., Lee, S. S., Brezovich, A., Lou, J. H., Turk, B. E., Aebersold, R., Ammerer, G., Peter, M., & Kraft, C. (2014). Early Steps in Autophagy Depend on Direct Phosphorylation of Atg9 by the Atg1 Kinase. *Molecular Cell*, *53*(3), 471–483. https://doi.org/10.1016/j.molcel.2013.12.011

Paris, C., Loiseau, P. M., Bories, C., & Bréard, J. (2004). Miltefosine Induces Apoptosis-Like Death in *Leishmania donovani* Promastigotes. *Antimicrobial Agents and Chemotherapy*, *48*(3), 852–859. https://doi.org/10.1128/AAC.48.3.852-859.2004

Parsons, M., Nelson, R. G., Watkins, K. P., Agabian, N. (1984). Trypanosome mRNAs share a common 5' spliced leader sequence. *Cell*, *38*(1), 309–316. https://doi.org/10.1016/0092-8674(84)90552-x

Parzych, K. R., & Klionsky, D. J. (2014). An Overview of Autophagy: Morphology, Mechanism, and Regulation. *Antioxidants & Redox Signaling*, *20*(3), 460–473. https://doi.org/10.1089/ars.2013.5371

Paumet, F., Brügger, B., Parlati, F., McNew, J. A., Söllner, T. H., & Rothman, J. E. (2001). A t-SNARE of the endocytic pathway must be activated for fusion. *Journal of Cell Biology*, *155*(6), 961–968. https://doi.org/10.1083/jcb.200104092

Peng, R., & Gallwitz, D. (2002). Sly1 protein bound to Golgi syntaxin Sed5p allows assembly and contributes to specificity of SNARE fusion complexes. *Journal of Cell Biology*, *157*(4), 645–655. https://doi.org/10.1083/jcb.200202006

Peters, N. C., Egen, J. G., Secundino, N., Debrabant, A., Kimblin, N., Kamhawi, S., Lawyer, P., Fay, M. P., Germain, R. N., & Sacks, D. (2008). In Vivo Imaging Reveals an Essential Role for Neutrophils in Leishmaniasis Transmitted by Sand Flies. *Science*, *321*(5891), 970–974. https://doi.org/10.1126/science.1159194

Pevsner, J., Hsu, S.-C., Braun, J. E. A., Calakos, N., Ting, A. E., Bennett, M. K., & Scheller, R. H. (1994). Specificity and regulation of a synaptic vesicle docking complex. *Neuron*, *13*(2), 353–361. https://doi.org/10.1016/0896-6273(94)90352-2

Phizicky, E. M., & Fields, S. (1995). Protein-protein interactions: methods for detection and analysis. *Microbiological Reviews*, *59*(1), 94–123. https://doi.org/10.1128/mr.59.1.94-123.1995

Piper, R. C., Whitters, E. A., & Stevens, T. H. (1994). Yeast Vps45p is a Sec1p-like protein required for the consumption of vacuole-targeted, post-Golgi transport vesicles. *European Journal of Cell Biology*, *65*(2), 305–318.

Poirier, M. A., Xiao, W., Macosko, J. C., Chan, C., Shin, Y.-K., & Bennett, M. K. (1998). The synaptic SNARE complex is a parallel four-stranded helical bundle. *Nature Structural Biology*, *5*(9), 765–769. https://doi.org/10.1038/1799

Polando, R., Dixit, U. G., Carter, C. R., Jones, B., Whitcomb, J. P., Ballhorn, W., Harintho, M., Jerde, C. L., Wilson, M. E., & McDowell, M. A. (2013). The roles of complement receptor 3 and Fcγ receptors during Leishmania phagosome maturation. *Journal of Leukocyte Biology*, *93*(6), 921–932. https://doi.org/10.1189/jlb.0212086

Price, H. P., Menon, M. R., Panethymitaki, C., Goulding, D., McKean, P. G., & Smith, D. F. (2003). Myristoyl-CoA:Protein N-Myristoyltransferase, an Essential Enzyme and Potential Drug Target in Kinetoplastid Parasites. *Journal of Biological Chemistry*, *278*(9), 7206–7214. https://doi.org/10.1074/jbc.M211391200

Proud, C. G. (2007). Signalling to translation: how signal transduction pathways control the protein synthetic machinery. *Biochemical Journal*, *403*(2), 217–234. https://doi.org/10.1042/BJ20070024

Pruzinova, K., Sadlova, J., Seblova, V., Homola, M., Votypka, J., & Volf, P. (2015). Comparison of Bloodmeal Digestion and the Peritrophic Matrix in Four Sand Fly Species Differing in Susceptibility to Leishmania donovani. *PLOS ONE*, *10*(6), e0128203. https://doi.org/10.1371/journal.pone.0128203

Rafati, S., Hassani, N., Taslimi, Y., Movassagh, H., Rochette, A., & Papadopoulou, B. (2006). Amastin Peptide-Binding Antibodies as Biomarkers of Active Human Visceral Leishmaniasis. *Clinical and Vaccine Immunology*, *13*(10), 1104–1110. https://doi.org/10.1128/CVI.00188-06

Ramakrishnan, S., Gohlke, A., Li, F., Coleman, J., Xu, W., Rothman, J. E., Pincet, F. (2018). High-Throughput Monitoring of Single Vesicle Fusion Using Freestanding Membranes and Automated Analysis. *Langmuir*, *34*(20), 5849–5859. https://doi.org/10.1021/acs.langmuir.8b00116

Ravikumar, B., Moreau, K., Jahreiss, L., Puri, C., & Rubinsztein, D. C. (2010). Plasma membrane contributes to the formation of pre-autophagosomal structures. *Nature Cell Biology*, *12*(8), 747–757. https://doi.org/10.1038/ncb2078

Ready, P. D. (2013). Biology of Phlebotomine Sand Flies as Vectors of Disease Agents. *Annual Review of Entomology*, *58*(1), 227–250. https://doi.org/10.1146/annurev-ento-120811-153557

Reggiori, F., Tucker, K. A., Stromhaug, P. E., & Klionsky, D. J. (2004). The Atg1-Atg13 Complex Regulates Atg9 and Atg23 Retrieval Transport from the Pre-Autophagosomal Structure. *Developmental Cell*, *6*(1), 79–90. https://doi.org/10.1016/S1534-5807(03)00402-7

Rigden, D. J., Michels, P., & Ginger, M. L. (2009). Autophagy in protists: examples of secondary loss, lineage-specific innovations, and the conundrum of remodeling a single mitochondrion. *Autophagy*, *5*(6), 784–794. https://doi.org/10.4161/auto.8838

Ritter, U., Frischknecht, F., & van Zandbergen, G. (2009). Are neutrophils important host cells for Leishmania parasites? *Trends in Parasitology*, *25*(11), 505–510. https://doi.org/10.1016/j.pt.2009.08.003

Rogers, M. E. (2012). The Role of Leishmania Proteophosphoglycans in Sand Fly Transmission and Infection of the Mammalian Host. *Frontiers in Microbiology*, *3*. https://doi.org/10.3389/fmicb.2012.00223

Rogers, M. E., Chance, M. L., & Bates, P. A. (2002). The role of promastigote secretory gel in the origin and transmission of the infective stage of *Leishmania mexicana* by the sandfly *Lutzomyia longipalpis*. *Parasitology*, *124*(5), 495–507. https://doi.org/10.1017/S0031182002001439

Rogers, M. E., Ilg, T., Nikolaev, A. v., Ferguson, M. A. J., & Bates, P. A. (2004). Transmission of cutaneous leishmaniasis by sand flies is enhanced by regurgitation of fPPG. *Nature*, *430*(6998), 463–467. https://doi.org/10.1038/nature02675

Rogers, M. E., Kropf, P., Choi, B-S., Dillon, R., Podinovskaia, M., Bates, P., Müller, I. (2009) Proteophosophoglycans Regurgitated by *Leishmania*-Infected Sand Flies Target the L-Arginine Metabolism of Host Macrophages to Promote Parasite Survival. *PLOS Pathogens, 5*(8), e1000555. https://doi.org/10.1371/journal.ppat.1000555

Rossi, V., Banfield, D., Vacca, M., Dietrich, L., Ungermann, C., Desposito, M., Galli, T., & Filippini, F. (2004). Longins and their longin domains: regulated SNAREs and multifunctional SNARE regulators. *Trends in Biochemical Sciences, 29*(12), 682–688. https://doi.org/10.1016/j.tibs.2004.10.002

Roth, M. G. (2004). Phosphoinositides in Constitutive Membrane Traffic. *Physiological Reviews, 84*(3), 699–730. https://doi.org/10.1152/physrev.00033.2003

Russell D. G. (1987). The macrophage-attachment glycoprotein gp63 is the predominant C3-acceptor site on Leishmania mexicana promastigotes. *European Journal of Biochemistry*. *164*(1), 213-21. https://doi.org/10.1111/j.1432-1033.1987.tb11013.x

Russell, R. C., Yuan, H.-X., & Guan, K.-L. (2014). Autophagy regulation by nutrient signaling. *Cell Research*, *24*(1), 42–57. https://doi.org/10.1038/cr.2013.166

Ruy, P. D. C., Monteiro-Teles, N. M., Miserani Magalhães, R. D., Freitas-Castro, F., Dias, L., Aquino Defina, T. P., Rosas De Vasconcelos, E. J., Myler, P. J., & Kaysel Cruz, A. (2019). Comparative transcriptomics in *Leishmania braziliensis* : disclosing differential gene expression of coding and putative noncoding RNAs across developmental stages. *RNA Biology*, *16*(5), 639–660. https://doi.org/10.1080/15476286.2019.1574161

Sádlová, J., Price, H. P., Smith, B. A., Votýpka, J., Volf, P., & Smith, D. F. (2010). The stage-regulated HASPB and SHERP proteins are essential for differentiation of the protozoan parasite Leishmania major in its sand fly vector, Phlebotomus papatasi. *Cellular Microbiology*, *12*(12), 1765–1779. https://doi.org/10.1111/j.1462-5822.2010.01507.x

Sarkar, A., Khan, Y. A., Laranjeira-Silva, M. F., Andrews, N. W., & Mittra, B. (2018). Quantification of Intracellular Growth Inside Macrophages is a Fast and Reliable Method for Assessing the Virulence of Leishmania Parasites. *Journal of Visualized Experiments, 133*. https://doi.org/10.3791/57486

Schweitzer, J.K., Burke, E.E., Goodson, H.V., D'Souza-Schorey, C. (2005) Endocytosis resumes during late mitosis and is required for cytokinesis. *Journal of Biological Chemistry*, *280*(50), 41628–41635. https://doi.org/10.1074/jbc.M504497200

Serafim, T. D., Coutinho-Abreu, I. v., Oliveira, F., Meneses, C., Kamhawi, S., & Valenzuela, J. G. (2018). Sequential blood meals promote Leishmania replication and reverse metacyclogenesis augmenting vector infectivity. *Nature Microbiology*, *3*(5), 548–555. https://doi.org/10.1038/s41564-018-0125-7

Shan, Q., Ma, F., Wei, J., Li, H., Ma, H., & Sun, P. (2020). Physiological Functions of Heat Shock Proteins. *Current Protein & Peptide Science*, *21*(8), 751–760. https://doi.org/10.2174/1389203720666191111113726

Shanks, S. G., Carpp, L. N., Struthers, M. S., McCann, R. K., & Bryant, N. J. (2012). The Sec1/Munc18 Protein Vps45 Regulates Cellular Levels of Its SNARE Binding Partners Tlg2 and Snc2 in Saccharomyces cerevisiae. *PLoS ONE*, *7*(11). https://doi.org/10.1371/journal.pone.0049628

Shen, C., Liu, Y., Yu, H., Gulbranson, D. R., Kogut, I., Bilousova, G., Zhang, C., Stowell, M. H. B., & Shen, J. (2018). The N-peptide–binding mode is critical to Munc18-1 function in synaptic exocytosis. *Journal of Biological Chemistry*, *293*(47), 18309–18317. https://doi.org/10.1074/jbc.RA118.005254

Shpilka, T., Mizushima, N., & Elazar, Z. (2012). Ubiquitin-like proteins and autophagy at a glance. *Journal of Cell Science*, *125*(10), 2343–2348. https://doi.org/10.1242/jcs.093757

Shrivastava, R., Tupperwar, N., Drory-Retwitzer, M., & Shapira, M. (2019). Deletion of a Single LeishIF4E-3 Allele by the CRISPR-Cas9 System Alters Cell Morphology and Infectivity of *Leishmania*. *MSphere*, *4*(5). https://doi.org/10.1128/mSphere.00450-19

Siegel, T. N., Hekstra, D. R., Kemp, L. E., Figueiredo, L. M., Lowell, J. E., Fenyo, D., Wang, X., Dewell, S., & Cross, G. A. M. (2009). Four histone variants mark the boundaries of polycistronic transcription units in *Trypanosoma brucei*. *Genes & Development*, *23*(9), 1063–1076. https://doi.org/10.1101/gad.1790409

Sievers, F., Wilm, A., Dineen, D., Gibson, T. J., Karplus, K., Li, W., Lopez, R., McWilliam, H., Remmert, M., Söding, J., Thompson, J. D., & Higgins, D. G. (2011). Fast, scalable generation of high-quality protein multiple sequence alignments using Clustal Omega. *Molecular Systems Biology*, *7*(1), 539. https://doi.org/10.1038/msb.2011.75

Song, Q., Meng, B., Xu, H., & Mao, Z. (2020). The emerging roles of vacuolar-type ATPase-dependent Lysosomal acidification in neurodegenerative diseases. *Translational Neurodegeneration*, *9*(1), 17. https://doi.org/10.1186/s40035-020-00196-0

Sosa, N., Pascale, J. M., Jiménez, A. I., Norwood, J. A., Kreishman-Detrick, M., Weina, P. J., Lawrence, K., McCarthy, W. F., Adams, R. C., Scott, C., Ransom, J., Tang, D., & Grogl, M. (2019). Topical paromomycin for New World cutaneous leishmaniasis. *PLOS*

Neglected Tropical Diseases, *13*(5), e0007253. https://doi.org/10.1371/journal.pntd.0007253

Späth, G. F., Garraway, L. A., Turco, S. J., & Beverley, S. M. (2003). The role(s) of lipophosphoglycan (LPG) in the establishment of Leishmania major infections in mammalian hosts. *Proceedings of the National Academy of Sciences of the United States of America*, *100*(16), 9536–9541. https://doi.org/10.1073/pnas.1530604100

Stathopulos, P. B., Scholz, G. A., Hwang, Y.-M., Rumfeldt, J. A. O., Lepock, J. R., & Meiering, E. M. (2008). Sonication of proteins causes formation of aggregates that resemble amyloid. *Protein Science*, *13*(11), 3017–3027. https://doi.org/10.1110/ps.04831804

Stepensky, P., Saada, A., Cowan, M., Tabib, A., Fischer, U., Berkun, Y., Saleh, H., Simanovsky, N., Kogot-Levin, A., Weintraub, M., Ganaiem, H., Shaag, A., Zenvirt, S., Borkhardt, A., Elpeleg, O., Bryant, N. J., & Mevorach, D. (2013). The Thr224Asn mutation in the VPS45 gene is associated with the congenital neutropenia and primary myelofibrosis of infancy. *Blood*, *121*(25), 5078–5087. https://doi.org/10.1182/blood-2012-12-475566

Stephan, J. S., Yeh, Y.-Y., Ramachandran, V., Deminoff, S. J., & Herman, P. K. (2009). The Tor and PKA signaling pathways independently target the Atg1/Atg13 protein kinase complex to control autophagy. *Proceedings of the National Academy of Sciences*, *106*(40), 17049–17054. https://doi.org/10.1073/pnas.0903316106

Struthers, M. S., Shanks, S. G., MacDonald, C., Carpp, L. N., Drozdowska, A. M., Kioumourtzoglou, D., Furgason, M. L. M., Munson, M., & Bryant, N. J. (2009). Functional homology of mammalian syntaxin 16 and yeast Tlg2p reveals a conserved regulatory mechanism. *Journal of Cell Science*, *122*(13), 2292–2299. https://doi.org/10.1242/jcs.046441

Sundar, S., & Chakravarty, J. (2008). Paromomycin in the treatment of leishmaniasis. *Expert Opinion on Investigational Drugs*, *17*(5), 787–794. https://doi.org/10.1517/13543784.17.5.787

Sundar, S., More, D. K., Singh, M. K., Singh, V. P., Sharma, S., Makharia, A., Kumar, P. C. K., & Murray, H. W. (2000). Failure of Pentavalent Antimony in Visceral Leishmaniasis in India: Report from the Center of the Indian Epidemic. *Clinical Infectious Diseases*, *31*(4), 1104–1107. https://doi.org/10.1086/318121

Sunter, J., & Gull, K. (2017). Shape, form, function and *Leishmania* pathogenicity: from textbook descriptions to biological understanding. *Open Biology*, *7*(9), 170165. https://doi.org/10.1098/rsob.170165

Sunter, J., Yanase, R., Wang, Z., Catta-Pretta, C. M. C., Moreira-Leite, F., Myskova, J., Pruzinova, K., Volf, P., Mottram, J. C., Gull, K (2019) *Leishmania* flagellum attachment zone is critical for flagellar pocket shape, development in the sand fly, and pathogenicity in the host. *Proceedings of the National Academy of Sciences of the United States of America, 116*(13), 6351–6360. https://doi.org/10.1073/pnas.1812462116

Sutton, R. B., Fasshauer, D., Jahn, R., & Brunger, A. T. (1998). Crystal structure of a SNARE complex involved in synaptic exocytosis at 2.4 Å resolution. *Nature*, *395*(6700), 347–353. https://doi.org/10.1038/26412

Suzuki, K., Kubota, Y., Sekito, T., & Ohsumi, Y. (2007). Hierarchy of Atg proteins in pre-autophagosomal structure organization. *Genes to Cells*, *12*(2), 209–218. https://doi.org/10.1111/j.1365-2443.2007.01050.x

Takahashi, Y., Meyerkord, C. L., Hori, T., Runkle, K., Fox, T. E., Kester, M., Loughran, T. P., & Wang, H.-G. (2011). Bif-1 regulates Atg9 trafficking by mediating the fission of Golgi membranes during autophagy. *Autophagy*, *7*(1), 61–73. https://doi.org/10.4161/auto.7.1.14015

Tang, B. L. (2019). Syntaxin 16's Newly Deciphered Roles in Autophagy. *Cells*, *8*(12), 1655. https://doi.org/10.3390/cells8121655

Thermo Fisher Scientific. (2022). *Traditional Methods of Cell Lysis for Protein Extraction*. Https://Www.Thermofisher.Com/Uk/En/Home/Life-Science/Protein-Biology/Protein-Biology-Learning-Center/Protein-Biology-Resource-Library/Pierce-Protein-Methods/Traditional-Methods-Cell-Lysis.Html.

Togneri, J., Cheng, Y.-S., Munson, M., Hughson, F. M., & Carr, C. M. (2006). Specific SNARE complex binding mode of the Sec1/Munc-18 protein, Sec1p. *Proceedings of the National Academy of Sciences*, *103*(47), 17730–17735. https://doi.org/10.1073/pnas.0605448103

Tomomori-Sato, C., Sato, S., Conaway, R. C., & Conaway, J. W. (2013). *Immunoaffinity Purification of Protein Complexes from Mammalian Cells* (pp. 273–287). https://doi.org/10.1007/978-1-62703-284-1_22

Tsigankov, P., Gherardini, P. F., Helmer-Citterich, M., Späth, G. F., Myler, P. J., & Zilberstein, D. (2014). Regulation Dynamics of Leishmania Differentiation: Deconvoluting Signals and Identifying Phosphorylation Trends. *Molecular & Cellular Proteomics*, *13*(7), 1787–1799. https://doi.org/10.1074/mcp.M114.037705

Tsukada, M., & Ohsumi, Y. (1993). Isolation and characterization of autophagy-defective mutants of Saccharomyces cerevisiae. *FEBS Letters*, *333*(1–2), 169–174. https://doi.org/10.1016/0014-5793(93)80398-E

Ullrich, O., Horiuchi, H., Bucci, C., & Zerial, M. (1994). Membrane association of Rab5 mediated by GDP-dissociation inhibitor and accompanied by GDP/GTP exchange. *Nature*, *368*(6467), 157–160. https://doi.org/10.1038/368157a0

Ungar, D., & Hughson, F. M. (2003). SNARE Protein Structure and Function. *Annual Review of Cell and Developmental Biology*, *19*(1), 493–517. https://doi.org/10.1146/annurev.cellbio.19.110701.155609

van Bockstal, L., Sádlová, J., Suau, H. A., Hendrickx, S., Meneses, C., Kamhawi, S., Volf, P., Maes, L., & Caljon, G. (2019). Impaired development of a miltefosine-resistant Leishmania infantum strain in the sand fly vectors Phlebotomus perniciosus and Lutzomyia longipalpis. *International Journal for Parasitology: Drugs and Drug Resistance*, *11*, 1–7. https://doi.org/10.1016/j.ijpddr.2019.09.003

van Zandbergen, G., Bollinger, A., Wenzel, A., Kamhawi, S., Voll, R., Klinger, M., Muller, A., Holscher, C., Herrmann, M., Sacks, D., Solbach, W., & Laskay, T. (2006). Leishmania disease development depends on the presence of apoptotic promastigotes in the virulent inoculum. *Proceedings of the National Academy of Sciences*, *103*(37), 13837–13842. https://doi.org/10.1073/pnas.0600843103

van Luenen, H. G. A. M., Farris, C., Jan, S., Genest, P.-A., Tripathi, P., Velds, A., Kerkhoven, R. M., Nieuwland, M., Haydock, A., Ramasamy, G., Vainio, S., Heidebrecht, T., Perrakis, A., Pagie, L., van Steensel, B., Myler, P. J., & Borst, P. (2012). Glucosylated Hydroxymethyluracil, DNA Base J, Prevents Transcriptional Readthrough in Leishmania. *Cell*, *150*(5), 909–921. https://doi.org/10.1016/j.cell.2012.07.030

Verhage, M., Maia, A. S., Plomp, J. J., Brussaard, A. B., Heeroma, J. H., Vermeer, H., Toonen, R. F., Hammer, R. E., van den, T. K., Berg, Missler, M., Geuze, H. J., & Südhof, T. C.

(2000). Synaptic Assembly of the Brain in the Absence of Neurotransmitter Secretion. *Science*, *287*(5454), 864–869. https://doi.org/10.1126/science.287.5454.864

Vilboux, T., Lev, A., Malicdan, M. C. v., Simon, A. J., Järvinen, P., Racek, T., Puchalka, J., Sood, R., Carrington, B., Bishop, K., Mullikin, J., Huizing, M., Garty, B. Z., Eyal, E., Wolach, B., Gavrieli, R., Toren, A., Soudack, M., Atawneh, O. M., … Somech, R. (2013). A Congenital Neutrophil Defect Syndrome Associated with Mutations in *VPS45*. *New England Journal of Medicine*, *369*(1), 54–65. https://doi.org/10.1056/NEJMoa1301296

Volf, P., Hajmova, M., Sadlova, J., & Votypka, J. (2004). Blocked stomodeal valve of the insect vector: similar mechanism of transmission in two trypanosomatid models. *International Journal for Parasitology*, *34*(11), 1221–1227. https://doi.org/10.1016/j.ijpara.2004.07.010

Walters, R. W., & Parker, R. (2015). Coupling of Ribostasis and Proteostasis: Hsp70 Proteins in mRNA Metabolism. *Trends in Biochemical Sciences*, *40*(10), 552–559. https://doi.org/10.1016/j.tibs.2015.08.004

Wang, H., He, M., Willard, B., & Wu, Q. (2019). Cross-linking, Immunoprecipitation and Proteomic Analysis to Identify Interacting Proteins in Cultured Cells. *BIO-PROTOCOL*, *9*(11). https://doi.org/10.21769/BioProtoc.3258

Weber, T., Zemelman, B. v, McNew, J. A., Westermann, B., Gmachl, M., Parlati, F., Söllner, T. H., & Rothman, J. E. (1998). SNAREpins: Minimal Machinery for Membrane Fusion. *Cell*, *92*(6), 759–772. https://doi.org/10.1016/S0092-8674(00)81404-X

Wen, X., & Klionsky, D. J. (2016). An overview of macroautophagy in yeast. *Journal of Molecular Biology*, *428*(9), 1681–1699. https://doi.org/10.1016/j.jmb.2016.02.021

Wheeler, R. J., Gluenz, E., & Gull, K. (2011). The cell cycle of Leishmania: morphogenetic events and their implications for parasite biology. *Molecular Microbiology*, *79*(3), 647–662. https://doi.org/10.1111/j.1365-2958.2010.07479.x

Wheeler, R. J., Gluenz, E., & Gull, K. (2015). Basal body multipotency and axonemal remodelling are two pathways to a 9+0 flagellum. *Nature Communications*, *6*(1), 8964. https://doi.org/10.1038/ncomms9964

WHO. (2021a). *Leishmaniasis - Global Health Observatory (GHO) data*. WHO. https://www.who.int/data/gho/data/themes/topics/gho-ntd-leishmaniasis

WHO. (2021b, May 20). *Leishmaniasis - Key Facts*. WHO - Leishmaniasis Fact Sheet. https://www.who.int/news-room/fact-sheets/detail/leishmaniasis

Williams, R. A. M., Mottram, J. C., & Coombs, G. H. (2013). Distinct Roles in Autophagy and Importance in Infectivity of the Two ATG4 Cysteine Peptidases of Leishmania major. *Journal of Biological Chemistry*, *288*(5), 3678–3690. https://doi.org/10.1074/jbc.M112.415372

Williams, R. A. M., Smith, T. K., Cull, B., Mottram, J. C., & Coombs, G. H. (2012). ATG5 Is Essential for ATG8-Dependent Autophagy and Mitochondrial Homeostasis in Leishmania major. *PLoS Pathogens*, *8*(5), e1002695. https://doi.org/10.1371/journal.ppat.1002695

Williams, R. A. M., Woods, K. L., Juliano, L., Mottram, J. C., & Coombs, G. H. (2009). Characterization of unusual families of ATG8-like proteins and ATG12 in the protozoan parasite *Leishmania major*. *Autophagy*, *5*(2), 159–172. https://doi.org/10.4161/auto.5.2.7328

Williams, R. A., Tetley, L., Mottram, J. C., & Coombs, G. H. (2006). Cysteine peptidases CPA and CPB are vital for autophagy and differentiation in Leishmania mexicana. *Molecular Microbiology*, *61*(3), 655–674. https://doi.org/10.1111/j.1365-2958.2006.05274.x

Wiwanitkit, V. (2012). Interest in paromomycin for the treatment of visceral leishmaniasis (kala-azar). *Therapeutics and Clinical Risk Management*, 323. https://doi.org/10.2147/TCRM.S30139

Wu, Y., el Fakhry, Y., Sereno, D., Tamar, S., & Papadopoulou, B. (2000). A new developmentally regulated gene family in Leishmania amastigotes encoding a homolog of amastin surface proteins. *Molecular and Biochemical Parasitology*, *110*(2), 345–357. https://doi.org/10.1016/S0166-6851(00)00290-5

Yamaguchi, T., Dulubova, I., Min, S.-W., Chen, X., Rizo, J., & Südhof, T. C. (2002). Sly1 Binds to Golgi and ER Syntaxins via a Conserved N-Terminal Peptide Motif. *Developmental Cell*, *2*(3), 295–305. https://doi.org/10.1016/S1534-5807(02)00125-9

Yang, B., Gonzalez, L., Prekeris, R., Steegmaier, M., Advani, R. J., & Scheller, R. H. (1999). SNARE Interactions Are Not Selective. *Journal of Biological Chemistry*, *274*(9), 5649–5653. https://doi.org/10.1074/jbc.274.9.5649

Yang, S., Park, D., Manning, L., Hill, S. E., Cao, M., Xuan, Z., Gonzalez, I., Dong, Y., Clark, B., Shao, L., Okeke, I., Almoril-Porras, A., Bai, J., De Camilli, P., Colón-Ramos, D. A. (2022). Presynaptic autophagy is coupled to the synaptic vesicle cycle via ATG-9. *Neuron, 110*(5), 824–840. https://doi.org/10.1016/j.neuron.2021.12.031

Yanik, M., Gurel, M. S., Simsek, Z., & Kati, M. (2004). The psychological impact of cutaneous leishmaniasis. *Clinical and Experimental Dermatology*, *29*(5), 464–467. https://doi.org/10.1111/j.1365-2230.2004.01605.x

Yimam, Y., & Mohebali, M. (2020). Effectiveness of insecticide-impregnated dog collars in reducing incidence rate of canine visceral leishmaniasis: A systematic review and meta-analysis. *PLOS ONE*, *15*(9), e0238601. https://doi.org/10.1371/journal.pone.0238601

Yin, Z., Pascual, C., & Klionsky, D. (2016). Autophagy: machinery and regulation. *Microbial Cell*, *3*(12), 588–596. https://doi.org/10.15698/mic2016.12.546

Yoshii, S. R., & Mizushima, N. (2017). Monitoring and Measuring Autophagy. *International Journal of Molecular Sciences*, *18*(9), 1865. https://doi.org/10.3390/ijms18091865

Young, A. R. J., Chan, E. Y. W., Hu, X. W., Köchl, R., Crawshaw, S. G., High, S., Hailey, D. W., Lippincott-Schwartz, J., Tooze, S. A. (2006). Starvation and ULK1-dependent cycling of mammalian Atg9 between the TGN and endosomes. *Journal of Cell Science, 119*(18), 3888–3900. https://doi.org/10.1242/jcs.03172

Yu, X., Long, Y. C., & Shen, H.-M. (2015). Differential regulatory functions of three classes of phosphatidylinositol and phosphoinositide 3-kinases in autophagy. *Autophagy*, *11*(10), 1711–1728. https://doi.org/10.1080/15548627.2015.1043076

Yuan, H.-X., Russell, R. C., & Guan, K.-L. (2013). Regulation of PIK3C3/VPS34 complexes by MTOR in nutrient stress-induced autophagy. *Autophagy*, *9*(12), 1983–1995. https://doi.org/10.4161/auto.26058

Zens, B., Sawa-Makarska, J., & Martens, S. (2015). In vitro systems for Atg8 lipidation. *Methods*, *75*, 37–43. https://doi.org/10.1016/j.ymeth.2014.11.004

Zijlstra, E. E. (2016). The immunology of post-kala-azar dermal leishmaniasis (PKDL). *Parasites & Vectors, 9*(1), 464. https://doi.org/10.1186/s13071-016-1721-0

Zilberstein, D., & Shapira, M. (1994). The role of pH and temperature in the development of *Leishmania* parasites. *Annual Review of Microbiology*, *48*(1), 449–470. https://doi.org/10.1146/annurev.mi.48.100194.002313